Frank N. Crespilho *Editor*

COVID-19 Metabolomics and Diagnosis

Chemical Science for Prevention and Understanding Outbreaks of Infectious Diseases

Springer

COVID-19 Metabolomics and Diagnosis

Frank N. Crespilho
Editor

COVID-19 Metabolomics and Diagnosis

Chemical Science for Prevention and Understanding Outbreaks of Infectious Diseases

Springer

Editor
Frank N. Crespilho
University of Sao Paulo
Sao Paulo, Brazil

ISBN 978-3-031-15888-9 ISBN 978-3-031-15889-6 (eBook)
https://doi.org/10.1007/978-3-031-15889-6

This Springer imprint is published by the registered company Springer Nature Switzerland AG
The registered company address is: Gewerbestrasse 11, 6330 Cham, Switzerland

Contents

Trends in Electroanalytical Assays for COVID-19 Diagnosis

Thiago Martimiano do Prado and Sérgio Antonio Spinola Machado

Abstract The use of electrochemical biosensors is highlighted for SARS-CoV-2 detection and COVID-19 diagnosis. In a brief description of virus structure, fundamental features of proteins and nucleic acid are approached for a comprehensive strategy over biosensor designs. Relevant works are described and related to specific structural proteins used as viral biomarkers. Furthermore, the challenges and perspectives are pointed to the evolution of electroanalysis and the establishment of methods comparable to the gold standard, RT-PCR.

Keywords Electrochemical biosensors · SARS-CoV-2 detection · Electroanalysis · COVID-19 diagnosis · Virus structure

1 Introduction

After the SARS-CoV-2 pandemic declaration, worldwide health agencies adopted many strategies for the control of the virus widespread. Social distancing and sometimes lockdown is necessary, as well as the use of a mask and frequent hand washing and application of alcohol gel. With the development and distribution of vaccines is expected that the progressive immunization of the population can slow down the virus widespread until their effective control. Furthermore, the key strategy to contain the SARS-CoV-2 circulation is the constant testing of the population and isolation of infected individuals.

For many countries, the massive tests are a great challenge, since some issues are related to the purchasing power of populations, limited production of devices caused by laborious fabrication methods, or raw material shortage due to high demand, when it comes to rapid tests based on immunochromatographic assays. Although RT-qPCR is the gold standard method for SARS-CoV-2 detection, in many countries it is limited by high cost and the existence of a small amount of equipment to meet the high demand for tests.

T. M. do Prado (✉) · S. A. S. Machado
University of São Paulo—Chemistry Institute of São Carlos, São Carlos 13560-970, Brazil
e-mail: thipra@gmail.com

F. N. Crespilho (ed.), *COVID-19 Metabolomics and Diagnosis*,
https://doi.org/10.1007/978-3-031-15889-6_1

Considering all problems for mass testing mentioned above, alternative methods are needed and the research on the electroanalytical methods using biosensors presents promising results. In general terms, this chapter presents the strategies adopted for the detection of SARS-CoV-2, through devices with an electrochemical response. Thus, it is necessary to know the biosensor operation, electroanalytical methods, and the biomolecules that are part of the structure of SARS-CoV-2, some of which are used as a recognition element for detection.

1.1 Electrochemical Biosensor Operation

All needed elements for the electrochemical biosensor operation are illustrated in Fig. 1. In a brief explanation, an electrochemical biosensor is an analytical device that integrates a biolayer with bioreceptors (DNA, enzyme, antibody, microorganism), an electrochemical transducer, and, electrical signal conditioning and processing elements. The main aim is the acquisition of an electrical signal with magnitude or frequency proportionally to the target analyte in the sample.

A variation in the resistance, capacitance, or the occurrence of electrical current when the analyte from the sample contact the bioreceptor is identified by the transducer. Then, the electrical signal is acquired and processed. The acquisition, control, and visualization system inform the user if the analyte was detected or not. In special cases is needed a secondary biological element is labeled with an electroactive compound (electrochemical probe). This marker is linked to the analyte after their bioconjugation with the bioreceptor and under controlled potential application, an electrical current intensity is proportional to the amount of analyte. The controlled potential should be suitable for the oxidation or reduction of the electrochemical probe.

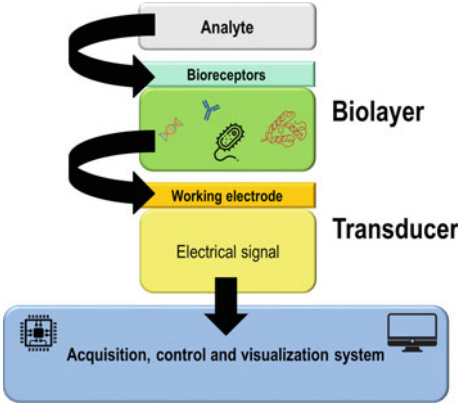

Fig. 1 Schematic representation of elements contained in an electrochemical biosensor

Biosensors developed for SARS-CoV-2 identification and COVID-19 diagnosis use some proteins or components of virus structure. Therefore, a detailed understanding of the SARS-CoV-2 structure is crucial to the development of the analytical strategy for their detection.

1.2 Structure of SARS-CoV-2

The genomic organization of the SARS-CoV-2 has structural proteins (4 types), nonstructural proteins (16 types), and accessory proteins (9 types). Here are described the main features of structural proteins: S protein; E protein; N protein; M protein (see Fig. 2); and the RNA viral, both used for the COVID-19 detection through electrochemical biosensors.

S protein

SARS-CoV-2 is a virus from the Coronaviridae family whose has spherical morphology, and its surface projections resemble the appearance of a "crown". These surface projections are compounds of structural proteins known as spike protein or S protein. During the organism infection S proteins are responsible for the virus linkage in receptors from the cellular membrane of the host, the human angiotensin 2 converting enzyme (hACE2). Walls and collaborators [1] performed studies over S protein from SARS-CoV-2 that showed the use of the S-B domain for the interaction with hACE2 similarly to the SARS-CoV S protein during the 2002–2003 SARS outbreak. Additionally, SARS-CoV-2 S protein has 80%, 80%, and 76% identity with Rinolophus sinicus ZC45 S glycoproteins, Rinolophus sinicus SARSr CoV ZXC21 S, and SARS-CoV S Urbani, respectively [2]. Also, the SARSr CoV RaTG13 has a 97% sequence identity of S glycoprotein to SARS-CoV-2 at [3].

In addition to the B domain, the receptor-binding domain (RBD) also presents information about the identity between SARS-CoV-2 and SARS-CoV. RBD is composed of interconnected helixes and loops core and a receptor-binding motif (RBM), which have interactions with the hACE2 [4]. For the S proteins, SARS-CoV

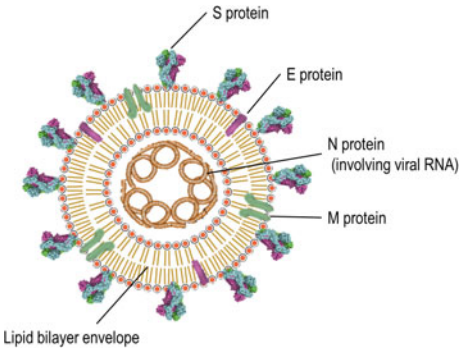

Fig. 2 Structure of SARS-CoV-2

and SARS-CoV-2 present about 50% identity in RBMs within the B domain and 75% identity in the S-B domain [5].

S protein of SARS-CoV-2 was the most frequently mutated protein, along with the pandemic between 2020 and 2021. It should be considered to assess whether a particular device that uses protein S for the diagnosis of COVID-19 is appropriate for the identification of disease caused by any existing type of virus strain.

E protein

Envelope proteins, also known as E proteins are an important structural protein class that forms the outer capsid of SARS-CoV-2. They have a size range of 8.4 to 12 KDa and around 76–109 amino acids [6]. During coronaviruses infection, E protein plays an important role in morphogenesis and pathogenesis [7]. Furthermore, they are responsible for the ions channel formation on the virus surface. The importance of E proteins is related to the virus assembly and infectivity [8].

Although the structure of SARS-CoV-2 protein E is not fully understood, studies on its functions can be done in a comparative way with SARS-CoV protein E, which is well solved. A charged cytoplasmic tail and a large hydrophobic domain have been identified in SARS-CoV. So, the hydrophobic domain is known as the transmembrane domain (TMD) containing 25 amino acids, within oligomerized alpha-helix that forms an ions channel in TMD. The abundance of leucine and valine comes with hydrophobicity in TMD [9–12].

Under the invasion, the coronavirus has a different location inside the host cell, and during virus assembly, the E protein occurs mainly in the endoplasmic reticulum and Golgi body (ERGIC) [13]. There are no concrete results about what region of the E protein is responsible for their directing in the ERGIC. Some studies with epitope-tagged SARS-CoV protein E indicate that it may be present by binding of groups N-terminal or C-terminal [14, 15]. Most information about the targeting of protein E in the Golgi apparatus is associated with binding to the C-terminal of the protein, with additional information being related to the N-terminal.

E protein also has its subcellular traffic and interactions with other proteins affected by various post-translational modifications. One such modification occurs in TMD cysteine in the protein, known as palmitoylation, according to observations made for SARS-CoV [16]. The importance of palmitoylation in viral assembly was observed by experiments with mutated E protein, with blocking of the modification, reduction of viral load, and protein instability. Another effect that is unique to the SARS-CoV E protein is ubiquitination. In this case, the CoV nsp3 interacts with the E protein via the N-terminal of nsp3, showing a negative correlation with the half-life and stability of the protein [17, 18].

There is a well-characterized interaction among coronaviruses proteins between E and M proteins. This occurs for viral assembly in the ERGIC, through the C-termini of the two proteins, resulting in the removal of the C-terminus and the reduction in virus-like proteins (VLPs) [7, 15, 19, 20]. Also, E protein interacts with itself by homo-oligomerization for the formation of the ion channel [21]. The interaction of E protein and S protein in SARS-CoV occurs by TMD of the E protein involving three cysteine residues and three cysteines in the C-terminus of the S protein [10, 22].

E protein interacts with five host cell proteins: stomatin, syntenin, e. Bcl-xL, PALS1 and sodium/potassium (Na^+/K^+) ATPase α-1 subunit. Both interactions with E protein can be related to some symptoms in the patients affected by SARS like the disruption of epithelial sodium channels, inflammatory cytokines, lymphopenia, and breach of the alveolar wall [23–27].

E protein presented very low mutation during the 2020–2021 pandemic, which can be favorable to the development of a unique strategy for diagnosis of COVID-19 caused by different virus strains.

N protein

The coronavirus has a nucleocapsid protein, also known as N protein, which is found in the helical ribonucleoprotein complex formed with the RNA genome. Additionally, it regulates the viral RNA synthesis, replication, and transcription, and affected cell metabolism [28–30]. The N protein plays a shield function over the viral ribonucleotides and supports the stability of the RNA inside the virus.

The primary function of N protein is to act for genomic RNA protection. So, recognizes the genomic RNA to form a capsid [31]. Other roles are associated with N protein such as the manipulation of the host cellular machinery; deregulation of the host cell cycle [32–34]; downregulation of the gene products [31] and; inhibition of interferon production [31]. There are studies over N protein upregulation in the production of cyclooxygenase-2 (COX_2) protein, an important proinflammatory induced under coronavirus infection [35]. Furthermore, some experimental studies demonstrated N protein correlation with the control over host-antigen interactions, progression of the host cell cycle, and apoptosis [33, 36, 37].

X-ray crystallography experiments were used to solve the crystal structure of SARS-CoV-2-N-NTD (N-terminal RNA-binding domain) and comparison to SARS-CoV-N-NTD [38]. The SARS-CoV-N-NTD has two different packing modes, a cubic and a monoclinic, whereas the SARS-CoV-2-N-NTD shows an orthorhombic crystal packing mode. Thus, the difference between crystal packing suggests that SARS-CoV-2 may have the formation of the ribonucleoprotein complex by different contacts [38].

N-NTD in SARS-CoV-2 and HCoV-OC43, the coronavirus that causes mild cold symptoms, has distinct structures. Information over the SARS-CoV-2-N-NTD ribonucleotide-binding site was disclosed by the superposition of SARS-CoV-2-N-NTD with HCoV-OC43-N-NTD-AMP.

N protein was the second most mutated in the 2020–2021 pandemic, after S protein. This protein has 419 amino acids long and occurred 16 mutations with a rate higher than the threshold of 0.01 [39]. This information is important for the evaluation of the analytical strategy used to detect different virus strains.

M protein

The membrane protein is also known as M protein. In general, it is a coronaviruses protein crucial to the virus assembly, including SARS-CoV-2. Their role is performed through interactions with themselves and other structural proteins like the N protein and S protein [40].

Interaction of M–S proteins occurs for the transmembrane fusion during a host cell invasion. M protein is found in abundance in the coronavirus virions, being important to the viral assembly and morphogenesis [41, 42].

There are three N-terminal domains in membrane M glycoprotein. After the expression of the M protein, it is glycosylated in the Golgi. Their combination with S protein, N protein, and itself occurs during the virus assembly [43]. A specific interaction occurs between the M protein and N protein involving the creation of a complex with the genomic RNA. The complex acts for the activation and the development of virions in the intermediate endoplasmic reticulum and Golgi apparatus [43, 44].

M protein present in SARS-CoV-2 has 669 nucleotides responsible for the encoding of 222 amino acids [45]. This sequence of SARS-CoV-2 M protein has an identity around 90% of the membrane M protein of SARS-CoV [46].

Common structural characteristics are present in all M proteins from CoV, which is the presence of three transmembrane domains endowed with a long carboxy-terminal tail and a short glycosylated amino-terminal domain [7, 40]. As well to the E protein, the M protein presented a very low mutation in the SARS-CoV-2 proteome in the 2020–2021 pandemic period [39]. It is important to predict the application of M protein-based analytical strategies for COVID-19 diagnosis by different virus strains.

RNA viral

SARS-CoV-2 is a ribonucleic acid virus (RNA) whose genetic material is represented by a unique RNA+ molecule. All their genome contains around 30.000 nucleotides, each compound with one ribose molecule, one phosphoric acid, and one nitrogen basis. RNA+ is protected within the virus by a nucleocapsid compound mainly by N proteins [47]. Because it is an RNA virus the nitrogen bases are adenine, cytosine, guanine, and uracil.

SARS-CoV-2 is classified as an RNA+ virus due to its direction in 5′3’ way, which means that it can be directly read by the cellular structures. Furthermore, is a considerate messenger RNA type, traversed by ribosomes and induces the production of viral proteins [48].

Another interesting feature of RNA+ is the presence of RNA polymerase protein, following the virus or produced by the host cell. The production of several RNA+ clone molecules within the host cell occurs out of transitory RNA− template molecules produced from the original RNA+ [48].

The use of appropriate sample processing and bioreceptors become the RNA detection useful for COVID-19 diagnosis.

1.3 RT-qPCR Versus Biosensors

The polymerase chain reaction (PCR) revolutionized the quantitative analysis of DNA and RNA. This technique has evolved rapidly in recent years and the growing interest in PCR applications has favored the development of quantitative real-time

PCR, also known as qPCR. When RNA has been analyzed their conversion to complementary DNA is needed. So, a specific step is performed for the reverse transcription reaction (RT) and the technique is known as RT-qPCR. This technique is considered the gold standard by the World Health Organization (WHO), for diagnosing COVID-19 [49].

Before the analysis, the nasopharyngeal sample is collected with aid of a swab that is kept immersed in a preservative solution, the viral transport medium, until the RNA extraction, through sequential washing steps with appropriate buffer solutions and centrifugation.

Three steps summarize the performance of PCR in a thermocycler [50], as shown in Fig. 3. First, the genomic DNA containing the sequence to be amplified is denatured offering the separation of the double-strand. Then in the annealing step, the molecules known as primers, specify to certain DNA sequence that binds to the strand of DNA to be amplified. Each primer is specifically complementary to the strand of the DNA double helix and the other strand. They will identify which stretch of DNA should be copied. In the third step, Taq polymerase binds in a complementary way to the strand signaled by the primer. The elongation of the new DNA fragment begins, forming a double strand of DNA again. This cycle is performed countless times until reaching millions of copies.

In RT-qPCR, the result is visualized immediately in a spectrofluorimeter, due to the addition of fluorescent probes to the PCR reactions. During the qPCR process, the amplification of the target DNA is monitored and the level of fluorescence increases proportionately to the DNA amplification. The equipment is capable of detecting the fluorescence produced by the sample and thus the technique allows monitoring of the reaction and the presentation of results in real-time [51].

In addition, the amount of target DNA present in the original sample is accurately determined by monitoring the rate of increase in fluorescence in the PCR reaction. The primers and fluorophores used may be chosen according to the genome region

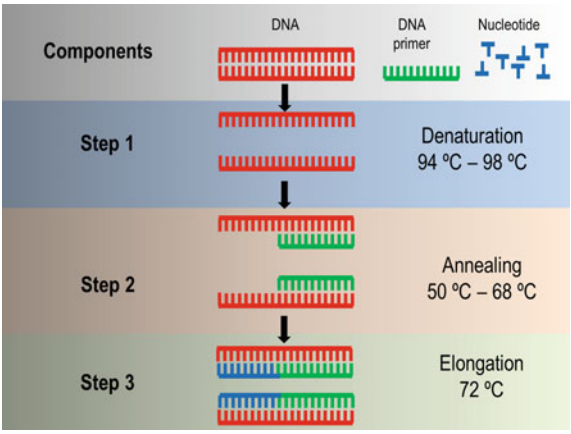

Fig. 3 Schematic representation of the PCR cycle

selected for the analysis and the detector specification of the spectrofluorimeter, respectively.

Although the RT-qPCR is a gold standard due to its high specificity, the sample processing from the swab collection until the RNA extraction is very laborious and demands a laboratory structure with centrifuges and accessories for sample handling. Also, the performance at specific laboratories is due to the not portables thermocyclers and spectrofluorimeter for the analysis. Furthermore, the steps in the thermocycler demand around an hour and a half time, which can be considered time-consuming when it is necessary to analyze many samples.

In this context, the biosensors arise as an alternative to RT-qPCR, due to their specificity, simple sample processing, and potential miniaturization for use in the point-of-care. In the further sections, the operation of biosensors for COVID-19 diagnosis is detailed allowing a deep analysis of their issues beyond the advantages of front RT-qPCR.

2 S Protein-Based Electrochemical Biosensors

The use of a specific antibody as a bioreceptor on the transducer surface is the main strategy embraced by the S protein-based biosensor. Besides, this strategy is often applied with S protein label-free detection. This means that the signal presented by the biosensor corresponds directly to the spike protein and an electroactive probe is non-needed for the measurements.

Lokman and collaborators [52] designed a voltammetric biosensor involving bovine serum albumin (BSA), SARS-CoV-2 spike antibody (AB), and functionalized graphene oxide (f-GO). The response of the biosensor was correlated to the current of oxidation attributed to the antibody-antigen protein interaction over two different transducers, glassy carbon electrode (GCE) and screen-printed carbon electrode (SPE). The AB immobilization occurred by terminus amino groups, which were linked to carboxyl groups from f-GO. Thus, the graphene oxide functionalization with N-(3-Dimethylaminopropyl)-N′-ethylcarbodiimide hydrochloride (EDC) and N-Hydroxysuccinimide (NHS) was crucial to the antibody attaching. The detection of SARS-CoV-2 spike protein was evaluated in synthetic, saliva, and oropharyngeal swabs samples. The analysis time was 5 min and 35 min for the SPE and GCE, respectively. Comparison with RT-PCR was performed in saliva sample and the developed method had 92.5% specificity and 93.3% sensitivity.

The use of label-free electrochemical biosensors may cause doubts over the attribution of the response to the specific bioconjugation since the potential interferers from the analysis matrix can be subjected to redox reactions. Nevertheless, Zeinab and collaborators [53] adopted the IgG anti-SARS-CoV-2 spike antibody ordered orientation as a key point to the fabrication of an immunosensor for SARS-CoV-2 spike protein detection. The ordered orientation was due to the presence of Staphylococcal protein A (ProtA), which plays the role of a strong immunological instrument due to its ability to strongly bind to the fragment crystallizable region of IgG

antibodies. So, an impedimetric biosensor was fabricated from an SPE modified with Cu_2O nanocubes (Cu_2O NCs) and immobilized antibodies with a well-defined orientation that increases antigen-binding capacity and improves the function of the detection system. The modified surface provides a large surface area in a very small space and, allowed a great ProtA loading on the electrode surface.

The proposed biosensor presented specific binding that allowed the establishment of a linear relationship between the charge transfer resistance (R_{ct}) and spike protein. Still, on a label-free strategy, the spectroelectrochemistry biosensor may provide supplementary responses that increase the reliability of the results. It was presented in the work of Waleed [54]. An immunoassay based on the S protein recognition by monoclonal antibody IgG1was performed by Raman spectroscopy and square-wave voltammetry (SWV). Raman spectroscopy is considered a promising labelless analytical methodology. The fingerprint's biochemical composition of the analyzed samples shown in Raman provides specificity to the analysis. Moreover, this technique allows accurate, sensitive, and nondestructive assays. On the other hand, the SWV correlates the oxidation current peaks with the interaction between the IgG1 and the SARS-CoV-2 spike protein. For the biosensor construction, the porous graphene oxide (rPGO) decorated with gold nanoparticles (Au NPs) was used to modify an ITO electrode. The uniform film of Au NPs@rPGO over the ITO surface provides enhanced Raman signal and electric conductivity. Thus, the IgG1 was immobilized onto the modified electrode and was used as a probe to capture SARS-CoV-2 spike protein in human serum. Figure 4 shows a schematic representation of the biosensor construction.

Table 1 summarizes other works that bring this same proposal, beyond the above-mentioned label-free electrochemical biosensors for COVID-19 diagnosis through S

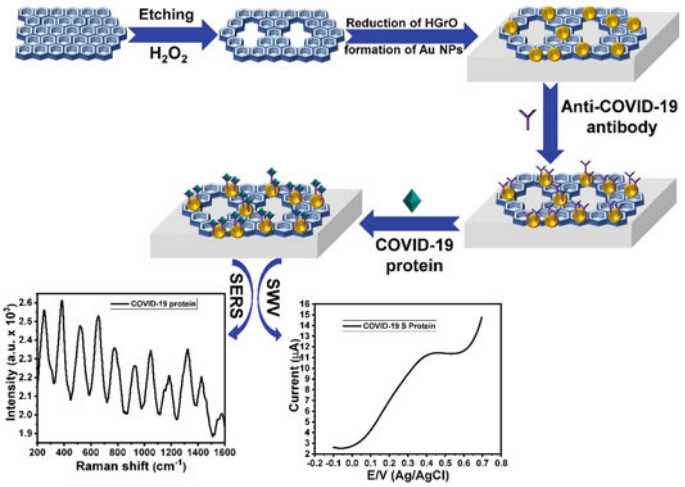

Fig. 4 Schematic representation of Spectroelectrochemical biosensor for SARS-CoV-2 spike protein detection. Reprinted from [54] with the permission of Elsevier

Table 1 Main features of label-free biosensors for COVID-19 diagnosis using S protein as a biomarker

Electrode	Sample	Electrochemical technique	Limit of detection	Reference
GCE/*f*-GO and SPE/*f*-GO	Oropharyngeal swab	SWV	10.0 fg mL^{-1}	[52]
SPE/Cu_2O NCs	Saliva, artificial nasal, and UTM	EIS	0.04 fg mL^{-1}	[53]
ITO/rPGO@Au NPs	serum	SWV plus Raman	39.5 fmol L^{-1}	[54]
SPE graphene layer	serum	SWV	260 nmol L^{-1}	[55]
ITO/GNPs@MUA	artificial nasal secretion	EIS	0.58 fg mL^{-1}	[56]
SPE graphene layer	nasopharyngeal fluid	EIS	0.25 fg mL^{-1}	[57]

Note GCE/*f*-GO: glassy carbon electrode modified with functionalized graphene; SPE/*f*-GO: screen-printed carbon electrode modified with functionalized graphene; SPE/Cu_2O NCs: screen-printed carbon electrode modified with copper (II) oxide nanocubes; ITO/rPGO@Au NPs: Indium tin oxide electrode modified with porous graphene oxide and gold nanoparticles; ITO/GNPs@MUA: Indium tin oxide electrode modified with gold nanoparticles-capped 11-mercaptoundecanoic acid; UTM: universal transport medium; SWV: square-wave voltammetry; EIS: electrochemical impedance spectroscopy

protein as a biomarker. SWV and EIS are typical electrochemical techniques used in these label-free strategies and the signals related to the amount of S protein detected are oxidation peak current and charge transfer resistance, respectively. In all works is evident the existence of a linear correlation between the analytical signal and the S protein concentration, although the reason for these signals variation is not clearly explained.

3 N Protein-Based Electrochemical Biosensors

The N proteins present in nucleocapsid are interesting virus constituents for use as antigen biomarkers, due to their inner virus structure localization. Considering the crucial role of nucleocapsid as an RNA shield, N proteins are intrinsically less susceptible to degradation than the other structural proteins (S, E, and M proteins). During assays for COVID-19 diagnosis, the inactivation of the virus probably present in the sample is a mandatory step for the safety assurance of the analyst and environment. This step may be performed by heating treatment or by chemicals. In this sense, the "robustness" of N protein ensures the integrity of their relative domain to the other structural proteins used as antigen biomarkers.

Among the published works on the use of the N protein for COVID-19 diagnosis, those which use the sandwich-type bioconjugation are highlighted. Karaman and collaborators [58] developed a sandwich-type electrochemical immunosensor based

on the capture of nucleocapsid protein from saliva samples. This proposal used the bismuth tungstate/bismuth sulfide composite (Bi_2WO_6/Bi_2S_3) and graphitic carbon nitride sheet decorated with gold nanoparticles (Au NPs) and, the tungsten trioxide sphere composite (g-C_3N_4/Au/WO_3) as signal amplification.

For the capture probe operation was made the Bi_2WO_6/Bi_2S_3 deposition over the glassy carbon electrode (GCE), followed by the immobilization of the capture human monoclonal antibody c-SARS-CoV-2-Ab1 by electrostatic interactions, and the subsequent surface blocking with BSA and the bioconjugation with the nucleocapsid protein (SARS-CoV-2-NP) that results in the SARS-CoV-2-NP/BSA/SARS-CoV-2-Ab1/GCE. Then, the amplification was made by the formation of the nanocomposite g-C_3N_4/Au/WO_3 and the immobilization of the detection monoclonal anti-SARS-CoV-2 nucleocapsid antibody (d-SARS-CoV-2-Ab2) resulting in the d-SARS-CoV-2-Ab2/g-C_3N_4/Au/WO_3. The bioconjugation between the composites formed the sandwich. Even as the electro-oxidation of the H_2O_2 in the sandwich surface is performed through differential-pulse voltammetry (DPV).

The g-C_3N_4/Au/WO_3 composite acts as signal amplification for the electrochemical SARS-CoV-2-NP immunosensor. Since the g-C_3N_4/WO_3 had a Z-scheme heterojunction which cause the decrease of the electron transfer is needed the use of AuNPs as a mediator to facilitate the electron transfer at the interface. The AuNPs have a large specific surface area, promote charge separation, and allow easy antibody immobilization. Hence, g-C_3N_4/Au/WO_3 composite provides the development of a sensitive immunosensor and low limit of detection, LOD = 3.00 fg mL^{-1}. The choice of H_2O_2 as a redox probe by the authors was due to its easy oxidation into O_2 and continuous monitoring.

Beyond the immunosensor, the aptasensor belongs to another kind of electrochemical biosensor that may be applied using the sandwich strategy. In the aptasensor, the bioreceptors and amplification are based on aptamer immobilization. The aptamer is an oligonucleotide or peptide that binds to a specific target molecule. Aptamers are normally created through selection from a set of random sequences, although they also occur naturally as part of riboswitches. Among several applications, aptamers can be used for both basic research and clinical purposes, as they can act as macromolecular drugs. Additionally, aptamers can be combined with ribozymes to self-cleave in the presence of the target molecule. For application in aptasensors, the aptamers should have a specific binding site to the bioconjugation with the target molecule used as the antigen biomarker.

Tian and collaborators developed an aptasensor based on the metal–organic frameworks (MOFs), decorated with metallic nanoparticles and enzymes for the detection of the SARS-CoV-2 N protein present in serum samples. The MOFs used are MIL-53(Al), the enzymes were the hemin/G-quadruplex (GQH) DNAzyme and horseradish peroxidase (HRP), whereas the metallic nanoparticle was core–shell Au@Pt.

The nanoprobes were composed of hemin/GQH DNAzyme, HRP, Au@Pt/MIL-53(Al). The presence of free amino groups in the MOFs allowed the assembly of the Au@Pt NPs. The anchoring was carried out with thiolated modified aptamers (SH-2G-N48 and SH-2G-N61) containing a double G-quadruplex sequence. The

HRP was decorated onto the Au@Pt NPs and, the co-catalysis of HRP and GQH DNAzyme nanoprobe was synthesized in the presence of hemin.

For the immobilization of the thiolated modified dual aptamers (N48 and N61) on the gold electrode surface were used the Au–S bonds. Then, the dual-aptamer modified gold electrode had their unoccupied sites blocked with BSA. The electrode was then incubated for 1 h in a certain concentration of SARS-CoV-2 N protein. Next, the construction of the aptamer-protein-nanoprobe sandwich structure aptasensor was made by the addition of the nanoprobe onto the gold electrode surface. Finally, the DPV signal was collected in the PBS solution containing H_2O_2 and hydroquinone (HQ). The nanoprobe catalyzes the oxidation of HQ with H_2O_2 giving rise to amplifying the electrochemical signal with the sharp peak current indicating that the SARS-CoV-2 N protein is captured.

Also, there are SARS-CoV-2 N protein electrochemical biosensors based on the label-free strategy. Although label-free biosensors have fabrication procedures more simple than the sandwich-type, their present less sensitivity and susceptibility to the cross-reactions with probable interferers present in the matrix, as well discussed in Sect. 4. The main features of some published works about label-free SARS-CoV-2 N protein are summarized in Table 2.

The reference [62] from Table 2 is highlighted due to an innovative feature of the immunosensor proposed, which is the use of the electrode in sample collection. For this, the virus nucleocapsid (N) protein was immobilized on carbon nanofiber-modified screen-printed electrodes. Thus, the virus antigen was detected after swabbing and immersion of the electrode in the solution for the competitive assay using a fixed amount of N protein antibody.

Table 2 Main features of label-free biosensors for COVID-19 diagnosis using N protein as a biomarker

Electrode	Sample	Electrochemical technique	Limit of detection	Reference
SPE/AuNPs	Nasopharyngeal swab	SWV	0.40 pg mL^{-1}	[59]
AuTFE/MIP	Nasopharyngeal swab	DPV	50.0 fmol L^{-1}	[60]
AuIDE/carbon nanodiamond	Serum	EIS	0.39 fmol L^{-1}	[61]
SPE/cotton-tipped	Nasopharyngeal swab	SWV	0.80 pg mL^{-1}	[62]

Keynotes AuTFE/MIP: gold thin film electrode modified with a molecularly imprinted polymer; AuIDE/carbon nanodiamond: gold interdigitate electrode modified with carbon nanodiamond

4 RNA-Based Electrochemical Biosensors

The electrochemical biosensors devoted to nucleic acid detection can also be called electrochemical genossensors. Generally, these devices use the working electrode modified with a capture probe, which hybridizes with the complementary target nucleotide onto the sensor surface. Specifically for the COVID-19 diagnosis, a DNA probe should be used to capture the RNA single strand from the virus. This bioconjugation methodology is the most similar to PCR among all the ones discussed here. Therefore, is expected that electrochemical genossensors for COVID-19 to be the direct alternative method to compete with PCR.

Moreover, portability, low cost, and low time consumption are fundamental features that increase the competitiveness of the electrochemical biosensors front PCR. Alafeef and collaborators [63] developed a device that probably could be a strong competitor to PCR if large-scale production becomes viable. The operation of the biosensor is based on a paper-based electrochemical platform. The sensing probes immobilized onto the transducer are composed of gold nanoparticles, capped with highly specific antisense oligonucleotides (ssDNA) used to capture the viral nucleocapsid phosphoprotein (N-gene). The target readout can be recorded with a simple hand-held reader. The biosensor chip was applied for analysis in samples of nasopharyngeal and oropharyngeal swabs. Figure 5 shows the representation of the operation principle of the COVID-19 electrochemical sensing platform.

In step A occurs the collection of the samples from the nasal swab or saliva of the patients, followed by step B, which consists of the viral SARS-CoV-2 RNA extraction extracted. Next, in step C the viral RNA is added over the graphene-ssDNA-AuNP platform, then in step D occur the sample incubation for 5 min and, finally, in step E the electrochemical response will be recorded.

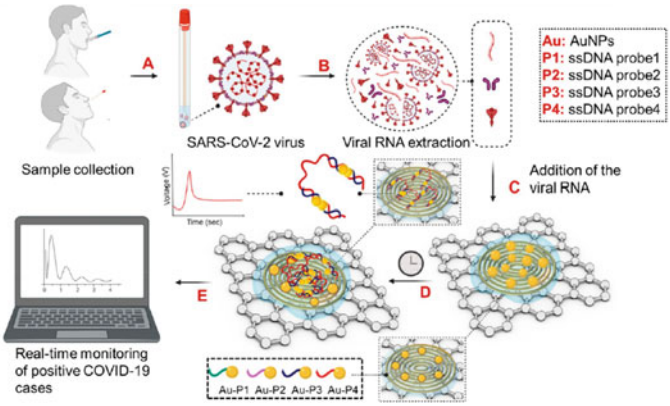

Fig. 5 Representation of the operation principle of the electrochemical sensing platform. Reprinted from [63] with permission of ACS Publications

Note that different capture probes are used (Au-P1, Au-P2, AuP3, and Au-P4), and each interacts with a specific region of the virus genome resulting in high specificity. The electrochemical response of the device is based on the resistive sensor model and the monitored potential increases proportionally to the target concentration.

$$\Delta V = R\frac{dq}{dt} \tag{1}$$

where ΔV is the change in the voltage across the sensor chip, R is the resistance and q is the charge. Thus, the hybridization of target RNA with ssDNA probe results in the decrease of the resistance across the sensor chip. The analysis takes place with 5 min of incubation time, has a sensitivity of 231 copies μL^{-1} and a limit of detection of 6.9 copies μL^{-1} without any further amplification.

The use of magnetic beads modified with capture probes is considered an efficient strategy in the sample processing for the hybridization with the target. It is due to the magnetic separation in the washing steps of the sample, which ensures the elimination of matrix interferences. This procedure is common in the methods that use the signal amplification by a second labeled probe to form a sandwich, as can be seen in the reference [64]. Figure 6 shows the representative steps of the detection procedure.

The capture probe and amplification element were designed as premix A and premix B, respectively.

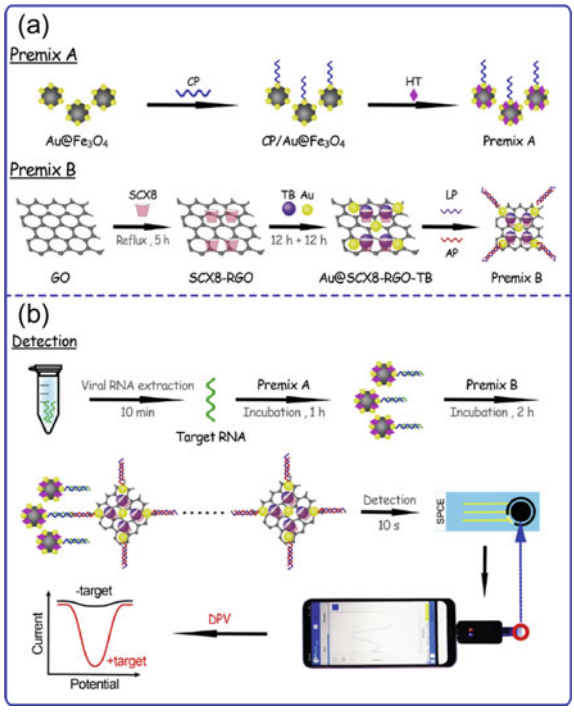

Fig. 6 Representative steps of detection procedure using a sandwich-type electrochemical genossensor. Reprinted from [64] with permission of Elsevier

The premix A composition has Fe_3O_4 NPs decorated with gold, $Au@Fe_3O_4$ with the capture probe immobilized onto the surface, and hexane-1-thiol (HT) occupying free sites to avoid non-specific binds. The premix B consists of reduced graphene oxide particles (RGO) decorated with gold and toluidine blue (TB) immobilized onto the surface.

After sample collection and RNA extraction the premix A is incubated with the sample for the target capture. Then, the sample is washed and the particles are separated by a magnet for incubation with the premix B forming the sandwich. Next, the sandwich is washed and separated as in the previous step. Finally, the solution with the sandwich is added onto the screen-printed electrode surface and the current peak of TB reduction is correlated to the target concentration/presence. This method presented the limit of detection of 200 copies mL^{-1} for the clinical specimen. Furthermore, the results show that the developed method is promising for application in point-of-care analysis (POC) due to the use of a smartphone for the measure and the ultra-sensitivity and accuracy.

There are other manuscripts over electrochemical genossensors for COVID-19 diagnosis that it is recommended to read in addition to these sensors discussed so far. Then, we highlighted the reference [65], which deals with a microfluidic platform based on molecular DNA nanostructures for viral RNA recognition, with electrochemical signal enhancement. Another interesting work [66] presents the development of a device capable of discriminating the distinct infection phases from amplified cDNA samples. The device is promised to reduce the overall cost and achieve low detection limits comparable to RT-qPCR-based tests.

5 Challenges and Perspectives

Some challenges must be overcome in terms of large-scale production and reproducibility since most of the developed devices use nanomaterials not commercially offered and with synthesis methods that do not have great yield. Withal, the key challenge is the creation of commercial electrochemical sensors for the point-of-care (POC) for the application in remote areas, and the monitoring of the infection of people in self-isolation.

From the point of view of electrochemistry, some problems should be avoided and considered for the development of analytical methods. The interference and electrode fouling can occur by matrix influence, resulting in weak molecular absorption and low electrochemical activity. Therefore, sample processing is crucial and the use of bioreceptors immobilized onto magnetic beads is a trend that can offer the clean-up of the sample with a decrease in matrix interference.

The time of analysis is very important to POC applications. Beyond the sample processing steps, the response acquisition time should be considered. In this sense, the size of the electrode is a determiner of the response time. As smaller, the electrode radial diffusion of the species became predominant and occurs a faster mass transport. Thus, smaller electrodes allow a faster electrochemical reaction to take place.

Potential or current measurements commonly have an error associated with the drop in potential resulting from the resistance between the reference electrode and the working electrode. This error changes the potential at the working electrode and when resistance and current (IR) can be corrected, a value is assigned to the resistance of the solution. Knowing the resistance of the solution, the current–potential curves (I-V) are corrected and the Ohmic drop is deduced through I–R.

Problems related to the counter electrode should also be avoided, once the counter electrode completes the circuit, allowing the application of the input potential to the working electrode and the flow of charges. To guarantee their correct functioning, they must be manufactured from an inert material and have a size at least two and a half times larger than the working electrode. This guarantees that there will be no current limitations.

The COVID-19 pandemic started an urgent run for the development of analytical methods for massive tests through devices with portability, robustness, and high sensibility. Once time that the present challenges could be overcome, the electrochemical biosensors are a serious candidate to be an efficient tool for disease widespread monitoring.

References

1. A.C. Walls, Y.J. Park, M.A. Tortorici, A. Wall, A.T. McGuire, D. Veesler, Structure, function, and antigenicity of the SARS-CoV-2 Spike glycoprotein. Cell **181**, 281 (2020). https://doi.org/10.1016/J.CELL.2020.02.058
2. X.Y. Ge, J.L. Li, X. Lou Yang, A.A. Chmura, G. Zhu, J.H. Epstein, J.K. Mazet, B. Hu, W. Zhang, C. Peng, Y.J. Zhang, C.M. Luo, B. Tan, N. Wang, Y. Zhu, G. Crameri, S.Y. Zhang, L.F. Wang, P. Daszak, Z.L. Shi, Isolation and characterization of a bat SARS-like coronavirus that uses the ACE2 receptor. Nature **503**, 535 (2013). https://doi.org/10.1038/NATURE12711
3. P. Zhou, X. Lou Yang, X.G. Wang, B. Hu, L. Zhang, W. Zhang, H.R. Si, Y. Zhu, B. Li, C.L. Huang, H.D. Chen, J. Chen, Y. Luo, H. Guo, R. Di Jiang, M.Q. Liu, Y. Chen, X.R. Shen, X. Wang, X.S. Zheng, K. Zhao, Q.J. Chen, F. Deng, L.L. Liu, B. Yan, F.X. Zhan, Y.Y. Wang, G.F. Xiao, Z.L. Shi, A pneumonia outbreak associated with a new coronavirus of probable bat origin. Nature **579**(7798), 270–273 (2020). https://doi.org/10.1038/s41586-020-2012-7
4. J. Lan, J. Ge, J. Yu, S. Shan, H. Zhou, S. Fan, Q. Zhang, X. Shi, Q. Wang, L. Zhang, X. Wang, Structure of the SARS-CoV-2 spike receptor-binding domain bound to the ACE2 receptor. Nature **581**(7807), 215–220 (2020). https://doi.org/10.1038/s41586-020-2180-5
5. Y. Wan, J. Shang, R. Graham, R.S. Baric, F. Li, Receptor recognition by the novel coronavirus from Wuhan: an analysis based on decade-long structural studies of SARS coronavirus. J. Virol. **94** (2020). https://doi.org/10.1128/JVI.00127-20/ASSET/EA9A0885-A970-4B62-B79A-99D6CA7D96E0/ASSETS/GRAPHIC/JVI.00127-20-F0004.JPEG
6. L. Kuo, K.R. Hurst, P.S. Masters, Exceptional flexibility in the sequence requirements for coronavirus small envelope protein function. J. Virol. **81**, 2249–2262 (2007). https://doi.org/10.1128/JVI.01577-06/ASSET/6B3DC561-FE54-4049-AB4A-94E0CA5237C7/ASSETS/GRAPHIC/ZJV0050788110008.JPEG
7. B.G. Hogue, C.E. Machamer, Coronavirus structural proteins and virus assembly. Nidoviruses 179–200 (2014). https://doi.org/10.1128/9781555815790.CH12
8. C. Verdiá-Báguena, J.L. Nieto-Torres, A. Alcaraz, M.L. Dediego, L. Enjuanes, V.M. Aguilella, Analysis of SARS-CoV E protein ion channel activity by tuning the protein and lipid charge.

Biochim. Biophys. Acta. **2013**, 2026–2031 (1828). https://doi.org/10.1016/J.BBAMEM.2013.05.008
9. Y. Du, F.A. Zuckermann, D. Yoo, Myristoylation of the small envelope protein of porcine reproductive and respiratory syndrome virus is non-essential for virus infectivity but promotes its growth. Virus Res. **147**, 294 (2010). https://doi.org/10.1016/J.VIRUSRES.2009.11.016
10. Q. Wu, Y. Zhang, H. Lü, J. Wang, X. He, Y. Liu, C. Ye, W. Lin, J. Hu, J. Ji, J. Xu, J. Ye, Y. Hu, W. Chen, S. Li, J. Wang, J. Wang, S. Bi, H. Yang, The E protein is a multifunctional membrane protein of SARS-CoV, Genomics. Proteom. Bioinform. **1**, 131–144 (2003). https://doi.org/10.1016/S1672-0229(03)01017-9
11. J.L. Nieto-Torres, M.L. DeDiego, C. Verdiá-Báguena, J.M. Jimenez-Guardeño, J.A. Regla-Nava, R. Fernandez-Delgado, C. Castaño-Rodriguez, A. Alcaraz, J. Torres, V.M. Aguilella, L. Enjuanes, Severe acute respiratory syndrome coronavirus envelope protein ion channel activity promotes virus fitness and pathogenesis. PLOS Pathog. **10**, e1004077 (2014). https://doi.org/10.1371/JOURNAL.PPAT.1004077
12. Y. Li, W. Surya, S. Claudine, J. Torres, Structure of a conserved Golgi complex-targeting signal in coronavirus envelope proteins. J. Biol. Chem. **289**, 12535–12549 (2014). https://doi.org/10.1074/JBC.M114.560094
13. T.R. Ruch, C.E. Machamer, The coronavirus E protein: assembly and beyond, viruses **4**, 363–382 (2012). https://doi.org/10.3390/V4030363
14. J.R. Cohen, L.D. Lin, C.E. Machamer, Identification of a golgi complex-targeting signal in the cytoplasmic tail of the severe acute respiratory syndrome coronavirus envelope protein. J. Virol. **85**, 5794–5803 (2011). https://doi.org/10.1128/JVI.00060-11/ASSET/B6CCA532-3E5F-439C-B1AA-8C4908FE6D72/ASSETS/GRAPHIC/ZJV9990946100008.JPEG
15. E. Corse, C.E. Machamer, The cytoplasmic tail of infectious bronchitis virus E protein directs Golgi targeting. J. Virol. **76**, 1273–1284 (2002). https://doi.org/10.1128/JVI.76.3.1273-1284.2002
16. L.A. Lopez, A.J. Riffle, S.L. Pike, D. Gardner, B.G. Hogue, Importance of conserved cysteine residues in the coronavirus envelope protein. J. Virol. **82**, 3000–3010 (2008). https://doi.org/10.1128/JVI.01914-07
17. C.T. Keng, S. Åkerström, C.S.W. Leung, L.L.M. Poon, J.S.M. Peiris, A. Mirazimi, Y.J. Tan, SARS coronavirus 8b reduces viral replication by down-regulating E via an ubiquitin-independent proteasome pathway. Microbes Infect. **13**, 179–188 (2011). https://doi.org/10.1016/J.MICINF.2010.10.017
18. E. Álvarez, M.L. DeDiego, J.L. Nieto-Torres, J.M. Jiménez-Guardeño, L. Marcos-Villar, L. Enjuanes, The envelope protein of severe acute respiratory syndrome coronavirus interacts with the non-structural protein 3 and is ubiquitinated. Virology **402**, 281–291 (2010). https://doi.org/10.1016/J.VIROL.2010.03.015
19. E. Mortola, P. Roy, Efficient assembly and release of SARS coronavirus-like particles by a heterologous expression system. FEBS Lett. **576**, 174–178 (2004). https://doi.org/10.1016/J.FEBSLET.2004.09.009
20. K.P. Lim, D.X. Liu, The missing link in coronavirus assembly. Retention of the avian coronavirus infectious bronchitis virus envelope protein in the pre-Golgi compartments and physical interaction between the envelope and membrane proteins. J. Biol. Chem. **276,** 17515–17523 (2001). https://doi.org/10.1074/JBC.M009731200
21. K. Pervushin, E. Tan, K. Parthasarathy, X. Lin, F.L. Jiang, D. Yu, A. Vararattanavech, W.S. Tuck, X.L. Ding, J. Torres, Structure and inhibition of the SARS coronavirus envelope protein ion channel. PLOS Pathog. **5**, e1000511 (2009). https://doi.org/10.1371/JOURNAL.PPAT.1000511
22. M.A. Tortorici, D. Veesler, Structural insights into coronavirus entry. Adv. Virus Res. **105**, 93–116 (2019). https://doi.org/10.1016/BS.AIVIR.2019.08.002
23. Y. Yang, Z. Xiong, S. Zhang, Y. Yan, J. Nguyen, B. Ng, H. Lu, J. Brendese, F. Yang, H. Wang, X.F. Yang, Bcl-xL inhibits T-cell apoptosis induced by expression of SARS coronavirus E protein in the absence of growth factors. Biochem. J. **392**, 135–143 (2005). https://doi.org/10.1042/BJ20050698

24. K.T. Teoh, Y.L. Siu, W.L. Chan, M.A. Schlüter, C.J. Liu, J.S.M. Peiris, R. Bruzzone, B. Margolis, B. Nal, The SARS coronavirus E protein interacts with PALS1 and alters tight junction formation and epithelial morphogenesis. Mol. Biol. Cell. **21**, 3838–3852 (2010). https://doi.org/10.1091/MBC.E10-04-0338/ASSET/IMAGES/LARGE/ZMK0221096610009.JPEG
25. J.M. Jimenez-Guardeño, J.L. Nieto-Torres, M.L. DeDiego, J.A. Regla-Nava, R. Fernandez-Delgado, C. Castaño-Rodriguez, L. Enjuanes, The PDZ-binding motif of severe acute respiratory syndrome coronavirus envelope protein is a determinant of viral pathogenesis. PLOS Pathog. **10**, e1004320 (2014). https://doi.org/10.1371/JOURNAL.PPAT.1004320
26. D. Schoeman, B.C. Fielding, Coronavirus envelope protein: current knowledge, Virol. J. **161**(16), 1–22 (2019). https://doi.org/10.1186/S12985-019-1182-0
27. J.L. Nieto-Torres, M.L. DeDiego, E. Álvarez, J.M. Jiménez-Guardeño, J.A. Regla-Nava, M. Llorente, L. Kremer, S. Shuo, L. Enjuanes, Subcellular location and topology of severe acute respiratory syndrome coronavirus envelope protein. Virology **415**, 69–82 (2011). https://doi.org/10.1016/J.VIROL.2011.03.029
28. Q. Huang, L. Yu, A.M. Petros, A. Gunasekera, Z. Liu, N. Xu, P. Hajduk, J. Mack, S.W. Fesik, E.T. Olejniczak, Structure of the N-Terminal RNA-binding domain of the SARS CoV nucleocapsid protein. Biochemistry **43**, 6059–6063 (2004). https://doi.org/10.1021/BI036155B
29. S.A. Stohlman, R.S. Baric, G.N. Nelson, L.H. Soe, L.M. Welter, R.J. Deans2, Specific interaction between coronavirus leader RNA and nucleocapsid protein. J. Virol. **62,** 4288–4295 (1988). https://doi.org/10.1128/JVI.62.11.4288-4295.1988
30. G.W. Nelson, S.A. Stohlman, S.M. Tahara, High affinity interaction between nucleocapsid protein and leader/intergenic sequence of mouse hepatitis virus RNA. J. Gen. Virol. **81**, 181–188 (2000). https://doi.org/10.1099/0022-1317-81-1-181/CITE/REFWORKS
31. M. Surjit, S.K. Lal, The SARS-CoV nucleocapsid protein: a protein with multifarious activities. Infect. Genet. Evol. **8**, 397–405 (2008). https://doi.org/10.1016/J.MEEGID.2007.07.004
32. Y.H. Li, J. Li, X.E. Liu, L. Wang, T. Li, Y.H. Zhou, H. Zhuang, Detection of the nucleocapsid protein of severe acute respiratory syndrome coronavirus in serum: comparison with results of other viral markers. J. Virol. Methods. **130**, 45–50 (2005). https://doi.org/10.1016/J.JVIROMET.2005.06.001
33. M. Surjit, B. Liu, V.T.K. Chow, S.K. Lal, The nucleocapsid protein of severe acute respiratory syndrome-coronavirus inhibits the activity of cyclin-cyclin-dependent kinase complex and blocks S phase progression in mammalian cells. J. Biol. Chem. **281**, 10669–10681 (2006). https://doi.org/10.1074/JBC.M509233200
34. F.Q. Li, H. Xiao, J.P. Tam, D.X. Liu, Sumoylation of the nucleocapsid protein of severe acute respiratory syndrome coronavirus. FEBS Lett. **579**, 2387–2396 (2005). https://doi.org/10.1016/J.FEBSLET.2005.03.039
35. X. Yan, Q. Hao, Y. Mu, K.A. Timani, L. Ye, Y. Zhu, J. Wu, Nucleocapsid protein of SARS-CoV activates the expression of cyclooxygenase-2 by binding directly to regulatory elements for nuclear factor-kappa B and CCAAT/enhancer binding protein. Int. J. Biochem. Cell Biol. **38**, 1417–1428 (2006). https://doi.org/10.1016/J.BIOCEL.2006.02.003
36. P.-K. Hsieh, S.C. Chang, C.-C. Huang, T.-T. Lee, C.-W. Hsiao, Y.-H. Kou, I.-Y. Chen, C.-K. Chang, T.-H. Huang, M.-F. Chang, Assembly of severe acute respiratory syndrome coronavirus RNA packaging signal into virus-like particles is nucleocapsid dependent. J. Virol. **79**, 13848–13855 (2005). https://doi.org/10.1128/JVI.79.22.13848-13855.2005
37. L. Du, G. Zhao, Y. Lin, C. Chan, Y. He, S. Jiang, C. Wu, D.Y. Jin, K.Y. Yuen, Y. Zhou, B.J. Zheng, Priming with rAAV encoding RBD of SARS-CoV S protein and boosting with RBD-specific peptides for T cell epitopes elevated humoral and cellular immune responses against SARS-CoV infection. Vaccine. **26**, 1644–1651 (2008). https://doi.org/10.1016/J.VACCINE.2008.01.025
38. S. Kang, M. Yang, Z. Hong, L. Zhang, Z. Huang, X. Chen, S. He, Z. Zhou, Z. Zhou, Q. Chen, Y. Yan, C. Zhang, H. Shan, S. Chen, Crystal structure of SARS-CoV-2 nucleocapsid protein RNA binding domain reveals potential unique drug targeting sites. Acta Pharm. Sin. B. **10**, 1228 (2020). https://doi.org/10.1016/J.APSB.2020.04.009

39. S. Vilar, D.G. Isom, One year of SARS-CoV-2: how much has the virus changed? Biology **10**, 91 (2021). https://doi.org/10.3390/BIOLOGY10020091
40. A.L. Arndt, B.J. Larson, B.G. Hogue, A conserved domain in the coronavirus membrane protein tail is important for virus assembly. J. Virol. **84**, 11418–11428 (2010). https://doi.org/10.1128/JVI.01131-10/ASSET/768BA1AF-FED2-4BA9-BEEB-3B634490CC9E/ASSETS/GRAPHIC/ZJV9990938260008.JPEG
41. K. Narayanan, A. Maeda, J. Maeda, S. Makino, Characterization of the coronavirus M protein and nucleocapsid interaction in infected cells. J. Virol. **74**, 8127–8134 (2000). https://doi.org/10.1128/JVI.74.17.8127-8134.2000
42. J. Armstrong, H. Niemann, S. Smeekens, P. Rottier, G. Warren, Sequence and topology of a model intracellular membrane protein, E1 glycoprotein, from a coronavirus. Nature **308**, 751–752 (1984). https://doi.org/10.1038/308751a0
43. C.A.M. de Haan, L. Kuo, P.S. Masters, H. Vennema, P.J.M. Rottier, Coronavirus particle assembly: primary structure requirements of the membrane protein. J. Virol. **72**, 6838–6850 (1998). https://doi.org/10.1128/JVI.72.8.6838-6850.1998/FORMAT/EPUB
44. D. Escors, J. Ortego, H. Laude, L. Enjuanes, The membrane M protein carboxy terminus binds to transmissible gastroenteritis coronavirus core and contributes to core stability. J. Virol. **75**, 1312–1324 (2001). https://doi.org/10.1128/JVI.75.3.1312-1324.2001
45. F. Wu, S. Zhao, B. Yu, Y.M. Chen, W. Wang, Z.G. Song, Y. Hu, Z.W. Tao, J.H. Tian, Y.Y. Pei, M.L. Yuan, Y.L. Zhang, F.H. Dai, Y. Liu, Q.M. Wang, J.J. Zheng, L. Xu, E.C. Holmes, Y.Z. Zhang, A new coronavirus associated with human respiratory disease in China. Nature **579,** 265–269 (2020). https://doi.org/10.1038/s41586-020-2008-3
46. Y. Hu, J. Wen, L. Tang, H. Zhang, X. Zhang, Y. Li, J. Wang, Y. Han, G. Li, J. Shi, X. Tian, F. Jiang, X. Zhao, J. Wang, S. Liu, C. Zeng, J. Wang, H. Yang, The M protein of SARS-CoV: basic structural and immunological properties, genomics. Proteom. Bioinform. **1**, 118–130 (2003). https://doi.org/10.1016/S1672-0229(03)01016-7
47. P.S. Masters, The molecular biology of coronaviruses. Adv. Virus Res. **66**, 193 (2006). https://doi.org/10.1016/S0065-3527(06)66005-3
48. S. Hussain, J. Pan, Y. Chen, Y. Yang, J. Xu, Y. Peng, Y. Wu, Z. Li, Y. Zhu, P. Tien, D. Guo, Identification of novel subgenomic RNAs and noncanonical transcription initiation signals of severe acute respiratory syndrome coronavirus. J. Virol. **79**, 5288–5295 (2005). https://doi.org/10.1128/JVI.79.9.5288-5295.2005/ASSET/C5613E8F-8935-4D26-82FA-4C617C92254A/ASSETS/GRAPHIC/ZJV0090561290005.JPEG
49. Y. Jiang, S. Zhang, H. Qin, S. Meng, X. Deng, H. Lin, X. Xin, Y. Liang, B. Chen, Y. Cui, Y.H. Su, P. Liang, G.Z. Zhou, H. Hu, Establishment of a quantitative RT-PCR detection of SARS-CoV-2 virus. Eur. J. Med. Res. **26**, 1–7 (2021). https://doi.org/10.1186/S40001-021-00608-5/FIGURES/4
50. H. Kuang, W. Ma, L. Xu, L. Wang, C. Xu, Nanoscale superstructures assembled by polymerase chain reaction (pcr): programmable construction, structural diversity, and emerging applications. Acc. Chem. Res. **46**, 2341–2354 (2013). https://doi.org/10.1021/AR300206M
51. S. Bustin, A. Coward, G. Sadler, L. Teare, T. Nolan, CoV2-ID, a MIQE-compliant sub-20-min 5-plex RT-PCR assay targeting SARS-CoV-2 for the diagnosis of COVID-19. Sci. Rep. **10** (2020). https://doi.org/10.1038/S41598-020-79233-X
52. L. Liv, G. Çoban, N. Nakiboğlu, T. Kocagöz, A rapid, ultrasensitive voltammetric biosensor for determining SARS-CoV-2 spike protein in real samples. Biosens. Bioelectron. **192**, 113497 (2021). https://doi.org/10.1016/j.bios.2021.113497
53. Z. Rahmati, M. Roushani, H. Hosseini, H. Choobin, Electrochemical immunosensor with Cu_2O nanocube coating for detection of SARS-CoV-2 spike protein. Microchim. Acta. **188**, 1–9 (2021). https://doi.org/10.1007/S00604-021-04762-9/TABLES/2
54. W.A. El-Said, A.S. Al-Bogami, W. Alshitari, Synthesis of gold nanoparticles@reduced porous graphene-modified ITO electrode for spectroelectrochemical detection of SARS-CoV-2 spike protein, Spectrochim. Acta Part A Mol. Biomol. Spectrosc. **264**, 120237 (2022). https://doi.org/10.1016/J.SAA.2021.120237

55. B. Mojsoska, S. Larsen, D.A. Olsen, J.S. Madsen, I. Brandslund, F. Alzahra'a Alatraktchi, Rapid SARS-CoV-2 detection using electrochemical immunosensor, (2021). https://doi.org/10.3390/s21020390
56. E.B. Aydın, M. Aydın, M.K. Sezgintürk, Highly selective and sensitive sandwich immunosensor platform modified with MUA-capped GNPs for detection of spike receptor binding domain protein: a precious marker of COVID 19 infection. Sens. Actuators B Chem. **345**, 130355 (2021). https://doi.org/10.1016/J.SNB.2021.130355
57. M.A. Ehsan, S.A. Khan, A. Rehman, Screen-Printed Graphene/Carbon Electrodes On Paper Substrates As Impedance Sensors For Detection Of Coronavirus In Nasopharyngeal Fluid Samples. Diagnostics **11**, 1030 (2021). https://doi.org/10.3390/DIAGNOSTICS11061030
58. C. Karaman, B.B. Yola, O. Karaman, N. Atar, İ Polat, M.L. Yola, Sensitive sandwich-type electrochemical SARS-CoV-2 nucleocapsid protein immunosensor. Microchim. Acta. **188**, 1–13 (2021). https://doi.org/10.1007/S00604-021-05092-6/FIGURES/6
59. S. Eissa, H.A. Alhadrami, M. Al-Mozaini, A.M. Hassan, M. Zourob, Voltammetric-based immunosensor for the detection of SARS-CoV-2 nucleocapsid antigen. Microchim. Acta. **188**, 1–10 (2021). https://doi.org/10.1007/S00604-021-04867-1/FIGURES/5
60. A. Raziq, A. Kidakova, R. Boroznjak, J. Reut, A. Öpik, V. Syritski, Development of a portable MIP-based electrochemical sensor for detection of SARS-CoV-2 antigen. Biosens. Bioelectron. **178**, 113029 (2021). https://doi.org/10.1016/j.bios.2021.113029
61. S. Ramanathan, S.C.B. Gopinath, Z.H. Ismail, M.K. Md Arshad, P. Poopalan, Aptasensing nucleocapsid protein on nanodiamond assembled gold interdigitated electrodes for impedimetric SARS-CoV-2 infectious disease assessment. Biosens. Bioelectron. **197,** 113735 (2022). https://doi.org/10.1016/J.BIOS.2021.113735
62. S. Eissa, M. Zourob, Development of a low-cost cotton-tipped electrochemical immunosensor for the detection of SARS-CoV-2. Anal. Chem. **93**, 1826–1833 (2020). https://doi.org/10.1021/ACS.ANALCHEM.0C04719
63. M. Alafeef, K. Dighe, P. Moitra, D. Pan, Rapid, ultrasensitive, and quantitative detection of SARS-CoV-2 using antisense oligonucleotides directed electrochemical biosensor chip. ACS Nano **14**, 17028–17045 (2020). https://doi.org/10.1007/S00604-021-04867-1/SUPPL_FILE/NN0C06392_SI_001.PDF
64. H. Zhao, F. Liu, W. Xie, T.C. Zhou, J. OuYang, L. Jin, H. Li, C.Y. Zhao, L. Zhang, J. Wei, Y.P. Zhang, C.P. Li, Ultrasensitive supersandwich-type electrochemical sensor for SARS-CoV-2 from the infected COVID-19 patients using a smartphone. Sens. Actuators B Chem. **327**, 128899 (2021). https://doi.org/10.1016/J.SNB.2020.128899
65. H. Zhao, Y. Zhang, Y. Chen, N.R.Y. Ho, N.R. Sundah, A. Natalia, Y. Liu, Q.H. Miow, Y. Wang, P.A. Tambyah, C.W.M. Ong, H. Shao, Accessible detection of SARS-CoV-2 through molecular nanostructures and automated microfluidics. Biosens. Bioelectron. **194**, 113629 (2021). https://doi.org/10.1016/J.BIOS.2021.113629
66. K.Y.P.S. Avelino, G.S. dos Santos, I.A.M. Frías, A.G. Silva-Junior, M.C. Pereira, M.G.R. Pitta, B.C. de Araújo, A. Errachid, M.D.L. Oliveira, C.A.S. Andrade, Nanostructured sensor platform based on organic polymer conjugated to metallic nanoparticle for the impedimetric detection of SARS-CoV-2 at various stages of viral infection. J. Pharm. Biomed. Anal. **206**, 114392 (2021). https://doi.org/10.1016/J.JPBA.2021.114392

Microfluidic Devices with Electrochemical Detection Towards Covid-19 Detection

Fabio Roberto Caetano, Marcia Gabriela Pianaro Valenga, Dhésmon Lima, Bruno C. Janegitz, Márcio F. Bergamini, and Luiz H. Marcolino-Junior

Abstract Over the decades, scientists have made efforts to enhance the performance of analytical procedures whether by creating simpler and faster assays, eliminating unnecessary/laborious steps or by improvements on hardware setup. In this context, microfluidics is the science related to manipulation and control of fluids physically constrained to submillimeter dimensions. This field emerged due to the use of microfabrication techniques for microelectronics purposes such as microchips and microcircuits. As an immediate consequence, the miniaturization of components either by creating new types of microstructures or recreating existing structures (e.g. channels, valves, storage containers, pumps, couplers,) allows the possibility of an entire laboratory in a single micro-sized device (Squires and Quake in RMP 77:977–1026, 2005 1), performing remarkable tasks in biological and chemical (Chiu et al. in Chem 2:201–223, 2017; Alam et al. in Anal Chim Acta 1044:29–65, 2018; Velve-Casquillas et al. in Nano Today 5:28–47, 2010 [2–4]) analysis. Especially for analytical chemistry, a direct consequence of the miniaturization of hardware dimensions impact on less consumption of reagents and minimum sample amount, typically nano or picoliter volumes and hence reduction of chemical waste.

Keywords Microfluidics · Electrochemical detection · COVID-19 · Sars-CoV-2 · Biosensors

F. R. Caetano · M. G. P. Valenga · D. Lima · M. F. Bergamini · L. H. Marcolino-Junior (✉)
Laboratory of Electrochemical Sensors (LabSensE), Department of Chemistry, Federal University of Paraná, 81.531-980, Curitiba, PR, Brazil
e-mail: luiz1berto@ufpr.br

B. C. Janegitz
Department of Nature Sciences, Mathematics and Education, Federal University of São Carlos, Araras, SP 13600-970, Brazil

F. N. Crespilho (ed.), *COVID-19 Metabolomics and Diagnosis*,
https://doi.org/10.1007/978-3-031-15889-6_2

1 A Brief Historic Overview: Types of Substrates, Fabrication Methods and Systems of Detection

Although the first report of microfluidic devices started at the end of the 1970s [5, 6] performing the separation of several hydrocarbons in a handheld dimension silicon wafer substrate by gas chromatography in less than ten seconds, was only in the 1990s, they received attention. Manz et. al. [7] developed a silicon-based chip (5 × 5 mm) containing an open tubular channel constructed for chemical separation by liquid chromatography and introduced the concept of micro total analysis system (μTAS), where sample pretreatment, separation and detection were performed in the same dispositive.

In this early period, the lack of progress on substrates for microfluidics can be understood for some aspects: (i) As the channel dimensions are dramatically reduced, high pressure is required to pump liquids through microchannels. Therefore, efforts on mechanical improvement of micropumps [8], microvalves [9], and system of injection [10] and integration of all components took the researchers attention. Therefore, principles of capillary electrophoresis (CE) were applied to μTAS using glass and silicon substrates. Since the separation is driven by an electric field across de entire microchannels length when a voltage is applied, the good efficiency of electroosmotic flow (EOF) pumping without the use of microvalves to control the flux was extensively explored [11, 12] (ii) studies were majority focused on the enhancement of the analytical performance of separation techniques (chromatography and CE) than in advantages such as reduction size or carrier/reagent economy (iii) the dependence of technological development since the microfluidics is one of the fields of microfabrication, which originate from microelectronics industry [13].

The introduction of polymeric materials in microfluidic devices was reported in 1993 when Fettinger et al. [14] created six unique and complementary elements made of polished plexiglass containing holes with 1 mm diameter, creating a stacked three-dimensional and rotationally independent flow system, enabling different combinations of channels and the use of flow to control injection. Since then, numerous techniques and combinations of processes have been proposed for polymer-based microfluidic devices. During the late 1990s, elastomeric substrates were introduced [15].

In this context, microfabrication is defined as a set of procedures that can be applied to obtain microstructures. Subtractive methods are those removing part of the rigid bulk substrate, (e.g. laser ablation assisted [16], plasma etching [17], soft lithography [18]) or replicative methods where the devices are built using molding techniques (e.g. hot embossing [19], microcontact printing [20], etc.).

Nowadays 3D printing method has gained attention in microfabrication. In this method, computer software uses a sequence of two-dimensional patterns creating a three-dimensional structure through the layer-by-layer deposition and hence accumulation of polymeric materials. In the last 20 years, the commercially available machinery, material, and supplies [21] become 3D printing an interesting alternative for microfabrication, even though high definition printers are not affordable.

After the 2000s, the development of substrates was marked by the appearance of low-cost materials. Paper has presented as a remarkable substrate for microfluidics due mainly to the capillary effect, which provides the spontaneous flow of solution and the ease of production, compatible with the well-established printing process, become microfluidic paper analytical devices (μPADs) a good option showing simplicity, low cost and fast production [22, 23].

In addition to paper, the use of threads in microfluidics emerged in the 2010s. Although the devices are still rudimental, threads are naturally in microchannel form constraining solution at the surface/air interface, dispensing the need for physical barriers [24, 25].

2 In a Microfluidic World, Why Does Size Matter?

When a fluid is confined in a microdimensional environment, its specific surface area increases, thus presenting divergent behavior from those at the macroscopic scale, which can be characterized by efficient mass and heat transfer, the dominance of viscous over inertial forces, and significant surface effects [26].

Reynolds number (Re), is a dimensionless number, which is used to describe the flow regime of a fluid over a given surface, predicting whether the fluid flow is laminar or turbulent [27], especially useful for transport phenomena issues (velocity of mixing and concentration of reagents, temperature, etc.) described by Eq. 1:

$$\mathrm{Re} = \frac{\rho v L}{\mu} \tag{1}$$

Here, ρ is the density, v is the average velocity of flux, L is the characteristic linear dimension of the system and μ is the dynamic viscosity. When a fluid is constrained in a relatively reduced dimension, Re is also reduced, presenting a laminar regime when Re falls below 2000 and turbulent flow is predominant when Re is above 4000. In many cases, laminar flow is preferable to turbulent behavior, because it became more predictable, allowing simplified mathematical modeling. For microfluidic systems, Re range between 10^{-3} and 10^{-5} is common, providing effective control of parameters such as the velocity of mixing, temperature, and concentration of reagents.

The mass transport phenomena in microfluidic devices are diffusion-controlled. Péclet Number (Pe, Eq. 2) gives information on mass transport behavior by the ratio between convectional and diffusional processes [28].

$$Pe = \frac{vL}{D} \tag{2}$$

Here D is the solute diffusion coefficient. In a microfluidic environment, the small value of L decreases the convection, forcing the mass transport processes to occur by

diffusion (Pe $\leq$ 1). T sensors [29, 30] filtration without membranes (H filters) [31, 32] are analytical applications of reduced Pe when the differences in solute diffusion rates play a key role.

3 Microfluidic Devices with Electrochemical Detection

Integration of detectors is a challenging topic for microfluidics. In this context, electrochemical detection is one of the most suitable options since it has remarkable features. The advances in electrode materials and geometries, and miniaturization of electronic devices allow in situ analysis. Furthermore, the wide hall of electrochemical detection techniques (e.g. potentiometry, voltammetry, electrochemical impedance spectroscopy, etc.) provided an interesting set of microfluidic electrochemical-based sensors for countless analytes such as organic, inorganic, and biological targets [33, 34] with low cost. Figure 1 presents some examples of microfluidic systems with electrochemical detection aiming to illustrate the diversity of substrates, electrodes, microchannels design, and applications these systems can offer.

As shown in examples 1E and 1F, the electrode surface can be modified to anchor biomolecules such as enzymes, antibodies, and nucleic acids. This special class of sensors, called biosensors are very attractive for microfluidics since they allow real-time analysis with high sensitivity and specificity, and only require small reagent and sample volumes [41, 42]. Also, these systems are ideal for multiplexing, enabling the detection of multiple analytes in a single chip [43], especially convenient for multiple antibodies and/or genetic content analysis for early diagnostics.

The working principle of electrochemical microfluidic biosensing devices is similar to traditional electrochemical biosensors: The small amount of sample containing the analyte flows through the microchannels and reaches the reaction chamber, where it interacts with biorecognition elements conveniently immobilized on the WE surface, generating or promoting variations in electrochemical parameters such as current [44, 45], potential [46, 47], and impedance [48, 49] (Fig. 2). Changes in analytical signal response are then monitored and can be directly associated with the presence of the molecule(s) under investigation. The electrochemical transduction system presents important advantages such as fast response, portability, and ultrahigh sensitivity, providing quick detection of analytes even in low concentrations.

Another important advantage of such detection systems is the fact that microfluidic technologies enable the development of fully automated assays, from sample preparation to analysis [41], avoiding cross-contamination and increasing feasibility. Moreover, microfluidic biosensors are suitable for industrial mass production, and the possibility of using low-cost materials and small amounts of biochemical reactants [50, 51] makes their use even more attractive. In this context, the most widely commercially available device is the glucometer which has gained unprecedented success, being a model of point-of-care testing devices [52]. Composed of test

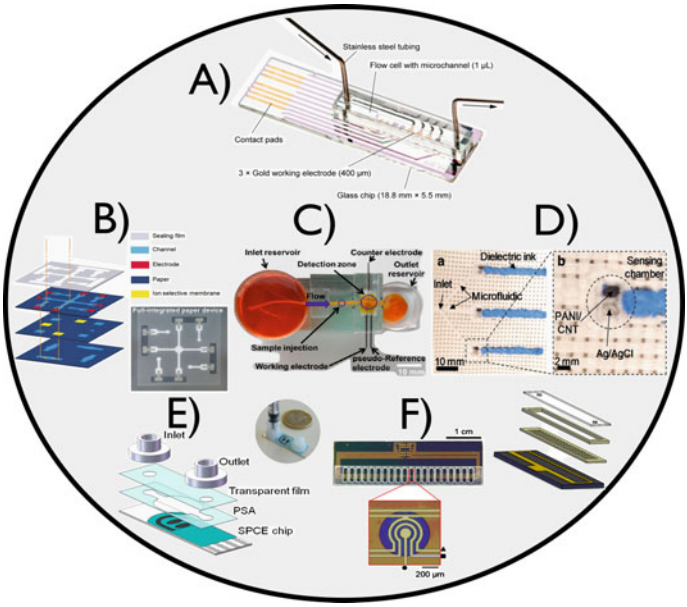

Fig. 1 Few examples of electrochemical-based microfluidic devices: **a** flow cell composed of three electrodeposited gold as working electrodes (WEs), platinum as a counter electrode (CE) and deposited onto a glass substrate, and poly(methylmethacrylate) for glyphosate detection in water samples [35]. **b** Potentiometric paper-based microfluidic electrochemical device with three different permeable membranes and Ag/AgCl printed electrodes to detect physiological ions in biological samples (Cl^-, Na^+, K^+, and Ca^{2+}) [36]. **c** Microfluidic device using cotton threads as microchannels and graphite electrodes onto glass plates substrate for simultaneous determination of acetaminophen (ACT) and diclofenac (DCF) [37]. **d** *a* Thread-based electrodes: Carbon nanotubes coated with doped poly-aniline and Ag/AgCl cotton threads sewn into a hydrophobic fabric substrate for pH measurements, *b* Zoomed-in image of threads [38]. **e** Microfluidic immuno-biochip containing carbon screen-printed electrodes, microchannels made of double-sided pressure-sensitive adhesive transparency film, and home-made syringe ports to detect tumor necrosis alpha biomarker [39]. **f** Multiplex detection of three specific bladder cancer DNA markers using 20 gold electrodes array deposited onto silicon layer and an individual sensor image with the working electrode. Microfluidic channel design consisted of three layers: The bottom was made of double-sided adhesive while the top layer thin sheet of plastic [40]. (Adapted with permission from [35], Copyright (2021), American Chemical Society; from [39] with permission of Elsevier)

strips (microfluidic channel on a disposable electrode modified with glucose oxidase enzyme) and portable potentiostat, only a few microliters of blood are necessary to perform a fast test of glucose levels, especially relevant for diabetes patients [53].

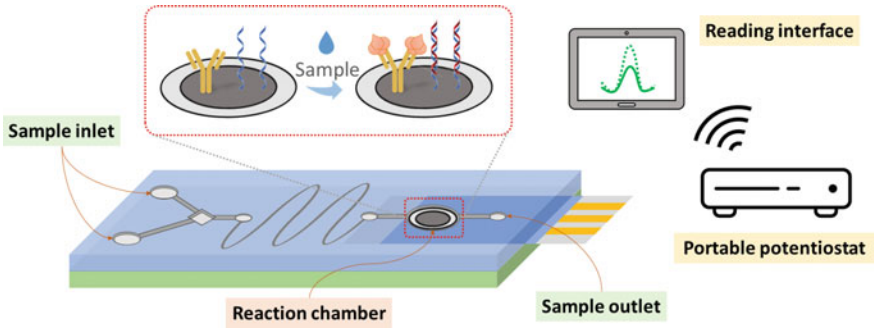

Fig. 2 General working principle of an electrochemical microfluidic biosensor

4 Electrochemical Biosensing of COVID-19 Using Microfluidics

Respiratory viral diseases are one of the most common health issues caused by a diversity of pathogens. Considering the pivotal role played by the respiratory system in the body, such types of infection can be a serious threat for patients in all age groups [54, 55]. Lower respiratory infections such as pneumonia, bronchitis, and bronchiolitis were the sixth leading cause of mortality for all ages and the leading cause for children under 5 years in 2016 [56]. These mortality rates have dramatically increased after the onset of the COVID-19 pandemic, which has been responsible for millions of infections and deaths worldwide [57]. Even after two years and the widespread use of effective vaccines, SARS-CoV-2 infections are still a significant health issue around the globe, mainly due to the high mutation rates of the novel coronavirus, which can decrease the efficiency of the immune system to prevent new infections [58].

The accurate diagnostics of COVID-19 and isolation of infected individuals are among the most efficient measures to minimize the spread of the virus and therefore control measures are still necessary for the ongoing pandemic. The main strategies currently employed to diagnose the disease rely mostly on assays to detect the presence of the viral genome or proteins in nasopharyngeal swab specimens or SARS-CoV-2-related antibodies in whole blood or serum samples. Methods such as reverse-transcription polymerase chain reaction (RT-PCR), enzyme-linked immunosorbent assay (ELISA), and immunochromatography have been widely used in clinical laboratories [59]. Despite their good detection performance, these methods present features that can significantly limit their applications and widespread commercialization. For example, RT-PCR and ELISA are time-consuming methods that require labor-intensive procedures and highly skilled personnel to be executed. In addition, the need for costly reagents (such as fluorescent probes and enzyme-labeled biomolecules) and expensive analytical and non-portable instrumentation brings additional drawbacks to the use of such techniques [60]. On the other hand, despite their miniaturized size and portability, immunochromatography-based tests such as

lateral flow immunoassays often present sensitivity and selectivity issues that may lead to expressive rates of false-positive, false-negative, or inconclusive results [61].

In this scenario, electrochemical biosensing strategies emerge as promising alternatives to provide faster, cheaper, and more reliable determinations compared to the traditional methods. The use of microfluidics can further benefit bioelectrochemical COVID-19 diagnostics since it enables the development of miniaturized, cost-effective, and portable detection systems, which are suitable for the design of point-of-care testing devices [52].

4.1 COVID-19 Diagnostic Strategies in Bioelectrochemical Microfluidics

Considering the advantages presented by microfluidic detection systems and the positive features of electrochemical transduction mechanisms, it can be stated that the integration of both technologies can potentially enable the creation of novel and more efficient platforms for COVID-19 clinical diagnostics. Recent achievements in microfluidics-based electrochemical biosensing approaches are proof of the great promise offered by such devices toward the detection of biomarkers related to the disease [42, 62–65].

As in other biosensing platforms, the detection of respiratory viruses including SARS-CoV-2 using microfluidics can be achieved through direct and indirect approaches. The direct methods are usually based on the detection of viral nucleic acids or proteins whereas indirect determinations consist in detecting biomarkers such as antibodies in patient samples. Both approaches are based on specific events such as oligonucleotide hybridization and antibody-antigen interactions taking place on the biosensing device. The use of microfluidic technology combined with electrochemical biosensing for COVID-19 diagnostics has been mainly focused on immunoassay development [45, 48, 63, 66]. However, promising approaches to the detection of genetic sequences of SARS-CoV-2 have also been reported [64, 67]. Considering the versatility of bioelectrochemical platforms, microfluidic devices developed for detecting other viral gene fragments could be easily adapted for COVID-19 detection simply by changing biorecognition probes.

Microfluidic electrochemical COVID-19 immunoassays have been designed to detect viral proteins (such as the spike (S) and nucleocapsid (N) proteins) and immunoglobulins produced in the body upon infection (IgM and IgG). When viral components are targeted in the assay, usually specific capture antibodies are immobilized on the sensing platform. On the other hand, antigens are employed as biorecognition elements when antibodies are the targets. Both approaches can be conducted through label-free or labeled detection strategies. The electrochemical response generated in direct label-free immunoassays depends solely on the interaction between antigens and antibodies on the working electrode, without the need for specific reagents and further detection procedures (Fig. 2). This approach has the

advantage of being cheaper, simple, and quicker since the detection of the target is accomplished in a single step [68]. It was recently used for the impedimetric detection of anti-S protein antibodies by using a microfluidic electrochemical bioassay [48].

Labeled bioelectrochemical assays are usually configured as sandwich assays and rely on the use of labeled reagents to generate the analytical signal. In this strategy, antigens or antibodies immobilized on the working electrode recognize and bind to their corresponding target in the first step of the assay. Afterward, the system is coated with secondary antibodies usually labeled with an enzyme, which catalyzes the oxidation of a substrate. The oxidized substrate is electroactive and can be reduced on the working electrode surface, generating current signals. Despite being more expensive and complex when compared to label-free analysis, labeled assays are usually more sensitive and less prone to cross-reactions [68]. Microfluidic biosensing devices devoted to COVID-19 diagnostics have been based on the use of secondary antibodies conjugated to horseradish peroxidase (HRP) as the labeled reagent, as is usual for electrochemical biosensors. Tetramethyl benzidine (TMB) has been employed as the enzyme–substrate, and the reduction of its oxidized form results in pronounced cathodic currents usually detected by using chronoamperometry. This strategy was recently employed in the detection of N protein [65] and related antibodies [45] in electrochemical microfluidic biodevices.

4.2 Materials and Immobilization Approaches

As is usual in the field of bioelectrochemical microfluidics, COVID-19 microfluidic biosensors have been mostly constructed on platforms based on gold [48, 65] and carbon [45, 67], which is possibly a consequence of the easier accessibility and relative affordability of such materials. The use of gold electrodes has been frequent in bioelectroanalysis as a result of their high stability and biocompatibility. Furthermore, the high affinity existing between gold and sulfur-containing biomolecules enables the obtention of highly stable and functional arrangements on the sensing surface [69]. These positive features make gold chips and electrodes a common choice for the production of microfluidic electrochemical biosensors [70–72]. Carbon-based electrodes have also been employed as effective platforms aiming for biosensing applications using microfluidics. Carbon surfaces are cost-effective and can be easily functionalized, enabling the attachment of different molecules and the immobilization of biomolecules to compose the biosensing system [73–75].

The use of nanomaterials such as graphene and metal nanoparticles has been frequent when developing microfluidics-based bioelectrochemical assays. The presence of nanostructured materials can enhance electrochemical signals and increase the sensitivity of the method, as a consequence of their high specific surface area, electrocatalytic properties, and pronounced electrical conductivity [34, 69]. Furthermore, these nanostructures can efficiently act as nanometric anchors to enable a proper immobilization of antibody or antigen molecules [69]. Graphene [66] and

reduced graphene oxide [48] were already employed as functional components in microfluidic electrochemical biosensors for COVID-19 diagnostics. The use of metal nanoparticles as signal amplifiers in microfluidic biosensors has been extensively described for the detection of several viral species [76–78]. However, the use of such nanostructured materials in microfluidic biosensing systems for SARS-Cov-2 detection is yet to be explored.

To ensure the proper functioning of the biosensing platform, the attachment of the biomolecules on the electrode must be carefully controlled. This step is crucial when developing any bioelectrochemical detection device, since important features such as sensitivity and selectivity may significantly decrease in case biomolecules are not suitable for immobilized on the platform. The immobilization of COVID-19 antibodies and antigens on microfluidic platforms has been achieved mainly by the use of classic coupling reactions with reagents such as 1-ethyl-3-(3-dimethylaminopropyl)carbodiimide (EDC) and *N*-hydroxysuccinimide (NHS) [48]. In this approach, surfaces functionalized with carboxylic groups are chemically activated to bind amine-containing biomolecules through covalent bonding (amide bond formation) [79]. Other immobilization approaches have been based on the previous functionalization of biomolecules such as antibodies and oligonucleotides with thiol groups [64, 65], in a way to enable their stable attachment to gold surfaces.

5 Detailed Approaches for Electrochemical Detection of COVID-19 Using Microfluidic Devices

The interest to use microfluidic devices for the detection of viruses is reflected by the prompt adaptability of these devices as a sensing platform soon after the pathogens first appear. In this sense, microfluidic devices for electrochemical detection of COVID-19 based on different targets and recognition sites as virus genetic material and proteins have been described.

For the sensing based on virus genetic material, Zhao et al. [64] proposed the use of a gold screen-printed electrode modified with hairpin signaling oligonucleotide sequences in a microfluidic system for direct detection of the SARS-CoV-2 S gene. In this case, the microfluidic device (Fig. 3) included a cover and a substrate layer made from poly(methylmethacrylate) (PMMA), a microchannel layer fabricated through poly(dimethylsiloxane) (PDMS) molding, and the functionalized screen-printed electrode. To reduce any carryover contamination, vacuum loaders were incorporated into the device and a miniaturized pumping system with an in-house developed interface was used to automatically load assay reagents from the inlets to on-chip reservoirs by generating negative pressure. Also, a liquid front guider composed of an array of laser-engraved pillars patterned on the roof of the reaction chamber was incorporated to spread the fluid front towards sidewalls, aiming at filling the reaction chamber.

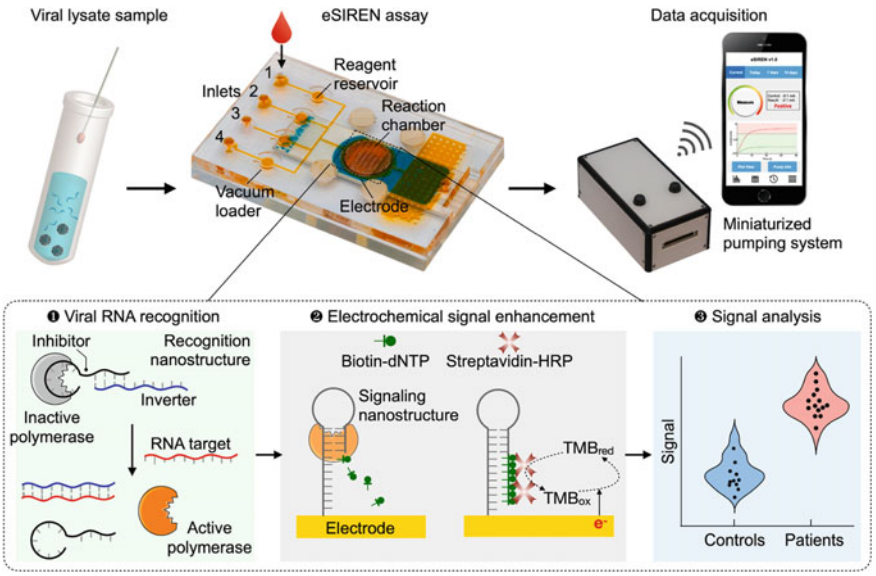

Fig. 3 Schematics of the eSIREN platform for SARS-CoV-2 detection. Reprinted from [64] with the permission of Elsevier

This platform was termed an electrochemical system integrating reconfigurable enzyme–DNA nanostructures (eSIREN) and used the DNA nanostructures to achieve three functional steps: (i) *Viral RNA recognition*: clinical lysate samples containing the target genes were mixed with a recognition structure composed of DNA strands bound to a Taq DNA polymerase. In the presence of complementary target RNA, upon target hybridization with the inverter sequence, the nanostructure dissociates and liberates polymerase activity; (ii) *Electrochemical signal enhancement*: as the active polymerase elongates a self-primed hairpin signaling nanostructure, it incorporates biotin-modified deoxynucleotide triphosphates (biotin-dNTPs) into the signaling nanostructure, thus incorporating streptavidin-conjugated HRP. The HRP incorporation enhances the response of the TMB electroactive species near the working electrode surface, increasing the electrochemical signal; (iii) *Signal analysis*: the resultant electrochemical current changes are used to measure SARS-CoV-2 RNA targets and detect infections. The current generated through the entire detection process was recorded using a miniaturized potentiostat and, for each sample, positive and negative controls were run concurrently for data normalization.

The target was determined in clinical samples of extracted RNA of nasopharyngeal swab samples and inactivated swab lysates. Sensitivity of 92.3% and specificity of 87.5% were acquired, in addition to an overall accuracy of 90.5% across 21 tested clinical samples, compared with results from gold-standard RT-qPCR assay.

Crevillen et al. [67] also proposed a genosensing microfluidic system for electrochemical detection of a SARS-CoV-2 RNA fragment. For this purpose, the device was made from a PDMS layer containing a single open channel, two reservoirs,

and a glass substrate. Two syringes were connected to the microchip inlet using a Y-connector; one contained PBS solution and the other SARS-CoV-2 RNA solution, and a dual syringe pump was used to infuse liquid at 10 μL min^{-1}. A 200 μL plastic electrochemical cell was inserted into the microchip outlet and 3D pen-printed electrodes (3D-PP) were immersed in it. Those were printed using a 3D printing pen and a conductive graphene/polylactic acid filament, and chemically and electrochemically activated by, respectively, immersion in 1 mol L^{-1} NaOH solution for 30 min and cyclic voltammetry (50 cycles, from 0 to +2.0 V, scan rate of 1 V s^{-1}) in PBS solution. The working electrode was placed right at the exit of the microchip channel, inside the outlet reservoir. Previously, single-stranded DNA (ssDNA) probe (antisense oligonucleotide) was physically adsorbed over this electrode surface, to obtain the genosensor.

The measurement protocol consisted of (i) *incubation step*: the sample was pumped from the inlet for 5 min. If the sample contained the SARS-CoV-2 target RNA, it hybridizes with ssDNA probe, leading to desorption by its adduction from the surface of the 3D-PP electrode; (ii) *cleaning step*: PBS solution was pumped from the inlet for 2 min, and *iii) detection step:* differential pulse voltammetry (DPV) analysis was performed and the signal generated by the oxidation of adenines present in ssDNA was monitored. If no hybridization occurred, a larger peak area was obtained, compared to the peak area after hybridization of the probe with the target.

By that, the device was able to discriminate the signal of SARS-CoV-2 RNA from the blank in 7 min. Also, the authors used a similar approach of working electrode construction and applied it in a three-electrode conventional cell to assess some analytical parameters. In this case, a linear working range from 10 to 500 nmol L^{-1} and a 15 nmol L^{-1} limit of detection were demonstrated. In addition, a response similar to the blank was obtained for a non-complementary target sequence, indicating the method selectivity.

In the scenario of using viral proteins and antibodies, current assays for the detection of SARS-CoV-2 infections are based on spike (S) and/or nucleocapsid (N) proteins. Based on that, Li et al. [65] constructed a microfluidic immunosensor for the detection of the virus N protein in serum. For that, capture antibodies (cAb) were immobilized on screen-printed gold electrodes (SPGE), which were then integrated with a microfluidic chip. Two sensing platforms were proposed for the use of a potentiostat connected to either a desktop PC or a smartphone. Both devices were fabricated from a polyethylene terephthalate (PET) film stacked with a PMMA cartridge, with the incorporation of microchannels, inlets, and outlets in the layers using a CO_2 laser cutter. For the desktop platform, the chip consisted of a reaction chamber encompassing the immunosensor connected to the inlet and outlet (Fig. 4a). For the smartphone-based device, a reaction chamber connected to a waste reservoir was designed (Fig. 4b).

Dually-labeled magnetic nanobeads (DMB) were prepared and modified with HRP and detection antibody (dAb), and then mixed with serum spiked with SARS-CoV-2 N protein or clinical serum samples: if the samples contained the target antigen, is bound to the DMB forming an immunocomplex. The mixture was added to the platform, using a syringe pump for the desktop platform or a capillary tube and

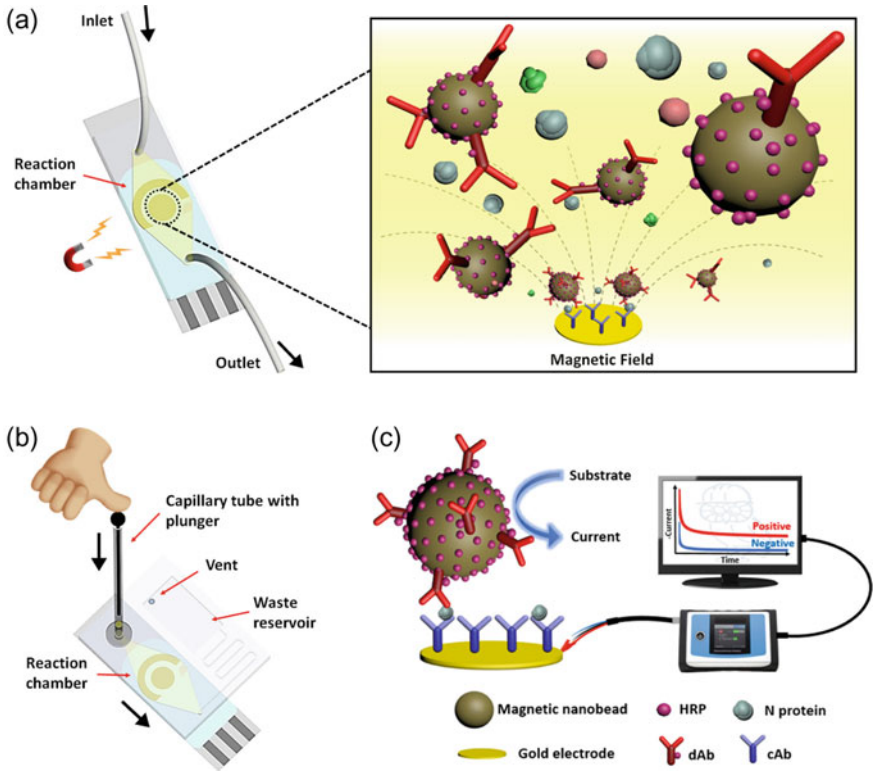

Fig. 4 Schematic illustrations of **A** microfluidic immunosensor chip for PC desktop-based device, highlighting the magnetic concentration of DMB to the sensor surface, **b** microfluidic immunosensor chip for the smartphone-based diagnostic device, and **c** electrochemical sensing scheme using the PC desktop-based platform. Reprinted with permission from [65], Copyright (2021), American Chemical Society

plunger for the smartphone-based device, and the chip was placed on a neodymium magnet for 1 min to concentrate the DMB on the working electrode (WE), where DMB-antigen bound to the immobilized cAb. Then it was incubated in the dark for 50 min or 25 min, for whole serum samples or five-times diluted samples, respectively. A washing buffer (PBS + 0.05% Tween-20) was flushed through the chip, followed by TMB flushing. After 2 min, chronoamperometric measurements were performed by applying a −0.2 V potential for 100 s. The HRP-coated DMB catalyzes the reduction of TMB, which generates an amperometric current that is proportional to the concentration of the target antigen attached to the sensor surface (Fig. 4c).

For both desktop and smartphone-based devices, a linear working range was established ranging from 0 to 10 ng mL^{-1}, and for the smartphone-based device limits of detection (LOD) of 230 and 100 pg mL^{-1} were obtained for the whole sample serum and five-times diluted samples, respectively. The sensor was selective to SARS-CoV-2 N protein when the current response was compared to the response

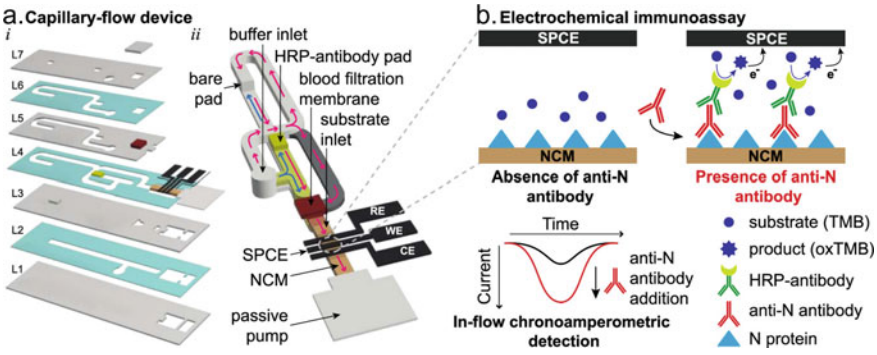

Fig. 5 Schematic view **a** and detection mechanism **b** of the electrochemical capillary-flow immunoassay. Reprinted with permission from [45], Copyright (2021), American Chemical Society

of samples spiked with RBD, SARS-Cov N protein, and MERS-CoV N protein. In addition, the microfluidic magneto immunosensor could differentiate the response of positive and negative samples, confirmed by RT-PCR assay.

Samper et al. [45] described an electrochemical capillary-flow immunoassay for detecting anti-SARS-CoV-2 N protein antibodies in blood samples. The device was fabricated by stacking four layers of hydrophilic polyester film intercalated with layers of double-tape adhesive; on each layer, channels, inlets, outlets, and vent holes were cut with a CO_2 laser cutter to create the design presented in Fig. 5a. The design of the device also included a blood-filtration membrane, to retain blood cells and deliver plasma to the microfluidic channel, and a separated channel for plasma flow, so the other reagents did not have to pass through the blood-filtration membrane. A nitrocellulose membrane (NCM) striped with N protein was inserted into the platform, and a waste pad was placed over the end of the NCM to create a passive pump for the fluidic system. The authors prepared SPCE using a stencil-printing method over the polyester film and the electrode was placed on top of NCM, upside-down so that the WE was in contact with the N protein strip.

For device operation, the blood sample was added to the blood-filtration membrane, and washing buffer (PBS–Tween80) was added to the buffer inlet. If the sample contained anti-N antibodies, they bound to the immobilized N proteins. Then HRP-antibody was released and delivered to the NCM, bounding to anti-N antibodies. The excess HRP-antibody was washed off automatically by the washing buffer and then TMB was added to the substrate inlet on the NCM. Once the buffer had started to flow through the NCM, a 0.0 V potential was applied to the WE and chronoamperometry recording started. In the presence of HRP in the detection zone, TMB gets oxidized and its product is then reduced at the electrode surface, generating an increase in the cathodic current, used for sensing purposes (Fig. 5b).

Under flow conditions, delivery of TMB to the detection zone produced a transient increase in the cathodic current that correlated to the concentration of anti-N antibody in the sample; from concentrations ranging from 0 to 100 ng mL^{-1}, a 4PL model was established to correlate target concentration and current delta. In addition, the

electrochemical capillary-flow device was coupled to a potentiostat operated by a smartphone, and this portable system was used to detect anti-N antibodies. Blank and spiked PBS-based samples were run in the device and the discrimination between positive and negative responses was achieved.

For the use of spike (S) proteins for SARS-CoV-2 detection, Ali et al. [48] proposed a biosensing platform created by 3D nanoprinting of three-dimensional electrodes, coated by nanoflakes of reduced graphene oxide (RGO) in which specific viral antigens were immobilized. The electrode was integrated with a microfluidic device and used for the detection of antibodies to SARS-CoV-2 spike S1 protein and its receptor-binding-domain (RBD) via impedance spectroscopy. The COVID-19 test chip was manufactured using a glass substrate with a gold film forming the base for WE, counter electrode (CE), and reference electrode (RE). An Aerosol Jet nanoparticle 3D printing was employed to convert gold ink into an aerosol and then used to form micropillars over the WE. Next, a PDMS housing containing a microfluidic channel was fabricated using replica molding, and the test chip was formed by placing the PDMS housing with the microfluidic channel on the glass substrate with the micropillar electrodes. Before this step, the micropillar electrodes were functionalized with RGO and SARS-CoV-2 spike S1 or RBD antigens.

The electrochemical transduction was performed by impedance spectroscopy, using electrolyte phosphate buffer saline solution mixed with ferro/ferricyanide. When the fluid containing antibodies to the viral antigens was introduced in the microfluidic chamber, the target antibodies bound to the corresponding antigens on the electrode, which increased the charge transfer resistance (R_{ct}). This strategy enabled detection concentrations as low as 2.8×10^{-15} mol L^{-1} and 16.9×10^{-15} mol L^{-1} of anti S1 antibodies and anti-RBD antibodies, respectively. The authors also described the possibility of regenerating the electrode, by eluting the antibodies with a 1.0 mol L^{-1} formic acid solution (pH = 2.5) flow in the device for 60 s, with the possibility of reusing the device ten times without significant losses in sensitivity and detection capacity.

An electrochemical approach for the determination of SARS-CoV-2 antibodies has been described by Ko et al. [63] based on microfluidic separation of capture from detection. The device (Fig. 6) was fabricated from a polymer substrate with laminated microfluidics and included three inlets (A, B, and C), two outlets (W1 and W2), and a capture region and reaction chamber (M). A three-electrode sensor chip prepared by sputtering gold through a mask onto polycarbonate was also incorporated into the platform. A Y-junction was included to direct the sample and the TMB either to the waste (W1) or over the sensor.

The device was applied to the detection of COVID-19 IgG antibodies. For that, initially, the W1 outlet was opened while the W2 outlet was closed, and carboxylate beads conjugated with RBD protein were introduced through inlet A for immobilization within the reaction chamber. Then diluted plasma samples were introduced through inlet A, and incubated for 20 s over the magnetic beads followed by washing with PBST. Captured AntiS from the sample was labeled by the addition of mouse anti-Human IgG secondary Antibody-HRP, followed by PBST washing. TMB solution was introduced through inlet C and incubated for 5 min over the beads; in the

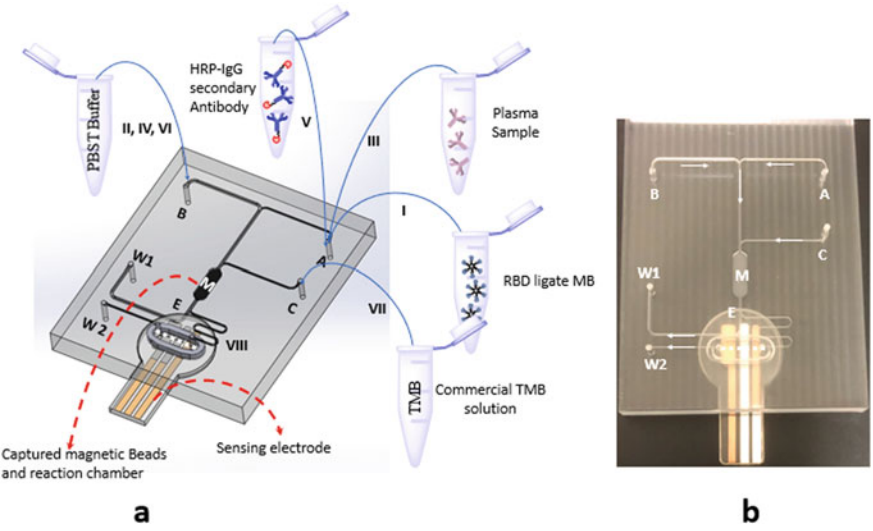

Fig. 6 Schematic (**a**) and picture (**b**) of the chip used to demonstrate the separation of capture from detection to SARS-CoV-2 antibodies. Reprinted from [63] with the permission of Elsevier

presence of HRP, TMB is oxidized. After that, W2 outlet is opened and oxidized TMB species flow is diverted over the sensor electrode, in which its reduction is measured by applying a −0.2 V potential.

The approach allowed capture, washing, reacting, and incubation of the sample in a reaction chamber within the microfluidics, without the possibility of contaminating the sensors electrodes prior to measurement. Also, the independent inlet for TMB eliminates its interaction with non-specifically bound HRP complexes and thus false positive responses. Using this proposal, electrochemical detection of COVID-19 patient samples and controls (commercially supplied ELISA) was performed and results showed a clear discrimination between positive and negative samples.

Conclusion and perspectives

Manipulation in microscale has proved to be an interesting choice for analytical tasks. In this chapter, a brief historical overview focusing on substrates and physical properties such as flow behavior in microfluidics have been summarized and discussed, with a special focus on the electrochemical biosensing of COVID-19-related biomarkers. Among the set of possible detection techniques, the combination of factors such as facile miniaturization and compatibility over a wide range of substrates provided by a variety of electrode materials and geometries, several modalities of signal responses and relatively low cost make electrochemical detection as a suitable technique for sensors and biosensors based on microfluidic systems.

A wide range of different substrate materials, electrode modifiers, and detection approaches can enable the creation of highly sensitive and robust detection devices to support COVID-19 diagnostics. Microfluidics-based electrochemical biosensing

offers a great promise that can considerably improve currently used detection strategies for SARS-CoV-2 infections. The use of these miniaturized, ultra-sensitive, and selective devices can consist in a valuable strategy to support all efforts made worldwide to control the ongoing pandemic.

Due to the recent discovery of SARS-CoV-2 infection in humans, resulting in emergence of Covid-19, the need for further detailed fundamental studies in molecular biology, genomics and proteomics are crucial for development of new sensitive and selective microfluidics devices combining different strategies of detection.

Acknowledgements The authors thank the financial support from Fundação de Amparo à Pesquisa do Estado de São Paulo (FAPESP) (2013/22127-2), Conselho Nacional de Desenvolvimento Científico e Tecnológico (CNPq) (303338/2019-9; 408309/2018-0; 311290/2020-5, 309803/2020-9 and 402195/2020-5), Fundação Araucária (PBA2022011000056) and Coordenação de Aperfeiçoamento de Pessoal de Nível Superior (CAPES) – Finance Code 001 and Epidemias 88887.504861/2020-0.

References

1. T.M. Squires, S.R. Quake, Microfluidics: fluid physics at the nanoliter scale. RMP **77**, 977–1026 (2005)
2. D.T. Chiu, A.J. de Mello, D. di Carlo et al., Small but perfectly formed? Successes, challenges, and opportunities for microfluidics in the chemical and biological sciences. Chem. **2**, 201–223 (2017)
3. M.K. Alam, E. Koomson, H. Zou et al., Recent advances in microfluidic technology for manipulation and analysis of biological cells (2007–2017). Anal. Chim. Acta **1044**, 29–65 (2018)
4. G. Velve-Casquillas, M. le Berre, M. Piel, P.T. Tran, Microfluidic tools for cell biological research. Nano Today **5**, 28–47 (2010)
5. S.C. Terry, J.H. Jerman, J.B. Angell, A gas chromatographic air analyzer fabricated on a silicon wafer. IEEE Trans. Electron Devices **26**, 1880–1886 (1979)
6. D.J. Harrison, A. Manz, Z. Fan et al., Capillary electrophoresis and sample injection systems integrated on a planar glass chip. Anal. Chem. **64**, 1926–1932 (1992)
7. A. Manz, D. Jed Harrison, J.E.M. Verpoorte et al., Planar chips technology for miniaturization and integration of separation techniques into monitoring systems—capillary electrophoresis on a chip. J. Chromatogr. **593**, 253–258 (1992)
8. M. Esashi, Integrated micro flow control systems. Sens. Actuators A21-A23, 161–167 (1990)
9. J. Ruzicka, E.H. Hansen, Integrated microconduits for flow injection analysis. Anal. Chim. Acta **161**, 1–25 (1984)
10. A.R. Razali, Y. Qin, A review on micro-manufacturing, micro-forming and their key issues. Procedia Eng. **53**, 665–672 (2013)
11. S. Shoki, M. Esashi, T. Matsuo, Prototype miniature blood gas analyser fabricated on a silicon wafer. Sens. Actuators **14**, 101–107 (1988)
12. H.T.G. van Lintel, F.C.M. van de Pol, S. Bouwstra, A piezoelectric micropump based on micromachining silicon. Sens. Actuators **15**, 153–167 (1988)
13. P. Papakonstantinou, N.A. Vainos, C. Fotakis, Microfabrication by UV femtosecond laser ablation of Pt, Cr and indium oxide thin films. Appl. Surf. Sci. 151:159–170
14. J.C. Fettinger, A. Manz, H. Ludi, H.M. Widmer, Stacked modules for micro flow systems in chemical analysis: concept and studies using an enlarged model. Sens. Actuators B **17**, 19–25 (1993)

15. E. Kim, Y. Xia, G.M. Whitesides, Polymer microstructures formed by moulding in capillaries. Nature **376**, 581–584 (1995)
16. M.A. Roberts, J.S. Rossier, P. Bercier et al., UV laser machined polymer substrates for the development of microdiagnostic systems. Anal. Chem. **69**, 2035–2042 (1997)
17. S.M. Ford, J. Davies, B. Kar et al., Micromachining in plastics using X-ray lithography for the fabrication of micro-electrophoresis devices. J. Biomech. Eng. **121**, 13–21 (1999)
18. P. Kim, K.W. Kwon, M.C. Park et al., Soft litography for microfluidics: a review. Biochip J. **2**, 1–11 (2008)
19. H. Becker, U. Heim, Hot embossing as a method for the fabrication of polymer high aspect ratio structures. Sens. Actuators A **83**, 130–135 (2000)
20. A. Kumar, H.A. Biebuyck, G.M. Whitesides, Patterning self-assembled monolayers: applications in materials science. Langmuir **10**, 1498–1511 (1994)
21. A.A. Yazdi, A. Popma, W. Wong et al, 3D printing: an emerging tool for novel microfluidics and lab-on-a-chip applications. Microfluid Nanofluid **20**, 50 (2016)
22. C. Parolo, A. Merkoçi, Paper-based nanobiosensors for diagnostics. Chem. Soc. Rev. **42**, 450–457 (2013)
23. R.S.P. Malon, L.Y. Heng, E.P. Córcoles, Recent developments in microfluidic paper-, cloth-, and thread-based electrochemical devices for analytical chemistry. Rev. Anal. Chem. **36**, 1–19 (2017)
24. D. Agustini, F.R. Caetano, R.F. Quero et al., Microfluidic devices based on textile threads for analytical applications: State of the art and prospects. Anal. Methods **13**, 4830–4857 (2021)
25. J. Berthier, K.A. Brakke, D. Gosselin et al., Thread-based microfluidics: flow patterns in homogeneous and heterogeneous microfiber bundles. Med. Eng. Phys. **48**, 55–61 (2017)
26. L. Shang, Y. Cheng, Y. Zhao, Emerging droplet microfluidics. Chem. Rev. **117**, 7964–8040 (2017)
27. O. Reynolds, An experimental investigation of the circumstances which determine whether the motion of water shall be direct or sinuous, and of the law of resistance in parallel channels. Philos. Trans. R. Soc. 935–981 (1883)
28. S.V. Von, *Numerical heat transfer and fluid flow* (McGraw Hill Book Company, New York, 1980)
29. A.E. Kamholz, B.H. Weigl, B.A. Finlayson, P. Yager, Quantitative analysis of molecular interaction in a microfluidic channel: the T-sensor. Anal. Chem. **71**, 5340–5347 (1999)
30. B.H. Weigl, P. Yager, Microfluidic diffusion-based separation and detection. Science **283**, 346–347 (1999)
31. J.P. Brody, P. Yager, Diffusion-based extraction in a microfabricated device. Sens. Actuators A **58**, 13–18 (1997)
32. J.P. Brody, P. Yager, R.E. Goldstein, R.H. Austin, Biotechnology at low Reynolds numbers. Biophys. J. **71**, 3430–3441 (1996)
33. J. Kudr, O. Zitka, M. Klimanek et al., Microfluidic electrochemical devices for pollution analysis—a review. Sens. Actuators B **246**, 578–590 (2017)
34. Z. Fattahi, M. Hasanzadeh, Nanotechnology-assisted microfluidic systems for chemical sensing, biosensing, and bioanalysis. TrAC **152**, 116637 (2022)
35. B. Uka, J. Kieninger, G.A. Urban, A. Weltin, Electrochemical microsensor for microfluidic glyphosate monitoring in water using MIP-based concentrators. ACS Sens. **6**, 2738–2746 (2021)
36. J.H. Jin, J.H. Kim, S.K. Lee et al., A fully integrated paper-microfluidic electrochemical device for simultaneous analysis of physiologic blood ions. Sensors **18**, 104 (2018)
37. D. Agustini, M.F. Bergamini, L.H. Marcolino-Junior, Low cost microfluidic device based on cotton threads for electroanalytical application. Lab Chip **16**, 345–352 (2016)
38. P. Mostafalu, M. Akbari, K.A. Alberti, et al., A toolkit of thread-based microfluidics, sensors, and electronics for 3D tissue embedding for medical diagnostics. Microsyst. Nanoeng. **2**, 16039 (2016)
39. U. Eletxigerra, J. Martinez-Perdiguero, S. Merino, Disposable microfluidic immuno-biochip for rapid electrochemical detection of tumor necrosis factor alpha biomarker. Sens. Actuators B **221**, 1406–1411 (2015)

40. J.P. Pursey, Y. Chen, E. Stulz et al., Microfluidic electrochemical multiplex detection of bladder cancer DNA markers. Sens. Actuators B **251**, 34–39 (2017)
41. E.A. Tarim, B. Karakuzu, C. Oksuz et al., Microfluidic-based virus detection methods for respiratory diseases. Emergent Mater. **4**, 143–168 (2021)
42. Y. Song, B. Lin, T. Tian et al., Recent progress in microfluidics-based biosensing. Anal. Chem. **91**, 388–404 (2019)
43. A. Parihar, P. Ranjan, S.K. Sanghi et al., Point-of-care biosensor-based diagnosis of COVID-19 holds promise to combat current and future pandemics. ACS Appl. Bio Mater. **3**, 7326–7343 (2020)
44. R. Bruch, J. Baaske, C. Chatelle, et al., CRISPR/Cas13a-powered electrochemical microfluidic biosensor for nucleic acid amplification-free miRNA diagnostics. Adv. Mater. **31**, 1905311 (2019)
45. I.C. Samper, A. Sánchez-Cano, W. Khamcharoen et al., Electrochemical capillary-flow immunoassay for detecting anti-SARS-CoV-2 nucleocapsid protein antibodies at the point of care. ACS Sens. **6**, 4067–4075 (2021)
46. R. Vinoth, T. Nakagawa, J. Mathiyarasu, A.M.V. Mohan, Fully printed wearable microfluidic devices for high-throughput sweat sampling and multiplexed electrochemical analysis. ACS Sens. **6**, 1174–1186 (2021)
47. T. Ozer, C.S. Henry, Microfluidic-based ion-selective thermoplastic electrode array for point-of-care detection of potassium and sodium ions. Microchim. Acta **189**, 152 (2022)
48. A. Ali, C. Hu, S. Jahan, et al., Sensing of COVID-19 antibodies in seconds via aerosol jet nanoprinted reduced-graphene-oxide-coated 3D electrodes. Adv. Mater. **33**, 2006647 (2021)
49. A.K. Bavil, D. Sticker, M. Rothbauer et al., A microfluidic microparticle-labeled impedance sensor array for enhancing immunoassay sensitivity. Analyst **146**, 3289–3298 (2021)
50. J.F.C. Loo, A.H.P. Ho, A.P.F. Turner, W.C. Mak, Integrated printed microfluidic biosensors. Trends Biotechnol. **37**, 1104–1120 (2019)
51. Y. Xie, L. Dai, Y. Yang, Microfluidic technology and its application in the point-of-care testing field. Biosens. Bioelectron. X **10**, 100109 (2022)
52. D.G. Rackus, M.H. Shamsi, A.R. Wheeler, Electrochemistry, biosensors and microfluidics: a convergence of fields. Chem. Soc. Rev. **44**, 5320–5340 (2015)
53. P.L. Edmiston, T.R. Williams, An analytical laboratory experiment in error analysis: repeated determination of glucose using commercial glucometers. J. Chem. Ed. **77**, 377–379 (2000)
54. H.F. Boncristiani, M.F. Criado, E. Arruda, *Respiratory Viruses* (Elsevier, Viruses, 2009)
55. N.H.L. Leung, Transmissibility and transmission of respiratory viruses. Nat. Rev. Microbiol. **19**, 528–545 (2021)
56. C. Troeger, B. Blacker, I.A. Khalil et al., Estimates of the global, regional, and national morbidity, mortality, and aetiologies of lower respiratory infections in 195 countries, 1990–2016: a systematic analysis for the global burden of disease study 2016. Lancet Infect. Dis. **18**, 1191–1210 (2018)
57. Our World in Data, COVID-19 data explorer. Available at: https://ourworldindata.org/explorers/coronavirus-data-explorer?time=2020-03-01..latest&facet=none&uniformYAxis=0&pickerSort=asc+&pickerMetric=location&Metric=Confirmed+cases&Interval=Cumulative&Relative+to+Population=false&Color+by+test+positivity=false&country=~OWID_WRL. Access: 2nd April 2022 (2022)
58. W.T. Harvey, A.M. Carabelli, B. Jackson et al., SARS-CoV-2 variants, spike mutations and immune escape. Nat. Rev. Microbiol. **19**, 409–424 (2021)
59. L.J. Carter, L.V. Garner, J.W. Smoot et al., Assay techniques and test development for COVID-19 diagnosis. ACS Cent. Sci. **6**, 591–605 (2020)
60. J.A. Berkenbrock, R. Grecco-Machado, S. Achenbach, Microfluidic devices for the detection of viruses: aspects of emergency fabrication during the COVID-19 pandemic and other outbreaks. Proc. R. Soc. A 476 (2020)
61. Y. Liu, L. Zhan, Z. Qin et al., Ultrasensitive and highly specific lateral flow assays for point-of-care diagnosis. ACS Nano **15**, 3593–3611 (2021)

62. L.M. Schmidt-Speicher, K. Länge, Microfluidic integration for electrochemical biosensor applications. Curr. Opin. Electrochem. **29**, 100755 (2021)
63. D.H. Ko, A. Hosseini, H. Karaosmanoglu, et al., Microfluidic separation of capture from detection and its application for determination of COVID-19 antibodies. Sens. Actuators B **351**, 130918 (2022)
64. H. Zhao, Y. Zhang, Y. Chen, et al., Accessible detection of SARS-CoV-2 through molecular nanostructures and automated microfluidics. Biosens. Bioelectron. **194**, 113629 (2021)
65. J. Li, P.B. Lillehoj, Microfluidic magneto immunosensor for rapid, high sensitivity measurements of SARS-CoV-2 nucleocapsid protein in serum. ACS Sens. **6**, 1270–1278 (2021)
66. Y. Li, Z. Peng, N.J. Holl et al., MXene-graphene field-effect transistor sensing of influenza virus and SARS-CoV-2. ACS Omega **6**, 6643–6653 (2021)
67. A.G. Crevillen, C.C. Mayorga-Martinez, J.V. Vaghasiya, M. Pumera, 3D-printed SARS-CoV-2 RNA genosensing microfluidic system. Adv. Mater. Technol. 2101121 (2022)
68. A. Koyappayil, M.H. Lee, Ultrasensitive materials for electrochemical biosensor labels. Sensors **21**, 1–19 (2021)
69. D. Lima, A.C.M. Hacke, B. Ulmer, S. Kuss, Electrochemical sensing of trypanosome- and flavivirus-related neglected tropical diseases. Curr. Opin. Electrochem. **30**, 100838 (2021)
70. J. Aleman, T. Kilic, L.S. Mille et al., Microfluidic integration of regeneratable electrochemical affinity-based biosensors for continual monitoring of organ-on-a-chip devices. Nat. Protoc. **16**, 2564–2593 (2021)
71. J.A. Hondred, Z.T. Johnson, J.C. Claussen, Nanoporous gold peel-and-stick biosensors created with etching inkjet maskless lithography for electrochemical pesticide monitoring with microfluidics. J. Mat. Chem. C **8**, 11376–11388 (2020)
72. A.C. Soares, J.C. Soares, V.C. Rodrigues et al., Microfluidic-based genosensor to detect human papillomavirus (HPV16) for head and neck cancer. ACS App. Mater. Interfaces **10**, 36757–36763 (2018)
73. F.R. Caetano, E.A. Carneiro, D. Agustini et al., Combination of electrochemical biosensor and textile threads: a microfluidic device for phenol determination in tap water. Biosens. Bioelectron. **99**, 382–388 (2018)
74. C. Kalinke, V. Wosgrau, P.R. Oliveira et al., Green method for glucose determination using microfluidic device with a non-enzymatic sensor based on nickel oxyhydroxide supported at activated biochar. Talanta **200**, 518–525 (2019)
75. S. Boonkaew, A. Yakoh, N. Chuaypen, et al., An automated fast-flow/delayed paper-based platform for the simultaneous electrochemical detection of hepatitis B virus and hepatitis C virus core antigen. Biosens. Bioelectron. **193**, 113543 (2021)
76. T.A. Freitas, C.A. Proença, T.A. Baldo, et al., Ultrasensitive immunoassay for detection of citrus tristeza virus in citrus sample using disposable microfluidic electrochemical device. Talanta **205**, 120110 (2019)
77. R. Chand, S. Neethirajan, Microfluidic platform integrated with graphene-gold nano-composite aptasensor for one-step detection of norovirus. Biosens. Bioelectron. **98**, 47–53 (2017)
78. M. Regiart, A.M. Gimenez, A.T. Lopes et al., Ultrasensitive microfluidic electrochemical immunosensor based on electrodeposited nanoporous gold for SOX-2 determination. Anal. Chim. Acta **1127**, 122–130 (2020)
79. C. Wang, Q. Yan, H.B. Liu et al., Different EDC/NHS activation mechanisms between PAA and PMAA brushes and the following amidation reactions. Langmuir **27**, 12058–12068 (2011)

Carbon-Based Materials for Electrochemical Sensing of SARS-CoV-2

Paulo Roberto de Oliveira, Cristiane Kalinke, Juliano Alves Bonacin, Luiz Humberto Marcolino-Junior, Márcio Fernando Bergamini, and Bruno Campos Janegitz

Abstract One of the most important aspects of the development of an electrochemical biosensor is the choice of materials used in the manufacturing process. This statement is based, not only on the use of the material with a good ability to conduct electrons but also on the use of a material that provides a good linkage between the electron transducer and the biological material. In this meaning, carbon-based conductive materials have been widely used in the development of electrochemical bioassays. This is because these materials present high electrical conductivity, low current background, stability, low cost, and mainly the potentiality the use as a material biological host system, after the association with enzymes, antibodies, DNA, and RNA fragments, among others. In this respect, electrochemical biosensors have played an important role in disease diagnosis, especially in the last few years for the sensing of SARS-CoV-2. Carbon-based materials can be classified according to their dimensionalities and structures, which can influence their properties (Li and Mu in Appl Energy 242:695–715, 2019 1). In addition, surface treatments have been widely used for the activation or functionalization of carbon-based materials, which can improve sensor immobilization. Thus, the properties, treatments, and applications of carbon-based materials for the fabrication of biosensors for the detection of SARS-CoV-2 will be addressed and discussed in this chapter.

Keywords Biosensing · COVID-19 · Carbon-based materials · Biocompability · Versatility

P. R. de Oliveira · B. C. Janegitz (✉)
Laboratory of Sensors, Nanomedicine, and Nanostructured Materials, Federal University of São Carlos (UFSCar), Araras, São Paulo 13600-970, Brazil
e-mail: brunocj@ufscar.br

C. Kalinke · J. A. Bonacin
Institute of Chemistry, University of Campinas (Unicamp), Campinas, São Paulo 13083-859, Brazil

L. H. Marcolino-Junior · M. F. Bergamini
Laboratory of Electrochemical Sensors (LabSensE), Department of Chemistry, Federal University of Paraná (UFPR), Curitiba, Paraná 81531-980, Brazil

F. N. Crespilho (ed.), *COVID-19 Metabolomics and Diagnosis*,
https://doi.org/10.1007/978-3-031-15889-6_3

1 Introduction

From the electrochemical point of view, the use of conductive carbonaceous materials for bioanalysis, firstly and evidently, is based on the high electrical conductivity, which allows the electron transduction and the current monitoring [2–4]. This property is attributed to the sp^2 hybridization of the carbon atoms for almost all carbon conductive materials, which generate covalent bonds in a two-dimensional hexagonal chain [5, 6]. This structure allows electrons to migrate along the carbon chain, which makes it possible to monitor the electrochemical reactions generated on the materials surface.

Otherwise, there are other interesting physical and chemical properties that deserve to be highlighted. Carbon-based materials have also high thermal conductivity, mechanical strength (except for some materials, such as graphite), chemical inertia, good stability, durability, as well as low cost, and abundance, which made these materials excellent alternatives to the use of metals in several areas, such as in the electrochemistry [7–9].

Beyond the electrical conductivity, biocompatibility is one of the main and most attractive properties of carbon-based materials for the development of biosensors aiming the diagnosis of diseases, such as those caused by virus [10–12]. Biocompatibility is understood as the complex characteristic attributed to a determinate biological system that is dependent on the interactions between the electrochemical system/material and the biological specie [4]. Therefore, the use of carbon materials with chemical inertness, low toxicity, presence of pores, or a compatible shape with the desired biomaterial to be incorporated is interesting for the construction of biosensors [13, 14]. These characteristics are observed mainly due to their chemical composition based on carbon and hydrogen, with the possibility of smaller amounts of oxygen and nitrogen, among other low toxic compounds [14, 15].

Some desirable characteristics of biosensors, such as good conductivity, high sensitivity, and active or immobilization sites can be achieved or improved by the surface modification of the electrode. This normally is performed by drop-casting of several materials, such as core–shell nanocomposites [16], magnetic and metal nanoparticles [17–20], carbon nanodots [21, 22], carbon nanotubes [23, 24], graphene [25–30], and other carbon nanostructures. As seen, the anchoring of nanomaterials can be promising for the improvement of selectivity and sensing of biosensors, which is due to their high surface area, electron transfer, and stability [31, 32]. Carbon-based nanomaterials such as single- or multi-walled carbon nanotubes [1], carbon black [33], graphene [34], and carbon dots or nanodots [35] can be highlighted for this approach, which is due to their biocompatibility, and easy immobilization ability by the presence of functional groups and other active sites.

For the development of biosensors, the number of interactions between the biological material and the electrode surface can influence the events of signal generation. In the other words, in electrochemical bioanalysis, nanomaterials with a higher overall surface area should be considered [36]. For example, the level of the linkage between SARS-CoV-2 RNA fragments and different carbon-based nanomaterials can

be correlated (Fig. 1). In this case, different kinds of fullerenes, carbon nanotubes, and graphene were evaluated regarding the total potential energy interaction affinity with RNA fragments, by van der Waals forces and electrostatic bond energies. By computational analysis, the authors identified variations in the total energy interactions between the carbon materials and the RNA fragment. However, the potential energy from electrostatic interactions presented the greatest contribution to the detriment of van der Waals interactions. Knowing that all carbon nanomaterials have the same chemical composition, two important factors must be considered here. First, carbon nanomaterials are charge neutral materials, and the RNA fragments are positively charged; thus, the most significant interaction consists of the ion-induced dipole force. The second one is that the increase in the overall surface area of the carbon materials led to a higher value of total potential energy interaction, which is explained by the greater number of available sites on the material. In this way, an increasing scale of the interaction of carbon nanomaterials with RNA fragments is suggested, as a function of the interaction affinity: fullerenes < graphenes < carbon nanotubes, which is the same behavior observed for the overall surface area.

Although some works in the literature describe the possibility of linkage between the electrode and the biological material, when biological species are randomly immobilized on the electrode surface, usually there is no control over the sites these species will be linked. This is an important point to be considered, probably, being one of the most critical events in the biocompatibility of the system [4]. Also, the orientation of this material towards the incorporation of antibodies into the electrochemical system is crucial for obtaining an immunosensor with high sensitivity and selectivity. Therefore, the biological immobilization step has been considered one of the greatest challenges to be overcome in the development of biosensors [37]. Some

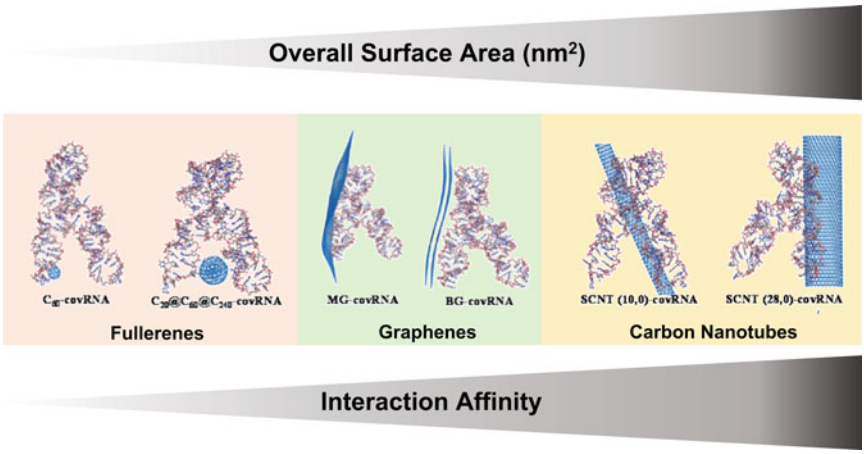

Fig. 1 Correlation between the surface area and the dimensionalities of carbon-based materials and their interaction affinity with SARS-CoV-2 RNA fragments. 0D: zero-dimension; 1D: one-dimension; 2D: two-dimension materials. Reprinted adapted with permission from F. Zhang et al. *Ecotoxicology Environmental Safety*, 219, 112,357, Copyright (2021), Elsevier [36]

strategies can be used to enable the orientation of the biological material, maybe the more extensively explored consists of the generation of immobilization sites, through the formation of functional groups on the surface of the host material [38].

Carbon-based materials can be functionalized or exfoliated by using different approaches, including chemical, physical, and electrochemical methods [39–41]. The functionalization methods can oxidize or reduce the carbon surface, introducing functional groups. Thus, the immobilization of biological species (i.e., enzymes, antibodies, proteins, DNA/RNA) in the carbon structure can be made by covalent interaction with oxygenated functional groups, mainly carboxylic, of the carbon with amine groups of the biological materials. This can occur directly on the carbon material surface, or by using ligands immobilization, such as EDC (1-ethyl-3-(3-dimethylamino) propyl carbodiimide) and NHS (N-hydroxysuccinimide), by a covalent crosslinking mechanism [17, 42, 43]. On the other hand, carbon materials can also interact non-covalently with biomolecules by van der Walls, $\pi - \pi$ stacking, and hydrophobic interactions [25, 44].

2 Carbon-Based Materials Applied for SARS-CoV-2 Biosensing

Regarding the different kinds of macro- or nanomaterials, as well as the possibilities of treatments for these materials, carbon-based biosensors have been applied for the detection of SARS-CoV-2 in several samples, which include biological (i.e., blood, urine, saliva, and nasopharyngeal), and environmental samples (i.e., wastewater), as summarized in Table 1.

2.1 Macro-Materials: Graphite and Diamond

Some examples of conductive carbon-based materials used for biosensing consist of widespread macro-scale materials applied in electrochemical sensing for decades, such as graphite and boron-doped diamond-based electrodes [54]. Graphite is an abundant carbon allotrope mineral, which makes its low cost one of the main advantages of its use [55]. This material is composed of several layers of graphene sheets bonded to each other by van der Waals force, which makes the graphite material with low mechanical strength [56]. For this reason, as well as the low cost and easy handling, most applications of this material in electroanalysis are made by use of graphite-based materials electrodes.

As an example, graphitic carbon foils were functionalized and exfoliated to improve the immobilization of anti-SARS-CoV-2 antibodies [50]. The material was treated in an acid medium, in which the graphitic carbon showed the surface partial oxidation. The intercalation of ions in the layers of the material was also

Table 1 Carbon-based biosensors for the sensing of SARS-CoV-2

Biosensor	Biosensor type	Technique	Redox probe/Label	Immobilization/Recognition	Target
Carbon paste-SPCE	Genosensor	SWV	Methylene blue	Methylene blue and DNA amplicon complex formation	N-protein and ORF1ab gene
SiO_2@UiO-66-SPCE	Immunosensor	EIS	Label-free	ACE2 and S-protein interaction	S-protein
MNP-SPCE	Immunosensor	DPV	–	S1 and S2 proteins immobilization by EDC/NHS reaction	Anti-S1, anti-S2, and antibody cocktail
$Ni(OH)_2$ NP-SPCE	Immunosensor	DPV	$[Fe(CN)_6]^{4-/3-}$	S-protein and $Ni(OH)_2$ NP covalent bond. Antibody/antigen interaction	IgM/IgG antibody
MB-ACE2-AuNPs-SPCE	Immunosensor	DPV	AuNPs	ACE2 covalent immobilization by thiol-gold interaction. ACE2 and S-protein interaction	S-protein
MB-CB-SPE	Immunosensor	DPV	1-naphthyl phosphate	Sandwich assay: antibody, antigen, antibody labeled with alkaline phosphatase enzyme. MB and antibody interaction	S- and N-proteins
G-SPE	Immunosensor	SWV	$[Fe(CN)_6]^{4-/3-}$	Antibody and EDC/PBASE covalent bond. Antibody/antigen interaction	S1 protein
SPCE	Immunosensor	Potentiometry	–	Antibody/antigen interaction	S-protein

(continued)

Table 1 (continued)

Biosensor	Biosensor type	Technique	Redox probe/Label	Immobilization/Recognition	Target
MoS_2-Thi-CNDs/SPCE	Genosensor	DPV	Thi-CNDs	Thiolated DNA probe covalent bond on MoS_2	ORF1ab gene
AuSPE-CDs/AuNMs	Genosensor	ECL	CDs/$[Ru(bpy)_3]^2$	Thiolated DNA probe immobilization on AuNM by thiol-gold interaction	ORF1ab gene
Au@SCX8-RGO-TB	Genosensor	DPV	Toluidine blue	Sandwich assay. CX8 recognition for TB	ORF1ab gene
GO-8H-AuNS SPCE	Immunosensor	DPV	AuNS	S-protein functional groups and NHS hydrogen bonds and electrostatic interactions	S2 and S2 proteins
GNPs-AuNP	Genosensor	Electrophoresis	-	Thiolated ssDNA probe-capped gold by thiol-gold interaction	N-gene
Flexible GCF	Immunosensor	DPV	$[Fe(CN)_6]^{4-/3-}$	Anti-SARS-CoV-2 and EDA-GCF covalent bond	S-protein
AuNF/NC/SPCE	Genosensor	DPV	Methylene blue	Methylene blue tagged biothiolated reporter RNA probe immobilization on AuNF	ORF gene_crRNA
Pd-Au nanosheets/MNPs CGE	Immunosensor	DPV	H_2O_2	Sandwich assay. Antibody-functionalized MNP, S1 protein, and antibody interaction	S1 protein
BDD thin films	Immunosensor	EIS	$[Fe(CN)_6]^{3-}$	Biotinylated S1 protein. Antibody covalent bond	S1 protein
MWCNT or rGO/AuNS or AgNW GCE	Immunosensor	DPV	$[Fe(CN)_6]^{4-/3-}$	Monoclonal IgG antibodies against S1 protein	S1 protein

(continued)

Table 1 (continued)

Biosensor	Biosensor type	Technique	Redox probe/Label	Immobilization/Recognition	Target
Laser engraved graphene electrodes	Multiplex immunosensor	DPV and amperometry	HQ	Antibodies HRP labeled or unlabeled/functionalized graphene covalent bond	NP-protein, S1-IgM and S1-IgG, and CRP
ND-AuIDE	Aptasensor	EIS	$[Fe(CN)_6]^{4-/3-}$	Anti-NCP aptamer binding on nanodiamond using CDI	NC protein
GONC/DEPChip	Genosensor	DPV	$[Fe(CN)_6]^{4-/3-}$	RdRp-COVID non-covalent bond	RdRp-COVID

Biosensor	LDR	LOD	Sample application	Response/Analysis time	Ref
Carbon paste-SPCE	$0.001 - 10{,}000 \times 10^{-3}$ ng μL^{-1}	0.038×10^{-3} ng μL^{-1}	Wastewater	–	[45]
SiO_2@UiO-66-SPCE	100 fg mL^{-1} – 10 ng mL^{-1}	100 fg mL^{-1}	Nasal	5 min	[16]
MNP-SPCE	1.0–200 ng mL^{-1}	0.53–0.99 ng mL^{-1}	Nasopharyngeal	–	[17]
$Ni(OH)_2$ NP-SPCE	1.0 fg mL^{-1} – 1.0 μg mL^{-1}	0.3 fg mL^{-1}	Blood serum	20 min	[18]
MB-ACE2-AuNPs-SPCE	0.0009–360 fg mL^{-1}	0.35 ag mL^{-1}	Saliva	60 min	[19]
MB-CB-SPE	–	19 and 8.0 ng mL^{-1}	Saliva	30 min	[46]
G-SPE	260 – 1040 nmol L^{-1}	260 nmol L^{-1}	Recombinant SARS-CoV-2	45 min	[43]
SPCE	10 fmol L^{-1} – 00 nmol L^{-1}	10 fmol L^{-1}	Saliva	1 min	[47]
MoS_2-Thi-CNDs/SPCE	1.0 pmol L^{-1} – 1.00 nmol L^{-1}	1.01 pmol L^{-1}	–	–	[21]
AuSPE-CDs/AuNMs	50 fmol L^{-1} – 100 nmol L^{-1}	514 amol L^{-1}	Blood serum	–	[48]
Au@SCX8-RGO-TB	$1.0 \times 10^{-17} - 1.0 \times 10^{-12}$ mol L^{-1}	200 copies mL^{-1}	Sputum, throat swab, urine, feces, plasma, serum, blood, oral swabs, and saliva	–	[29]

(continued)

Table 1 (continued)

Biosensor	LDR	LOD	Sample application	Response/Analysis time	Ref
GO-8H-AuNS SPCE	–	1.68×10^{-22} μg mL^{-1}	Blood, oropharyngeal, and saliva	1 min	[30]
GNPs-AuNP	585 – 5.85×10^{7} copies μL^{-1}	6.9 copies μL^{-1}	Infected cells, nasopharyngeal, and saliva	5 min	[49]
Flexible GCF	2 to 1000 pg mL^{-1}	27 pg ml^{-1}	Blood plasma	30 min	[50]
AuNF/NC/SPCE	1.0×10^{-1} – 1.0×10^{5} fg mL^{-1}	4.4×10^{-2} fg mL^{-1}	Artificial saliva	90 min	[20]
Pd-Au nanosheets/MNPs CGE	0.01 – 1,000 ng mL^{-1}	0.0072 ng mL^{-1}	Nasopharyngeal	–	[51]
BDD thin films	1.0 – 1000 fg mL^{-1}	1 fg mL^{-1}	Cell culture media	5 min	[52]
MWCNT or rGO/AuNS or AgNW GCE	0.0013–0.028, 0.0076–0.036 and 0.0012–0.025 fg mL^{-1}	0.0011, 0.0065 and 0.0010 fg mL^{-1}	Human plasma and aquatic biological medium	1 min	[25]
Laser engraved graphene electrodes	–	–	Human serum and saliva	5 min	[27]
ND-AuIDE	1.0 fmol L^{-1}–100 pmol L^{-1}	0.389 fmol L^{-1}	Human serum	–	[53]

(continued)

Table 1 (continued)

Biosensor	LDR	LOD	Sample application	Response/Analysis time	Ref
GONC/DEPChip	$1.0 \times 10^{-5} - 1.0 \times 10^{-10}$ mol L^{-1}	186 nmol L^{-1}	Human serum and saliva	30 min	[28]

SPCE: Screen printed carbon electrode; SWV: Square-Wave Voltammetry; SiO_2@UiO-66-SPCE: Screen printed carbon electrode modified with SiO_2 nanoparticles in zirconium (IV) carboxylate MOF (UiO-66); EIS: Electrochemical Impedance Spectroscopy; ACE2: Angiotensin-converting enzyme 2; S-protein: Spike protein; MNP-SPCE: Magnetic nanoparticle-based SPCE; DPV: Differential pulse voltammetry; $Ni(OH)_2$ NP-SPCE: Nickel hydroxide nanoparticles modified SPCE; MB-ACE2-AuNP-SPCE: Magnetic beads and gold nanoparticles modified with ACE2 peptide SPCE; MB-CB-SPE: Magnetic beads combined with carbon black-based SPE; N-protein: Nucleocapsid protein; G-SPE: Graphene SPE functionalized with PBSAE (1-pyrene butyric acid N-hydroxysuccinimide ester linker); MoS_2-Thi-CNDs/SPCE: Thionine functionalized carbon nanodots on molybdenum disulphide SPCE; AuSPE-CDs/AuNMs: Gold nanomaterials and carbon dost screen-printed gold electrode; ECL: Electrochemiluminescent; Au@SCX8-RGO-TB: Calixarene (p-sulfocalix[8]arene) functionalized graphene oxide modified with gold nanoparticles and toluidine blue SPCE; GO-8H-AuNS SPCE: Graphene oxide decorated with 8-hydroxyquinoline (8H) coupled with gold nanostars SPCE; Flexible GCF: Flexible graphitic carbon foil; EDA: ethylenediamine; AuNF/NC/SPCE: Screen printed carbon electrode modified with graphene-based nanocomposite and nanoflowers of gold; Pd-Au nanosheets/MNPs CGE: Pd-Au nanosheets and functionalized superparamagnetic nanoparticles glassy carbon electrode; BDD: Boron doped diamond; MWCNT or rGO/AuNS or AgNW GCE: Multi-walled carbon nanotubes or graphene oxide immunosensor modified with gold nanostars or silver nanowires GCE; HQ: hydroquinone; HRP: horseradish peroxidase; ND-AuIDE: Nanodiamond assembled gold interdigitated electrodes; CDI: 1,1′ -Carbonyldiimidazole; NC-protein: Nucleocapsid protein; GONC/DEPChip: Graphene oxide nanocolloids disposable electrical printed chip; RdRp-COVID: COVID RNA-dependent RNA polymerase

achieved. After, thermal treatment in presence of ethylenediamine was performed, which bonds to functional groups at the edges and basal planes and promoted the partial exfoliation of the material (Fig. 2a). The introduction of amine groups was also reported in the material, which is interesting for the immobilization of antibodies. The immunosensor was applied for the biosensing of SARS-CoV-2 S-protein in blood plasma using $[Fe(CN)_6]^{3-/4-}$ probe by DPV (Fig. 2b).

Regarding the carbon-based macro-electrodes, perhaps, the most widespread are carbon paste electrodes [57, 58], glassy carbon electrodes [59, 60], and 2D screen-printed electrodes [61, 62]. Considering bioanalysis applications, screen-printed carbon electrodes (SPCE) based have been most used. This 2D type electrode can be purchased [16] or easily fabricated by printing a conductive ink or paste onto a substrate [63]. In this case, graphite, graphene, and carbon black can be used for this purpose. In general, screen-printed electrodes are more compact devices

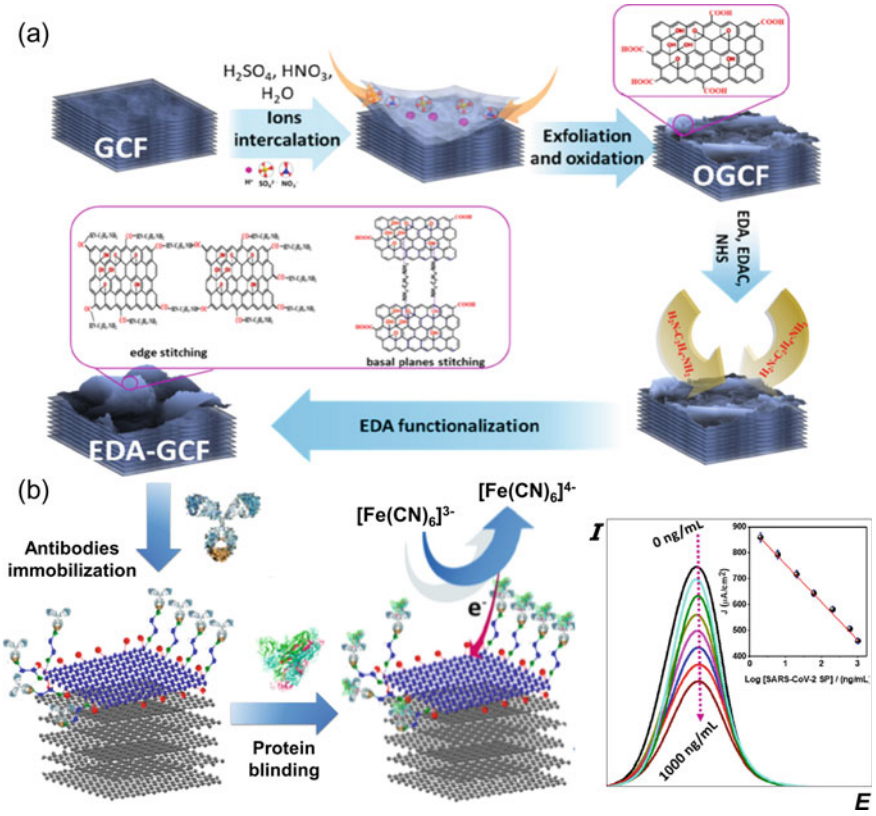

Fig. 2 **a** Graphitic carbon surface activation (exfoliation and functionalization). **b** Anti-SARS-CoV-2 antibodies immobilization for the detection of SARS-CoV-2 protein using $[Fe(CN)_6]^{3-/4-}$ probe by DPV. Reprinted adapted with permission from M. Adeel et al. *Sensors and Actuators: B. Chemical*, 359, 131,591, Copyright (2022), Elsevier [50]

than conventional electrodes, leading to less waste generation, portable and large-scale production abilities [64]. The properties presented by SPCEs, associated with the biocompatibility attributed to carbon materials, allowed their wide use in the development of biosensors or bio arrays for electrochemical determination [62, 65], including SARS-CoV-2 sensing, as demonstrated by Mahari et. al [47]. In this work, the development of an e-sensing device coupled to a commercial SPCE for SARS-CoV-2 monitoring was reported. Anti-SARS-CoV-2 antibodies were immobilized on the working electrode surface, and the measures before and after incubation with SARS-CoV-2 S1 protein were performed by potentiometry. In addition to the biocompatibility and stability of the bioanalysis system, a high simplicity of device construction and analysis was also observed in this work.

Concerning diamond, the structure is composed of carbon atoms with sp^3 hybridization, unlike graphite, in which the carbon atoms make 4 sigma bonds (σ), a tetragonal bond [66, 67]. This structure, as well as high binding energy, makes the diamond exhibit high hardness and good thermal conductivity [67, 68]. On the other hand, sp^3 hybridization promotes this material a low electron conductivity, which would make its use in the development of electrochemical sensors unfeasible. However, p- or n-type doping using boron allows the generation of electron conduction sites [69]. Hence, the boron-doped diamond electrodes, especially thin film-based electrodes, consisting of a conductive carbon material widely used as electrochemical sensors and biosensors, mainly because of the biocompatibility, low background of current, and wide potential window [70, 71]. Therefore, boron-doped diamond is a material with high potential for the construction of electrochemical biosensors [72, 73], such as for the sensing and monitoring of SARS-CoV-2, as described by Witt et al. [52]. In this work, the authors performed an impedimetric determination of SARS-CoV-2 spike protein in human cells culture medium, after interaction with anti-SARS-CoV-2 antibodies immobilized on the boron-doped diamond electrode. The main positive points highlighted were the low limit of detection, which allows the dilution of the sample that reduced some possible matrix effects, and the high stability of the system during the measurements.

2.2 Nanostructured Materials

2.2.1 Carbon Nanotubes

Carbon nanotubes are 2D carbon nanomaterials with cylindrical structures obtained by twisted sheets of graphite, classified as single or multi-walled carbon nanotubes [1]. The walls of the nanotubes are composed of rolled-up sheets of graphene, in other words, consisting of an electron conductive material with a hexagonal arrangement of sp^2 hybridized carbon atoms [74, 75]. These characteristics give this material excellent electrochemical properties, mainly high thermal and electrical conductivities. Like other carbon-based materials, carbon nanotube-based electrodes have slow kinetics of carbon oxidation, which allows these devices to have a wide potential

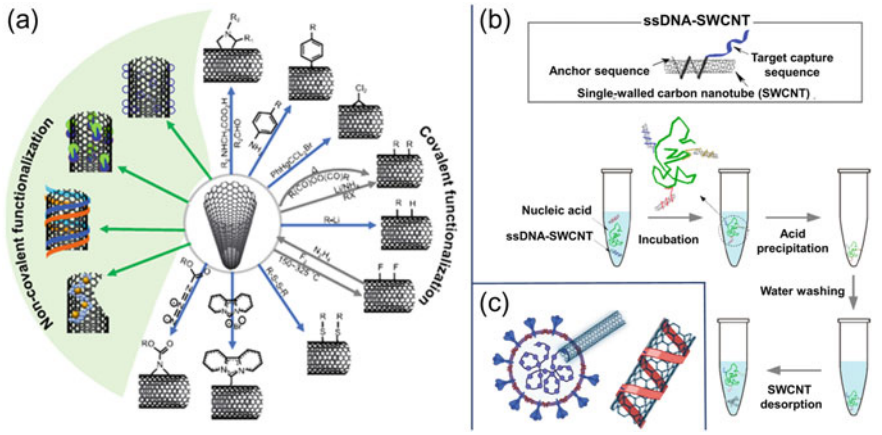

Fig. 3 **a** Carbon nanotubes covalent and non-covalent functionalization and **b** binding with SARS-CoV-2 biological materials. **c** SARS-CoV-2 nucleic acid extract by using target capture sequence (ssDNA) anchored on single-walled carbon nanotubes. Reprinted adapted with permission from E. N. Ozmen et al. *Materials Science & Engineering C*, 129, 112,356, Copyright (2021), Elsevier [3]; R. Varghese et al. *Colloid and Interface Science Communications*, 46, 100,544, Copyright (2022), Elsevier [24]; S. Jeong et al. *ACS Nano*, 15, 10,309–10,317, Copyright (2021), American Chemical Society [81]

range [76]. In sensing applications, carbon nanotubes are widely applied in association with other materials, more precisely as modifiers of electrochemical transducers, which can be metallic or carbon-based, such as glassy carbon electrodes and screen-printed carbon electrodes [2, 77]. The presence of carbon nanotubes increases the electrochemical surface area, as well as electrical conductivity, and biocompatibility, making it an excellent platform for the anchor or determination of biological species [78].

For carbon nanotubes, a purification step can be performed by using oxidants (i.e., HNO_3, $KMnO_4$, and H_2SO_4) to separate undesirable impurities from the nanotubes. The functionalization is widely used for the oxidation of carbon nanotubes, which can be covalently done by direct binding of functional groups on the surface or by carboxylic acids attached to the sides or ends of the nanotubes [79, 80] (Fig. 3a). The cabon nanotubes structure also allows the immobilization of biological materials inside or outside the nanotubes (Fig. 3b) [24]. Another interesting strategy has been explored to extract nucleic acids of SARS-CoV-2 by using single-walled carbon nanotubes with capture single-stranded DNA sequences (Fig. 3c), improving the detection sensitivity [81].

2.2.2 Graphenes

Graphene is a two-dimensional carbon structure with carbon atoms arranged in hexagonal sp^2 hybridized structures with properties like carbon nanotubes, as

presented before. Graphene normally can be synthesized by physical and chemical methods from pristine graphite and presents interesting properties, such as elasticity and flexibility, high hardness, thermal conductivity, surface area, and electrical conductivity [82, 83]. This nanomaterial can be synthesized from graphite, by the Hummers method or modified Hummers methods, which allows the formation of oxygenated functional groups on the material, conferring hydrophilic and lipophilic characteristics to the material [1]. An example of graphene oxide nanocolloids application for SARS-CoV-2 monitoring was developed by Ang et al. [28]. The material was used not only for the construction of the sensor but also as a platform for anchoring and recognizing the biological material in saliva samples by the DPV technique. The sensor was used for the detection of 2019-nCoV genomic sequences, in which the electrode was modified with a DNA fragment and the monitoring of the genomic sequence was performed by suppressing the voltammetric signal after the incubation of the complementary DNA fragment (target). High selectivity was registered using this genosensor for SARS-CoV-2 monitoring, which also presented portability and low cost, allowing the integration of the bio arrays for *in loco* monitoring, for example.

The presence of functional groups can interfere with the honeycomb structure of graphene, affecting its thermal and electrical conductivity. Thus, a reduction method is commonly employed by using chemical agents, photochemical or electrochemical methods, leading to the formation of defects in the structure and obtaining the reduced graphene oxide (rGO) [3, 25, 84, 85] (Fig. 4a, b). A comparison between carbon-based materials (i.e., multi-walled carbon nanotubes, graphene oxide, and reduced graphene oxide) immunossensors was reported for the detection of SARS-CoV-2 (Fig. 4c) [25]. The immobilization of monoclonal IgG antibodies was performed by using EDC/NHS couple. Gold nanostars and silver nanowires were also tested as amplifying agents. In this case, graphene-based immunosensor (rGO modified with gold nanostars) showed the best detection of SARS-CoV-2 spike protein in biological samples. This is correlated to the highest effective surface area, electron transfer rate and electrical conductivity of the single-layer reduced graphene oxide compared to multi-walled carbon nanotube [25, 36].

2.2.3 Carbon Dots and Nanodots

Carbon quantum dots, or 0D carbon materials, are compounds mostly based on carbon. However, they can present significant amounts of oxygen, hydrogen, and nitrogen, depending on the synthesis or treatments of these materials [86, 87]. Due to their extremely small size (diameter of 10 nm or less), carbon quantum dots have a higher surface area and amount of edge sites compared to other carbon materials, which increases their chemical and electrochemical activities [88]. They also show high solubility, and the ability to be synthesized from compounds abundant in nature without the use of solvents [89], increasing the interest in greener materials. Graphene quantum dots have been used for the immobilization of antibodies (Fig. 5a), this demonstrates their ability for the development of biosensors [90].

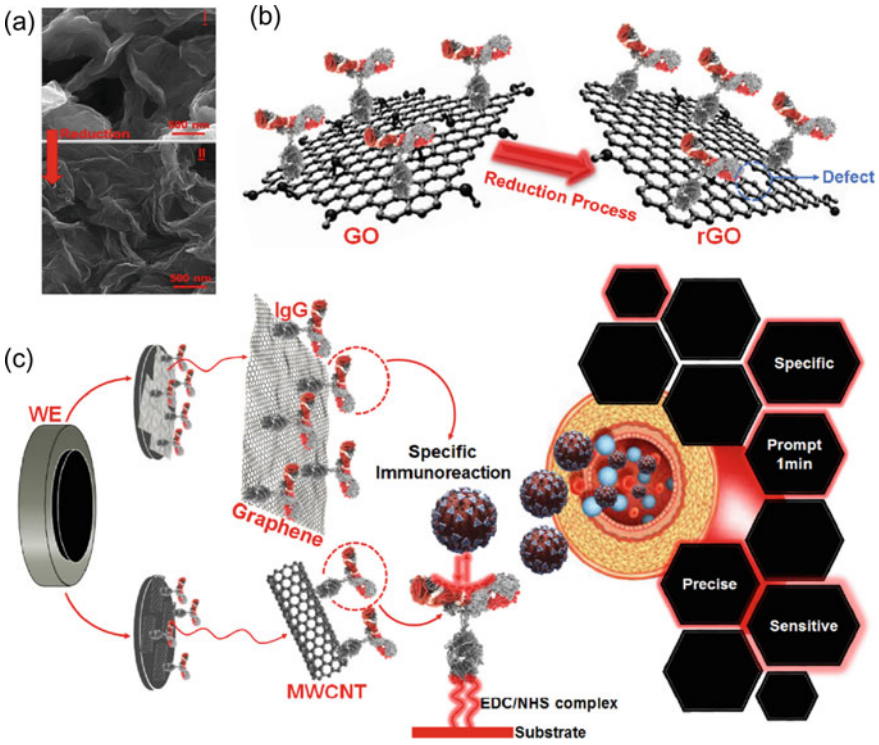

Fig. 4 **a** Field emission scanning electron microscopy images and **b** structures for graphene oxide reduction process. **c** Comparison between graphene- and carbon nanotubes-based immunosensors for the sensing of SARS-CoV-2. Reprinted adapted with permission from S. A. Hashemi et al. *Talanta*, 239, 123,113 Copyright (2022), Elsevier [25]

Regarding COVID-19 monitoring, carbon nanodots functionalized with thionine were applied as electrochemical indicators of the hybridization reaction, allowing the detection of SARS-CoV-2 DNA sequences at picomolar levels (Fig. 5b) [21]. In another work, carbon nanodots have been used as co-reactant agents to improve the electrochemiluminescence for the detection of SARS-CoV-2 DNA sequences in human serum samples [48]. This emphasizes their application in different strategies for the biosensing approaches, including for SARS-CoV-2 determination.

3 Tendencies and Perspectives

As can be seen, carbon-based materials have been extensively used as conductive materials or modifiers for the construction of biosensors for the detection of

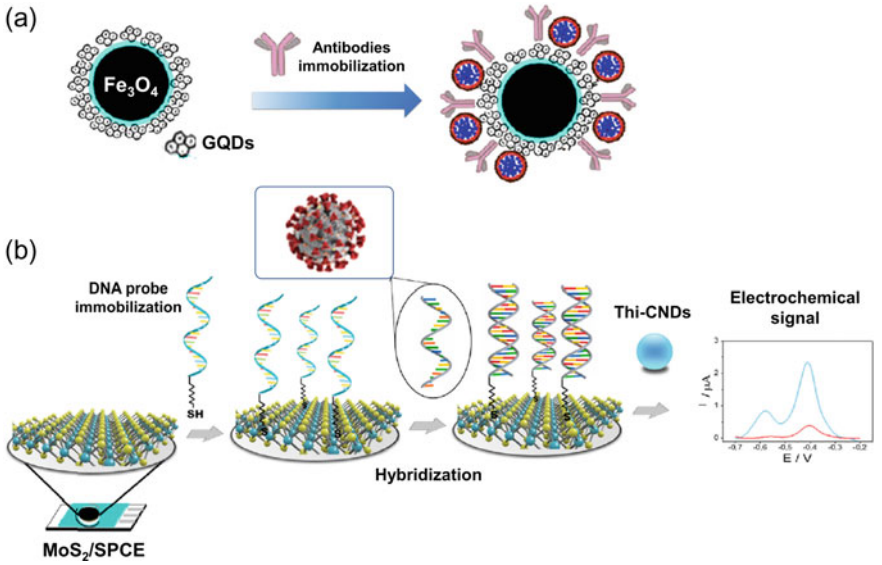

Fig. 5 **a** Graphene quantum dots used for antibodies immobilization. **b** Carbon nanodots application as a redox indicator of the hybridization for the sensing of SARS-CoV-2. Reprinted adapted with permission from X. Wang et al. *Biosensors and Bioelectronics*, 47, 171–177 Copyright (2013), Elsevier [90]; E. Martínez-Periñán et al. *Biosensors and Bioelectronics*, 189, 113,375, Copyright (2021), Elsevier [21]

SARS-CoV-2. Different approaches of carbon-based biosensors have been developed, mainly immunosensors, for the monitoring of antigens (proteins) and antibodies; and genosensors, for the monitoring of genetical materials (RNA or corresponding c-DNA). Recently, the change in the levels of some biomarkers has been also attached to the COVID-19 infection, such as glutamate [91, 92], cytokines [93, 94], interleukins [95], C-reactive protein [96], dopamine [97], among others [98, 99].

Carbon-based sensors are also versatile to be used as disposable test strips [45], and combined with portable potentiostats and other devices [27, 43, 46, 47] allowing the fast and low cost detection of SARS-CoV-2, as point-of-care devices. An interesting work proposed a multiplex device for the simultaneous determination of four different biomarkers in saliva and human blood serum samples, correlated with symptom severity in COVID 19 disease [27]. This device consisted of a 2D electrode constructed of laser-engraved graphene and the four working electrodes were modified with antibodies for SARS-CoV-2, IgG, IgM, and C-reactive protein. It is important to highlight that the device allowed the monitoring of these species simultaneously making it possible to correlate the data obtained with the disease severity, possible infection, and immune response. The different levels of each biomarker were wirelessly transmitted by Bluetooth, which allowed the application of the device in medical appointments or diagnoses via telemedicine (Fig. 6).

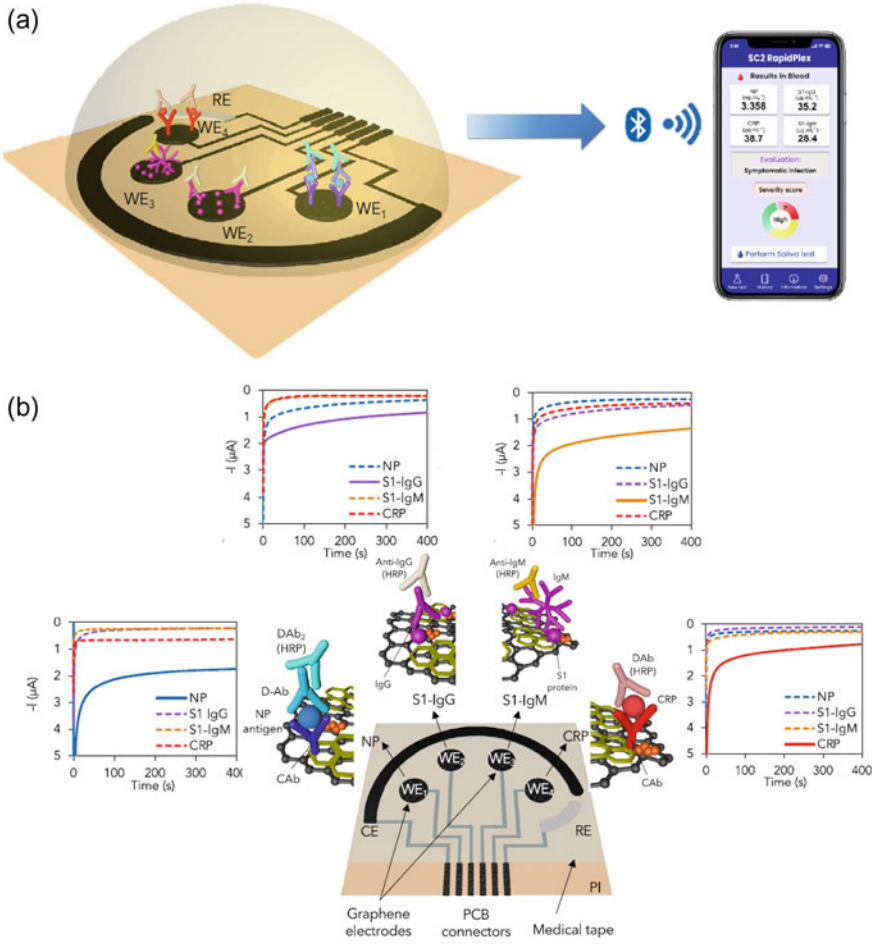

Fig. 6 **a** Laser-engraved graphene immunosensors multiplex wireless sensor. **b** Application of the device for SARS-CoV-2 nucleocapsid protein, IgG, IgM, and C-reactive protein sensing. Reprinted adapted with permission from R. M. Torrente-Rodríguez et al., *Matter*, 3, 1981–1998, Copyright (2020), Elsevier [27]

The use of conductive carbon-based inks on flexible surfaces is another important point to be highlighted. These approaches make it possible to use these materials on different surfaces, even with irregular morphology as the human body, for the development of wearable sensors for COVID-19 monitoring or other existing or emerging diseases. Wherein, carbon-based devices can be used for real-time monitoring of numerous species, such as endocrine regulators, toxins, and diseases, such as COVID-19, depending on the recognition center immobilized on the electrode.

Physical and chemical characteristics presented by conductive carbon-based materials, at macro-scale or nanoscale, promote interesting bioelectrochemical properties for these sensors, as mentioned above.

In addition, the use of carbon-based materials can reduce the environmental impact due their low chemical inertia and low toxicity, as already mentioned previously addressed. This impact can be further reduced with the possibility of reusing or recycling these devices after application. The recycling of the sensors into another material could be a feasible and interesting alternative from the circular economy point of view [100]. For example, carbon-based paper or cotton fabric sensors for SARS-CoV-2 monitoring devices could be pyrolyzed after use, generating bio-charcoal. This new material could be embedded into the environment, as a soil conditioner, or it could also be re-used as a modifier in other electrochemical devices [101], since it has interesting intereaction properties for the development of biosensors.

Faced with the COVID-19 pandemic that has plagued the world since 2019, there was an immediate need for searching alternatives to contain and identify this virus. The use of carbon-based materials plays an important role in the development of reliable, fast, environmentally friendly, and low cost devices for the sensing of SARS-CoV-2. Given the above, especially concerning the different types and versatility of applications, carbon-based materials can enable the immobilization and monitoring of nucleic acids, proteins, antibodies, as well as potential biomarkers recently related to COVID-19 in biological and environmental samples.

References

1. M. Li, B. Mu, Effect of different dimensional carbon materials on the properties and application of phase change materials: a review. Appl. Energy **242**, 695–715 (2019)
2. A.C. Power, B. Gorey, S. Chandra, J. Chapman, Carbon nanomaterials and their application to electrochemical sensors: a review. Nanotechnol. Rev. **7**, 19–41 (2018)
3. E.N. Özmen, E. Kartal, M.B. Turan, A. Yazıcıoğlu, J.H. Niazi, A. Qureshi, Graphene and carbon nanotubes interfaced electrochemical nanobiosensors for the detection of SARS-CoV-2 (COVID-19) and other respiratory viral infections: a review. Mater. Sci. Eng., C **129**, 112356 (2021)
4. D.F. Williams, There is no such thing as a biocompatible material. Biomaterials **35**, 10009–10014 (2014)
5. S. Takabayashi, M. Yang, S. Ogawa, H. Hayashi, R. Ješko, T. Otsuji, Y. Takakuwa, Relationship between the structure and electrical characteristics of diamond-like carbon films. J. Appl. Phys. **116**, 093507 (2014)
6. P. Glover, Graphite and electrical conductivity in the lower continental crust: a review. Phys. Chem. Earth **21**, 279–287 (1996)
7. F. Cesano, M.J. Uddin, K. Lozano, M. Zanetti, D. Scarano, All-carbon conductors for electronic and electrical wiring applications. Front. Mater. **7**, 219 (2020)
8. A.A. Balandin, Thermal properties of graphene and nanostructured carbon materials. Nat. Mater. **10**, 569–581 (2011)
9. K. Kinoshita, *Carbon: Electrochemical and Physicochemical Properties*. John Wiley & Sons (1988)

10. G. Martins, J.L. Gogola, L.H. Budni, B.C. Janegitz, L.H. Marcolino-Junior, M.F. Bergamini, 3D-printed electrode as a new platform for electrochemical immunosensors for virus detection. Anal. Chim. Acta **1147**, 30–37 (2021)
11. L.C. Brazaca, A.H. Imamura, N.O. Gomes, M.B. Almeida, D.T. Scheidt, P.A. Raymundo-Pereira, O.N. Oliveira, B.C. Janegitz, S.A.S. Machado, E. Carrilho, Electrochemical immunosensors using electrodeposited gold nanostructures for detecting the S proteins from SARS-CoV and SARS-CoV-2, Analyt. Bioanalyt. Chem. (2022)
12. L.C. Brazaca, P.L. Dos Santos, P.R. de Oliveira, D.P. Rocha, J.S. Stefano, C. Kalinke, R.A. Abarza Muñoz, J.A. Bonacin, B.C. Janegitz, E. Carrilho, Biosensing strategies for the electrochemical detection of viruses and viral diseases—a review. Analyt. Chimica Acta, **1159,** 338384 (2021)
13. Z. Wang, Z. Dai, Carbon nanomaterial-based electrochemical biosensors: an overview. Nanoscale **7**, 6420–6431 (2015)
14. C. Grabinski, S. Hussain, K. Lafdi, L. Braydich-Stolle, J. Schlager, Effect of particle dimension on biocompatibility of carbon nanomaterials. Carbon **45**, 2828–2835 (2007)
15. S. Smart, A. Cassady, G. Lu, D. Martin, The biocompatibility of carbon nanotubes. Carbon **44**, 1034–1047 (2006)
16. M. Mehmandoust, Z.P. Gumus, M. Soylak, N. Erk, Electrochemical immunosensor for rapid and highly sensitive detection of SARS-CoV-2 antigen in the nasal sample. Talanta **240**, 123211 (2022)
17. C. Durmus, S. Balaban Hanoglu, D. Harmanci, H. Moulahoum, K. Tok, F. Ghorbanizamani, S. Sanli, F. Zihnioglu, S. Evran, C. Cicek, R. Sertoz, B. Arda, T. Goksel, K. Turhan, S. Timur, Indiscriminate SARS-CoV-2 multivariant detection using magnetic nanoparticle-based electrochemical immunosensing, Talanta **243,** 123356 (2022)
18. Z. Rahmati, M. Roushani, H. Hosseini, H. Choobin, An electrochemical immunosensor using SARS-CoV-2 spike protein-nickel hydroxide nanoparticles bio-conjugate modified SPCE for ultrasensitive detection of SARS-CoV-2 antibodies. Microchem. J. **170**, 106718 (2021)
19. E.D. Nascimento, W.T. Fonseca, T.R. de Oliveira, C.R.S.T.B. de Correia, V.M. Faça, B.P. de Morais, V.C. Silvestrini, H. Pott-Junior, F.R. Teixeira, R.C. Faria, COVID-19 diagnosis by SARS-CoV-2 Spike protein detection in saliva using an ultrasensitive magneto-assay based on disposable electrochemical sensor, Sens. Actuators B: Chem. **353,** 131128 (2022)
20. W. Heo, K. Lee, S. Park, K.-A. Hyun, H.-I. Jung, Electrochemical biosensor for nucleic acid amplification-free and sensitive detection of severe acute respiratory syndrome coronavirus 2 (SARS-CoV-2) RNA via CRISPR/Cas13a trans-cleavage reaction. Biosens. Bioelectron. **201**, 113960 (2022)
21. E. Martínez-Periñán, T. García-Mendiola, E. Enebral-Romero, R. del Caño, M. Vera-Hidalgo, M. Vázquez Sulleiro, C. Navío, F. Pariente, E.M. Pérez, E. Lorenzo, A MoS_2 platform and thionine-carbon nanodots for sensitive and selective detection of pathogens. Biosens. Bioelectron. **189,** 113375 (2021)
22. M. Amouzadeh Tabrizi, L. Nazari, P. Acedo, A photo-electrochemical aptasensor for the determination of severe acute respiratory syndrome coronavirus 2 receptor-binding domain by using graphitic carbon nitride-cadmium sulfide quantum dots nanocomposite. Sens. Actuators B: Chem. **345,** 130377 (2021)
23. M.A. Zamzami, G. Rabbani, A. Ahmad, A.A. Basalah, W.H. Al-Sabban, S. Nate Ahn, H. Choudhry, Carbon nanotube field-effect transistor (CNT-FET)-based biosensor for rapid detection of SARS-CoV-2 (COVID-19) surface spike protein S1, Bioelectrochemistry **143,** 107982 (2022)
24. R. Varghese, S. Salvi, P. Sood, J. Karsiya, D. Kumar, Carbon nanotubes in COVID-19: A critical review and prospects. Colloid Interface Sci. Commun. **46**, 100544 (2022)
25. S.A. Hashemi, S. Bahrani, S.M. Mousavi, N. Omidifar, N.G.G. Behbahan, M. Arjmand, S. Ramakrishna, A.M. Dimiev, K.B. Lankarani, M. Moghadami, M. Firoozsani, Antibody mounting capability of 1D/2D carbonaceous nanomaterials toward rapid-specific detection of SARS-CoV-2. Talanta **239**, 123113 (2022)

26. J. Gao, C. Wang, Y. Chu, Y. Han, Y. Gao, Y. Wang, C. Wang, H. Liu, L. Han, Y. Zhang, Graphene oxide-graphene Van der Waals heterostructure transistor biosensor for SARS-CoV-2 protein detection. Talanta **240**, 123197 (2022)
27. R.M. Torrente-Rodríguez, H. Lukas, J. Tu, J. Min, Y. Yang, C. Xu, H.B. Rossiter, W. Gao, SARS-CoV-2 RapidPlex: a graphene-based multiplexed telemedicine platform for rapid and low-cost COVID-19 diagnosis and monitoring. Matter **3**, 1981–1998 (2020)
28. W.L. Ang, R.R.X. Lim, A. Ambrosi, A. Bonanni, Rapid electrochemical detection of COVID-19 genomic sequence with dual-function graphene nanocolloids based biosensor. FlatChem **32**, 100336 (2022)
29. H. Zhao, F. Liu, W. Xie, T.-C. Zhou, J. OuYang, L. Jin, H. Li, C.-Y. Zhao, L. Zhang, J. Wei, Y.-P. Zhang, C.-P. Li, Ultrasensitive supersandwich-type electrochemical sensor for SARS-CoV-2 from the infected COVID-19 patients using a smartphone. Sens. Actuators, B Chem. **327**, 128899 (2021)
30. S.A. Hashemi, N.G. Golab Behbahan, S. Bahrani, S.M. Mousavi, A. Gholami, S. Ramakrishna, M. Firoozsani, M. Moghadami, K.B. Lankarani, N. Omidifar, Ultra-sensitive viral glycoprotein detection nanosystem toward accurate tracing SARS-CoV-2 in biological/non-biological media. Biosens. Bioelectron. **171,** 112731 (2021)
31. S.I. Kaya, L. Karadurmus, G. Ozcelikay, N.K. Bakirhan, S.A. Ozkan, Electrochemical virus detections with nanobiosensors. In *Nanosensors for Smart Cities*. Elsevier, 303–26 (2020)
32. G. Ozcelikay, B. Dogan-Topal, S.A. Ozkan, An electrochemical sensor based on silver nanoparticles-benzalkonium chloride for the voltammetric determination of antiviral drug tenofovir. Electroanalysis **30**, 943–954 (2018)
33. T.A. Silva, F.C. Moraes, B.C. Janegitz, O. Fatibello-Filho, Electrochemical biosensors based on nanostructured carbon black: a review. J. Nanomater. **2017**, 4571614 (2017)
34. C.I. Justino, A.R. Gomes, A.C. Freitas, A.C. Duarte, T.A. Rocha-Santos, Graphene based sensors and biosensors. Trends Anal. Chem. **91**, 53–66 (2017)
35. C. Ji, Y. Zhou, R.M. Leblanc, Z. Peng, Recent developments of carbon dots in biosensing: a review. ACS Sensors **5**, 2724–2741 (2020)
36. F. Zhang, Z. Wang, M.G. Vijver, W.J. Peijnenburg, Probing nano-QSAR to assess the interactions between carbon nanoparticles and a SARS-CoV-2 RNA fragment. Ecotoxicol. Environ. Saf. **219**, 112357 (2021)
37. G. Balkourani, A. Brouzgou, M. Archonti, N. Papandrianos, S. Song, P. Tsiakaras, Emerging materials for the electrochemical detection of COVID-19. J. Electroanal. Chem. **893**, 115289 (2021)
38. A.K. Trilling, J. Beekwilder, H. Zuilhof, Antibody orientation on biosensor surfaces: a minireview. Analyst **138**, 1619–1627 (2013)
39. D.D.L. Chung, Exfoliation of graphite. J. Mater. Sci. **22**, 4190–4198 (1987)
40. P.-C. Ma, N.A. Siddiqui, G. Marom, J.-K. Kim, Dispersion and functionalization of carbon nanotubes for polymer-based nanocomposites: a review. Composites Part A: Appl. Sci. Manuf. **41**, 1345–1367 (2010)
41. F. Yan, Y. Jiang, X. Sun, Z. Bai, Y. Zhang, X. Zhou, Surface modification and chemical functionalization of carbon dots: a review. Microchim. Acta **185**, 1–34 (2018)
42. L. Liv, Electrochemical immunosensor platform based on gold-clusters, cysteamine and glutaraldehyde modified electrode for diagnosing COVID-19. Microchem. J. **168**, 106445 (2021)
43. B. Mojsoska, S. Larsen, D.A. Olsen, J.S. Madsen, I. Brandslund, F.A. Alatraktchi, Rapid SARS-CoV-2 detection using electrochemical immunosensor. Sensors **21**, 390 (2021)
44. N.K. Mehra, V. Mishra, N.K. Jain, A review of ligand tethered surface engineered carbon nanotubes. Biomaterials **35**, 1267–1283 (2014)
45. R.G. Ramírez-Chavarría, E. Castillo-Villanueva, B.E. Alvarez-Serna, J. Carrillo-Reyes, R.M. Ramírez-Zamora, G. Buitrón, L. Alvarez-Icaza, Loop-mediated isothermal amplification-based electrochemical sensor for detecting SARS-CoV-2 in wastewater samples. J. Environ. Chem. Eng. **10**, 107488 (2022)

46. L. Fabiani, M. Saroglia, G. Galatà, R. De Santis, S. Fillo, V. Luca, G. Faggioni, N. D'Amore, E. Regalbuto, P. Salvatori, G. Terova, D. Moscone, F. Lista, F. Arduini, Magnetic beads combined with carbon black-based screen-printed electrodes for COVID-19: a reliable and miniaturized electrochemical immunosensor for SARS-CoV-2 detection in saliva. Biosens. Bioelectron. **171**, 112686 (2021)
47. S. Mahari, A. Roberts, D. Shahdeo, S. Gandhi, eCovSens-ultrasensitive novel in-house built printed circuit board based electrochemical device for rapid detection of nCovid-19 antigen, a spike protein domain 1 of SARS-CoV-2, *BioRxiv*, (2020)
48. L. Gutiérrez-Gálvez, R. del Caño, I. Menéndez-Luque, D. García-Nieto, M. Rodríguez-Peña, M. Luna, T. Pineda, F. Pariente, T. García-Mendiola, E. Lorenzo, Electrochemiluminescent nanostructured DNA biosensor for SARS-CoV-2 detection. Talanta **240**, 123203 (2022)
49. M. Alafeef, K. Dighe, P. Moitra, D. Pan, Rapid, ultrasensitive, and quantitative detection of SARS-CoV-2 using antisense oligonucleotides directed electrochemical biosensor chip. ACS Nano **14**, 17028–17045 (2020)
50. M. Adeel, K. Asif, V. Canzonieri, H.R. Barai, M.M. Rahman, S. Daniele, F. Rizzolio, Controlled, partially exfoliated, self-supported functionalized flexible graphitic carbon foil for ultrasensitive detection of SARS-CoV-2 spike protein. Sens. Actuators, B Chem. **359**, 131591 (2022)
51. J. Zhao, Z. Fu, H. Li, Y. Xiong, S. Cai, C. Wang, Y. Chen, N. Han, R. Yang, Magnet-assisted electrochemical immunosensor based on surface-clean Pd-Au nanosheets for sensitive detection of SARS-CoV-2 spike protein. Electrochim. Acta **404**, 139766 (2022)
52. S. Witt, A. Rogien, D. Werner, J. Siegenthaler, R. Lesiyon, N. Kurien, R. Rechenberg, N. Baule, A. Hardy, M. Becker, Boron doped diamond thin films for the electrochemical detection of SARS-CoV-2 S1 protein. Diam. Relat. Mater. **118**, 108542 (2021)
53. S. Ramanathan, S.C.B. Gopinath, Z.H. Ismail, M.K. Md Arshad, P. Poopalan, Aptasensing nucleocapsid protein on nanodiamond assembled gold interdigitated electrodes for impedimetric SARS-CoV-2 infectious disease assessment. Biosens. Bioelectron. **197,** 113735 (2022)
54. M.D. Angione, R. Pilolli, S. Cotrone, M. Magliulo, A. Mallardi, G. Palazzo, L. Sabbatini, D. Fine, A. Dodabalapur, N. Cioffi, Carbon based materials for electronic bio-sensing. Mater. Today **14**, 424–433 (2011)
55. J. Pappis, S. Blum, Properties of pyrolytic graphite. J. Am. Ceram. Soc. **44**, 592–597 (1961)
56. H. Lee, N. Lee, Y. Seo, J. Eom, S. Lee, Comparison of frictional forces on graphene and graphite. Nanotechnology **20**, 325701 (2009)
57. I. Švancara, K. Vytřas, K. Kalcher, A. Walcarius, J. Wang, Carbon paste electrodes in facts, numbers, and notes: a review on the occasion of the 50-years jubilee of carbon paste in electrochemistry and electroanalysis. Electroanalysis **21**, 7–28 (2009)
58. I. Švancara, K. Vytřas, J. Barek, J. Zima, Carbon paste electrodes in modern electroanalysis. Crit. Rev. Anal. Chem. **31**, 311–345 (2001)
59. W. Van der Linden, J.W. Dieker, Glassy carbon as electrode material in electro-analytical chemistry. Anal. Chim. Acta **119**, 1–24 (1980)
60. L.S. Vieira, A review on the use of glassy carbon in advanced technological applications. Carbon **186**, 282–302 (2022)
61. M. Li, Y.-T. Li, D.-W. Li, Y.-T. Long, Recent developments and applications of screen-printed electrodes in environmental assays—a review. Anal. Chim. Acta **734**, 31–44 (2012)
62. A. Smart, A. Crew, R. Pemberton, G. Hughes, O. Doran, J. Hart, Screen-printed carbon based biosensors and their applications in agri-food safety. TrAC, Trends Anal. Chem. **127**, 115898 (2020)
63. J.R. Camargo, L.O. Orzari, D.A.G. Araújo, P.R. de Oliveira, C. Kalinke, D.P. Rocha, A. Luiz dos Santos, R.M. Takeuchi, R.A.A. Munoz, J.A. Bonacin, B.C. Janegitz, Development of conductive inks for electrochemical sensors and biosensors. Microchem. J. **164**, 105998 (2021)
64. A. Hayat, J.L. Marty, Disposable screen printed electrochemical sensors: tools for environmental monitoring. Sensors **14**, 10432–10453 (2014)

65. W.-J. Guan, Y. Li, Y.-Q. Chen, X.-B. Zhang, G.-Q. Hu, Glucose biosensor based on multi-wall carbon nanotubes and screen printed carbon electrodes. Biosens. Bioelectron. **21**, 508–512 (2005)
66. J. Robertson, Properties of diamond-like carbon. Surf. Coat Technol. **50**, 185–203 (1992)
67. J.E. Field, The mechanical and strength properties of diamond. Rep. Prog. Phys. **75**, 126505 (2012)
68. C.A. Brookes, E.J. Brookes, Diamond in perspective: a review of mechanical properties of natural diamond. Diamond Relat. Mater. **1**, 13–17 (1991)
69. R. Kalish, Doping of diamond. Carbon **37**, 781–785 (1999)
70. Y. Zhou, J. Zhi, The application of boron-doped diamond electrodes in amperometric biosensors. Talanta **79**, 1189–1196 (2009)
71. C.E. Nebel, B. Rezek, D. Shin, H. Uetsuka, N. Yang, Diamond for bio-sensor applications. J. Phys. D Appl. Phys. **40**, 6443 (2007)
72. H. Jin, M. Wei, J. Wang, Electrochemical DNA biosensor based on the BDD nanograss array electrode. Chem. Cent. J. **7**, 1–6 (2013)
73. Y.L. Zhou, R.H. Tian, J.F. Zhi, Amperometric biosensor based on tyrosinase immobilized on a boron-doped diamond electrode. Biosens. Bioelectron. **22**, 822–828 (2007)
74. A. Merkoçi, Carbon nanotubes in analytical sciences. Microchim. Acta **152**, 157–174 (2006)
75. T. Yamabe, K. Fukui, *The Science and Technology of Carbon Nanotubes*. Elsevier (1999)
76. Y. Lin, W. Yantasee, J. Wang, Carbon nanotubes (CNTs) for the development of electrochemical biosensors. Front. Biosci. **10**, 582 (2005)
77. S. Cinti, F. Arduini, M. Carbone, L. Sansone, I. Cacciotti, D. Moscone, G. Palleschi, Screen-printed electrodes modified with carbon nanomaterials: a comparison among carbon black, carbon nanotubes and graphene. Electroanalysis **27**, 2230–2238 (2015)
78. K. Balasubramanian, M. Burghard, Biosensors based on carbon nanotubes. Anal. Bioanal. Chem. **385**, 452–468 (2006)
79. Y.-P. Sun, K. Fu, Y. Lin, W. Huang, Functionalized carbon nanotubes: properties and applications. Acc. Chem. Res. **35**, 1096–1104 (2002)
80. S. Mallakpour, S. Soltanian, Surface functionalization of carbon nanotubes: fabrication and applications. RSC Adv. **6**, 109916–109935 (2016)
81. S. Jeong, E. González-Grandío, N. Navarro, R.L. Pinals, F. Ledesma, D. Yang, M.P. Landry, Extraction of viral nucleic acids with carbon nanotubes increases SARS-CoV-2 quantitative reverse transcription polymerase chain reaction detection sensitivity. ACS Nano **15**, 10309–10317 (2021)
82. C. Soldano, A. Mahmood, E. Dujardin, Production, properties and potential of graphene. Carbon **48**, 2127–2150 (2010)
83. D.S.L. Abergel, V. Apalkov, J. Berashevich, K. Ziegler, T. Chakraborty, Properties of graphene: a theoretical perspective. Adv. Phys. **59**, 261–482 (2010)
84. C. Kalinke, N.V. Neumsteir, G.O. Aparecido, T.V.B. Ferraz, P.L. Santos, B.C. Janegitz, J.A. Bonacin, Comparison of activation processes for 3D printed PLA-graphene electrodes: electrochemical properties and application for sensing of dopamine. Analyst **145**, 1207–1218 (2020)
85. P.L. dos Santos, R.A. Timm, L.T. Kubota, J.A. Bonacin, Modulation of electrochemical properties of graphene oxide by photochemical reduction using UV-light emitting diodes. ChemistrySelect **1**, 1168–1175 (2016)
86. Y. Chen, G. Huang, Y. Gao, Q. Chen, J. Bi, Up-conversion fluorescent carbon quantum dots decorated covalent triazine frameworks as efficient metal-free photocatalyst for hydrogen evolution. Int. J. Hydrogen Energy **47**, 8739–8748 (2022)
87. Y. Liang, D. Hou, Z. Ni, M. Cao, L. Cai, Preparation, characterization of naringenin, β-cyclodextrin and carbon quantum dot antioxidant nanocomposites. Food Chem. **375**, 131646 (2022)
88. X.T. Zheng, A. Ananthanarayanan, K.Q. Luo, P. Chen, Glowing graphene quantum dots and carbon dots: properties, syntheses, and biological applications. Small **11**, 1620–1636 (2015)

89. F. Rigodanza, L. Đorđević, F. Arcudi, M. Prato, Customizing the electrochemical properties of carbon nanodots by using quinones in bottom-up synthesis. Angew. Chem. **130**, 5156–5161 (2018)
90. X. Wang, L. Chen, X. Su, S. Ai, Electrochemical immunosensor with graphene quantum dots and apoferritin-encapsulated Cu nanoparticles double-assisted signal amplification for detection of avian leukosis virus subgroup J. Biosens. Bioelectron. **47**, 171–177 (2013)
91. J.L. Scoggin, C. Tan, N.H. Nguyen, U. Kansakar, M. Madadi, S. Siddiqui, P.U. Arumugam, M.A. DeCoster, T.A. Murray, An enzyme-based electrochemical biosensor probe with sensitivity to detect astrocytic versus glioma uptake of glutamate in real time in vitro. Biosens. Bioelectron. **126**, 751–757 (2019)
92. J. Schultz, Z. Uddin, G. Singh, M.M.R. Howlader, Glutamate sensing in biofluids: recent advances and research challenges of electrochemical sensors. Analyst **145**, 321–347 (2020)
93. Z. Wang, Z. Hao, S. Yu, C. Huang, Y. Pan, X. Zhao, A wearable and deformable graphene-based affinity nanosensor for monitoring of cytokines in biofluids. Nanomaterials **10**, 1503 (2020)
94. Z. Hao, Y. Pan, W. Shao, Q. Lin, X. Zhao, Graphene-based fully integrated portable nanosensing system for on-line detection of cytokine biomarkers in saliva. Biosens. Bioelectron. **134**, 16–23 (2019)
95. A.R. Cardoso, M.H. de Sá, M.G.F. Sales, An impedimetric molecularly-imprinted biosensor for Interleukin-1β determination, prepared by in-situ electropolymerization on carbon screen-printed electrodes. Bioelectrochemistry **130**, 107287 (2019)
96. S. Jampasa, W. Siangproh, R. Laocharoensuk, T. Vilaivan, O. Chailapakul, Electrochemical detection of c-reactive protein based on anthraquinone-labeled antibody using a screen-printed graphene electrode. Talanta **183**, 311–319 (2018)
97. M.T. Hwang, I. Park, M. Heiranian, A. Taqieddin, S. You, V. Faramarzi, A.A. Pak, A.M. van der Zande, N.R. Aluru, R. Bashir, Ultrasensitive detection of dopamine, IL-6 and SARS-CoV-2 proteins on crumpled graphene FET biosensor. Adv. Mater. Technol. **6**, 2100712 (2021)
98. S. Kotru, M. Klimuntowski, H. Ridha, Z. Uddin, A.A. Askhar, G. Singh, M.M.R. Howlader, Electrochemical sensing: a prognostic tool in the fight against COVID-19. TrAC, Trends Anal. Chem. **136**, 116198 (2021)
99. M. Kaur, S. Tiwari, R. Jain, Protein based biomarkers for non-invasive Covid-19 detection. Sens. Bio-Sens. Resear. **29**, 100362 (2020)
100. H. Salmenperä, K. Pitkänen, P. Kautto, L. Saikku, Critical factors for enhancing the circular economy in waste management. J. Clean. Prod. **280**, 124339 (2021)
101. C. Kalinke, P.R. de Oliveira, J.A. Bonacin, B.C. Janegitz, A.S. Mangrich, L.H. Marcolino-Junior, M.F. Bergamini, State-of-the-art and perspectives in the use of biochar for electrochemical and electroanalytical applications. Green Chem. **23**, 5272–5301 (2021)

Electrochemical Immunosensor for Diagnosis of COVID-19

Steffane Quaresma Nascimento and Frank N. Crespilho

Abstract An immunosensor is a biosensor that detects antigen interactions using a particular antibody bound on the transducer's surface. These biosensors have high selectivity and sensitivity due to their interaction specificity. Owing to this characteristic, this type of sensor is attractive for several applications, especially in the medical area and bioanalysis. Among the types of immunosensors, electrochemical immunosensors have gained prominence due to their simplicity and portability, potentially enabling in situ detection as promising characteristic for analysis in emergency care. In this chapter, the potential of electrochemical immunosensors is presented, especially in applications related to clinical examinations and mainly in the diagnosis of SARS-CoV-2.

Keywords SARS-CoV-2 · Electrochemical immunosensor · Biomarker · Point-of-care

1 Introduction

The World Health Organization (WHO) declared COVID-19, caused by SARS-CoV-2, a pandemic in 2019 owing to its fast transmission via aerosol droplets, contact, fecal–oral, fomites, and blood. COVID-19 has a high reproduction number of approximately 2.2, a figure that indicates that this disease is highly contagious. Once infected with COVID-19, an individual can be asymptomatic, which makes it more difficult to detect and contain this virus [1, 2]. Given the severity of COVID-19 symptoms, and the high rates of hospitalization and fatality, quick diagnostic tests integrated with current health procedures are needed to track the virus's dissemination and limit the course of the pandemic [3]. The virus is detected using two types of tests: nucleic acid tests, which detect viral RNA; and serological tests, which detect antibodies produced against SARS-CoV-2 antigens [4]. However, due the limitations of nucleic acid tests, such as the need for specialized personnel, robust equipment,

S. Q. Nascimento · F. N. Crespilho (✉)
Laboratory of Bioelectrochemistry and Interfaces—Institute of Chemistry of São Carlos (IQSC), University of São Paulo, São Carlos, São Paulo 13566-590, Brazil
e-mail: frankcrespilho@iqsc.usp.br

F. N. Crespilho (ed.), *COVID-19 Metabolomics and Diagnosis*,
https://doi.org/10.1007/978-3-031-15889-6_4

and a long analysis time, rapid and large-scale diagnosis, and consequently, mild or asymptomatic infections are not diagnosed [5].

Electrochemical immunosensors are an attractive choice due to their high sensitivity, low cost, easy operation, the possibility of miniaturization, and point-of-need diagnostics [6–9]. Electrochemical approaches can be used to identify small changes caused by the recognition event of biomolecules, thereby enabling the use of this type of sensor. In electrochemical sensors, a redox probe is used to indirectly show the effect of this biorecognition reaction through a quantifiable variation in the electrode/solution interface of these devices [10].

In this chapter, we discussed the advances in the development of electrochemical immunosensors for the detection of COVID19 biomarkers, and emphasized the production of miniaturized, portable, sensitive, selective, and flexible biosensors, ultimately revealing biosensors that enable direct or indirect detection. Additionally, we aimed to highlight recent publications in this area. In this chapter, we discussed the following:

(I) Biomarkers: their definition and classification, and the main biomarkers of COVID 19.
(II) Immunosensors: their definition and a description of how they are used. Some literature findings are also presented.
(III) Electrochemical immunosensors: their definition and the main techniques employed with this type of device. Some literature are also presented.
(IV) The recent advances in the diagnosis of COVID19.

2 Biomarkers

A biomarker is a measure used to assess the physiological condition of an organism, the progression of a disease, and the effectiveness of a therapeutic intervention [11]. Biomarkers are employed in several areas, such as the development of new drugs, safety assessment, and clinical analysis [12]. Glucose, RNA, DNA, antigens, proteins, blood pressure, and other chemical and biological components are examples of biomarkers.

Biomarkers are divided into four categories based on their utility: (1) predictive biomarkers, (2) diagnostic biomarkers, (3) prognosis biomarkers, and (4) monitoring biomarkers [13]. Predictive biomarkers provide information that may be used to select the best therapy for a certain condition [14]. Diagnostic biomarkers are biomolecules or chemical reagents that may be used to diagnose or confirm the presence of a disease or condition. A prognostic biomarker is a molecule that indicates whether an event is caused by illness progression or death. [15]. Monitoring biomarkers set the state of a disease or medical condition, and are used in medical tests to identify disease-causing agents [11].

3 Immunosensors

Immunosensors are analytical devices based on the detection of antibody-antigen interaction. This interaction causes a signal change according to the concentration of the analyte under investigation. Immunosensors differ from conventional sensors as they possess great sensitivity, selectivity, stability, and the capacity to detect many targets [16]. The type, quantity, spatial orientation, reactivity, and immobilization method are relevant issues in the development of these devices [17]. It is also critical to select an immunoassay format and transducer that match the features of the material under investigation [18]. Table 1 shows some examples of immunosensors mentioned in the literature.

3.1 Antibodies

Antibodies (immunoglobulins) are specific glycoproteins of the immune system that are produced by the body after contact with an antigen. In serum, antibodies specifically bind to the antigen to neutralize them before they cause harm to the organism [13]. Figure 1 shows a typical image of an antibody. The antibody consists of four polypeptides—two identical heavy chains (VH) and two light chains (VL) [25].

Heavy chains are composed of three constants (CH1, CH2, and CH3) and one variable (VH) that are linked to the hinge region by numerous disulfide bonds that differ depending on the antibody subclass and the host. Light chains consist of two domains—a constant (C_L) and a variable (V_L) linked by disulfide bonds and non-covalent interactions [25]. The heavy chains are found in the Fab and Fc areas, whereas the light chains are found in the Fab region. Three complementarity determining regions (CDRs) are found in the antibody structure. These regions are responsible for the formation of the binding site with the antigen (the region where the antibody interacts with the epitope of the antigen) [26]. In the recognition process, some factors are relevant, such as the antigen and antibody, and the distance between them [27]. When these characteristics are adequate, the formation of non-covalent bonds or hydrogen bonds occurs, which are responsible for immunocomplex formation, and, consequently, responsible for the specific recognition of these molecules. This occurs in the Fab region of the antibody, which is responsible for identifying and engaging with the matching antigen, whereas the Fc region binds to several receptors in a non-specific manner and is mostly employed for antibody immobilization on a surface. Furthermore, the oligosaccharide component (CH2 domain) of the Fc region is important for antibody immobilization [13].

Antibodies differ in terms of antigen specificity and affinity for binding. They can be polyclonal, monoclonal, recombinant, mono or bispecific, chemically modified, or fragmented [28]. Furthermore, amino acid composition, functional binding sites, amount of carbohydrates, size, and charge also differ from antibody to antibody, which indicates that, the choice of an appropriate antibody is essential. Usually, the

Table 1 Immunosensors found in the literature

Biomarker	Biosensor	Detection method	Application	Detection limit	References
P24	PtNCs	Optical/(LFIA)	HIV virus	0.8 pg.mL^{-1}	[19]
NS1	AuNPs	Optical/(LFIA)	Dengue virus	4.5 ŋg.mL^{-1}	[20]
TcdA and TcdB	AuNPs	EIS	Detection of *clostridium difficile*	TcdA: 0.61 pg.mL^{-1} TcdB: 0.60 pg.mL^{-1}	[21]
NDPK-A	CdS nanoparticles and $Mn2^{+}$	PEC	Detection of deterioration of lung cancer and non-Hodgkin lymphoma	0.3 pg mL^{-1}	[22]
CysC	TiO2 nanotube	PEC	Detection of Renal function	0.14 pM	[23]
Apo B-100	Biotinylated	EIS	Detection of Coronary artery disease	0.03 ng mL^{-1}	[24]

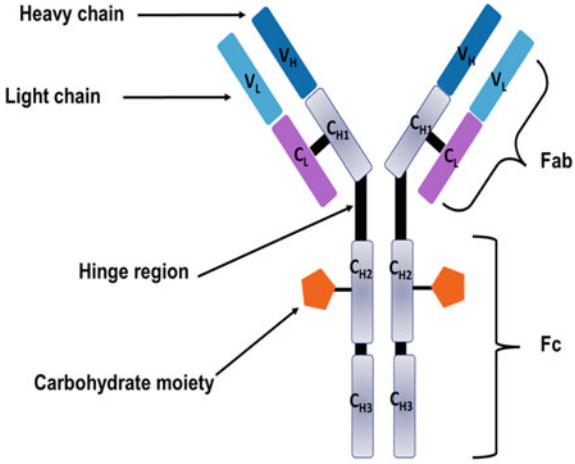

Fig. 1 Typical image of an antibody

immunoglobulin G (IgG) antibodies are selected owning to their greater quantity, better stability, and higher affinity among the immunoglobulin classes [29].

3.2 Immobilization Methods

The antibody and the immobilization method must be considered in the development of sensitive and selective immunosensors for use in samples [30]. For such assays, the antigen-binding on the surface of the antibody and its binding capacity are key characteristics. To obtain a stronger antibody response, the antigen-binding sites must be immobilized correctly. Antibody immobilization methods are divided into two groups random immobilization and targeted immobilization [31] (Fig. 2).

In random immobilization, antibodies are immobilized by physical adsorption. In this configuration, the hydrophobic and electrostatic interactions predominate. This method of immobilization is simple, quick, and affordable, and can produce

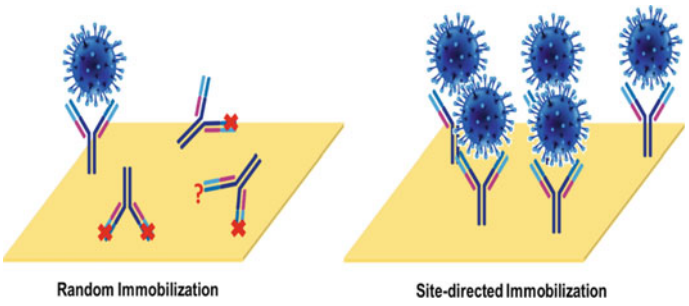

Fig. 2 Antibody immobilization methods—random immobilization and targeted immobilization

strong analytical signals in some instances [32]. However, some antibodies, might denature or undergo conformational changes following interaction with the substrate as it is a physical adsorption. This situation can cause a deficiency in their binding capacity and result in reproducibility problems for this sensor [32]. This problem can be solved with another random immobilization method, in which antibodies are covalently linked to substrates [33]. By using various chemical reagents, the antibody is immobilized in a pre-modified substrate containing active functional groups. Covalent bond formation, repeatability, stability, and appropriate sensitivity are advantages of this approach. Due to the random orientation of the antigen–antibody binding sites, the fundamental drawback of this technique is the reduced availability of antigen–antibody binding sites [31].

Two strategies were reported to solve the random immobilization problem. The first strategy involves the use of the affinity between the Fc region of the antibody with some proteins (protein A, protein G, and domain Z) and other antibodies. These proteins are employed to guarantee correct targeting, in which antibody sites are available for antigen binding, resulting in higher antibody density on the sensor surface than random antibody immobilization approaches [34]. The second technique is based on the binding of the oligosaccharide in Fc region of the antibody, especially in the CH2 domain. This connection can be accomplished via two approaches: the surface Schiff-based formation binds to the oligosaccharide sections of oxidized antibodies (diols converted to aldehydes), or the oligosaccharide portions engage with a boronic acid-modified substrate [35].

In addition to these methods, a new methodology has currently emerged. In this new method, chemically (or genetically) modified antibody fragments are used to interact and promote this orientation [36]. Dithiothreitol can be used to decrease the disulfide linkages in the hinge region of the antibody in this method. In such circumstances, free sulfhydryl groups are employed to covalent immobilization of semiantibody fragments on the pre-modified substrate [36].

Using randomly immobilized antibodies, sensitive, selective, and stable immunosensors may be developed. However, other investigations show that antigen-binding ability is reduced owing to antigen-binding sites on the surface being oriented incorrectly [37]. To build sensitive and selective immunosensors, antibodies must be properly selected and immobilized.

3.3 Immunusensors Format

Three types of immunoassay formats are reported in the literature: (1) direct, (2) sandwich, and (3) competitive. (Fig. 3) [38].

Antibodies are mounted on the sensor surface and interact directly with analytes in a direct immunoassay. Typically, a large quantity of antigen in the sample is required in these sensors to provide superior analytical findings. As a result, without the signal amplification stage, this format is the fastest, simplest, and cheapest, but is also the least sensitive. This format detects large biomarkers [39].

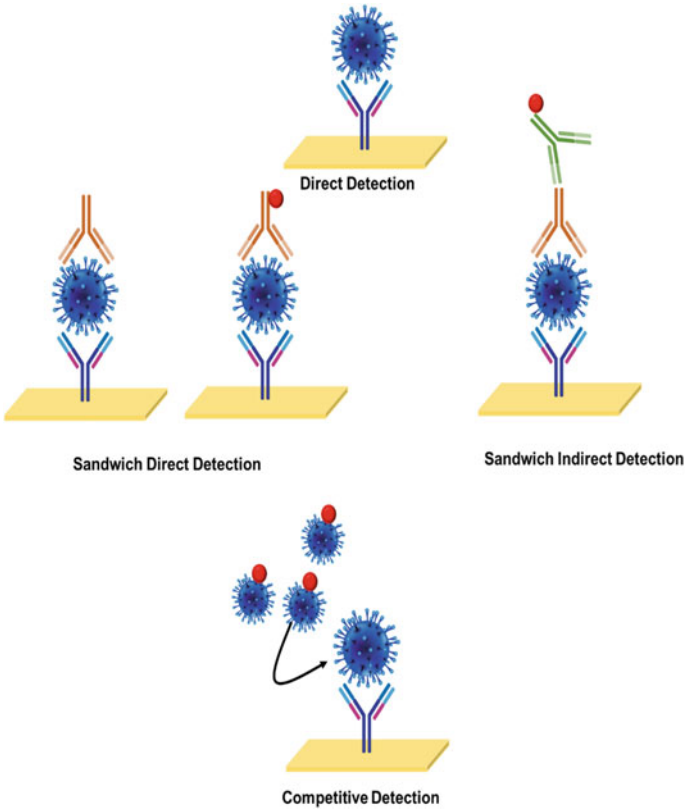

Fig. 3 Types of immunoassay format

The antibodies of capture and detection are utilized in the sandwich immunoassay format. This format is broken down into two parts. In the first stage, capture antibodies mounted on the surface identify and bind with biomarkers. In the second stage, tagged secondary antibodies that bind with the detection antibody (indirect sandwich format) are employed, allowing the analytical signal to be amplified [40]. This immunosensor format allows biomarkers to be detected or quantified in a highly specific and sensitive manner; however, multi-step analysis is associated with a markedly longer duration. Further, it is necessary to select antibodies that bind to different epitopes and that efficiently and do not interfere with each other [40].

In the competitive test (inhibition assay), the antibodies (unlabeled or labeled conjugates) are first interacted with the sample containing the biomarker. The biomarker-antibody combination is then applied to the sensor's surface, which has been pre-modified with a reference biomarker [41]. Binding site antibodies present in the solution depend on the number of biomarkers in the sample. As a result, the reference biomarker competes for binding sites. Immobilized biomarkers can only interact with free antibodies. Further, the quantity of antibodies must remain constant for this

sort of essay; otherwise, the analysis will fail. A competitive immunosensor is used to identify low molecular weight biomarkers. The competitive immunosensor does not suffer from matrix effects and does not require any sample preparation [41].

4 Techniques in Electrochemical Immunosensors

Several electrochemical techniques have been used in immunoassays, such as voltammetric, amperometric, and impedimetric approaches (Fig. 4). Typically, electrochemical experiments are carried out using a three-electrode method (working electrode, reference electrode, and auxiliary electrode) [42]. The working electrode is the component of an electrochemical immunosensor that has been modified with biorecognition elements (antibody or antigen) deposited on the working surface using a ligand [43]. This section covers the methods used to evaluate the effectiveness of such immunosensors.

4.1 Voltammetry

Voltammetry is an electrochemical analytical method that evaluates the current generated as a function of the application of a potential sweep [16]. In electrochemical immunosensors, several voltammetric methods are employed, such as cyclic voltammetry (CV), differential pulse voltammetry (DPV), linear scan voltammetry (LSV), square wave voltammetry (SWV), stripping voltammetry (SV), however, CV, DPV, and SWV. The ability to determine attributes of the materials employed

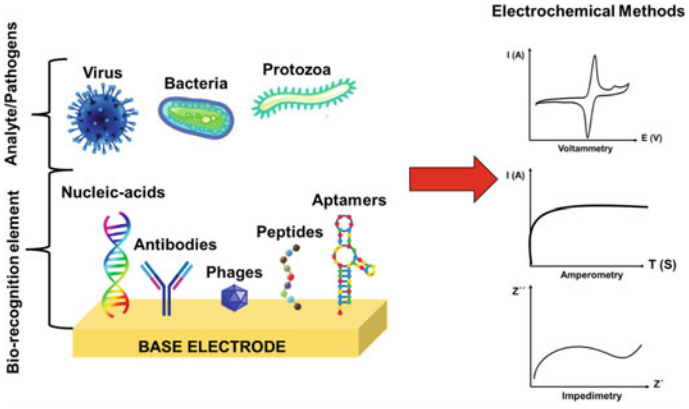

Fig. 4 Techniques used in immunoassays

in the biosensor, such as equilibrium constant in coupled processes, electrochemical reversibility, and electron transfer, is an advantage of voltammetric approaches [44]. Voltammetry is mainly utilized in analytical immunodetection investigations to determine the LOD, LR, sensitivity, and other parameters. Figure 5 shows the main voltammetric techniques and their respective voltammograms

Cyclic voltammetry (CV) is a voltammetric technique that provides information on the electrochemical behavior of electroactive analytes on electrode surfaces [45]. CV is normally used to obtain information about the analyte, such as its mechanism, the number of electrons involved in the feed, the presence of coupled reactions, or whether any adsorption process resulting from the redox reaction exists [45]. Therefore, in electroanalysis, the first step involves recording a cyclic voltammogram. In CV, the potential is swept from an initial potential, E i, (V, volts) at a specific sweep rate (mV/s) to switching or reverse potential (E λ), at which the potential is reversed (digitized in the opposite direction) to the initial potential at the same sweep rate. Several cycles can be performed. If the sweep starts at a potential well below (negative) the formal potential (E^o) of the redox process, only non-faradaic currents flow, that is, current from the redox process of the analyte [45].

The most important parameters obtained by CV are the peak potential (characteristic of each analyte) and peak current (faradaic current correlated with the concentration of the analyte), which are important for the identification of analytes [46]. Thus, CV is a complementary technique to other voltammetric techniques as some information is obtained and used by other voltammetry techniques, such as DPV and SWV.

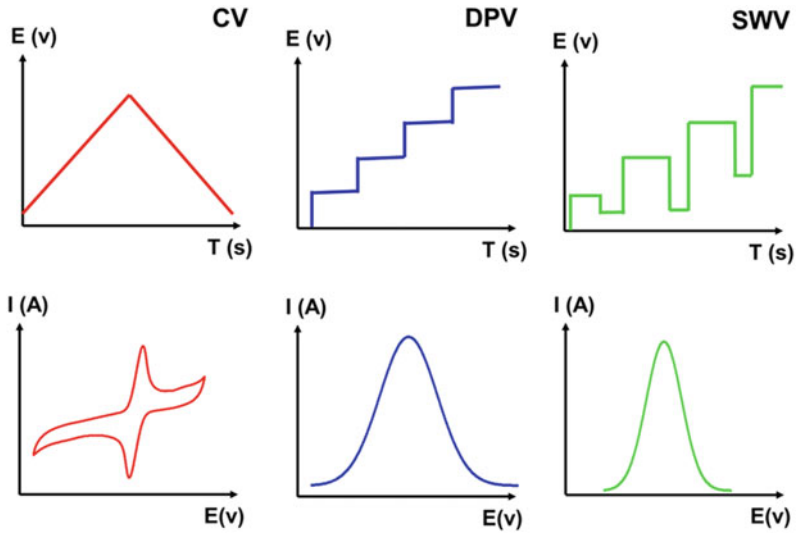

Fig. 5 The main voltammetric techniques with their respective voltammograms.

As previously mentioned, DPV and SWV are the most used electroanalytic techniques. These techniques are more sensitive due to the potential pulse approach. The central principle of these techniques lies in the difference in decay rates between faradaic and non-faradaic currents. Non-faradaic current decays exponentially and thus decay much faster than faradaic current; this is because as faradaic current is inversely proportional to the square root of time. Therefore, in DPV and SWV techniques the non-faradaic current (capacitive current) is negligible, potentially causing lower detection limit with higher sensitivity, which is ideal for bioanalysis [47]. The applicability of these techniques in electroanalysis is depicted in Table 2, which contain some works reported in the literature.

4.2 Amperometry

Amperometry is an electroanalytical technique that measures the current generated from an oxidation–reduction reaction under a constant potential that is proportional to the concentration of this analyte in solution [55]. In recent years, amperometry has been widely used in electroanalysis, due to some characteristics such as high sensitivity and selectivity for electroactive species and a wide range of linear concentration [56]. Owing to the simplicity of this technique, it is easily used in unusual environments and can be integrated into portable and low-cost instrumentation [57]. In biosensors, amperometry is normally used to detect the current variation as a function of the formation of the immune complex (Fig. 6).

Several amperometric biosensors are currently on the market, with glucose biosensors as the main type of amperometric biosensors. These sensors benefit from a large market for glucose biosensors, which are used daily by diabetic patients. Their technique combines the enzyme's selectivity in recognizing a specific target analyte with the direct conversion of the biocatalytic reaction rate into a current signal [45]. Table 3 shows some amperometric immunosensors reported in the literature.

4.3 Electrochemical Impedance Spectroscopy

Electrochemical impedance spectroscopy (EIS) is a technique that offers information on intermolecular interactions by observing the influence on electron transfer resistance (R_{ct}). EIS is an excellent technique for detecting minor changes on the surface of the biosensor and is utilized for interface characterization. The EIS analyzes different frequencies and identifies changes in the diffusion process of each interface from an impedance spectrum [65]. To obtain the R_{ct} values, the impedance spectrum is examined using an electrical equivalent circuit. As illustrated in Fig. 7a, this circuit consists of four elements: ohmic resistance (R), capacitance (Cd), stationary phase element (Rt), and Warburg impedance (Zd) [66].

Table 2 Voltammetric immunosensor found in the literature

Biosensor	Detection method	Linear range	Detection limit	Sample type	Ref
MWCNTs/Ab1	DPV	0.01–100 ng mL^{-1}	5.4 pg mL^{-1}	Serum	[48]
cMWCNTs/Ab1	LSV	0.18 fg mL^{-1}–450 ng mL^{-1}	0.1 fg mL^{-1}	Serum	[49]
MB-Au-rGO/Ab1	SWV	0.001–100 ng mL^{-1}	0.13 pg mL^{-1}	–	[50]
MWCNTs-CHIT/ssDNA-Aptamer	DPV	0.85–12.5 ng mL^{-1}	0.75 ng mL^{-1}	Serum	[51]
AuNPs/rGO/Thio/Aptamer	DPV and CV	0.05–200 ng mL^{-1}	10 pg mL^{-1}	Serum	[52]
MWCNTs-ERGO/AuNPs/Aptamer	DPV and EIS	DPV: 0.005–20 ng mL^{-1} and EIS: 0.005–100 ng mL^{-1}	DPV: 1 pg mL^{-1} and EIS: 1 pg mL^{-1}	Serum	[53]
nanoiniferter/polyEDGMA-CNTs-MnO_2-MIP	SWV and DPV	SWV: 0.99 fg mL^{-1}–5.99 pg mL^{-1} and DPV: 9.99 fg mL^{-1}–9.99 pg mL^{-1}	SWV: 0.25 fg mL^{-1} and DPV: 3.04 gf mL^{-1}	Serum urine	[54]

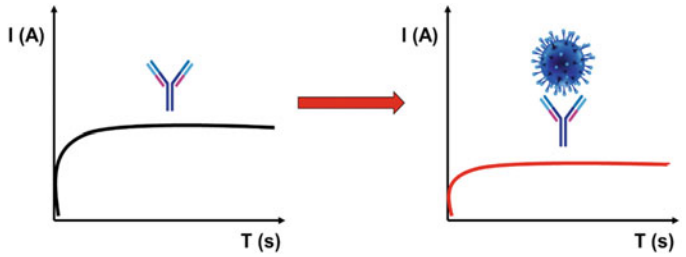

Fig. 6 Variation in amperometric current in function of the formation of the immune complex

To match experimental impedance data (Nyquist plot) with ideal impedance elements, electrical equivalent circuits (Fig. 7a) are utilized. Electrochemical factors such as electrolyte solution resistance, electrode polarization resistance, and double-layer capacitance are evaluated using the Nyquist plot. These numbers are needed to determine the activities in the interface [66]. In a complex plane, the Nyquist plot is given by Z′() and Z″(). EIS may also be studied using the Bode plot in addition to the Nyquist plot (Fig. 7b). The Bode plot is consists of log Z (impedance) on the X-axis and the log f (frequency) on the Y-axis, and the phase angle. Compared to the Nyquist graph, which has frequency values that are more implicit, this graph yields a more explicit explanation of the electrochemical system-dependent behavior and frequency by displaying frequency on one of the axes [67].

The EIS is divided into two categories: faradaic and non-faradaic processes. A redox species is alternatively oxidized/reduced in the faradaic process EIS. As a result, redox-active species and DC conditions must be introduced into the environment in a manner that prevents their consumption. In contrast, no extra reagents are required in EIS of non-faradaic processes, making non-faradaic investigations more appropriate for point-of-care applications [68].

Impedimetric biosensors, such as the biosensors mentioned above, are bioelectronic devices that rely on the unique interaction of a biomolecule with the transducer surface, which modifies the interface characteristics directly or indirectly in EIS investigations [69]. Recently, due to accessibility to impedance instrumentation, there has been an increase in studies on impedance-based biosensors [67]. In these studies, EIS is primarily utilized to regulate the biosensor production process but has also been employed to investigate biosensor diagnostic procedures in recent years [70]. Proteins, nucleic acids, cells, microbes, antibodies, and antigens are among the analytes studied, as indicated in Table 4, which summarizes some of the studies published in the literature.

Table 3 Amperometric immunosensors found in the literature

Biomarker	Biosensor	Linear range	Detection limit	Recovery (%)	Sample type	References
NSE	SiO_2-GOx-Ab_2-MBs	1 pg/mL–100 ng/mL	0.447 pg/mL	94.4–102	Human serum	[58]
CEA	Ab_2-HRP-Au@AgNPs	0.0001–100 ng/mL	0.05 pg/mL	80–100	Human serum	[59]
AFP	PIN-5-COOH	0.001–100 pg/mL	0.33 pg/mL	93.3–109	Human serum	[60]
N-matrix 22	AuNPs-PTNPs-MOFs	0.005–20 ng/mL	1.7 pg/mL	96–106	Urine	[61]
AFP	BSA/Ab/Cu_3Pt NFs	0.1–10,000 pg/mL	0.033 pg/mL	99.4–101.5	Human serum	[62]
Pseudopodium-k1	AuNPs-tagged-AntiPEAK1	10–10^6 pg/mL	10 pg/mL	103–104	Human serum	[63]
Tetrabromobisphenol A bis(2-hydroxyethyl)ether	PS@PEI@CAT@AuNPs@Ab_2	0–27 ng/mL	0.12 ng/mL	78–116	Pure, tap, pond, water	[64]

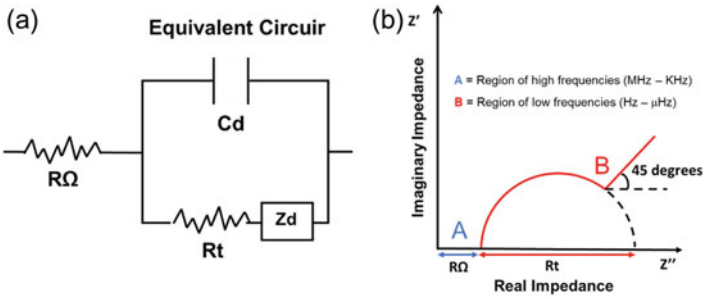

Fig. 7 **a** electrical equivalent circuit, **b** nyquist plot

5 Electrochemical Immunosensors for the Detection of COVID-19

COVID-19, caused by SARS-CoV-2, has been classified as a pandemic by the WHO due to its rapid spread via air droplets, contact, fecal–oral, fomites, and blood. COVID-19 has a high basic reproduction number of approximately 2.2 which highlights it as a highly contagious. Once infected, an individual can be asymptomatic, which makes it difficult to contain this virus [1, 80]. Owing to the severity of the symptoms of COVID-19 and the high rates of hospitalization and mortality, rapid diagnostic tests that are integrated with current health protocols to monitor the spread of the virus and control the progression of the pandemic [3]. In this section, the electrochemical sensors reported in the literature for the diagnosis of COVID19, which are sensors for virus proteins, RNA, and antibodies.

5.1 Electrochemical Detection of SARS-CoV-2 Proteins

The coronavirus nucleocapsid protein is a structural protein that assembles the virus genome and creates a complex with its RNA. According to studies, the large proportion of this protein makes it a possible biomarker for the identification of SARS-CoV-2. Eissa and colleagues (Fig. 8) created an electrochemical sensor that served as a detector and a sample collector for the detection of SARS-CoV-2 N protein using cotton fibers [9]. The viral N protein was immobilized on carbon nanofibers functionalized with benzoic acid through electrodeposition of the diazonium salt. In enriched nasal samples, this sensor employed square wave voltammetry (SWV) as the detection approach and had an LOD of 0.8 pg/mL, selectivity, and recovery of 91 to 95.5%.

A MIP-modified thin-film electrode was utilized by Raziq et al. to make an electrochemical sensor for N protein. Differential pulse voltammetry (DPV) in the presence

Table 4 Impedimetric immunosensors found in the literature

Biomarker	Biosensor	Linear range	Detection limit	Recovery (%)	Sample type	References
CA 19–9	CeO2/FeOx@mC	0.0001–10 U/mL	0.00001 U/mL	95.2–106.4	Human serum	[71]
IgM rheumatoid factor	IDWμE—SAM	1–200 IU/mL	0.22 IU/mL		Human serum	[72]
IFN-γ	PANI—G	5–1000 pg/mL	3.4 pg/mL	101–104	Human serum	[73]
Interleukin 6	PPy—ITO	0.02–16 pg/mL	6 fg/mL	97.10–101.25	Human serum	[74]
TNF α	PET-GPTES	0.01–1.5 pg/mL	3.1 fg/mL	96.51–100.90	Human serum	[75]
P21-k2	GPTMS-anti-PAK2	0.005–0.075 fg/mL	1.5 fg/mL	99.11–102.31	Human serum	[76]
NSE	ITO—P—Thi—g -Man	0.02–4 pg/mL	6.1 fg/mL	100.24–105.52	Human serum	[77]
k1	11-CUTMS	0.036–2.278 pg/mL	10.8 fg/mL	91–109.20	Human serum	[78]
IL 1β	PHA-anti-IL-1 β	0.025–3 pg/mL	7.5 fg/mL	96.7–105.4	Human serum	[79]

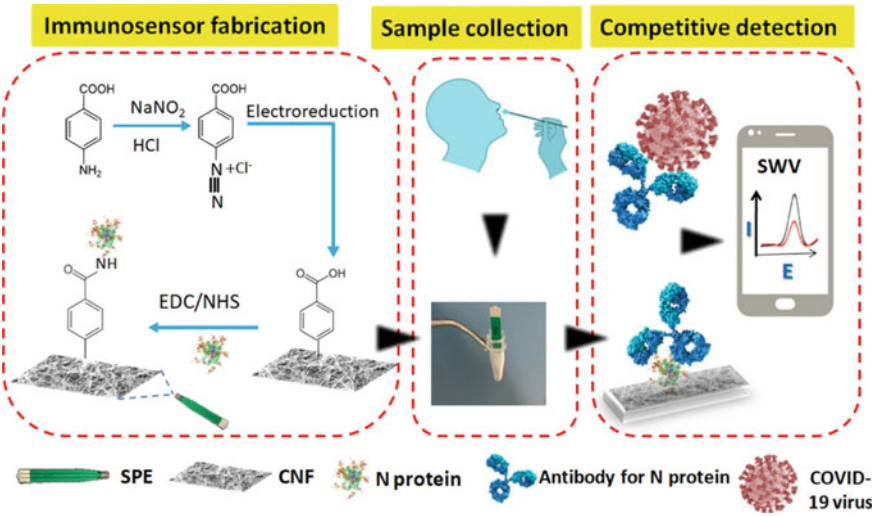

Fig. 8 Schematic electrochemical immunosensor; **a** cotton-tipped collector electrode, **b** carbon nanofiber electrode based biosensor, **c** principle of detection employing. Reprinted with permission of Ref. [9] Copyright2021@American Chemical Society

of a ferri/ferrocyanide redox pair was chosen as the method. The sensor's applicability was investigated in this study by using it on various nasopharyngeal samples from patients. The sensor was found to be repeatable up to a concentration of 111 fM, with LOD of 15 fM and LOQ of 50 fM [81].

The spike protein (Protein S), which plays a key role in the virus's entrance, fusion, and attachment in the organism and serves a potential biomarker, is another important protein for the detection of SARS-CoV-2. Protein S is employed as a diagnostic antigen because coronaviruses have diverse amino acid sequences that enable specific detection of SARS-CoV-2 [80, 82–84]. Vadlmani et al. reported the generation of a novel electrochemical sensor based on cobalt functionalized TiO2 nanotubes. The described sensor could detect the S-RBD protein in the low concentration range of 14–1400 nM, with a LOD of 0.7 nM and an analysis time [82].

Mahari et al. also reported the generation of a device for the detection of the SARS-CoV-2 S protein in enriched saliva samples, based on an internal device (eCovSens). To investigate variations in electrical conductivity using the potentiostat, and the the fluorine-doped tin oxide (FTO) modified with AuNPs and coated with SARS-CoV-2 antibody. The reported immunosensor was found to have a high sensitivity for the SARS-CoV-2 spike antigen, ranging from 1 fM to 1 M, and could detect it in 10–30 s [83].

Torres and associates created a portable real-time impedimetric detection 1.0 prototype (RAPID 1.0). The described immunosensor could measure the influence of the formation of an immune-complex between ACE2 and SARS-CoV-2 on the solution's resistance. With 10 μL of material, the biosensor could identify SARS-CoV-2 in 4 min. Furthermore, RAPID 1.0's specificity and sensitivity for saliva and

nasopharyngeal/oropharyngeal swab samples were 100%, 85.3%, 86.5%, and 100%, respectively, which are exceptional findings for this type of equipment [84].

5.2 Electrochemical Detection of SARS-CoV-2 RNA

Besides the SARS-CoV-2 proteins, devices that detect SARS-CoV-2 genes, RNA, and hybrid DNA have been mentioned in the literature. Alafeef and colleagues revealed a graphene-based biosensor for SARS-CoV-2 N gene detection. Four ssDNA probes were coupled with gold in this device to magnify the signal. With an average incubation period of 5 min, this sensor could detect the target RNA, yielding an LOD of 6.9 copies/L with 231 (copies/L^{-1}). In addition to routine analysis, the sensor was verified using RNA samples collected from SRAS-CoV-2 infected cells, which enabled the distinction of positive COVID-19 samples from negative samples with 100% accuracy and, specificity, and sensitivity, with no substantial difference in the response for samples that did not include a viral target section [85].

Chaibun and colleagues described a system for detecting SARS-CoV-2 genes. Unlike previous studies, their study not only discussed the detection of the N gene, but also S gene (Fig. 9). Of note, the rolling circle amplification (RCA) approach could collaborators. To detect the genes, the gadget employed a method called differential pulse voltammetry. The sensor was able to identify 1 copy/L of S or N viral genes in 2 h and provided 100% accurate findings in actual samples tested by qRT-PCR [1].

Sensors for the RNA and DNA of SARS-CoV-2 may be found in the literature, in addition to those for the genes. The growth of studies in molecular biology and nucleic acid detection methods, particularly during the application of principles used in RT-PCR analysis, has resulted in an increase in the number of publications on this type of sensor [2]. Hwang et al. reported an unlabeled capacitive DNA biosensor made with platinum/titanium electrodes to detect the DNA (Fig. 10). The sensor's sensitivity was 0.843 nF/nM. Furthermore, fluorescence intensity was used to demonstrate the virus's selective detection, and SARS-CoV-2 gene was identified with a fluorescent dye [86].

5.3 Electrochemical Detection of SARS-CoV-2 Antibodies

Antibodies, such as IgM and IgG, were the primary biomarkers used to diagnose SARS-CoV-2 infection at the start of the epidemic. As antibody detection indicates the dynamics of the immune response to the presence of the virus, and how these dynamics may be altered for asymptomatic and symptomatic individuals at different phases of viral infection. The antiviral antibodies, IgG and IgM, can be detected in human serum samples infected with SARS-CoV-2, according to recent research [87–90]. Yakoh and colleagues developed an electrochemical paper (ePAD)-based analytical apparatus for detecting SARS-CoV-2 IgG and IgM. (Fig. 11). The impact

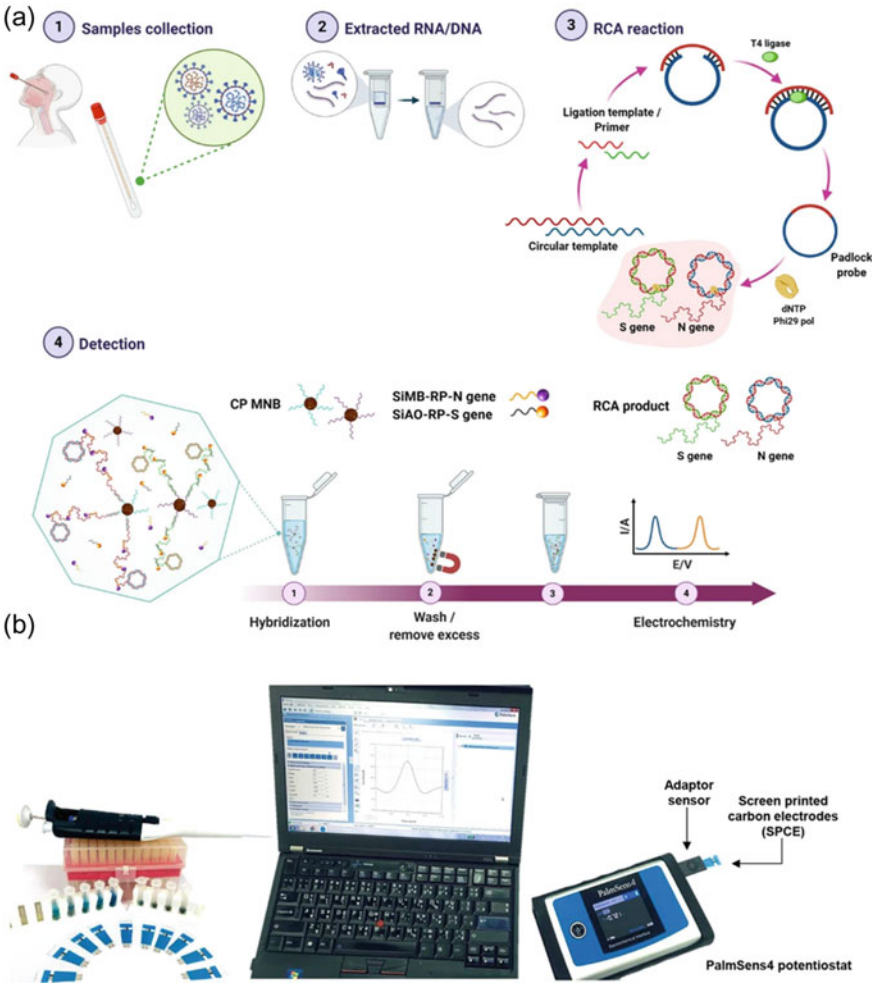

Fig. 9 The detecting platform is described in detail: **a** biosensor of RCA of N and S genes, **b** setup of detection device. Reprinted with permission from Ref. [1] Copyright 2021@Nature

of the presence of the antibody on the redox conversion of $[Fe(CN)_6]^{3/4-}$ was investigated using the square wave voltammetry method. For IgG and IgM, the sensor had an LOD of 0.96 ng/mL and 0.14 ng/mL, respectively. This protocol's cross-reactivity was also evaluated in the presence of different antibodies; however, no cross-reactivity was found [91].

Hashemi et al. presented a system that detect SARS-CoV-2 IgG monoclonal antibodies with extreme precision (Fig. 12). This gadget was created to analyze blood samples from COVID-19-infected individuals. Activated graphene oxide (GO) was combined with Au nanostars to create the sensor (G-Au NS). The sensor was found to have an a LOD of 0.1810 19 V/V and a sensitivity of 2.14 A. V/V cm^2,

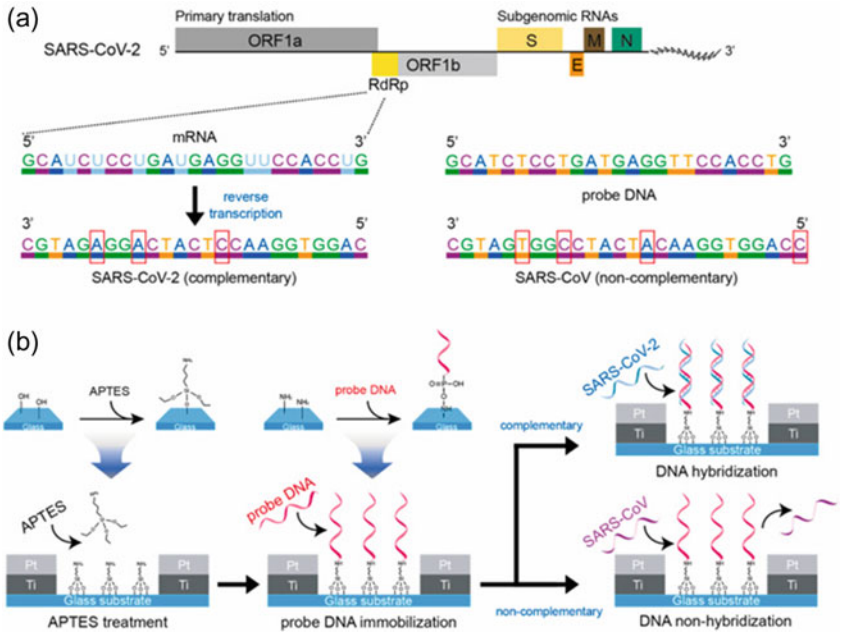

Fig. 10 The IDE biosensor's operating principles for detecting SARS-CoV-2 cDNA: **a** probe DNA sequence schematic using specific mRNA sequences; **b** schematics showing the biosensor fabrication and detection. Reprinted with permission of Ref. [86] Copyright 2021@Elsevier

exhibiting a remarkable correlation with the gold standard (ELISA assay). The sensor's specificity/selectivity were 100%/85% and 95%/100%, respectively [92].

.

A graphene-based Electrical-Electrochemical Vertical Device (EEVD), designed for the serological diagnostic of COVID-19, was proposed by Mattioli et al. [93]. The EEVD proposed by the authors quantifies the SARS-CoV-2 specific Ig G in serum samples, through interactions with the Receptor Binding Domain (RBD) immobilized in the biosensor surface. The combination of graphene basal plane, with high charge carrier mobility, high conductivity, lower intrinsic resistance, and interfacial sensibility to capacitance alterations. The EEVD was applied to real human serum samples. Because EEVD is a miniaturized device, it only requires 40 μL of sample for COVID-19 infection detection at the point-of-care. When compared to serologic assays such as ELISA and other immunochromatographic methods, EEVD has some advantages such as a shorter analysis time (15 min), sample preparation, and a lower limit of detection (LOD) of 1.0 pg mL^{-1}. We see that EEVD meets the principles of robustness and accuracy, which are desirable analytic parameters for pandemic control assays [93] (Fig. 13).

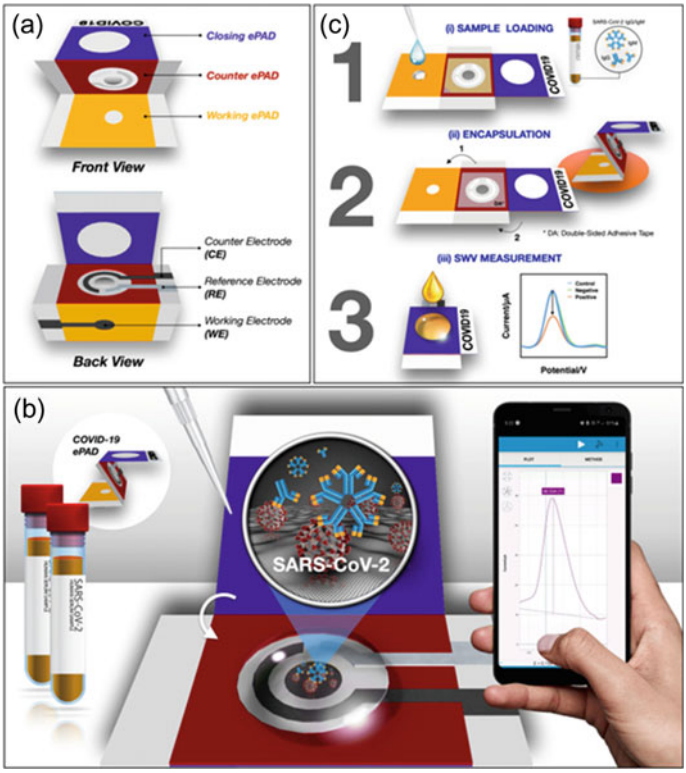

Fig. 11 The schematic figure of **a** biosensor components, **b** biosensor detection principle, and **c** analysis steps of the COVID-19 ePAD. Reprinted with permission of Ref. [91] Copyright 2021@Elsevier

6 Conclusion

The pandemic caused by SARS-CoV-2 revealed the need for low-cost devices and prompt care for the diagnosis of diseases. Currently, most clinical analysis methods are based on analytical techniques that usually require expensive and bulky equipment that are not practical to combat a global pandemic, such as the new coronavirus. Miniaturized electrochemical immunosensors have special advantages, such as portability, low cost, and applicability in emergency care, which reduces the total time of analysis and increases efficiency, characteristics required for coping with highly contagious diseases. As presented in this chapter, electrochemical immunosensors have emerged in the literature as alternatives to traditional methods for detecting SARS-CoV-2. Several factors, such as simplicity, high sensitivity, and selectivity, good compatibility with biological samples were found to be obtained with these biosensors. Finally, the production adopted in the development of each biosensor was presented herein, highlighting the suitability of this technology for application

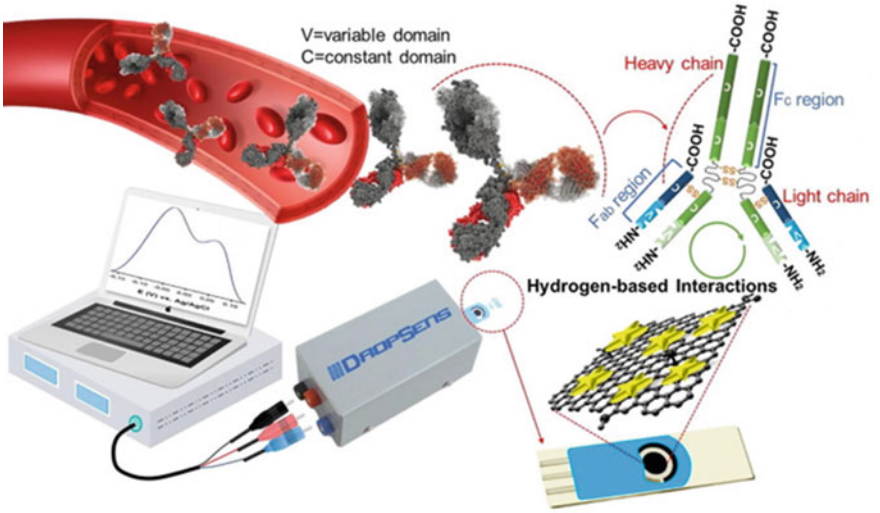

Fig. 12 Scheme of the interaction of the G-Au with IgG antibodies. Reprinted with permission from Ref. [92] Copyright 2021@ Elsevier

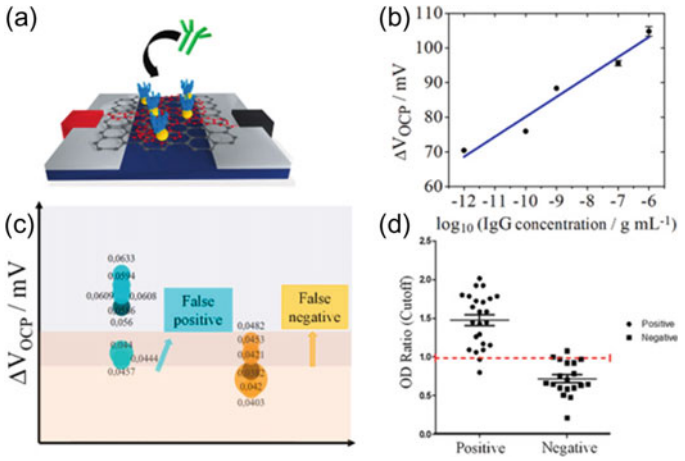

Fig. 13 EEVD biosensor: **a** schematic representation of G-PNR-AuNP/RBD interface; **b** calibration curve for IgG detections; **c** displacement values for positive and negative IgG detections; **d** analysis via ELISA assay from Ref. [93] Copyright 2022@ Elsevier

in clinical analysis. These biosensors are also promising devices for the diagnosis of diseases considering the exponential growth of publications in this area of research.

References

1. T. Chaibun, J. Puenpa, T. Ngamdee, N. Boonapatcharoen, P. Athamanolap, A.P. O'Mullane, S. Vongpunsawad, S. Yong Poovorawan, Y. Lee, B. Lertanantawong, Rapid electrochemical detection of coronavirus SARS-CoV-2. Nat. Commun. **12**, 802 (2021). https://doi.org/10.1038/s41467-021-21121-7
2. G. Qiu, Z. Gai, Y. Tao, J. Schmitt, G.A. Kullak-Ublick, J. Wang, Dual-functional plasmonic photothermal biosensors for highly accurate severe acute respiratory syndrome coronavirus 2 detection. ACS Nano **14**, 5268–5277 (2020). https://doi.org/10.1021/acsnano.0c02439
3. M.Z. Rashed, J.A. Kopechek, M.C. Priddy, K.T. Hamorsky, K.E. Palmer, N. Mittal, J. Valdez, J. Flynn, S.J. Williams, Rapid detection of SARS-CoV-2 antibodies using electrochemical impedance-based detector. Biosens Bioelectron **171** (2021). https://doi.org/10.1016/j.bios.2020.112709
4. I.A. Mattioli, A. Hassan, O.N. Oliveira, F.N. Crespilho, On the challenges for the diagnosis of SARS-CoV-2 based on a review of current methodologies. ACS Sensors **5**, 3655–3677 (2020). https://doi.org/10.1021/acssensors.0c01382
5. I.A. Mattioli, F.N. Crespilho, Problems of interpreting diagnostic tests for SARS-CoV-2: analytical chemistry concerns. Anais da Academia Brasileira de Ciências 92 (2020). https://doi.org/10.1590/0001-3765202020201208
6. J. Kudr, L. Zhao, E.P. Nguyen, H. Arola, T.K. Nevanen, V. Adam, O. Zitka, A. Merkoçi, Inkjet-printed electrochemically reduced graphene oxide microelectrode as a platform for HT-2 mycotoxin immunoenzymatic biosensing. Biosens. Bioelectron. **156**, 112109 (2020). https://doi.org/10.1016/j.bios.2020.112109
7. S. Kurbanoglu, S.A. Ozkan, A. Merkoçi, Nanomaterials-based enzyme electrochemical biosensors operating through inhibition for biosensing applications. Biosens. Bioelectron. **89**, 886–898 (2017). https://doi.org/10.1016/j.bios.2016.09.102
8. L.A. Layqah, S. Eissa, An electrochemical immunosensor for the corona virus associated with the middle east respiratory syndrome using an array of gold nanoparticle-modified carbon electrodes. Microchim. Acta**186** (2019). https://doi.org/10.1007/s00604-019-3345-5
9. S. Eissa, M. Zourob, Development of a low-cost cotton-tipped electrochemical immunosensor for the detection of SARS-CoV-2. Anal. Chem. **93**, 1826–1833 (2021). https://doi.org/10.1021/acs.analchem.0c04719
10. L. Rivas, C.C. Mayorga-Martinez, D. Quesada-González, A. Zamora-Gálvez, A. de la Escosura-Muñiz, A. Merkoçi, Label-free impedimetric aptasensor for ochratoxin—a detection using iridium oxide nanoparticles. Anal. Chem.**87** (2015). https://doi.org/10.1021/acs.analchem.5b00890
11. R.M. Califf, Biomarker definitions and their applications. Exp. Biol. Med. **243**, 213–221 (2018). https://doi.org/10.1177/1535370217750088
12. M.A. Robb, P.M. McInnes, R.M. Califf, Biomarkers and surrogate endpoints. JAMA **315**, 1107 (2016). https://doi.org/10.1001/jama.2016.2240
13. A. Ramanaviciene, K.M. Asta, P. Anton, B. Benediktas, R. Arunas, Design of immunosensors for rapid and sensitive detection of biomarkers. In *The Detection of Biomarkers*, pp. 303–333. Elsevier. (2022). https://doi.org/10.1016/B978-0-12-822859-3.00009-2
14. T.K. Khan, Introduction to Alzheimer's disease biomarkers. In *Biomarkers in Alzheimer's Disease*, pp. 3–23. Elsevier (2016). https://doi.org/10.1016/B978-0-12-804832-0.00001-8
15. L. Maurillo, R. Bassan, N. Cascavilla, F. Cascavilla, Quality of response in acute myeloid leukemia: the role of minimal residual disease. Cancers **11**, 1417 (2019). https://doi.org/10.3390/cancers11101417
16. F.S. Felix, L. Angnes, Electrochemical immunosensors—a powerful tool for analytical applications. Biosens. Bioelectron. **102**, 470–478 (2018). https://doi.org/10.1016/j.bios.2017.11.029
17. H.M. Salvi, G.D. Yadav, Process intensification using immobilized enzymes for the development of white biotechnology. Catal. Sci. Technol. **11**, 1994–2020 (2021). https://doi.org/10.1039/D1CY00020A

18. J.F. Hernández-Rodríguez, D. Rojas, A. Escarpa, Electrochemical sensing directions for next-generation healthcare: trends, challenges, and frontiers. Anal. Chem. **93**, 167–183 (2021). https://doi.org/10.1021/acs.analchem.0c04378
19. C.N. Loynachan, M.R. Thomas, E.R. Gray, D.A. Richards, J. Kim, B.S. Miller, J.C. Brookes et al., Platinum nanocatalyst amplification: redefining the gold standard for lateral flow immunoassays with ultrabroad dynamic range. ACS Nano **12**, 279–288 (2018). https://doi.org/10.1021/acsnano.7b06229
20. A. Fatima, H. Wang, K. Kang, L. Xia, Y. Wang, W. Ye, J. Wang, X. Wang, Development of VHH antibodies against dengue virus type 2 NS1 and comparison with monoclonal antibodies for use in immunological diagnosis. PLoS ONE **9**, e95263 (2014). https://doi.org/10.1371/journal.pone.0095263
21. Z. Zhu, L. Shi, H. Feng, H. Susan Zhou, Single domain antibody coated gold nanoparticles as enhancer for clostridium difficile toxin detection by electrochemical impedance immunosensors. Bioelectrochemistry **101**, 153–158 (2015). https://doi.org/10.1016/j.bioelechem.2014.10.003
22. A. Liu, K. Yin, L. Mi, M. Ma, Y. Liu, Y. Li, W. Wei, Y. Zhang, S. Liu, A novel photoelectrochemical immunosensor by integration of nanobody and ZnO nanorods for sensitive detection of nucleoside diphosphatase kinase-A. Anal. Chim. Acta **973**, 82–90 (2017). https://doi.org/10.1016/j.aca.2017.03.048
23. L. Mi, P. Wang, J. Yan, J. Qian, L. Jusheng, Y. Jiachao, Y. Wang et al., A novel photoelectrochemical immunosensor by integration of nanobody and TiO_2 nanotubes for sensitive detection of serum cystatin C. Anal. Chim. Acta **902**, 107–114 (2016). https://doi.org/10.1016/j.aca.2015.11.007
24. H. Li, J. Yan, O. Weijun, H. Liu, S. Liu, Y. Wan, Construction of a biotinylated cameloid-like antibody for lable-free detection of apolipoprotein B-100. Biosens. Bioelectron. **64**, 111–118 (2015). https://doi.org/10.1016/j.bios.2014.08.060
25. Q. Wang, Y. Chen, J. Park, X. Liu, H. Yifeng, T. Wang, K. McFarland, M.J. Betenbaugh, Design and production of bispecific antibodies. Antibodies **8**, 43 (2019). https://doi.org/10.3390/antib8030043
26. M.M. Al Qaraghuli, K. O. Karina, V.A. Ferro, P.A. Mulheran, Structural analysis of anti-hapten antibodies to identify long-range structural movements induced by Hapten binding. Front. Molecul. Biosci.**8** (2021). https://doi.org/10.3389/fmolb.2021.633526
27. K. Yang, S. Li, L. Liu, Y. Chen, W. Zhou, J. Pei, Z. Liang, L. Zhang, Y. Zhang, Epitope imprinting technology: progress, applications, and perspectives toward artificial antibodies. Adv. Mater. **31**, 1902048 (2019). https://doi.org/10.1002/adma.201902048
28. A.F. Labrijn, M.L. Janmaat, J.M. Reichert, P.W.H.I. Parren, Bispecific antibodies: a mechanistic review of the pipeline. Nat. Rev. Drug Discovery **18**, 585–608 (2019). https://doi.org/10.1038/s41573-019-0028-1
29. K.-L. Wu, Y. Chenfei, C. Lee, C. Zuo, Z.T. Ball, H. Xiao, Precision modification of native antibodies. Bioconjug. Chem. **32**, 1947–1959 (2021). https://doi.org/10.1021/acs.bioconjchem.1c00342
30. F. Ricci, G. Adornetto, G. Palleschi, A review of experimental aspects of electrochemical immunosensors. Electrochim. Acta **84**, 74–83 (2012). https://doi.org/10.1016/j.electacta.2012.06.033
31. A. Kausaite-Minkstimiene, A. Ramanaviciene, J. Kirlyte, A. Ramanavicius, Comparative study of random and oriented antibody immobilization techniques on the binding capacity of immunosensor. Anal. Chem. **82**, 6401–6408 (2010). https://doi.org/10.1021/ac100468k
32. Y. Liu, Y. Jie, Oriented immobilization of proteins on solid supports for use in biosensors and biochips: a review. Microchim. Acta **183**, 1–19 (2016). https://doi.org/10.1007/s00604-015-1623-4
33. Y. Cao, M. Zheng, W. Cai, Z. Wang, Enzyme-loaded liposome with biocatalytic precipitation for potentiometric immunoassay of thyroid-stimulating hormone in thyroid carcinoma. Chin. Chem. Lett. **31**, 463–467 (2020). https://doi.org/10.1016/j.cclet.2019.06.024

34. A. Makaraviciute, A. Ramanaviciene, Site-directed antibody immobilization techniques for immunosensors. Biosens. Bioelectron. **50**, 460–471 (2013). https://doi.org/10.1016/j.bios.2013.06.060
35. P.K. Qasba, Glycans of antibodies as a specific site for drug conjugation using glycosyltransferases. Bioconjug. Chem. **26**, 2170–2175 (2015). https://doi.org/10.1021/acs.bioconjchem.5b00173
36. J. Kalecki, Z. Iskierko, M. Cieplak, P.S. Sharma, Oriented immobilization of protein templates: a new trend in surface imprinting. ACS Sensors **5**, 3710–3720 (2020). https://doi.org/10.1021/acssensors.0c01634
37. Z. Balevicius, A. Ramanaviciene, I. Baleviciute, A. Makaraviciute, L. Mikoliunaite, A. Ramanavicius, Evaluation of intact- and fragmented-antibody based immunosensors by total internal reflection ellipsometry. Sens. Actuators, B Chem. **160**, 555–562 (2011). https://doi.org/10.1016/j.snb.2011.08.029
38. K.E. Sapsford, P.T. Charles, C.H. Patterson, F.S. Ligler, Demonstration of four immunoassay formats using the array biosensor. Anal. Chem. **74**, 1061–1068 (2002). https://doi.org/10.1021/ac0157268
39. D. Pan, G. Li, H. Huizhen, H. Xue, M. Zhang, M. Zhu, X. Gong, Y. Zhang, Y. Wan, Y. Shen, Direct immunoassay for facile and sensitive detection of small molecule aflatoxin B_1 based on nanobody. Chem. Eur. J. **24**, 9869–9876 (2018). https://doi.org/10.1002/chem.201801202
40. H. Ueda, Open sandwich immunoassay: a novel immunoassay approach based on the interchain interaction of an antibody variable region. J. Biosci. Bioeng. **94**, 614–619 (2002). https://doi.org/10.1016/S1389-1723(02)80203-1
41. S.A. Lim, M.U. Ahmed, CHAPTER 1. Introduction to Immunosensors, pp. 1–20 (2019). https://doi.org/10.1039/9781788016162-00001
42. J.Y. Kim, M. Park, Recent progress in electrochemical immunosensors. Biosensors **11**, 360 (2021). https://doi.org/10.3390/bios11100360
43. M. Kuldeep, S. Kumar, A. Srivastava, P.K. Maurya, R. Singh, P. Chandra, Electrochemical immunosensors. In *Handbook of immunoassay technologies*, 359–414 (2018). Elsevier. https://doi.org/10.1016/B978-0-12-811762-0.00014-1
44. N.J. Ronkainen, H. Brian Halsall, W.R. Heineman, Electrochemical biosensors. Chem. Soc. Rev. **39**, 1747 (2010). https://doi.org/10.1039/b714449k
45. A.J. Bard, L.R. Faulkner. *Electrochemical Methods: Fundamentals and Applications*
46. N. Elgrishi, K.J. Rountree, B.D. McCarthy, E.S. Rountree, T.T. Eisenhart, J.L. Dempsey, A practical beginner's guide to cyclic voltammetry. J. Chem. Educ. **95**, 197–206 (2018). https://doi.org/10.1021/acs.jchemed.7b00361
47. A. Chen, B. Shah, Electrochemical sensing and biosensing based on square wave voltammetry. Anal. Methods **5**, 2158 (2013). https://doi.org/10.1039/c3ay40155c
48. J. Yang, W. Wen, X. Zhang, S. Wang, Electrochemical immunosensor for the prostate specific antigen detection based on carbon nanotube and gold nanoparticle amplification strategy. Microchim. Acta **182**, 1855–1861 (2015). https://doi.org/10.1007/s00604-015-1523-7
49. X. Qin, X. Aigui, L. Liu, W. Deng, C. Chen, Y. Tan, F. Yingchun, Q. Xie, S. Yao, Ultrasensitive electrochemical immunoassay of proteins based on in situ duple amplification of gold nanoparticle biolabel signals. Chem. Commun. **51**, 8540–8543 (2015). https://doi.org/10.1039/C5CC01439E
50. J. Feng, H. Wang, Z. Ma, Ultrasensitive amperometric immunosensor for the prostate specific antigen by exploiting a Fenton reaction induced by a metal-organic framework nanocomposite of type Au/Fe-MOF with peroxidase mimicking activity. Microchim. Acta **187**, 95 (2020). https://doi.org/10.1007/s00604-019-4075-4
51. F. Tahmasebi, A. Noorbakhsh, Sensitive electrochemical prostate specific antigen aptasensor: effect of carboxylic acid functionalized carbon nanotube and glutaraldehyde linker. Electroanalysis **28**, 1134–1145 (2016). https://doi.org/10.1002/elan.201501014
52. B. Wei, K. Mao, N. Liu, M. Zhang, Z. Yang, Graphene nanocomposites modified electrochemical aptamer sensor for rapid and highly sensitive detection of prostate specific antigen. Biosens. Bioelectron. **121**, 41–46 (2018). https://doi.org/10.1016/j.bios.2018.08.067

53. E. Heydari-Bafrooei, N.S. Shamszadeh, Electrochemical bioassay development for ultrasensitive aptasensing of prostate specific antigen. Biosens. Bioelectron. **91**, 284–292 (2017). https://doi.org/10.1016/j.bios.2016.12.048
54. S. Patra, E. Roy, R. Madhuri, P.K. Sharma, Nano-iniferter based imprinted sensor for ultra trace level detection of prostate-specific antigen in both men and women. Biosens. Bioelectron. **66**, 1–10 (2015). https://doi.org/10.1016/j.bios.2014.10.076
55. A. Aziz, H. Mohammadi, Amperometry. In *Reference Module in Chemistry, Molecular Sciences and Chemical Engineering*. Elsevier (2018). https://doi.org/10.1016/B978-0-12-409547-2.14204-0
56. A.P.F. Turner, Biosensors: sense and sensibility. Chem. Soc. Rev. **42**, 3184 (2013). https://doi.org/10.1039/c3cs35528d
57. R.A.S. Couto, J.L.F.C. Lima, M.B. Quinaz, Recent developments, characteristics and potential applications of screen-printed electrodes in pharmaceutical and biological analysis. Talanta **146**, 801–814 (2016). https://doi.org/10.1016/j.talanta.2015.06.011
58. S. Yin, Z. Ma, "Smart" sensing interface for the improvement of electrochemical immunosensor based on enzyme-Fenton reaction triggered destruction of Fe^{3+} cross-linked alginate hydrogel. Sens. Actuators, B Chem. **281**, 857–863 (2019). https://doi.org/10.1016/j.snb.2018.11.030
59. P. Chen, X. Hua, J. Liu, H. Liu, F. Xia, D. Tian, C. Zhou, A dual amplification electrochemical immunosensor based on HRP-Au@Ag NPs for carcinoembryonic antigen detection. Anal. Biochem. **574**, 23–30 (2019). https://doi.org/10.1016/j.ab.2019.03.003
60. T. Yang, X. Ren, M. Yang, X. Li, K. He, A. Rao, Y. Wan, H. Yang, S. Wang, Z. Luo, A highly sensitive label-free electrochemical immunosensor based on poly(indole-5-carboxylicacid) with ultra-high redox stability. Biosens. Bioelectron. **141**, 111406 (2019). https://doi.org/10.1016/j.bios.2019.111406
61. S. Zhao, Y. Zhang, S. Ding, J. Fan, Z. Luo, K. Liu, Q. Shi, W. Liu, G. Zang, A highly sensitive label-free electrochemical immunosensor based on AuNPs-PtNPs-MOFs for nuclear matrix protein 22 analysis in urine sample. J. Electroanal. Chem. **834**, 33–42 (2019). https://doi.org/10.1016/j.jelechem.2018.12.044
62. A.-J. Wang, X.-Y. Zhu, Y. Chen, P.-X. Yuan, X. Luo, J.-J. Feng, A label-free electrochemical immunosensor based on rhombic dodecahedral Cu3Pt nanoframes with advanced oxygen reduction performance for highly sensitive alpha-fetoprotein detection. Sens. Actuators, B Chem. **288**, 721–727 (2019). https://doi.org/10.1016/j.snb.2019.03.061
63. K.S. Prasad, X. Cao, N. Gao, Q. Jin, S.T. Sanjay, G. Henao-Pabon, XiuJun Li, A low-cost nanomaterial-based electrochemical immunosensor on paper for high-sensitivity early detection of pancreatic cancer. Sens. Actuators, B Chem. **305**, 127516 (2020). https://doi.org/10.1016/j.snb.2019.127516
64. S. Dong, S. Wang, E. Gyimah, N. Zhu, K. Wang, W. Xiangyang, Z. Zhang, A novel electrochemical immunosensor based on catalase functionalized AuNPs-loaded self-assembled polymer nanospheres for ultrasensitive detection of tetrabromobisphenol A bis(2-hydroxyethyl) ether. Anal. Chim. Acta **1048**, 50–57 (2019). https://doi.org/10.1016/j.aca.2018.10.018
65. E.P. Randviir, C.E. Banks, Electrochemical impedance spectroscopy: an overview of bioanalytical applications. Anal. Methods **5**, 1098 (2013). https://doi.org/10.1039/c3ay26476a
66. F. Ciucci, Modeling electrochemical impedance spectroscopy. Curr. Opin. Electrochem. **13**, 132–139 (2019). https://doi.org/10.1016/j.coelec.2018.12.003
67. M.E. Strong, J.R. Richards, M. Torres, C.M. Beck, J.T. la Belle, Faradaic electrochemical impedance spectroscopy for enhanced analyte detection in diagnostics. Biosens. Bioelectron. **177**, 112949 (2021). https://doi.org/10.1016/j.bios.2020.112949
68. C. Ibau, M.K. Md Arshad, S.C.B. Gopinath, M.N. Nuzaihan, M.F.M. Fathil, S.A. Shamsuddin, Immunosensing prostate-specific antigen: faradaic vs non-Faradaic electrochemical impedance spectroscopy analysis on interdigitated microelectrode device. Int. J. Biol. Macromol. **162**, 1924–1936 (2020). https://doi.org/10.1016/j.ijbiomac.2020.08.125
69. F. Lisdat, D. Schäfer, The use of electrochemical impedance spectroscopy for biosensing. Anal. Bioanal. Chem. **391**, 1555–1567 (2008). https://doi.org/10.1007/s00216-008-1970-7

70. J.L. Hammond, N. Formisano, P. Estrela, S. Carrara, J. Tkac, Electrochemical biosensors and nanobiosensors. Essays Biochem. **60**, 69–80 (2016). https://doi.org/10.1042/EBC20150008
71. M. Wang, H. Mengyao, H. Bin, C. Guo, Y. Song, Q. Jia, L. He, Z. Zhang, S. Fang, Bimetallic cerium and ferric oxides nanoparticles embedded within mesoporous carbon matrix: electrochemical immunosensor for sensitive detection of carbohydrate antigen 19–9. Biosens. Bioelectron. **135**, 22–29 (2019). https://doi.org/10.1016/j.bios.2019.04.018
72. S.R. Chinnadayyala, J. Park, M.A. Abbasi, S. Cho, Label-free electrochemical impedimetric immunosensor for sensitive detection of IgM rheumatoid factor in human serum. Biosens. Bioelectron. **143**, 111642 (2019). https://doi.org/10.1016/j.bios.2019.111642
73. N. Ruecha, K. Shin, O. Chailapakul, N. Rodthongkum, Label-free paper-based electrochemical impedance immunosensor for human interferon gamma detection. Sens. Actuators, B Chem. **279**, 298–304 (2019). https://doi.org/10.1016/j.snb.2018.10.024
74. E.B. Aydın, Highly sensitive impedimetric immunosensor for determination of interleukin 6 as a cancer biomarker by using conjugated polymer containing epoxy side groups modified disposable ITO electrode. Talanta **215**, 120909 (2020). https://doi.org/10.1016/j.talanta.2020.120909
75. B.A. Elif, A label-free and sensitive impedimetric immunosensor for TNF α biomarker detection based on epoxysilane-modified disposable ITO-PET electrode. Int. J. Environ. Anal. Chem. **100**, 363–377 (2020). https://doi.org/10.1080/03067319.2019.1679807
76. N. Yılmaz, E.B. Aydın, M.K. Sezgintürk, An epoxysilane modified indium tin oxide electrode for the determination of PAK 2: application in human serum samples. Anal. Chim. Acta **1062**, 68–77 (2019). https://doi.org/10.1016/j.aca.2019.02.020
77. M. Aydın, E.B. Aydın, M.K. Sezgintürk, A highly selective poly(thiophene)-graft-poly(methacrylamide) polymer modified ITO electrode for neuron specific enolase detection in human serum. Macromol. Biosci. **19**, 1900109 (2019). https://doi.org/10.1002/mabi.201900109
78. H. Törer, E.B. Aydın, M.K. Sezgintürk, A label-free electrochemical biosensor for direct detection of RACK 1 by using disposable, low-cost and reproducible ITO based electrode. Anal. Chim. Acta **1024**, 65–72 (2018). https://doi.org/10.1016/j.aca.2018.04.031
79. E.B. Aydın, M.K. Sezgintürk, A disposable and ultrasensitive ITO based biosensor modified by 6-phosphonohexanoic acid for electrochemical sensing of IL-1β in human serum and saliva. Anal. Chim. Acta **1039**, 41–50 (2018). https://doi.org/10.1016/j.aca.2018.07.055
80. G. Liu, J.F. Rusling, COVID-19 antibody tests and their limitations. ACS Sensors **6**, 593–612 (2021). https://doi.org/10.1021/acssensors.0c02621
81. A. Raziq, A. Kidakova, R. Boroznjak, J. Reut, A. Öpik, V. Syritski, Development of a portable MIP-based electrochemical sensor for detection of SARS-CoV-2 antigen. Biosens. Bioelectron. **178**, 113029 (2021). https://doi.org/10.1016/j.bios.2021.113029
82. B.S. Vadlamani, T. Uppal, S.C. Verma, M. Misra, Functionalized TiO_2 nanotube-based electrochemical biosensor for rapid detection of SARS-CoV-2. Sensors **20**, 5871 (2020). https://doi.org/10.3390/s20205871
83. S. Mahari, A. Roberts, D. Shahdeo, S. Gandhi, eCovSens-ultrasensitive novel in-house built printed circuit board based electrochemical device for rapid detection of nCovid-19 antigen, a spike protein domain 1 of SARS-CoV-2. *BIORXIV* (2020)
84. M.D.T. Torres, W.R. de Araujo, L.F. de Lima, A.L. Ferreira, C. de la Fuente-Nunez, Low-cost biosensor for rapid detection of SARS-CoV-2 at the point of care. Matter **4**, 2403–2416 (2021). https://doi.org/10.1016/j.matt.2021.05.003
85. M. Alafeef, K. Dighe, P. Moitra, D. Pan, Rapid, ultrasensitive, and quantitative detection of SARS-CoV-2 using antisense oligonucleotides directed electrochemical biosensor chip. ACS Nano **14**, 17028–17045 (2020). https://doi.org/10.1021/acsnano.0c06392
86. C. Hwang, N. Park, E.S. Kim, S. Miran Kim, D. Kim, S. Park, N.Y. Kim, J.H. Kim, Ultrafast and recyclable DNA biosensor for point-of-care detection of SARS-CoV-2 (COVID-19). Biosens. Bioelectron. **185**, 113177 (2021). https://doi.org/10.1016/j.bios.2021.113177

87. X. Li, Z. Qin, F. Hao, T. Li, R. Peng, Z. Li, J.M. Rini, X. Liu, Enhancing the performance of paper-based electrochemical impedance spectroscopy nanobiosensors: an experimental approach. Biosens. Bioelectron. **177**, 112672 (2021). https://doi.org/10.1016/j.bios.2020.112672
88. N.P. Shetti, A. Mishra, S.D. Bukkitgar, S. Basu, J. Narang, K.R. Reddy, T.M. Aminabhavi, Conventional and nanotechnology-based sensing methods for SARS coronavirus (2019-nCoV). ACS Appl. Bio Mater. **4**, 1178–1190 (2021). https://doi.org/10.1021/acsabm.0c01545
89. Z. Fan, B. Yao, Y. Ding, J. Zhao, M. Xie, K. Zhang, Entropy-driven amplified electrochemiluminescence biosensor for RdRp gene of SARS-CoV-2 detection with self-assembled DNA tetrahedron scaffolds. Biosens. Bioelectron. **178**, 113015 (2021). https://doi.org/10.1016/j.bios.2021.113015
90. H. Ma, W. Zeng, H. He, D. Zhao, D. Jiang, P. Zhou, L. Cheng, Y. Li, X. Ma, T. Jin, Serum IgA, IgM, and IgG responses in COVID-19. Cell. Mol. Immunol. **17**, 773–775 (2020). https://doi.org/10.1038/s41423-020-0474-z
91. A. Yakoh, U. Pimpitak, S. Rengpipat, N. Hirankarn, O. Chailapakul, S. Chaiyo, Paper-based electrochemical biosensor for diagnosing COVID-19: detection of SARS-CoV-2 antibodies and antigen. Biosens. Bioelectron. **176**, 112912 (2021). https://doi.org/10.1016/j.bios.2020.112912
92. A. Hashemi, S.B. Seyyed, S.M. Mousavi, N. Omidifar, N.G.G. Behbahan, M. Arjmand, S. Ramakrishna et al., Ultra-precise label-free nanosensor based on integrated graphene with Au nanostars toward direct detection of IgG antibodies of SARS-CoV-2 in blood. J. Electroanal. Chem. **894**, 115341 (2021). https://doi.org/10.1016/j.jelechem.2021.115341
93. I.A. Mattioli, K.R. Castro, L.J.A. Macedo, G.C. Sedenho, M.N. Oliveira, I. Todeschini, P.M. Vitale et al., Graphene-based hybrid electrical-electrochemical point-of-care device for serologic COVID-19 diagnosis. Biosens. Bioelectron. **199**, 113866 (2022). https://doi.org/10.1016/j.bios.2021.113866

Optical Fibers Sensors for Detection of SARS-CoV-2 Infection

Daniel S. Francisco, Renato G. Capelo, Ricardo S. Baltieri, and Danilo Manzani

Abstract In this chapter, the main techniques that use light to monitor and detect viruses and biomolecules will be presented, including Surface-Enhanced Raman Spectroscopy (SERS), Localized-Surface Plasmon Resonance (SPR), luminescence, and others. It will also be discussed the devices used to build biosensors and, in addition, the chemical modifications in waveguides to improve and innovate such technologies. Besides, it will also address how optical devices and materials are being explored in the detection and diagnosis of the new coronavirus, as some aspects related to the biological structure of SARS-CoV-2 and its detection.

Keywords Optical biosensors · Photonic devices · Fiber optics

1 Fundamentals

Biosensors are devices that incorporate a biological sensing element and can detect biomolecules in chemically complex samples. Optical biosensors are the most reported class of sensors having many advantages including real-time detection, easy miniaturization, safety, and cost-effectiveness. As well as the small size, capacity of miniaturization, and the friendly use makes it an alternative method to be point-of-care for ills and virus detection [1]. The development of optical biosensors has been mainly regarding environmental applications and monitoring, the biotechnology industry, and healthcare for the detection of, for example, Ebola, triglycerides [2], HIV, influenza virus [3], dengue [4], and others [5].

In general, an optical biosensor involves an analyte to be monitored or detected and is constituted by a biorecognition element, an optical transducer, and signal output that is treated, as shown in Fig. 1 [6]. To achieve high specificity and sensitivity, the sensors need to use a suitable biorecognition element that includes biostructures like enzymes, antibodies, nucleic acids, cells, receptors, and so on. The choice of

D. S. Francisco · R. G. Capelo · R. S. Baltieri · D. Manzani (✉)
Laboratory of Inorganic and Vitreous Materials (LaMIV), São Carlos Institute of Chemistry, University of São Paulo, São Carlos, São Paulo, Brazil
e-mail: dmanzani@usp.br

F. N. Crespilho (ed.), *COVID-19 Metabolomics and Diagnosis*,
https://doi.org/10.1007/978-3-031-15889-6_5

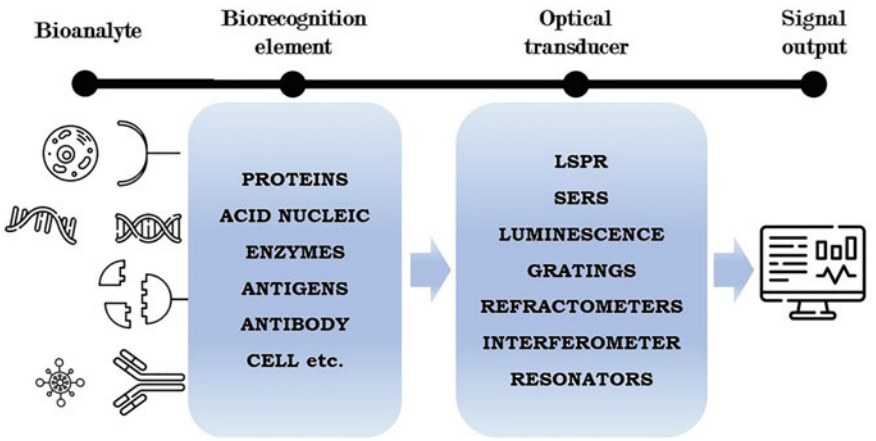

Fig. 1 General flowchart of an optical biosensor

biorecognition element occurs in the function of affinity and specificity interaction with the analyte which needs result in a distinguishable optical signal [7].

Regarding an optical signal, the optical biosensor can be divided into two broads: label-based and label-free. In summary, label-free sensors generate the signal directly by the interaction of the target molecule and the transducer. Localized-Surface Plasmon Resonance (SPR) and Surface-Enhanced Raman Scattering (SERS) based sensors, for instance, are often reported as label-free method. On the other hand, the label-based sensor involves an extra component, a label, that will generate a signal by a colorimetric, electric signal, or fluorescent method.

Particularly, biosensors must recognize a variety of complex samples. In the case of virus detection, many parts can be used to identify the ill like proteins or RNA sequence. The structure of SARS-CoV-2, like other viruses, is complex and can be hard to accurately diagnose with all desirable characteristics of an ideal biosensor. Such attributes include low cost, high sensibility and specificity, quantitative, reusable, easy to clean, and ability to operate with fast results [8]. Coronavirus pathogens have six main proteins in their structure: spike (S), small membrane (E), membrane (M), hemagglutinin-esterase (HE), nucleocapsid (N), and internal (I) proteins [9].

Each structural protein has a specific function in viral infection and replication into the body. Among these proteins, the main interest remains in the spike proteins and nucleocapsid proteins. The S protein is responsible for recognizing and entering the human cell through the Recognized Binding Domain (RBD) localized in one of its two subunits, S1 [9]. The N protein of SARS-CoV-2, differently from the other six coronavirus family with the largest RNA genome, is one of its functions that act in the genome packaging of viral RNA in the virus [10, 11]. Different optical approaches are used to detect such proteins, like SPR, SERS, and chemiluminescence (CL). Properties of N protein can be detected using specific RNA interaction as in the Reverse Transcription Polymerase Chain Reaction (RT-PCR) test. However,

variations in the test results were assigned to variations in the RNA sequences when using some genes such as ORF1ab gene and N genes can affect the test and thus cause false-negative diagnostics [12]. To overcome the issue of N protein mutations on RNA, some recent works have developed biological components that can selectively identify the SARS-CoV-2 from another virus, even for the SARS-CoV [13]. Using N protein as a target molecule is useful for early diagnosis because at this stage the human body does not start producing antibodies and the N protein is the most present protein in Covid-19 [14].

Although there are tests and technologies for N protein detection, they are not quantitative or require skilled labor and expansive equipment, for example, RT-PCR or Mass Spectrometry essay [15], that is suitable for research but not for large-scale use. Since the discovery of the first coronaviruses and their potential to cause Severe Acute Respiratory Syndrome (SARS), modifications have been sought to make their identification cheaper and easier, such as an enzyme-linked immunosorbent assay using chemiluminescence to identify SARS-Cov [16], Recently, aptamers-based sensors are explored to give high selectivity to biosensors. Aptamers are optimized for the nucleic acids (mainly RNA or DNA) for high-affinity binding to a given target. This biorecognition element originated from in vitro selection sequence libraries named Systematic Evolution of Ligands by Exponential Enrichment (SELEX), which, starting from random sequence libraries, is used with other elements to generate a signal output [17, 18]. This kind of device has been explored in Lateral Flow Assay with a Limit of Detection of 1 ng mL^{-1} by the naked eye [13]. A combination of aptamer immunocomplexes modified to bind specifically with SARS-Cov-2 with an optical analysis can provide a rapid and cost-effective test. In this case, DNA aptamers are used to bind with SARS-Cov-2 N protein and then generate a chemiluminescent signal quantified by fluorescent image analysis [19].

The antibody also can be used to detect Covid-19 as a recognition element for S or N proteins, which can be assembled in different ways to generate an optical output response. It is possible to use a sandwich assay as demonstrated by Divagar et al. [20] who used an optical fiber biosensor built as a sandwich immunoassay of AuNP/IgG1/Covid-19 N Protein/IgG2-Fiber for virus detection by localized plasmonic absorbance [20]. Sandwich immunoassay is the most common assembly used in optical biosensors, such as fluorescent sensors. They also can be arranged as a direct immunoassay, competitive immunoassay, or displacement immunoassay, as shown in Fig. 2. Direct detection works on the optical properties of the antigen that modifies a signal when bounded with the antibody. The competitive immunoassay shown in Fig. 2b has two modes, in the first one the antibody is immobilized and there is competition for the binding sites between the target molecule and a labeled target [21]. The second mode is quite similar but the target is immobilized and the antibody is labeled. The most used configuration for detecting target molecules is the sandwich immunoassay. Firstly, the target molecule in the solution is captured by an antibody immobilized on the substrate. Later, a second labeled antibody (reporter antibody or detection) binds to the target molecule resulting in a measured complex (Fig. 2c). At last, in displacement immunoassay, the immobilized antibody is firstly

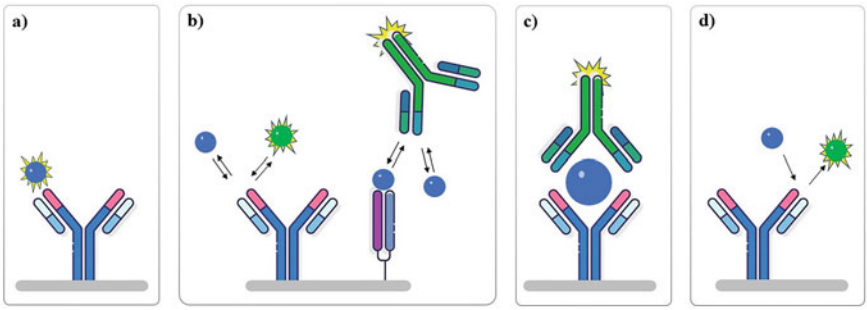

Fig. 2 Classification of (bio)mimetic **a** direct immunoassay; **b** competitive immunoassay; **c** sandwich immunoassay; **d** displacement immunoassay [22]

saturated with an excess of labeled antigen until getting a stable signal. Then, the addition of the target molecule leads to a displacement of the labeled antigen whose signal change is proportional to the concentration of the target molecule [22].

2 Optical Techniques for Covid-19 Detection

2.1 Surface-Enhanced Raman Spectroscopy (SERS)

Surface-enhanced Raman scattering (SERS) is a fundamental technique used in several fields including chemistry, biochemistry, and material science. The great use of this powerful tool is due to its intrinsic characteristics and technological advances that have reduced the cost and increased the sensitivity of SERS measurements. The SERS phenomenon was demonstrated for the first time by Fleischmann et al. in 1974 [23], showing an unpredictable broad Raman signal from pyridine adsorbed on a silver electrode. Thereafter, some researchers studied and confirmed the SERS by strong electrochemical electric fields on the metal surface [24], and then it was proposed that the phenomenon originated from the optical excitation of electrons collective oscillations on the surface of metallic nanostructures [25]. Additionally, subsequent studies have shown that the reason for the SERS enhancement is linked to the electromagnetic and to the chemical effect [26, 27]. In the last three decades, technological advances have been providing fundamental contributions to the development of instrumentation in the field of Raman/SERS spectroscopies [28]. The introduction of charged coupled devices (CCDs), for example, allowed a high improvement in the spectra signal/noise ratio; further, the holographic notch filters, and the use of solid-state lasers for excitation, meant important advances in the quality and scope of the technique [29]. The unique characteristics of SERS, as well as its instrumental advances, have boosted the use of this spectroscopic technique

in several fields, transforming a tool, which in the past, was used only by a limited number of specialized users, into a widely spread analytical technique [28].

Currently, researchers are working on many applications of SERS, such as sensing food additives or contaminants, explosives, and biological species, as well as its different uses in forensic science and monitoring reactions catalyzed by metallic nanoparticles [28]. Also, SERS has been widely reported in biological fields, especially to detect influenza and hepatitis B virus [30, 31]. However, the identification of biomacromolecules by SERS is still a major challenge, since the low compatibility of biomolecules with SERS hot spots, and the complexity of physiological environments, make it difficult to use SERS for this application [32].

At the current time, with an ongoing Covid-19 pandemic, healthcare systems have been overwhelmed across the world. In this context, early and rapid diagnosis of SARS-CoV-2 plays a key role in fighting the outbreak. In this context, one of the most requested and urgent demands was the application of a fast, cheap, and accessible monitoring system. As a possible alternative, SERS provides quantitative results and shows high specificity and sensitivity. A viable configuration for this is the so-called point-of-care (PoC) testing arrangement, such as SERS Based Lateral Flow Immunoassay (LFIA) [33]. SERS-LFIA devices have already been approved by the Food and Drug Administration (FDA) and by the Indian Council of Medical Research (ICMR) and are available commercially and for the diagnosis of SARS-CoV-2 [34, 35]. The great miniaturization potential of SERS-based sensors makes them good candidates for biosensors, being an interesting alternative to other more traditional diagnostic methods. For example, Liu et al. described a SERS-LFIA immunoassay for the simultaneous sensing of anti-SARS-CoV-2 IgM/IgG with high sensitivity [36]. New designs were made with two layers of Raman dye and coating with a complete Ag shell on the SiO_2 core (SiO_2@Ag), showing mainly good SERS signals and great stability. Briefly, anti-human IgM and IgG were immobilized on the two test lines of the strip to bind with formed SiO_2@Ag-spike (S) protein-anti-SARS-CoV-2 IgM/IgG immunocomplexes, as shown in Fig. 3. Thus, portable Raman equipment was able to detect the SERS signal intensities of the IgM and IgG, which allows the analysis of target IgM and IgG with 800 times higher limit of detection than standard Au nanoparticle based LFIA.

Another sensor configuration was studied by Chen et al., which developed a new platform for highly sensitive quantification of SARS-CoV-2 [37]. In a sensible detection, a spike protein deoxyribonucleic acid (DNA) aptamer was used as a receptor, and a gold surface as a SERS detection substrate, according to the scheme shown in Fig. 4. With this new design, the device allowed the performance of quantitative analysis of the SARS-CoV-2 lysate, by the change in the intensity of the SERS peak, which was caused by the new binding between the spike protein in the SARS-CoV-2 virus and the DNA of aptamer released from the gold surface. As a result, the limit of detection (LoD) was less than 10 PFU/mL within 15 min, which makes this technique a great alternative for clinical application in the diagnosis of SARS-Cov-2.

Finally, a different approach for SERS-based sensor was also studied and improved by Huang et al., using a deep learning-based SERS technique [38]. This work allowed a rapid, sensitive, and on-site detection of the SARS-CoV-2 antigen,

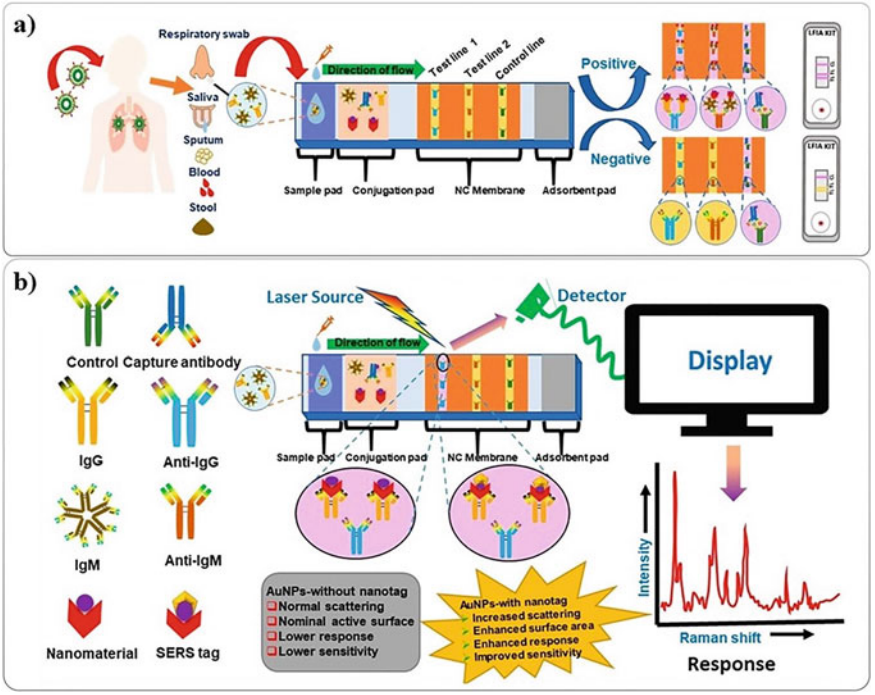

Fig. 3 Schematic representation of the fabrication and working principle of **a** conventional LFIA and **b** SERS-based LFIA for detection of SARS-CoV-2 (Reproduced with permission from [33])

through a Raman database based on the spike protein of SARS-CoV-2, therefore, combining experiments with human throat swabs, sputum, and theoretical calculations. The detection process can be seen in Fig. 4a, in which the enhanced local electric field (hot spot) is found in the nanogaps of neighboring AuNPs, and due to the nail shape of the spike protein (S) of the SARS-CoV-2 virus, with a width of 7 nm and a length of 23 nm, it has the highest probability of falling precisely in the SERS hot spots. In addition, to perform rapid detection, a supervised deep learning algorithm was developed with a database of pure protein S spectra and negative clinical specimens.

2.2 Localized-Surface Plasmon Resonance (LSPR)

The phenomenon of localized-surface plasmon resonance (LSPR) has been widely used for rapid, real-time, and in-situ sensors and biosensors [39, 40]. Especially, these devices can be applied for kinetic and thermodynamic analysis, and quantification of biomolecule concentrations, due to the high sensitivity to refractive index or changes in the medium around the metallic surface [41, 42]. Despite that, conventional LSPR

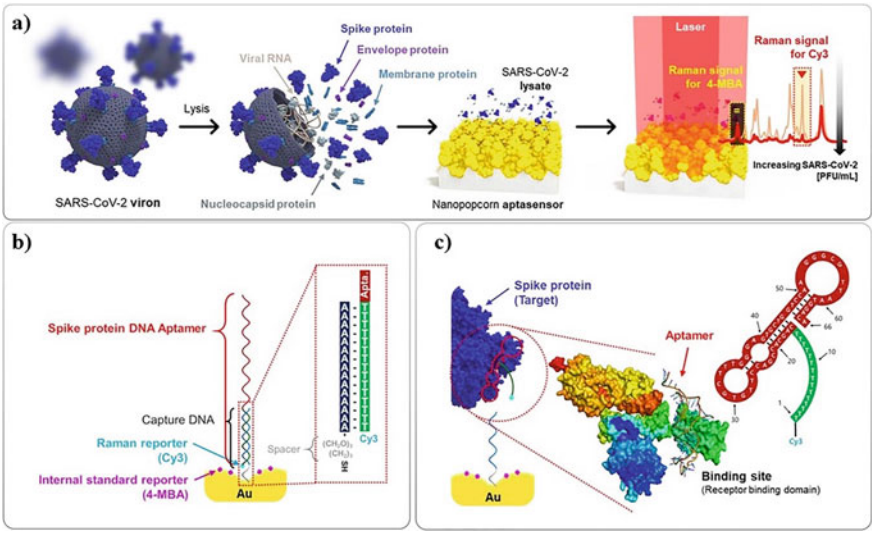

Fig. 4 Schematic illustration of the quantitative evaluation of SARS-CoV-2 using the SERS-based aptasensor. **a** After SARS-CoV-2 lysates release the target spike proteins, they are recognized by the aptamer DNAs on the Au nanopopcorn surfaces. The spike protein-bound aptamers move away from the Au nanopopcorn surfaces, leading to a decreased Raman peak intensity of Cy3 reporters. **b** Cy3-tagged aptamer DNAs are hybridized with capture DNAs on the Au nanopopcorn substrate. The internal standard 4-MBAs are immobilized along with aptamer DNAs on the Au nanopopcorn substrate. **c** Recognition of the spike protein of SARS-CoV-2 induces a conformational change of aptamer DNAs, enabling the aptamer DNAs to bind with the receptor-binding domain (RBD) on the spike protein (Reproduced with permission from [37])

sensors presented low sensitivity for detecting relatively small biomolecules, being very difficult to measure small concentrations by the LSPR technique [39].

Nowadays, several researchers have been aiming to enhance LSPR sensitivity, extending the use of LSPR sensors in low molecular weight and low concentration detection [43, 44]. In this context, three different materials are being mainly used for increasing the LSPR sensitivity: gold nanostructures, magnetic nanoparticles, and thin films with a high refractive index [39]. Generally, nanoparticles increase the refractive index of the analyte, resulting in enhanced shifts of resonance angle and then contributing to increased sensitivity of the LSPR sensor [45, 46]. Also, LSPR-based thin film sensors with a bimetallic layer can increase signal sensitivity by minimizing incident light reflectivity and subsequently maximizing the electromagnetic field intensity at the surface [47].

The spread of the novel coronavirus (SARS-CoV-2) has demanded rapid, accurate, and convenient methods for Covid-19 diagnosis. In this sense, localized surface plasmon resonance (LSPR) sensing transduction has been studied as a promising alternative due to its potential high selectivity and label-free detection [48]. One interesting sensor device was developed by Qiu et al., in which two-dimensional gold nanoislands (AuNIs) functionalized with complementary DNA receptors were tested

as a sensitive sensor for selected sequences from severe acute respiratory syndrome SARS-CoV-2 by nucleic acid hybridization [49]. Intending to a better detection sensibility, a thermoplasmonic heat was generated on the AuNIs chip focusing on their plasmonic resonance frequency. As a result, the localized plasmonic photothermal effect was capable to elevate the in-situ hybridization temperature and facilitating the accurate discrimination of two similar gene sequences [49].

Another important approach related to new coronavirus sensors development consists of the nanoplasmonic resonance sensor [50]. This biosensor type, widely used in several areas, provides direct and quickly optical measurements, which in the case of SARS-CoV-2, there is no need of sample preparation, and the analysis is carried out using a spike protein [51]. Thus, with an antibody surface functionalization, the nanoplasmonic sensor allowed the detection of concentrations lower than 370 vp/mL SARS-CoV-2 pseudovirus and virus concentrations in the range of 102–107 vp/mL through simultaneous measurements of diluted standard samples. Additionally, similar sensing potential was demonstrated using a low-cost handheld optical equipment controlled by a smartphone App, providing it a great potential for commercial application [51].

Recently, opto-microfluidic biosensor has also been used as an alternative to serological methods, based on previous works that reveal it as fast and cheap detecting [52]. Regarding Covid-19 sensing, an opto-microfluidic platform has been studied to quantify the concentration of anti-SARS-CoV-2 spike protein antibodies [53]. For this measure, diluted human plasma is used and the sensing is based on the wavelength shift of the localized surface plasmon resonance (LSPR) peak of gold nanostructures (AuNS) in the microfluidic device. The occurrence of binding interactions with the SARS-CoV-2 spike protein leads to a redshift of the LSPR peak of the AuNS, which allows the determination of antibody concentration [54]. Thus, a glass substrate covered by gold nanospike, fabricated by gold electrodeposition (ED), has been used as an optofluidic platform. The substrate is coupled to a microfluidic chip with a reflection probe, which can detect antibodies against the SARS-CoV-2 spike protein [53].

2.3 Luminescence

Luminescence is widely used in many types of sensors, such as chemical, thermal, and biological sensors. This wide area of application in sensing is due to the sensitivity of this technique, in addition to a high specificity to the analyte in focus. Among the luminescent sensors, there is a broad variety of methods and strategies, which can be applied for different environments. In the same way as other types of biosensors, the luminescent biosensors need a sample, where the target analyte can be, also needs a biorecognition sensing element attached to an optical transducer, where the luminescent component generates a signal output [6].

Many compounds and materials can exhibit luminescence, such as Metal–Organic Framework (MOF) [55, 56], rare earth ions [57, 58] or organic compounds [59]. In

view of this variety of luminescent elements, sensors with different excitation and emission wavelengths can be designed. The choice of components that form the biosensor occurs in the function of the interested molecule because the sensor must respond specifically to the target molecule, and then generate a suitable signal [6]. The luminescent signal can be followed with a simple linear regression as a function of the analyte concentration, or even establish a band-to-band ratio when there are bands in the fluorescence spectrum that do not change with the analyte concentration or are inversely proportional [60]. This sensor is called ratiometric based sensors due to the ratio established between the spectrum bands. The ratiometric sensors have the advantage of being self-standardized and, therefore, minimize possible errors arising from fluctuations in the equipment. Figure 5 represents the different types of ratiometric sensors with two different components or just one emitter component [61]. The ratiometric application was introduced by Montana et al. [62] to detect the changes in Hela cells membrane potential. Since that, it is widely used in thermal sensors [63] as well as for the detection and quantification of biomolecules such as viruses [64] and bacteria [65, 66].

Given the current pandemic scenario caused by the SARS-CoV-2 virus, different biosensing technologies have been developed to detect the biomolecules associated with the virus. In this context, Fan et al. [67] used a ratiometric electrochemiluminescence (ECL) to detect the virus RdRp gene SARS-CoV-2 with a limit of detection of 7.8 aM, making it a potential biosensor to use in situations where the concentration of virus in the body is still low and not detected by conventional biosensors [67, 68]. Elledge et al. [69] developed a methodology using luminescence enzyme split and binding to SARS-CoV-2 viral protein antigens. The proteins linked with enzyme fragments bind to antigen-binding (Fab) arms causing the approximation and recombination of NanoBiT luciferase enzyme and in this way producing an active luciferase signal. The choice of N and S proteins for antibody test is because these

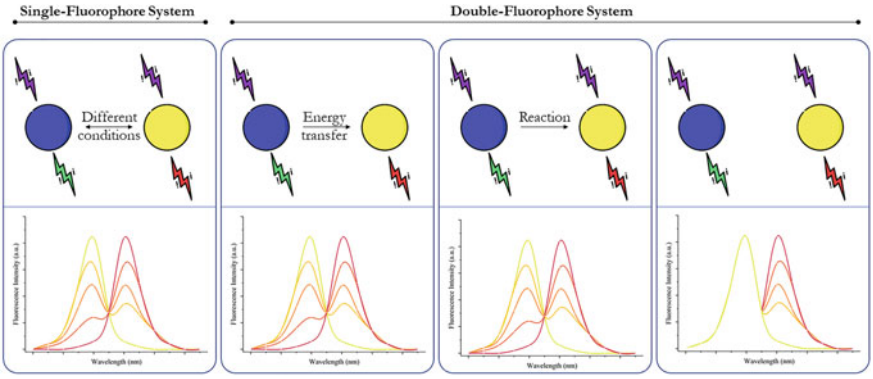

Fig. 5 Comparison of double-fluorophore system and single-fluorophore system. Double-fluorophore dual-emitting system can be ascribed to three ways, internal reference, energy transfer and reaction types. The fluorescence of single-fluorophore dual-emitting probe changes with conditions

proteins are the main used antigen tests for SARS-CoV-2. Which packages the viral genome and interacts with the enzyme ACE2 to entry in the cell, respectively [69].

Another way to use luminescence is to apply it in Lateral Flow Immunoassays, in this technique the solution containing the analyte runs through a chromatography plate and interacts with specific regions already functionalized, in general, this biosensor is qualitative generating a colorimetric signal. When combined with luminescence the Lateral Flow method can become quantitative by establishing a linear relationship between antibody concentration and fluorescence. This combination was demonstrated by Guo et al. [70], who inserted parts of fiber optic functionalized with up-conversion nanoparticles (UCNPs@mSiO_2) on chromatographic paper, to detect the Spike protein and nucleocapsid protein of the Coronavirus, obtaining a sensor with a limit of detection of 1.6 and 2.2 ng mL^{-1}, respectively, and with easy portability [70]. Table 1 shows some luminescent biosensors researched and developed for SARS-CoV-2.

Table 1 Examples and features of luminescent biosensors for Covid-19

Assay	Luminescent agent	Target biomolecule	LoD	Ref
CLEIA	Lumipulse Fujirebio	SARS-CoV-2 antigen	1.34 pg/mL	[71]
CLIA	MAGLUMI 2000 Plus*	2019-nCoV IgM	1.0 AU/mL	[72]
CLIA	MAGLUMI 800*	2019-nCoV IgG IgG	AU/mL 0.03 AU/mL	[73]
CLIA	iFlash1800*	IgM Anti-SARV-CoV-2 IgG Anti-SARV-CoV-2 IgM	0.58 AU/mL 7.1 AU/mL 10.0 AU/mL	[74]
ECL-RET	Au-g-C3N4	SARS-CoV-2 RdRp	7.8 aM	[67]
FI	GQDs	2019-nCoV mAb	50 fg/mL	[75]
LFIA	LNPs	anti-SARV-CoV-2 IgG	–	[76]
LFIA	UCNPs@mSiO_2	S protein N protein	1.6 ng/mL 2.2 ng/mL	[70]
MCLIA	FITC	IgM/IgG	–	[77]
Microfluidic	(FDG)	N protein	33.28 pg/mL	[19]
spLUC assay	NanoLuc enzyme	SARS-CoV-2 antibodies	0.1 nM	[69]

*Standard procediment or equipmnet

3 Optical Fiber for Biosensing

The dielectric cylindrical waveguide, or simply optical fibers as we know it today, represents centuries of research to describe the light's behavior through the unification of electromagnetism [78], total internal reflection phenomenon, light scattering, development of new materials, and so on [79]. Starting from the beginning of twentieth century, lots of research developed theoretical performance of wave transmission through a dielectric medium [79–83]. Parallelly, in material science the development of glass materials, mostly the silicates, with high transparence, economic benefits, and precursor availability, enabled the fabrication of very long, durable and low loss optical fibers [84]. In 1966, Kao and Hockham [85] evaluated the materials and the loss mechanisms in silica optical fibers, which drove numerous research towards the development of telecommunication. He was recognized with a Nobel Prize in Physics in 2009. Almost six decades later, optical fiber is nowadays the main means of global communication. Taking advantages of their intrinsic properties, it has received the attention to be used in several advanced applications, such as in optical sensing devices. Optical fibers are extensively explored in light-dependent sensors, either for guiding the electromagnetic wave through analysis instruments or as support for many types of chemical surface functionalization and core modifications. The latter indicates processes involving physical and chemical mechanisms to increase its sensing capacity, such as tapering process to reduce core diameter, changing on the refraction index, or simply bending the fiber in specific ways (e.g., U-bent configuration) to allow the interaction with the environment to be analyzed. For photonic devices, this section presents what has been developed and its perspectives for optical fibers applied in biomolecule sensing.

3.1 Propagation of Light

Light propagates through an optical fiber by means of a phenomenon named Total Internal Reflection, and to understand this it is necessary to take a few steps back. The speed that lights travels is closely dependent on the medium, in which the speed in vacuum is a constant of nature represented by c. The measure of this speed change is calculated using the refractive index (n_0), a dimensionless number that shows how many times light travels slower in a certain medium. Refractive index is obtained simply by dividing the speed of light in vacuum (c) by speed of light in the medium (v). When light passes from one medium to another of different n_0 means that there is a sudden change in its speed, also changing its propagation angle. The Snell's law describes this phenomenon by relating n_0 of a certain medium with the angle of this beam light, using a sine function, as shown in the equation $n_1 sin\theta_1 = n_2 sin\theta_2$. The angle θ is measured based on an axis perpendicular to the interface between the two media, as Fig. 6a shows considering $n_1 > n_2$. Besides the refracted beam, part of the light is reflected with the same angle as the incident light. There is an angle where the

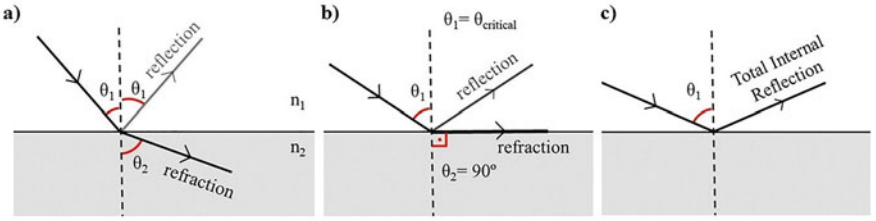

Fig. 6 **a** Refraction of a beam of light, **b** Refraction at the critical angle, and **c** Total internal reflection

refracted beam of light is exactly 90°, which according to the Snell equation, depends on the medium refractive index. In this case, the incident angle is called the *critical angle*, θ_c. Figure 6b shows the case where the incident beam generates a right-angle refraction. Thus, any incident angle above θ_c results in the total internal reflection (TIR) phenomenon, which allows one to control the path of light propagation, as can be seen in Fig. 6c.

In the case of waveguides, the light travel in the medium with higher n_0, such as in optical fibers and planar waveguides. A typical optical fiber has an external diameter of 125 mm and is composed of three parts: core (the inner part where light travels), cladding with a smaller n_0, and a polymeric coating. For guiding, the light must be launch into the core of the optical fiber with a proper angle to allow TIR [86]. The numerical aperture (NA) of an optical fiber is the measure for its angular acceptance of incident light and is defined as the product of refractive index and the sine of the largest incident light angle for TIR in the optical fiber core, e.g. $NA = n_{core}\theta_{max}$. A core with higher n_0 with respect to the cladding, means larger NA. The smallest allowed angle is named *fundamental mode*, while the others are *high-order* modes. This means that the diameter size and dopant concentration of the fiber's core are very important to avoid scattering light and control the allowed angles of a given optical fiber. Optical fiber with small core diameter that allow only one mode at a certain wavelength, is called single-mode fiber. If more than one mode is allowed, it is called multimode fiber. Moreover, the transverse refractive index profile in each fiber can be constant, called step-index fiber, and can also gradually decreases from the center to the core-cladding boundary, called graded-index fiber. Figure 7a–c schematically shows the transmission of light in the three types of optical fibers.

Fig. 7 **a** step-index fiber single mode; **b** step-index fiber multimode; **c** graded-index fiber multimode

3.2 *Chemically Modified Optical Fiber for Sensing*

For sensing applications, the use of optical fiber has brought some advantages such their electrical interference immunity, miniaturization, bend flexibility, remote and real-time acquisition of data for inaccessible or harsh environments, for instance. For the last decades, different applications and modifications have been developed and this section briefly present some of them. For applications in optical sensing, a little portion of the optical fiber must interact with the environment or analyte. This interaction must be strong enough to capture information, but not too strong that unable the guided light to reach the detector. In the case of optical fibers-based sensors, this interaction occurs directly on the glass surface in contact with the analyte. This type of light interaction happens due to the presence of an evanescent light that scape from the core, mainly observed in multimode optical fibers, bringing optical information about the analyte through the guided mode until to the detector. Figure 8 basically illustrate a usual behavior inside the fiber's core by the presence of an evanescent field formed on the cladding. In this sense, large core and exposed core fibers are used to take advantages from the evanescent field.

Other common physical modification besides the complete removal of the cladding (Fig. 9a), is the tapering process of optical fibers that consist of heating and stretching the fiber in a short length, reducing their core more than 10 times (Fig. 9b) [87, 88]. Although they are different processes and open possibilities for other modifications, both can be produced in the same piece of an optical fiber.

The cladding can be chemically removed by etching the surface with hydrofluoric acid, which strongly reacts with silica-based glasses. Some authors have described the process, including how to monitor the process and reach a more desirable diameter

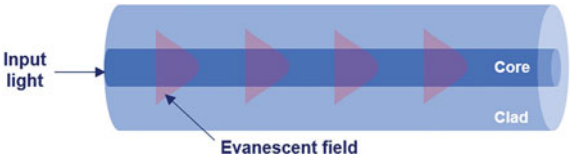

Fig. 8 Scheme of a multimode optical fiber and the evanescent field leaking to the cladding medium

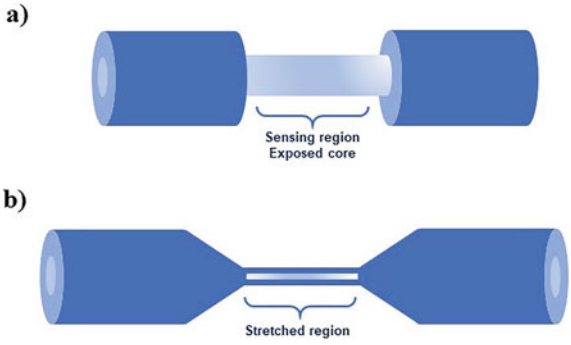

Fig. 9 **a** Cladding removal and **b** stretched optical fiber

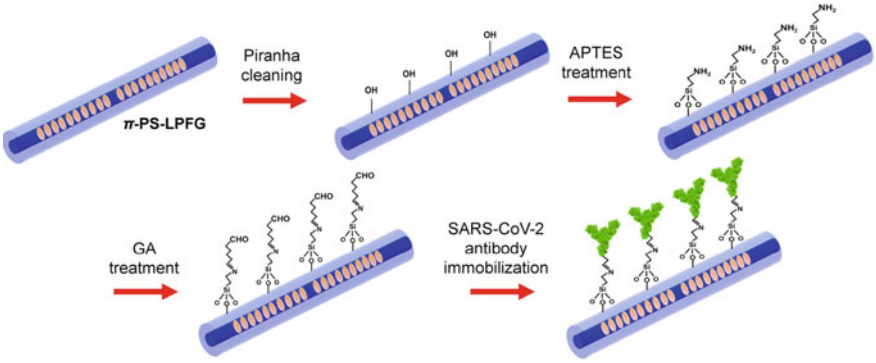

Fig. 10 Surface functionalization for application of optical fibers as substrates for biomolecule sensor (Reproduced with permission of [96])

[89–91]. The process of decreasing the size by stretching the optical fibers (tapering) needs a source of heating, like a flame or electric arc, and a way to mechanically control the pulling [92, 93]. From these two procedures, several configurations began to be proposed in the literature in recent years. Some examples, especially applied for biomolecule detection, are filling the gap where the cladding is removed and chemically modified the region by different optically active material such as organic dyes, fluorescent nanoparticles, or semiconductor quantum dots [94–96]. Moreover, optical fibers are used also as substrate when functionalized with molecules and biomolecules for increasing selectivity [95, 96], as shown in Fig. 10 by the use of antibody immobilization with crosslink molecules for proteins recognition, for example.

Bending the fiber in specific formats as the U-type [97] or S-type [98] increases the quantity of reflected light in the core's surface (evanescent field) and, consequently, the interaction of the guided light with the external environment. Lastly, complex systems with multiple cores or optical fibers interacting with each other [99–101]. Besides the core exposition and surface functionalization, it is possible to internally modify the fiber's core to control the light transmission and creating new concepts of optical sensors.

3.3 Fiber Bragg Grating

In this type of optical fibers, they are core modified to present periodic modulation of the refractive index. Such configuration reflects part of the incident light if the wavelength meets the Bragg condition, by successive coherent scattering from the index variations, transmitting the rest. The standard modification is uniform across the optical fiber width and periodic by its axis, with a few millimeters of extension. Along with the advantages of optical fibers themselves, this type of modification presents

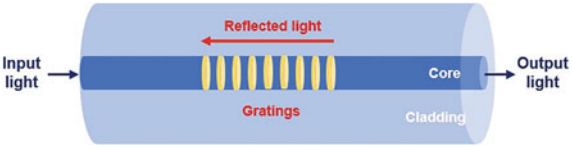

Fig. 11 A scheme of a fiber Bragg grating

intrinsic sensitivity of surrounding refractive index changes and allows several label-free sensing applications. Numerous processes can change the refraction index of a fiber's core, such as temperature, stretching, or composition. In the case of a common silica optical fiber, a germanium doped core can be exposed under UV radiation to permanently change their refractive indexes according to patterns and properties of the beam. Figure 11 shows a scheme of a Fiber Bragg Grating. Another way to produce this grating is by physical deformation, forming trenches, and it is referred to as a surface relief grating [102–105]. As aforementioned, the grating is usually a few millimeters of extension, the distance between each grid is by a few hundreds of nanometers, and they are all perpendicular to the direction of the incident wave. However, some other configurations are equally possible, such as rising the periodic distance to some micrometers, known as Long-Period Fiber Gratings, modifying the grating period from linear to quadratic, or changing the grid angles through the optical fiber axis. Each one of these represents a change in the signal, by the increase on the Surrounding Refractive Index (SRI) [96, 102–105].

3.4 Highlights and Final Comments

All presented optical fiber modification possibilities can be used for biomolecules sensing, and most of the recent research ends up mixing more than one of those methods. As can be seen in a label-free biosensor (protein and IgG probes), tapered microfiber described by Juste-Dolz [106]. Binding events on the surface of the bioreceptor increase the amount of matter constituting the Bragg Grating, thus creating a change in its modulation depth. Therefore, the system can detect the analyte when the receptor, imprinted on the microfiber surface, binds to its specific target, by using the reflection peak, as can be seen in Fig. 12. Another very common technique to immobilize metallic nanoparticles for detection is the functionalization of the optical fiber surface with modified silanes. The procedure usually starts by cleaning the surface with dilute acid and then using a piranha solution to create SiOH sites where the Organically Modified Silicates (ORMOSILs) bond. The metallic nanoparticles interact with specific groups, such as mercapto (-SH) or amine (-NH) in biomolecules [107–110]. Lastly, a single-mode tapered optical fiber used for light guiding close to the silica mesopore microspheres decorated with the nucleocapsid proteins (N-proteins) of the SARS-CoV-2 [111].

In conclusion, it was shown in this section the basics operation of optical fiber biosensor, the most common modifications in the literature for sensing, and potential

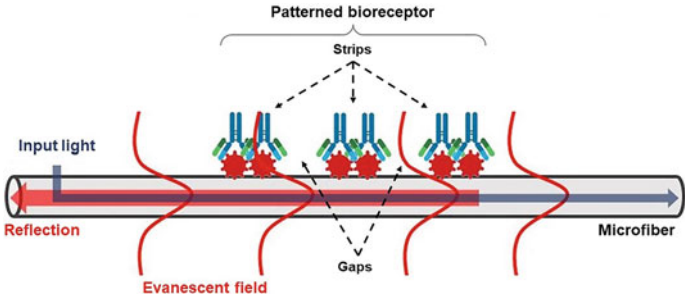

Fig. 12 Bioreceptor in the surface of a grated optical fiber (Reproduced with permission of [106])

applications for biomolecule detection in case of infections like the presence of Severe Acute Respiratory Syndrome-Corona Virus-2 (SARS-CoV-2).

4 Perspectives

We show in this chapter a briefly overview of some principles of photonic devices used to diagnose and monitor some biological elements and biomolecules. In special, the use of optical devices against the Virus of SARS-Cov-2 shows promise for large-scale tests of coronaviruses, with many advantages such as small size, low cost, sensibility, and possible Point of care diagnostic. With the vaccines, Covid-19 started to be suppressed and after 2 years the infections and deaths decreased, but detection is still necessary to help the reduction virus spread. The SARS-Cov family was discovered in 2003 and in 2019 a new variant, SARS-CoV-2, become a high infectious virus that causes the pandemic. Thus, the continuous development of efficient biosensors is important to defeat coronaviruses but also possible new unknown pathogens and virus variants.

Acknowledgements The authors are grateful to CAPES (Pandemias 8887.504861/2020-00) and FAPESP (2020/11038- 2 and 2020/12280-1) for the financial support.

References

1. H. Maddali, C. E. Miles, J. Kohn, D.M.O'Carroll, ChemBioChem **22**, 1176–1189 (2021)
2. L. Lu, L. Zhu, G. Zhu, M. Dong, Z. Zeng, IEEE Sens. J. **20**, 14173–14180 (2020)
3. M.J. Marín, A. Rashid, M. Rejzek, S.A. Fairhurst, S.A. Wharton, S.R. Martin, J.W. McCauley, T. Wileman, R.A. Field, D.A. Russell, Org. Biomol. Chem. **11**, 7101–7107 (2013)
4. Y.M. Kamil, M.A. Bakar, M. Mustapa, M. Yaacob, N. Abidin, A. Syahir, H. Lee, M. Mahdi, Sens. Actuators, B Chem. **257**, 820–828 (2018)
5. Y. Saylan, Ö. Erdem, S. Ünal, A. Denizli, Biosensors **9**, 65 (2019)

6. J. Svitel, J. Katrl et al., Essays. Biochem. **60**, 91–100 (2016)
7. C. Chen, J. Wang, Analyst **145**, 1605–1628 (2020)
8. I.A. Mattioli, A. Hassan, O.N. Oliveira Jr., F.N. Crespilho, ACS Sensors **5**, 3655–3677 (2020)
9. S.R. Weiss, J.L. Leibowitz, Adv. Virus Res. **81**, 85–164 (2011)
10. J. Cui, F. Li, Z.-L. Shi, Nat. Rev. Microbiol. **17**, 181–192 (2019)
11. Z. Bai, Y. Cao, W. Liu, J. Li, Viruses **13**, 1115 (2021)
12. Y. Wang, H. Kang, X. Liu, Z. Tong, Journal of Medical Virology 538–539 (2020)
13. L. Zhang, X. Fang, X. Liu, H. Ou, H. Zhang, J. Wang, Q. Li, H. Cheng, W. Zhang, Z. Luo, Chem. Commun. **56**, 10235–10238 (2020)
14. A. Savastano, A. Ibáñez de Opakua, M. Rankovic, M. Zweckstetter, Nat. Commun. **11**, 1–10 (2020)
15. L.H. Cazares, R. Chaerkady, S.H. Samuel Weng, C.C. Boo, R. Cimbro, H.-E. Hsu, S. Rajan, W. Dall'Acqua, L. Clarke, K. Ren et al., Analytical Chemistry **92**, 13813–13821 (2020)
16. K. Fujimoto, K.-H. Chan, K. Takeda, K.-F. Lo, R.H. Leung, T. Okamoto, J. Clin. Microbiol. **46**, 302–310 (2008)
17. J. Labuda, A.M.O. Brett, G. Evtugyn, M. Fojta, M. Mascini, M. Ozsoz, I. Palchetti, E. Paleček, J. Wang, Pure Appl. Chem. **82**, 1161–1187 (2010)
18. S. Song, L. Wang, J. Li, C. Fan, J. Zhao, TrAC, Trends Anal. Chem. **27**, 108–117 (2008)
19. C. Ge, J. Feng, J. Zhang, K. Hu, D. Wang, L. Zha, X. Hu, R. Li, Talanta **236**, 122847 (2022)
20. M. Divagar, R. Gayathri, R. Rasool, J.K. Shamlee, H. Bhatia, J. Satija, V. Sai, IEEE Sens. J. **21**, 22758–22766 (2021)
21. F. Ligler, *Biophotonics* (Springer, Berlin, 2008), pp.199–215
22. E. Benito-Peña, M.G. Valdés, B. Glahn-Martínez, M.C. Moreno-Bondi, Anal. Chim. Acta **943**, 17–40 (2016)
23. M. Fleischmann, P.J. Hendra, A.J. McQuillan, Chem. Phys. Lett. **26**, 163–166 (1974)
24. M.G. Albrecht, J.A. Creighton, J. Am. Chem. Soc. **99**, 5215–5217 (1977)
25. M. Moskovits, J. Chem. Phys. **69**, 4159–4161 (1978)
26. A. Otto, Journal of Raman Spectroscopy: An International Journal for Original Work in all Aspects of Raman Spectroscopy. Including Higher Order Processes, and also Brillouin and Rayleigh Scattering **36**, 497–509 (2005)
27. A. Otto, Quarterly. Phys. Rev. **3**, 1–14 (2017)
28. R. Pilot, R. Signorini, C. Durante, L. Orian, M. Bhamidipati, L. Fabris, Biosensors **9**, 57 (2019)
29. S. Xu, X. Ji, W. Xu, X. Li, L. Wang, Y. Bai, B. Zhao, Y. Ozaki, Analyst **129**, 63–68 (2004)
30. J.-Y. Lim, J.-S. Nam, H. Shin, J. Park, H.-I. Song, M. Kang, K.-I. Lim, Y. Choi, Anal. Chem. **91**, 5677–5684 (2019)
31. Y. Wang, Q. Ruan, Z.-C. Lei, S.-C. Lin, Z. Zhu, L. Zhou, C. Yang, Anal. Chem. **90**, 5224–5231 (2018)
32. C. Zong, M. Xu, L.-J. Xu, T. Wei, X. Ma, X.-S. Zheng, R. Hu, B. Ren, Chem. Rev. **118**, 4946–4980 (2018)
33. S. Yadav, M.A. Sadique, P. Ranjan, N. Kumar, A. Singhal, A.K. Srivastava, R. Khan, ACS Appl. Bio Mater. **4**, 2974–2995 (2021)
34. P. Pokhrel, C. Hu, H. Mao, ACS Sensors **5**, 2283–2296 (2020)
35. F. Li, M. You, S. Li, J. Hu, C. Liu, Y. Gong, H. Yang, F. Xu, Biotechnol. Adv. **39**, 107442 (2020)
36. H. Liu, E. Dai, R. Xiao, Z. Zhou, M. Zhang, Z. Bai, Y. Shao, K. Qi, J. Tu, C. Wang et al., Sens. Actuators, B Chem. **329**, 129196 (2021)
37. H. Chen, S.-G. Park, N. Choi, H.-J. Kwon, T. Kang, M.-K. Lee, J. Choo, ACS Sensors **6**, 2378–2385 (2021)
38. J. Huang, J. Wen, M. Zhou, S. Ni, W. Le, G. Chen, L. Wei, Y. Zeng, D. Qi, M. Pan et al., Anal. Chem. **93**, 9174–9182 (2021)
39. O. Tabasi, C. Falamaki, Anal. Methods **10**, 3906–3925 (2018)
40. J. Wang, H.S. Zhou, Anal. Chem. **80**, 7174–7178 (2008)
41. J. Wang, A. Munir, Z. Zhu, H.S. Zhou, Anal. Chem. **82**, 6782–6789 (2010)

42. H. Sota, Y. Hasegawa, M. Iwakura, Anal. Chem. **70**, 2019–2024 (1998)
43. L. Wang, Y. Sun, J. Wang, X. Zhu, F. Jia, Y. Cao, X. Wang, H. Zhang, D. Song, Talanta **78**, 265–269 (2009)
44. S. Zeng, D. Baillargeat, H.-P. Ho, K.-T. Yong, Chem. Soc. Rev. **43**, 3426–3452 (2014)
45. X. Yang, Q. Wang, K. Wang, W. Tan, H. Li, Biosens. Bioelectron. **22**, 1106–1110 (2007)
46. L. Wang, Y. Sun, J. Wang, J. Wang, A. Yu, H. Zhang, D. Song, Colloids Surf., B **84**, 484–490 (2011)
47. M. Wang, Y. Huo, S. Jiang, C. Zhang, C. Yang, T. Ning, X. Liu, C. Li, W. Zhang, B. Man, RSC Adv. **7**, 47177–47182 (2017)
48. G. Qiu, S.P. Ng, C.-M.L. Wu, Sens. Actuators, B Chem. **265**, 459–467 (2018)
49. G. Qiu, Z. Gai, Y. Tao, J. Schmitt, G.A. Kullak-Ublick, J. Wang, ACS Nano **14**, 5268–5277 (2020)
50. T. Dang, W. Hu, W. Zhang, Z. Song, Y. Wang, M. Chen, H. Xu, G.L. Liu, Biosens. Bioelectron. **142**, 111494 (2019)
51. L. Huang, L. Ding, J. Zhou, S. Chen, F. Chen, C. Zhao, J. Xu, W. Hu, J. Ji, H. Xu et al., Biosens. Bioelectron. **171**, 112685 (2021)
52. C. Dincer, R. Bruch, E. Costa-Rama, M.T. Fernández-Abedul, A. Merkoçi, A. Manz, G.A. Urban, F. Güder, Adv. Mater. **31**, 1806739 (2019)
53. R. Funari, K.-Y. Chu, A.Q. Shen, Biosens. Bioelectron. **169**, 112578 (2020)
54. K.M. Mayer, J.H. Hafner, Chem. Rev. **111**, 3828–3857 (2011)
55. B.-P. Xie, G.-H. Qiu, P.-P. Hu, Z. Liang, Y.-M. Liang, B. Sun, L.-P. Bai, Z.-H. Jiang, J.-X. Chen, Sens. Actuators, B Chem. **254**, 1133–1140 (2018)
56. L. Wang, K. Liang, W. Feng, C. Chen, H. Gong, C. Cai, Microchem. J. **164**, 106047 (2021)
57. M. Alafeef, K. Dighe, P. Moitra, D. Pan, ACS Sustainable Chemistry and Engineering 245–258 (2021)
58. H. Zhang, Z.-H. Chen, X. Liu, F. Zhang, Nano Res. **13**, 1795–1809 (2020)
59. L. Ding, Z. Qin, C. Xiang, G. Zhou, Journal of Materials Chemistry B **5**, 2750–2756 (2017)
60. R. Gui, H. Jin, X. Bu, Y. Fu, Z. Wang, Q. Liu, Coord. Chem. Rev. **383**, 82–103 (2019)
61. X. Pei, Y. Pan, L. Zhang, Y. Lv, Appl. Spectrosc. Rev. **56**, 324–345 (2021)
62. V. Montana, D.L. Farkas, L.M. Loew, Biochemistry **28**, 4536–4539 (1989)
63. E. Pan, G. Bai, L. Wang, L. Lei, L. Chen, S. Xu, ACS Applied Nano Materials **2**, 7144–7151 (2019)
64. M. Du, N. Li, G. Mao, Y. Liu, X. Wang, S. Tian, Q. Hu, X. Ji, Y. Liu, Z. He, Anal. Chim. Acta **1084**, 116–122 (2019)
65. M.B. Maas, G.H. Maybery, W.J. Perold, D.P. Neveling, L.M. Dicks, Curr. Microbiol. **75**, 150–155 (2018)
66. Y. Shen, T. Wu, Y. Zhang, N. Ling, L. Zheng, S.-L. Zhang, Y. Sun, X. Wang, Y. Ye, Anal. Chem. **92**, 13396–13404 (2020)
67. Z. Fan, B. Yao, Y. Ding, D. Xu, J. Zhao, K. Zhang, Chem. Eng. J. **427**, 131686 (2022)
68. C.Y. Lee, I. Degani, J. Cheong, J.-H. Lee, H.-J. Choi, J. Cheon, H. Lee, Biosens. Bioelectron. **178**, 113049 (2021)
69. S.K. Elledge, X.X. Zhou, J.R. Byrnes, A.J. Martinko, I. Lui, K. Pance, S.A. Lim, J.E. Glasgow, A.A. Glasgow, K. Turcios et al., Nat. Biotechnol. **39**, 928–935 (2021)
70. J. Guo, S. Chen, S. Tian, K. Liu, J. Ni, M. Zhao, Y. Kang, X. Ma, J. Guo, Biosens. Bioelectron. **181**, 113160 (2021)
71. C. Gandolfo, F. Morecchiato, M. Pistello, G.M. Rossolini, M.G. Cusi, Journal of Clinical Virology 104942 (2021)
72. A. Padoan, C. Cosma, L. Sciacovelli, D. Faggian, M. Plebani, Clinical Chemistry and Laboratory Medicine (CCLM) **58**, 1081–1088 (2020)
73. R. Soleimani, M. Khourssaji, D. Gruson, H. Rodriguez-Villalobos, M. Berghmans, L. Belkhir, J.-C. Yombi, B. Kabamba-Mukadi, J. Med. Virol. **93**, 1465–1477 (2021)
74. J. Xie, C. Ding, J. Li, Y. Wang, H. Guo, Z. Lu, J. Wang, C. Zheng, T. Jin, Y. Gao et al., J. Med. Virol. **92**, 2004–2010 (2020)
75. N. Li, L. Shi, X. Zou, T. Wang, D. Wang, Z. Gong, M. Fan, Microchem. J. **173**, 107046 (2022)

76. Z. Chen, Z. Zhang, X. Zhai, Y. Li, L. Lin, H. Zhao, L. Bian, P. Li, L. Yu, Y. Wu et al., Anal. Chem. **92**, 7226–7231 (2020)
77. Q.-X. Long, B.-Z. Liu, H.-J. Deng, G.-C. Wu, K. Deng, Y.-K. Chen, P. Liao, J.-F. Qiu, Y. Lin, X.-F. Cai et al., Nat. Med. **26**, 845–848 (2020)
78. J.C. Maxwell, Philosophical Transactions of the Royal Society of London 459–512 (1865)
79. J. Ballato, P. Dragic, Int. J. Appl. Glas. Sci. **7**, 413–422 (2016)
80. C.R. Doerr, H. Kogelnik, J. Lightwave Technol. **26**, 1176–1187 (2008)
81. D. Hondros, P. Debye, Ann. Phys. **337**, 465–476 (1910)
82. J.A. Stratton, *Electromagnetic Theory*, vol. 33 (Wiley, New Jersey, 2007)
83. E. Waves, *S.A. Schelkunoff* (1943)
84. J. Amalberti, P. Sarda, C. Le Losq, N. Sator, T. Hammouda, E. Chamorro-Pérez, B. Guillot, S. Le Floch, D.R. Neuville, Chem. Geol. **582**, 120413 (2021)
85. K.C. Kao, G.A. Hockham, in *Proceedings of the Institution of Electrical Engineers* (1966), pp. 1151–1158
86. Z. Fang, K. Chin, R. Qu, H. Cai, *Fundamentals of Optical Fiber Sensors*, vol. 226 (Wiley, New Jersey, 2012)
87. S. Lacroix, R. Bourbonnais, F. Gonthier, J. Bures, Appl. Opt. **25**, 4421–4425 (1986)
88. D. Marcuse, J. Lightwave Technol. **5**, 125–133 (1987)
89. H.S. Haddock, P. Shankar, R. Mutharasan, Mater. Sci. Eng., B **97**, 87–93 (2003)
90. P. Hoffmann, B. Dutoit, R.-P. Salathé, Ultramicroscopy **61**, 165–170 (1995)
91. F. Long, M. He, H. Shi, A. Zhu, Biosens. Bioelectron. **23**, 952–958 (2008)
92. V. Ahsani, F. Ahmed, M.B. Jun, C. Bradley, Sensors **19**, 1652 (2019)
93. K. Stasiewicz, R. Krajewski, L. Jaroszewicz, M. Kujawińska, R. Świłło, Opto-Electron. Rev. **18**, 102–109 (2010)
94. A.M. Abdi, S.S. Shastry, A.A. Nnanna, ASME International Mechanical Engineering Congress and Exposition pp. 49–53 (2008)
95. N. Rajil, A. Sokolov, Z. Yi, G. Adams, G. Agarwal, V. Belousov, R. Brick, K. Chapin, J. Cirillo, V. Deckert et al., Nanophotonics **10**, 235–246 (2021)
96. S.-L. Lee, J. Kim, S. Choi, J. Han, G. Seo, Y.W. Lee, Talanta **235**, 122801 (2021)
97. B. Gupta, N.K. Sharma, Sens. Actuators, B Chem. **82**, 89–93 (2002)
98. S. Chauhan, N. Punjabi, D. Sharma, S. Mukherji, Procedia Engineering **168**, 117–120 (2016)
99. K.I. Oberg, R. Hodyss, J. Beauchamp, Sens. Actuators, B Chem. **115**, 79–85 (2006)
100. Y. Zhan, Q. Liu, S. Feng, J. Ye, X. Wang, W. Sun, Y. Zhang, Appl. Phys. Lett. **117**, 171107 (2020)
101. J.M. Mauro, L.K. Cao, L.M. Kondracki, S.E. Walz, J.R. Campbell, Anal. Biochem. **235**, 61–72 (1996)
102. Z. Wang, J. Heflin, K. Van Cott, R.H. Stolen, S. Ramachandran, S. Ghalmi, Sens. Actuators, B Chem. **139**, 618–623 (2009)
103. P. Pilla, P.F. Manzillo, V. Malachovska, A. Buosciolo, S. Campopiano, A. Cutolo, L. Ambrosio, M. Giordano, A. Cusano, Opt. Express **17**, 20039–20050 (2009)
104. M.-J. Yin, B. Gu, Q.-F. An, C. Yang, Y.L. Guan, K.-T. Yong, Coord. Chem. Rev. **376**, 348–392 (2018)
105. F. Baldini, M. Brenci, F. Chiavaioli, A. Giannetti, C. Trono, Anal. Bioanal. Chem. **402**, 109–116 (2012)
106. A. Juste-Dolz, M. Delgado-Pinar, M. Avella-Oliver, E. Fernández, D. Pastor, M.V. Andrés, Á. Maquieira, Biosens. Bioelectron. **176**, 112916 (2021)
107. M.E. Martínez-Hernández, P.J. Rivero, J. Goicoechea, F.J. Arregui, Chemosensors **9**, 64 (2021)
108. P. Vaiano, B. Carotenuto, M. Pisco, A. Ricciardi, G. Quero, M. Consales, A. Crescitelli, E. Esposito, A. Cusano, Laser Photonics Rev. **10**, 922–961 (2016)
109. M. Pisco, A. Cusano, Sensors **20**, 4705 (2020)
110. A.K. Sharma, C. Marques, IEEE Sens. J. **19**, 7168–7178 (2019)
111. Y. Yue, H. Ding, C. Chen, J. Biophotonics **14**, e202000338 (2021)

Lateral Flow Assays for COVID-19

Karla R. Castro, Beatriz G. R. Silva, and Frank N. Crespilho

Abstract Rapid tests are essential tools for monitoring and containing the COVID-19 pandemic. Lateral flow assays (LFAs) have been introduced for the point-of-care COVID-19 diagnosis, using paper-based devices, and widely used for detecting antigen or antibody related to COVID-19. This book chapter includes a brief overview of the LFAs for rapid test of COVID-19, with focus on nanomaterials for bioconjugation, material selection, human sampling, antibody and antigen tests, viral nucleic acid detection, advantages, limitations, and future perspective.

Keywords Lateral flow · LFA · Immunosensors · Rapid test · COVID-19

1 Introduction

The damage caused by the COVID-19 pandemic in the last two years (2019–2021) is undeniable. The novel coronavirus (SARS-CoV-2), responsible for the coronavirus disease 2019 (COVID-19) has already more than 5 million deaths and 263 million confirmed cases worldwide [1]. Despite measures taken to decelerate the transmission rate, without global cooperation and mass testing, the virus will remain uncontrolled, as so, its mutants. Traditional laboratory-based analytical methods, such as enzyme-linked immunosorbent assay (ELISA) and real time polymerase chain reaction (RT-PCR) considered gold standard for detection of a large number of disease; however, they are laborious, time-consuming, and require certified molecular testing laboratories [2, 3].

Rapid tests can be a useful tool for monitoring and containing the COVID-19 pandemic. Immunochemical methods provide highly sensitive and specific results, and for that reason, the most utilized screening method for detection is based on immunoassays [2, 4]. Lateral flow assays (LFA) are paper based devices widely used for detecting a target analyte in different matrix [5]. When a LFA is based on the formation of an immunocomplex antigen (Ag)—antibody (Ab), they are called

K. R. Castro · B. G. R. Silva · F. N. Crespilho (✉)
Laboratory of Bioelectrochemistry and Interfaces, Institute of Chemistry of São Carlos (IQSC), University of São Paulo, São Carlos, São Paulo 13566-590, Brazil
e-mail: frankcrespilho@iqsc.usp.br

F. N. Crespilho (ed.), *COVID-19 Metabolomics and Diagnosis*,
https://doi.org/10.1007/978-3-031-15889-6_6

Lateral Flow Immunoassay (LFIA), which the efficacy is related to the efficiency of the Ab-Ag immunocomplex formation and its capacity to detect this phenomenon [6].

Among the assay-based methodologies, the immunochromatographic strip test (ICST), well-known as lateral flow immunoassay (LFIA) or even as rapid diagnostic test (RDT) may be an appropriated alternative solution to mass testing diagnosis of SARS-CoV-2, because it present advances, such as mass-production, rapid response, and good trial tool [7]. First designed in 1960 [8], this device became a breakthrough technology that not only changed the medical practice, but also the medical device market, globally.

The success of LFIA can be seen in their importance in the global market. Only in 2020, the lateral flow market was estimated to be US$7.8 billion, and it is projected to reach a size of US$11.6 billion in 2027, demonstrating that this device has already entered real-life applications [9]. The LFA are versatile in different fields, such as healthcare [10], food safety [11], environmental [12], and in therapeutic drug monitoring [13]. Despite innumerous efforts to improve their sensitivity, depending on the target analyte, in general, the LFIA already have an adequate sensitivity acceptable in diverse government agencies, such as Food and Drug Administration (FDA) [14], with a limit of detection (LOD), varying to 0.1 and 10 ng mL^{-1}[2].

Reviews about LFA already have provided a deep knowledge on specific topics, such as construction [15], Designs [16], formats [15], recognition elements [17], and instrumentalization [18]. Therefore, the aim of this chapter is to give a brief introduction on LFA, general improvements, and trends in lateral flow.

2 LFA Construction

Generally, the construction of LFA includes three principal items: membrane, biomolecules as biorecognition elements, and reporters as signal-transforming element [19]. In addition, the total construction also depends on other components shown in Table 1, which also play a crucial role in the confection of a good device [15, 16].

The detection mechanism is mainly based in capillarity phenomenon. Parameters, such as the fluid used also determine the flow behavior of the membrane, and in some cases, it requires a sample pretreatment (LFA is not an ideal platform for solid samples). Also, there are equations that can be used to predict variables such as the time of fluid transport, optimization of antibody concentration, label concentration and the length of the strip, as Washburn's equation in wet-out condition, for instance. The appropriated selection of reagents in LFAs also impacts their reproducibility. Steps, such as biomolecules immobilization, drying, washing and the time of the assay must be studied and controlled. Properties like pH, ionic strength, particle size, porosity, flow rate, and viscosity, may also contributes to LFA performance [20].

Table 1 Components of LFA and their functions

Component	Main material	Function
Sample pad	Cellulose, glass fiber	Transport of the sample through other components of lateral flow test strip
Conjugate pad	Glass fiber, polyesters	To preserve the dried biconjugate, allowing interaction with the target element, and to release them into membrane
Membrane	Nitrocellulose, polyvinylidene fluoride	Responsible for the signal generation and sensitivity. Generally, two lines are sprayed on the strip: a test line and a control line
Absorbent pad	Glass fiber	Helps to maintain the flow rate of the test
Backing card	Vinyl, PVC	Used as a support for the strip
Lateral flow cassettes	Plastic in general	Storage of the test; also helps in sample application

This device is used innumerous applications, as well as different samples with different characteristics, as we can see in the literature [16]. Further, it can be seen that the design of the LFA depends on two main points: (I) Target analyte and (II) Sample. Taking these points into consideration, it is important to remember that the confection of a reliable LFA is not trivial [21]. Some of the main advantages and disadvantages are present in Fig. 1.

The LFIA format is similar to ELISA, although it does not replace them, it can be used as trial tool, as mentioned beforehand. It uses almost the same components as the ELISA. One of the first reports of LFIA construction with immobilized antibodies on a chromatographic paper strip date in the mid of 1980. Combining the advantages of chromatographic principles and immunological recognition elements, lateral flow devices were consolidated as one of the main technologies for screening both in research and in the market [22].

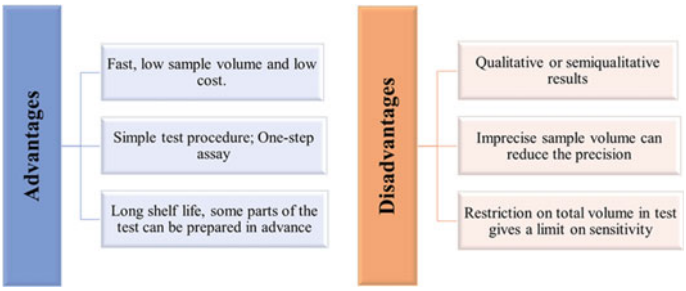

Fig. 1 Common advantages and disadvantages of LFIA. Adapted from [21]

Classified as a challenge, the biomolecule selection for LFA gives a wide possibility of bioreceptors that can be used. Antibodies can be employed as biorecognition elements on the test and control line. They are responsible for binding to the target analyte through the immunocomplex formation in the flux. Although there are commercially available LFIAs for diseases, contaminants, and hormones, they can be synthesized against specific analyte [23]. Aptamers, considered as artificial nucleic acids, are short single-stranded DNA or RNA, having a molecular weight that varies between 10 and 30 kD, and can replace antibodies in biorecognition events in the LFA. Synthesized in SELEX, aptamers can bind to target analytes due to the three-dimensional shape, hydrogen bonding, salt bridges, Van der Waals forces, electrostatic interaction, stacking of aromatic rings, and complementarity shape [24]. Nanobody is an antibody fragment, presenting with a small size (15 kD) and concave shape that can recognize and capture epitopes from antigens, which normally antibodies do not access. Due to the presence of fewer charged groups, there is less problem with cross-reaction phenomenon compared to the whole antibody; however, both only detect immunogenic molecules [25].

3 LFA for COVID-19

Normally, LFA for COVID-19 involves different types of detection: (I) Antibody (II) antigen and (III) nucleic acid detection, but commercially, until the date, only antibody and antigen detection are available. Antibody-based test do not confirm of the virus in organism, however, present a larger immunological window, stability of antibodies, and generally used as supplementary tool for monitoring immune response [26]. Although antigen-based LFAs are less sensitive than RT-PCR, is an economic way for mass testing and rapid response [7]. Besides, they can be combined with other techniques, including RT-PCR, Isothermal amplification, and CRISPR [27]. In addition, the use of nanomaterials for bioconjugate fabrication and, collection and handling of the sample is a crucial step for a good sensitivity, being as important as the manufacturing of the device. Here we only will discuss human sampling for COVID-19 detection in LFA, more information of different samples is widely discussed in literature [28].

3.1 Nanomaterials for Bioconjugation

In LFA, the use of labels is indispensable. They can be divided according to the type of readout, such as: (I) Naked-eye detection, (II) fluorescence detection, and (III) non-optical readout detection. The initial labels were the same enzymes applied for enzyme immunoassays [29]. Nowadays, new nanomaterials are classified as alternatives to enzymes, e.g., gold nanoparticles (GNPs), latex beads, carbon nanoparticles, quantum dots, magnetic nanoparticles (MNP) [16], and less often, selenium, carbon,

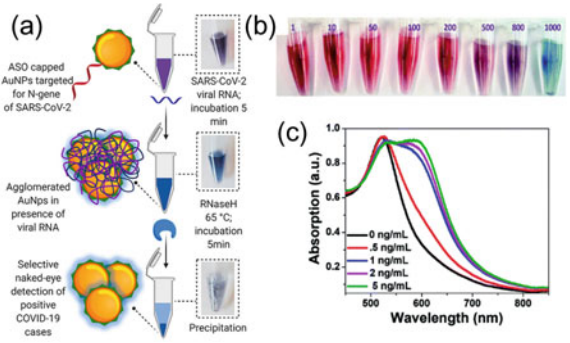

Fig. 2 **a** Schematic representation for the visual naked-eye detection of SARS-CoV-2. Reprinted from [33] with permission. ACS Copyright © 2022. **b** GNP/antibody bioconjugate change color in the presence of different concentration of COVID-19 antigen from 1 pg mL^{-1} to 1000 pg mL^{-1}. **c** UV–Vis of GNP/antibody bioconjugate at different concentration of antigen

or liposomes can be used as labels [21]. These nanomaterials help in improving their performance, as requested in real sample applications [30]. The limitations of using LFA remain in samples with low concentration of the target analytes, especially in early detection of diseases.

Nanomaterial-based assays still struggle in nonspecific biding in complex matrix. One way to control or minimize this phenomenon relies on manipulating biomolecular recognition events in the nanomaterial [31]. Bioconjugates that are design for naked detection normally involves equipment-free detection once they are based on the visual presence of test line on the LFA. Mainly for gold and silver nanoparticles, the bioconjugate monitoring can be based on localized surface plasmon resonance properties, that allow free electrons to oscillate so it is possible to absorption peaks in the visible regions, as can be seen in Fig. 2 [31]. There are several protocols for conjugation of molecules, biomolecules onto gold surface, as well different mechanism involved it, such as electrostatically, covalent, hydrophobic, ionic interaction, and chemisorption. Characteristics like nanoparticle shape, surface change, size and ligand located on nanoparticle surface show a great influence in the choice of bioconjugation process [32]. Other cautions as time of incubation, temperature, inappropriate tubes used in conjugation process, molecules/biomolecules purity, quantity, concertation of reagents, and buffer used may influence the whole process.

3.2 Human Sampling

For RT-qPCR, the nasopharyngeal, oropharyngeal swab, and saliva are the most specimens used for COVID-19 detection [34]. Also, the combination of nasopharyngeal and saliva is used to confirm viral infection, Once, the infection migrates from the upper to the lower respiratory area (nasopharyngeal, oropharyngeal), to replicate

[35]. The sample should be collected promptly, and in an appropriate manner to minimize or avoid false negative results. The collection should considerate which biomarker used, of instance, for acuate phase, virus or genetic material can be detect in 3–7 days onset. In situations that antibodies are the target, de collection of the sample should be 7–15 days after the last symptom [36] (Fig. 3).

Nasopharyngeal samples (NS) (used in antigen tests) require sterile, flexible, and long rayon swab. The use of calcium alginate swabs, wooden sticks is not allowed, once they may present substances that inactivated some viruses and can influence some molecular assays [37]. According to Centers for Disease Control and Prevention (CDC), the step of collection includes the gently and slowly insert a rayon swab through the nostril parallel to the palate until resistance is encountered. Next, the swab is rubbed and rolled leaving it in place for several seconds to absorb secretions. Then, the swab is slowly removed while rotating it, and finally placed into the transport tube. The storage respiratory specimens should be at 2–8 °C for 72 h after collection. For long store specimens, the temperature should be at −70 °C or below [38]. NS is preferably used for SARS-CoV-2 detection, especially for the reported a high sensitivity than other specimens, although its collection may be uncomfortable [39].

Presenting a similar collection protocol, oropharyngeal sample (OP) differentiate only that the insert of the swab is performed in throat. The swab is also rubbed over both tonsillar pillars and posterior oropharynx. However, studies found that using 19 positive samples for COVID-19, only nine tested positive, even when the samples where recollected [40]. A possible way that can be taken to reduce false negatives is collecting samples from multiple sites.

Blood, plasma, and serum samples are generally used for antigen or antibody detection in LFA. As already described in literature, one or two drops of blood is collected by fingerstick devices in middle or ring finger [38]. Saliva samples normally require 80 μL for the assay [41]. The storage also is taken at −20 to −80 °C [42]. The use of saliva samples is simpler, less invasive way for testing, especially for children, the main disadvantage is that the sensibility is variable [34]. Nowadays, self-test have gained attention and became commercially available, yet,

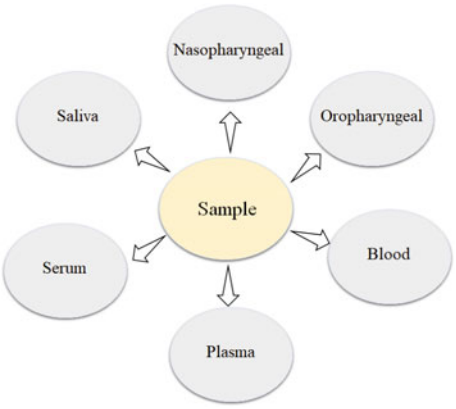

Fig. 3 Samples normally used in LFA for COVID-19, adapted from [28]

CDC reports that nasopharyngeal and oropharyngeal specimens are not appropriate for self-collection [38]. Furthermore, an important question arises: How do people will interpret the result? How will data be collected and analyzed for case tracking? A study carried with 360 adults, showed that a considerable portion misinterpreted the negative results [43].

3.3 Antibody Test

When an organism gets in contact with a pathogen, for example SARS-CoV-2, the immune system starts to produce antibodies against the infection, and this specific antibody can be useful to detect the virus using the LFIA platform [44]. This type of test is based on antigen–antibody immunocomplex formation. For example, in SARS-Cov-2, a part of the spike protein, or its immunogenic fragments, such as the Receptor-Binding Domain (RBD) can detect specific immunoglobulins (IgA, IgM and IgG) that are produced as a response to the infection, as described elsewhere [27]. Antibody tests presents some advantages compared to other configurations of LFA, for example, wider detection window, easy and safe for operators to collect blood samples than respiratory samples, higher stability, less susceptibility to degradation, uniform distribution of antibodies in blood and serum [45]. It can detect ongoing (IgM detections) or past infections (IgG detections), in order to understand the transmission dynamics of COVID-19 [46].

It is already reported that many companies provide LFA presenting results within 15–30 min. For example, Roche diagnostic produced Elecsys® Anti-SARS-CoV-2 for IgG antibody detection in serum and plasma with specificity of 99.5% [47]. Abbot developed an 10 min rapid test named Panbio™ COVID-19 IgG/IgM, presenting specificity for serum/plasma of 92.8%, fingerstick whole blood 100.0% and venous whole blood 95.8% [48]. FDA provide a complete open data for serologic test authorized is USA [49]. In academic field, it was reported a colorimetric-fluorescent dual detection of IgM and IgG for SARS-CoV-2 based on quantum dots nanobeads (SiO_2@Au@QD nanobeads (NBs) used as label [50]. Completed within 15 min and using 1 μL of serum sample, the LOD was 100 times more sensitive than the use of common GNPs. The proposed device presented 100% of specificity using a total of 16 positive serum human sample and 41 negatives from other viral infections.

The quantification of the SARS-CoV-2 antibodies using a 532 nm laser optical and gold nanoparticles was described [51]. The laser was directed at the LFIA strip, and the readout system provided the quantification of a conventional LFIA. The LOD of 4×10^8 IgG molecules was achieved. A SARS-CoV-2 antigen test immunoassay using latex microspheres to label the antibodies was reported in literature (Fig. 4a, b). This device was tested in 659 samples and showed the sensitivity and specificity of 98.22% and 97.93%, respectively [52]. At present, more than one hundred serology tests have been globally granted since the begin of the pandemic, still it is important to emphasize that antibody test is not recommended by CDC for COVID-19 diagnosis.

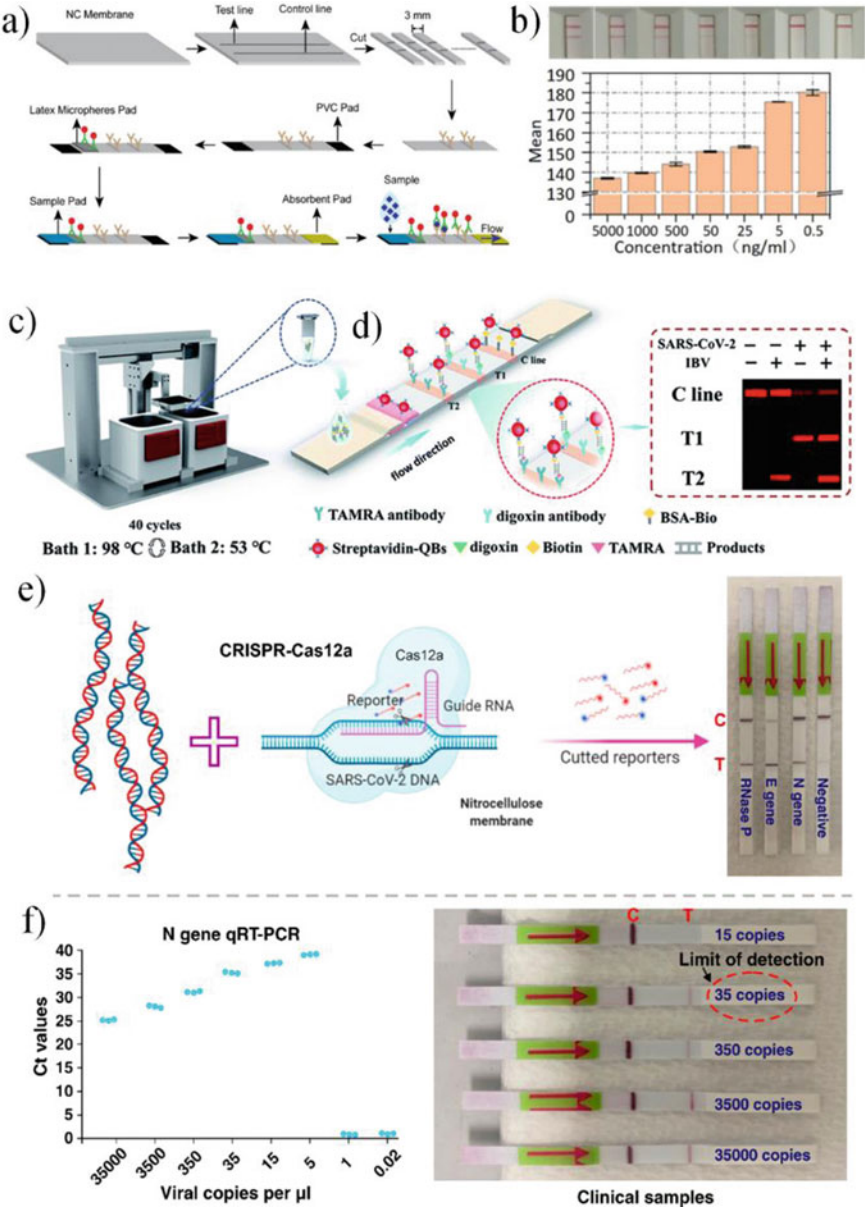

Fig. 4 Schematic representation showing the **a** Fabrication and detection principle for SARS-CoV-2 antigen test using latex microspheres; **b** Colorimetric signal of LFIA in different positive specimen dilutions. Reprinted from [52] with permission. Copyright © 2022, Wiley. **c** homemade water bath used; **d** the RT-PCR combined with LFA for the simultaneous detection of SARS-CoV-2 and influenza B virus. Reprinted from [63] with authorization. Copyright © 2022, Royal Society of Chemistry. **e** CRISPR-Cas12a reaction on pre-amplified SARS-CoV-2 target genes, and visualization of the lateral flow strips. **f** The detection limit of the RT-qPCR assay (left) using PCR machine and RT-LAMP/Cas12a assay (right) using clinical samples. Reprinted from [66] with authorization. Copyright © 2022, MDPI

3.4 Antigen Test

Governed by the same phenomenon as antibody test, the aim of this format is the detection of the antigens. This device is widely used to identify the presence of spike, membrane or nucleocapsid proteins of SARS-CoV-2 [10]. The development of antigen test for COVID-19 was considered late, and these first-generation devices have been gradually validated independently in literature [10, 53, 54]. The main obstacle remains in the identification of asymptomatic cases, once the diagnosis of COVID-19 is mostly for symptomatic individuals [10]. But successfully can identify symptomatic cases, helping in control the spread of the virus [55].

According to European commission directorate-general for health and food safety, data about commercial LFA antigen test approved for COVID-19 detection and continuous validations updates is required. Therefore, all LFA should present their efficacy to be keep in the market and recognize as a detection tool [56]. The effect of SARS-CoV-2 mutation are the main motivation for these strategies, not only for LFA but for Nucleic Acid Amplification Tests (NAAT) as well. Abbott Rapid Diagnostics created a LFA labelled as Panbio™ COVID-19 Ag Rapid Test, presenting a 98.1% of sensitivity and 99.8% specificity using nasal swab [57]. AAZ-LMB developed a self-test named COVID-VIRO ALL IN® for children. The adapted device has a different configuration for easy sample extraction. Within 15 min, the result can be read and the device presents a correlation of 97.5% with the nasopharyngeal PCR test [58].

Not only sensitivity and specificity, also positive predict value (PPV) and negative predict value (NPV) are essential to measure the risks and consequences of false positive and false negative results in guidance decision protocols in healthcare system. A prospection showed a relationship between test performance, predictive values, and disease prevalence. Here, they concluded that a lower prevalence means lower PPV and a higher number of false positive results. If it is observed an increase of the prevalence, higher is the PPV, consequently, the false positive results decrease. The sensitivity vary in elevated prevalence situations, once leads to lower NPV and a higher number of false negatives. The device should present sensitivity enough to minimize false negative results and, specific enough to avoid/minimize false positives in low prevalence scenarios [59]. The construction and correct use of an antigen test, as well as any type of test is a tiny balance of various factors that is crucial for appropriated results. A study showed an interesting pathway for a complete diagnose of COVID-19 antigen test for patients using LFA. The authors concluded that the device can be effectively adopted with POC-RT-PCR testing during periods of high and low disease prevalence [60].

3.5 Viral Nucleic Acid Detection

For viral detection, RT-PCR is the gold standard for most viral detection. Based on the reverse transcription of RNA and amplification of specific complementary DNA (cDNA) fragments, RT-PCR provides a quantitative information of viral loads in organism. The main advantage of this technique is that it is not limited by the analyte concentration; however, their accessibility may be difficult in remote regions, which requires trained staffs, and it is time-consuming with high cost of equipment and materials [27, 61]. When based on nucleic detection, LFA is named as Nucleic acid lateral flow assay (NALFA), and it is designed for testing the presence of an amplified double-stranded nucleic acid sequence using primers with two different tags [62]. Despite the limitations in early detection (since normally target concentrations can be low in the infected individual), the combination of different techniques (e.g. RT-PCR, LAMP, Clustered Regularly Interspaced Short Palindromic Repeats—CRISPR, and Loop-mediated Isothermal Amplification—LAMP) and LFA are a promising tool for a simple way to increase the accessibility of those molecular techniques [27, 61]. They are present in this chapter as improvement of the LFA.

4 General Improvements Using LFA

Nucleic acid rapid tests are extremely desired, and integration with different methods and techniques is an interesting way for popularization of this technology. In this way, a water bath PCR combined with fluorescent lateral flow assay for SARS-CoV-2 and influenza B detection was proposed (Fig. 4c, d). After the amplification process, the PCR targeted products were detected in an LFA with two test lines and streptavidin-conjugated quantum dot. The LOD were 8.44 copies per μL for SARS-CoV-2 and 14.23 copies per μL for influenza B virus [63]. Variations of RT-PCR have been proposed. Here a multiplex for three different regions of SARS-CoV-2 was developed. The device was able to detect the three genomic regions (ORF_{3a} RdRp, and N genes). The LoD was 10 copies/test, in a total time for the detection about 2 h (100 min PCR, 12 min LFA assay) [64].

A portable RT-LAMP machine combined with LFA and gold nanoparticles was described [65]. The device was designed for simultaneous detection of SARS-CoV-2 and the flu in a single reaction. The evaluation was proceeded after pre-amplified steps of viral loads and control RNA targets assays followed by the LFA readout. The LOD of 35 copies per liter was obtained in 35 min of test (Fig. 4e, 4f) [66]. The use of a near-infrared (NIR) and nanoparticle as the fluorescent labelled is reported elsewhere [65]. The aggregation-induced emission nanoparticle was designed for early detection of IgM and IgG for SARS-CoV-2 in serum sample. The LOD of IgM was 0.236 and IgG 0.125 $\mu g\ mL^{-1}$. The sensitivity was 78 and 95% for IgM and IgG respectively. The main difference was observed in the time of detecting IgM or

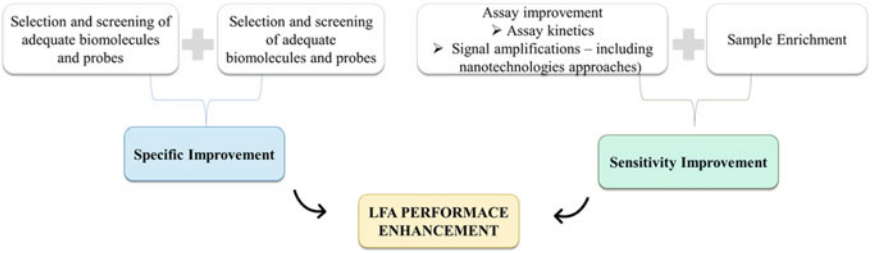

Fig. 5 Schematic representation of the main points for the enhancement of LFA detection performance. Adapted from [69]

IgG, that using the proposed label, clinical samples were analysed in 1–7 days after symptom onset, earlier than the common use of GNPs-based test strip (8–15 days).

The LAMP also can be optimized, a multiplex LAMP for SARS-CoV-2 was developed. The target genes N and ORF1ab were simultaneously amplified and detected using a LFA strip [67]. Completed within 1 h, the LOD obtained was 12 copies for both targets. Parameters such as sensitivity and the specificity were both 100%.

Electrophoresis, dialysis, and magnetic enrichment can be used to improve the performance of LFA [16, 68]. Extractions and pre-concentration based on two-phase system to obtain biomarkers before loading them on LFA can also be used. Other approaches can be focused on the components of the LFA, for example. NC membrane size change, inclusion of new components of LFA, such as wax barrier to delay the flux, different pre-treatments in sample and conjugate pad, blocking agents etc. [16, 68]. Figure 5 is a schematic representation of the general points for LFA enhancement.

LFA technology holds a great importance as an useful tool for screening and mass-testing for COVID-19 and different diseases. Despite to be easy handle, the construction itself is not trivial, and in the most of cases requires improvement of their performance. Obviously, the upgrade that have been applied in LFA assays were absurd in these almost 3 years. Validation steps are crucial, though, the access to positive and negative samples is not easy task in some cases, also, the poor sample collection, and the use of non-fresh specimen also impact in the device performance.

LFA also is vastly explored in multi target detection as already mentioned. This trend is clearly observed in the number of publications focusing in multi-target detection and in commercial tests available [70]. A great number of multiplexing technology in the LFA has been developed for a few years [71]. Additionally, different configurations of LFA is already described, such as the addition of two conjugate pads for the simultaneous detection of two proteins [5] and different conformations of LFA strips for the simultaneous detection of 10 different antibodies by using a 10-channel disc configuration for 10 different LFIA [72]. Lateral flow platform for COVID-19 might not be restricted to only to detect a single type of target, once the simultaneous detection of antibodies and antigens against SARS-CoV-2 and its

mutants by a single LFA can be a great instrument for vaccine and pathology studies. Understanding how each LFA test strip performs when different targets are utilized as test objects is critical to achieving this goal [27].

5 Future Perspectives

Lateral flow technology has date over 50 years ago and between all these years, innumerous applications such as medical, veterinary field, agricultural etc. have been developed. LFA shows great importance in the global market because their facilities as simplicity, since only few drops of the sample are required, with relativity low-cost production, compared to other technologies. However, the detection and diagnosis of many diseases, especially SARS-CoV-2 infection remains as a challenge for LFA to be accepted as a gold standard like RT-PCR or ELISA.

One of the principal limitations is the quantitative or semi-quantitative detections, of which some diseases require quantification of their biomarker. Ideally, rapid test must provide a reliable early detection, help to personalized treatment, or be used for mass-testing in healthcare. Various formats of LFA platform have sprung up in last 10 years, and the advance in nanomaterials field allows the achievement of lower LOD. In this way, the lateral flow assay is considered a helpful complement to RT-PCR and ELISA, once it is widely available in low-resource settings.

If large-scale testing of is already a reality, in the next few years, we might expect an efficient implementation of different technologies for performance, processing and collection of the data generated by lateral flow devices. Nevertheless, those technological integration of LFAs in the future can increase the cost of analysis, thereby making them unsuitable for self-test at home or in low-resource areas.

Acknowledgements The authors gratefully acknowledge the Coordinating Agency for Advanced Training of Graduate Personnel (CAPES), MeDiCo Network CAPES, Brazil grant number 88881.504532/2020-01 and 88887.511448/2020-00. Fundação de Amparo à Pesquisa do Estado de São Paulo—FAPESP, grant numbers: 2019/12053-8, 2019/15333-1, 2018/22214-6 and 2021/10911-7.

References

1. World Health Organization (WHO), *WHO Coronavirus (COVID-19) Dashboard*, (2021). https://covid19.who.int/info/
2. F. Di Nardo, M. Chiarello, S. Cavalera, C. Baggiani, L. Anfossi, Ten years of lateral flow immunoassay technique applications: trends, challenges and future perspectives. Sensors **21**, 5185 (2021). https://doi.org/10.3390/s21155185
3. I.A. Mattioli, A. Hassan, O.N. Oliveira Jr., F.N. Crespilho, O.N. Oliveira, F.N. Crespilho, On the challenges for the diagnosis of SARS-CoV-2 based on a review of current methodologies. ACS Sensors **5**, 3655–3677 (2020). https://doi.org/10.1021/acssensors.0c01382

4. J.M. Van Emon, *Immunoassay and Other Bioanalytical Techniques* (CRC Press, Boca Raton, 2016)
5. K.M. Koczula, A. Gallotta, Lateral flow assays. Essays Biochem. **60**, 111–120 (2016). https://doi.org/10.1042/EBC20150012
6. H. Chen, A.E.V. Hagström, J. Kim, G. Garvey, A. Paterson, F. Ruiz-Ruiz, B. Raja, U. Strych, M. Rito-Palomares, K. Kourentzi, J.C. Conrad, R.L. Atmar, R.C. Willson, Flotation immunoassay: masking the signal from free reporters in sandwich immunoassays. Sci. Rep. **6**, 24297 (2016). https://doi.org/10.1038/srep24297
7. B.D. Grant, C.E. Anderson, J.R. Williford, L.F. Alonzo, V.A. Glukhova, D.S. Boyle, B.H. Weigl, K.P. Nichols, SARS-CoV-2 coronavirus nucleocapsid antigen-detecting half-strip lateral flow assay toward the development of point of care tests using commercially available reagents. Anal. Chem. **92**, 11305–11309 (2020). https://doi.org/10.1021/acs.analchem.0c01975
8. R.S. Yalow, S.A. Berson, Immunoassay of endogenous plasma insulin in man. J. Clin. Invest. **39**, 1157–1175 (1960). https://doi.org/10.1172/JCI104130
9. R. and Markets, Lateral Flow Assays - Global Market Trajectory & Analytics, (2021). https://www.researchandmarkets.com/reports/4805627/lateral-flow-assays-global-market-trajectory (toegang verkry 12 Februarie 2022)
10. T. Peto, D. Affron, B. Afrough, A. Agasu, COVID-19: rapid antigen detection for SARS-CoV-2 by lateral flow assay: a national systematic evaluation of sensitivity and specificity for mass-testing. EClinicalMedicine. 36, 0–6 (2021). https://doi.org/10.1016/j.eclinm.2021.100924
11. J. Liu, S. Gao, L. Kang, B. Ji, W. Xin, J. Kang, P. Li, J. Gao, H. Wang, J. Wang, H. Yang, An ultrasensitive gold nanoparticle-based lateral flow test for the detection of active botulinum neurotoxin type A. Nanoscale Res. Lett. **12**, 227 (2017). https://doi.org/10.1186/s11671-017-1944-9
12. C. Liu, Q. Jia, C. Yang, R. Qiao, L. Jing, L. Wang, C. Xu, M. Gao, Lateral flow immunochromatographic assay for sensitive pesticide detection by using Fe_3O_4 nanoparticle aggregates as color reagents. Anal. Chem. **83**, 6778–6784 (2011). https://doi.org/10.1021/ac201462d
13. L. Bian, J. Liang, H. Zhao, K. Ye, Z. Li, T. Liu, J. Peng, Y. Wu, G. Lin, Rapid monitoring of vancomycin concentration in serum using europium (III) Chelate nanoparticle-based lateral flow immunoassay. Front. Chem. **9** (2021). https://doi.org/10.3389/fchem.2021.763686
14. FDA, EUA authorized serology test performance (2021). https://www.fda.gov/medical-devices/coronavirus-disease-2019-covid-19-emergency-use-authorizations-medical-devices/eua-authorized-serology-test-performance (toegang verkry 12 Februarie 2022)
15. M. Sajid, M. Daud, Designs, formats and applications of lateral flow assay: a literature review. J. Saudi Chem. Soc. **19**, 689–705 (2015). https://doi.org/10.1016/j.jscs.2014.09.001
16. C. Parolo, A. Sena-Torralba, J.F. Bergua, E. Calucho, C. Fuentes-Chust, L. Hu, L. Rivas, R. Álvarez-Diduk, E.P. Nguyen, S. Cinti, D. Quesada-González, A. Merkoçi, Tutorial: design and fabrication of nanoparticle-based lateral-flow immunoassays. Nat. Protoc. **15**, 3788–3816 (2020). https://doi.org/10.1038/s41596-020-0357-x
17. V. Perumal, U. Hashim, Advances in biosensors: principle, architecture and applications. J. Appl. Biomed. **12**, 1–15 (2014). https://doi.org/10.1016/j.jab.2013.02.001
18. W.C. Mak, V. Beni, A.P.F. Turner, Lateral-flow technology: from visual to instrumental. TrAC Trends Anal. Chem. **79**, 297–305 (2016). https://doi.org/10.1016/j.trac.2015.10.017
19. F. Li, M. You, S. Li, J. Hu, C. Liu, Y. Gong, H. Yang, F. Xu, Paper-based point-of-care immunoassays: recent advances and emerging trends. Biotechnol. Adv. **39**, 107442 (2020). https://doi.org/10.1016/j.biotechadv.2019.107442
20. S. Kasetsirikul, M.J.A. Shiddiky, N.-T. Nguyen, Challenges and perspectives in the development of paper-based lateral flow assays. Microfluid. Nanofluidics. **24**, 17 (2020). https://doi.org/10.1007/s10404-020-2321-z
21. G.A. Posthuma-Trumpie, J. Korf, A. van Amerongen, Lateral flow (immuno)assay: its strengths, weaknesses, opportunities and threats. A literature survey. Anal. Bioanal. Chem. **393**, 569–582 (2009). https://doi.org/10.1007/s00216-008-2287-2

22. D.J. Litman, T.M. Hanlon, E.F. Ullman, Enzyme channeling immunoassay: a new homogeneous enzyme immunoassay technique. Anal. Biochem. **106**, 223–229 (1980). https://doi.org/10.1016/0003-2697(80)90141-4
23. R.-M. Lu, Y.-C. Hwang, I.-J. Liu, C.-C. Lee, H.-Z. Tsai, H.-J. Li, H.-C. Wu, Development of therapeutic antibodies for the treatment of diseases. J. Biomed. Sci. **27**, 1 (2020). https://doi.org/10.1186/s12929-019-0592-z
24. M. Majdinasab, M. Badea, J.L. Marty, Aptamer-based lateral flow assays: current trends in clinical diagnostic rapid tests. Pharmaceuticals **15** (2022). https://doi.org/10.3390/ph15010090
25. Y. Liu, L. Zhan, Z. Qin, J. Sackrison, J.C. Bischof, Ultrasensitive and highly specific lateral flow assays for point-of-care diagnosis. ACS Nano **15**, 3593–3611 (2021). https://doi.org/10.1021/acsnano.0c10035
26. G. Liu, J.F. Rusling, COVID-19 antibody tests and their limitations. ACS Sens. **6**, 593–612 (2021). https://doi.org/10.1021/acssensors.0c02621
27. Y. Zhou, Y. Wu, L. Ding, X. Huang, Y. Xiong, Point-of-care COVID-19 diagnostics powered by lateral flow assay. Trends Analyt. Chem. **145**, 116452 (2021). https://doi.org/10.1016/j.trac.2021.116452
28. S. Purohit, P.K. Rao, D. Rawtani, in Sampling and Analytical Techniques for COVID-19 (Chap. 4), ed. by D. Rawtani, C.M. Hussain, N.B.T.-C.-19 in the E. Khatri (Reds) (Elsevier, 2022), bll 75–94. https://doi.org/10.1016/B978-0-323-90272-4.00008-7
29. M.G. Pappas, R. Hajkowski, W.T. Hockmeyer, Dot enzyme-linked immunosorbent assay (Dot-ELISA): a micro technique for the rapid diagnosis of visceral leishmaniasis. J. Immunol. Methods. **64**, 205–214 (1983). https://doi.org/10.1016/0022-1759(83)90399-X
30. D. Quesada-González, A. Merkoçi, Nanoparticle-based lateral flow biosensors. Biosens. Bioelectron. **73**, 47–63 (2015). https://doi.org/10.1016/j.bios.2015.05.050
31. A. Pramanik, Y. Gao, S. Patibandla, K. Gates, P.C. Ray, Bioconjugated nanomaterial for targeted diagnosis of SARS-CoV-2. Accounts Mater. Res. **3**, 134–148 (2022). https://doi.org/10.1021/accountsmr.1c00177
32. M.H. Jazayeri, H. Amani, A.A. Pourfatollah, H. Pazoki-Toroudi, B. Sedighimoghaddam, M. Hadi, H. Amani, A. Akbar, H. Pazoki-Toroudi, B. Sedighimoghaddam, M.H. Jazayeri, H. Amani, A.A. Pourfatollah, H. Pazoki-Toroudi, B. Sedighimoghaddam, Various methods of gold nanoparticles (GNPs) conjugation to antibodies. Sens. Bio-Sensing Res. **9**, 17–22 (2016). https://doi.org/10.1016/j.sbsr.2016.04.002
33. P. Moitra, M. Alafeef, K. Dighe, M.B. Frieman, D. Pan, Selective naked-eye detection of SARS-CoV-2 mediated by N gene targeted antisense oligonucleotide capped plasmonic nanoparticles. ACS Nano **14**, 7617–7627 (2020). https://doi.org/10.1021/acsnano.0c03822
34. M. Ahmadzadeh, H. Vahidi, A. Mahboubi, F. Hajifathaliha, L. Nematollahi, E. Mohit, Different respiratory samples for COVID-19 detection by standard and direct quantitative RT-PCR: a literature review, Iran. J. Pharm. Res. **20**, 285–299 (2021). https://doi.org/10.22037/ijpr.2021.115458.15383
35. D. Wang, B. Hu, C. Hu, F. Zhu, X. Liu, J. Zhang, B. Wang, H. Xiang, Z. Cheng, Y. Xiong, Y. Zhao, Y. Li, X. Wang, Z. Peng, Clinical characteristics of 138 hospitalized patients with 2019 novel coronavirus–infected pneumonia in Wuhan. China. JAMA **323**, 1061–1069 (2020). https://doi.org/10.1001/jama.2020.1585
36. J.A. Al-Mughales, T.J. Al-Mughales, O.I. Saadah, Monitoring specific IgM and IgG production among severe COVID-19 patients using qualitative and quantitative immunodiagnostic assays: a retrospective cohort study. Front. Immunol. **12** (2021). https://doi.org/10.3389/fimmu.2021.705441
37. Pan American Health Organization, Sample collection (2020). https://www3.paho.org/hq/index.php?option=com_content&view=article&id=7918:2012-videos-sample-collection&Itemid=40295&lang=pt (toegang verkry 27 April 2022)
38. Centers for Disease Control and Prevention, Interim guidelines for collecting and handling of clinical specimens for COVID-19 testing (2021). https://www.cdc.gov/coronavirus/2019-ncov/lab/guidelines-clinical-specimens.html (toegang verkry 27 April 2022)

39. H. Wang, Q. Liu, J. Hu, M. Zhou, M. Yu, K. Li, D. Xu, Y. Xiao, J. Yang, Y. Lu, F. Wang, P. Yin, S. Xu, Nasopharyngeal swabs are more sensitive than oropharyngeal swabs for COVID-19 diagnosis and monitoring the SARS-CoV-2 load. Front. Med. **7** (2020). https://doi.org/10.3389/fmed.2020.00334
40. C. Xie, L. Jiang, G. Huang, H. Pu, B. Gong, H. Lin, S. Ma, X. Chen, B. Long, G. Si, H. Yu, L. Jiang, X. Yang, Y. Shi, Z. Yang, Comparison of different samples for 2019 novel coronavirus detection by nucleic acid amplification tests. Int. J. Infect. Dis. IJID Off. Publ. Int. Soc. Infect. Dis. **93**, 264–267 (2020). https://doi.org/10.1016/j.ijid.2020.02.050
41. A. Roda, S. Cavalera, F. Di Nardo, D. Calabria, S. Rosati, P. Simoni, B. Colitti, C. Baggiani, M. Roda, L. Anfossi, Dual lateral flow optical/chemiluminescence immunosensors for the rapid detection of salivary and serum IgA in patients with COVID-19 disease. Biosens. Bioelectron. **172**, 112765 (2021). https://doi.org/10.1016/j.bios.2020.112765
42. B.S. Henson, D.T. Wong, in *Collection, Storage, and Processing of Saliva Samples for Downstream Molecular Applications BT—Oral Biology: Molecular Techniques and Applications*, ed. by G.J. Seymour, M.P. Cullinan, N.C.K. Heng (Reds) (Humana Press, Totowa, 2010), bll 21–30. https://doi.org/10.1007/978-1-60761-820-1_2
43. S. Woloshin, B. Dewitt, T. Krishnamurti, B. Fischhoff, Assessing how consumers interpret and act on results from at-home COVID-19 self-test kits a randomized clinical trial. JAMA Intern. Med. **182**, 332–341 (2022). https://doi.org/10.1001/jamainternmed.2021.8075
44. C. Wang, W. Li, D. Drabek, N.M.A. Okba, R. van Haperen, A.D.M.E. Osterhaus, F.J.M. van Kuppeveld, B.L. Haagmans, F. Grosveld, B.-J. Bosch, A human monoclonal antibody blocking SARS-CoV-2 infection. Nat. Commun. **11**, 2251 (2020). https://doi.org/10.1038/s41467-020-16256-y
45. R. Jalandra, A.K. Yadav, D. Verma, N. Dalal, M. Sharma, R. Singh, A. Kumar, P.R. Solanki, Strategies and perspectives to develop SARS-CoV-2 detection methods and diagnostics. Biomed. Pharmacother. **129**, 110446 (2020). https://doi.org/10.1016/j.biopha.2020.110446
46. A. Petherick, Developing antibody tests for SARS-CoV-2. Lancet **395**, 1101–1102 (2020). https://doi.org/10.1016/S0140-6736(20)30788-1
47. Roche Diagnostics, Elecsys® Anti-SARS-CoV-2 (2022). https://diagnostics.roche.com/global/en/products/params/elecsys-anti-sars-cov-2.html (toegang verkry 27 April 2022)
48. Abbott, PANBIO™ COVID-19 IgG/IgM rapid test device (2020). https://www.globalpointofcare.abbott/en/product-details/panbio-covid-19-igg-igm-antibody-test.html (toegang verkry 07 April 2022)
49. FDA, Independent evaluations of COVID-19 serological tests (2020). https://open.fda.gov/apis/device/covid19serology/
50. C. Wang, X. Yang, B. Gu, H. Liu, Z. Zhou, L. Shi, X. Cheng, S. Wang, Sensitive and simultaneous detection of SARS-CoV-2-specific IgM/IgG using lateral flow immunoassay based on dual-mode quantum dot nanobeads. Anal. Chem. **92**, 15542–15549 (2020). https://doi.org/10.1021/acs.analchem.0c03484
51. T. Peng, X. Liu, L.G. Adams, G. Agarwal, B. Akey, J. Cirillo, V. Deckert, S. Delfan, E. Fry, Z. Han, P. Hemmer, G. Kattawar, M. Kim, M.-C. Lee, C. Lu, J. Mogford, R. Nessler, B. Neuman, X. Nie, J. Pan, J. Pryor, N. Rajil, Y. Shih, A. Sokolov, A. Svidzinsky, D. Wang, Z. Yi, A. Zheltikov, M. Scully, Enhancing sensitivity of lateral flow assay with application to SARS-CoV-2. Appl. Phys. Lett. **117**, 120601 (2020). https://doi.org/10.1063/5.0021842
52. L. Shen, Q. Zhang, X. Luo, H. Xiao, M. Gu, L. Cao, F. Zhao, Z. Chen, A rapid lateral flow immunoassay strip for detection of SARS-CoV-2 antigen using latex microspheres. J. Clin. Lab. Anal. **35**, e24091 (2021). https://doi.org/10.1002/jcla.24091
53. A.K. Lindner, O. Nikolai, C. Rohardt, F. Kausch, M. Wintel, M. Gertler, S. Burock, M. Hörig, J. Bernhard, F. Tobian, M. Gaeddert, F. Lainati, V.M. Corman, T.C. Jones, J.A. Sacks, J. Seybold, C.M. Denkinger, F.P. Mockenhaupt, Diagnostic accuracy and feasibility of patient self-testing with a SARS-CoV-2 antigen-detecting rapid test. J. Clin. Virol. **141**, 104874 (2021). https://doi.org/10.1016/j.jcv.2021.104874
54. P. Merino et al., Multicenter evaluation of the Panbio™ COVID-19 rapid antigen-detection test for the diagnosis of SARS-CoV-2 infection. Clin. Microbiol. Infect. **27**, 758–761 (2021). https://doi.org/10.1016/j.cmi.2021.02.001

55. W.-Y. Hsieh, C.-H. Lin, T.-C. Lin, C.-H. Lin, H.-F. Chang, C.-H. Tsai, H.-T. Wu, C.-S. Lin, Development and efficacy of lateral flow point-of-care testing devices for rapid and mass COVID-19 diagnosis by the detections of SARS-CoV-2 antigen and anti-SARS-CoV-2 antibodies. Diagnostics (Basel, Switzerland). **11** (2021). https://doi.org/10.3390/diagnostics11101760
56. European Commission Directorate-General for Health and Food Safety, EU health preparedness: a common list of COVID-19 rapid antigen tests; a common standardised set of data to be included in COVID-19 test result certificates; and a common list of COVID-19 laboratory based antigenic assays (2021). https://ec.europa.eu/health/sites/health/files/preparedness_response/docs/common_testingapproach_covid-19_en.pdf
57. Abbott, PanbioTM COVID-19 Ag rapid test device (2022). https://www.abbott.co.uk/panbio.html
58. AAZ, Autotest covid suitable for children—autotest COVID-VIRO ALL IN® (2022). https://www.covid19aaz.com/en/autotest-covid-viro-all-in/
59. R.W. Peeling, P.L. Olliaro, D.I. Boeras, N. Fongwen, Scaling up COVID-19 rapid antigen tests: promises and challenges. Lancet Infect. Dis. **21**, e290–e295 (2021). https://doi.org/10.1016/S1473-3099(21)00048-7
60. B. Merrick, M. Noronha, R. Batra, S. Douthwaite, G. Nebbia, L.B. Snell, S. Pickering, R.P. Galao, J. Whitfield, A. Jahangeer, R. Gunawardena, T. Godfrey, R. Laifa, K. Webber, P.R. Cliff, E. Cunningham, S.J.D. Neil, H. Gettings, J.D. Edgeworth, H.L. Harrison, Real-world deployment of lateral flow SARS-CoV-2 antigen detection in the emergency department to provide rapid, accurate and safe diagnosis of COVID-19. Infect. Prev. Pract. **3**, 100186 (2021). https://doi.org/10.1016/j.infpip.2021.100186
61. S. Agarwal, C. Warmt, J. Henkel, L. Schrick, A. Nitsche, F.F. Bier, Lateral flow–based nucleic acid detection of SARS-CoV-2 using enzymatic incorporation of biotin-labeled dUTP for POCT use. Anal. Bioanal. Chem. (2022). https://doi.org/10.1007/s00216-022-03880-4
62. M. Blažková, M. Koets, P. Rauch, A. van Amerongen, Development of a nucleic acid lateral flow immunoassay for simultaneous detection of *Listeria* spp. and Listeriamonocytogenes in food. Eur. Food Res. Technol. **229**, 867 (2009). https://doi.org/10.1007/s00217-009-1115-z
63. H. Chen, Y. Wang, H. Wei, Z. Rong, S. Wang, A rapid water bath PCR combined with lateral flow assay for the simultaneous detection of SARS-CoV-2 and influenza B virus. RSC Adv. **12**, 3437–3444 (2022). https://doi.org/10.1039/d1ra07756b
64. S. Yu, S.B. Nimse, J. Kim, K.-S. Song, T. Kim, Development of a lateral flow strip membrane assay for rapid and sensitive detection of the SARS-CoV-2. Anal. Chem. **92**, 14139–14144 (2020). https://doi.org/10.1021/acs.analchem.0c03202
65. R. Chen, C. Ren, M. Liu, X. Ge, M. Qu, X. Zhou, M. Liang, Y. Liu, F. Li, Early detection of SARS-CoV-2 seroconversion in humans with aggregation-induced near-infrared emission nanoparticle-labeled lateral flow immunoassay. ACS Nano **15**, 8996–9004 (2021). https://doi.org/10.1021/acsnano.1c01932
66. M. Rezaei, S. Razavi Bazaz, D. Morshedi Rad, O. Shimoni, D. Jin, W. Rawlinson, M. Ebrahimi Warkiani, A portable RT-LAMP/CRISPR machine for rapid COVID-19 screening. Biosensors **11** (2021). https://doi.org/10.3390/bios11100369
67. X. Zhu, X. Wang, L. Han, T. Chen, L. Wang, H. Li, S. Li, L. He, X. Fu, S. Chen, M. Xing, H. Chen, Y. Wang, Multiplex reverse transcription loop-mediated isothermal amplification combined with nanoparticle-based lateral flow biosensor for the diagnosis of COVID-19. Biosens. Bioelectron. **166**, 112437 (2020). https://doi.org/10.1016/j.bios.2020.112437
68. Y. Deng, H. Jiang, X. Li, X. Lv, Recent advances in sensitivity enhancement for lateral flow assay. Mikrochim. Acta. **188**, 379 (2021). https://doi.org/10.1007/s00604-021-05037-z
69. L. Napione, Integrated nanomaterials and nanotechnologies in lateral flow tests for personalized medicine applications. Nanomaterials **11** (2021). https://doi.org/10.3390/nano11092362
70. F. Mahmoudinobar, D. Britton, J.K. Montclare, Protein-based lateral flow assays for COVID-19 detection. Protein Eng. Des. Sel. **34** (2021). https://doi.org/10.1093/protein/gzab010
71. L. Anfossi, F. Di Nardo, S. Cavalera, C. Giovannoli, C. Baggiani, Multiplex lateral flow immunoassay: an overview of strategies towards high-throughput point-of-need testing. Biosensors **9**, 2 (2018). https://doi.org/10.3390/bios9010002

72. Y. Zhao, H. Wang, P. Zhang, C. Sun, X. Wang, X. Wang, R. Yang, C. Wang, L. Zhou, Rapid multiplex detection of 10 foodborne pathogens with an up-converting phosphor technology-based 10-channel lateral flow assay. Sci. Rep. **6**, 21342 (2016). https://doi.org/10.1038/srep21342

The Use of NMR Based Metabolomics to Discriminate Patients with Viral Diseases

Banny Silva Barbosa Correia, Priscila Marques Firmiano Dalle Piagge, Luísa Souza Almeida, Gabriel Henrique Ribeiro, Cristina de Souza Peixoto, Luiz Alberto Colnago, and Daniel Rodrigues Cardoso

Abstract Infectious diseases are one of the most common conditions impacting global health, being a matter of concern for health agencies due to their contagious capacity and periodic outbreaks of new diseases, such as the global pandemic COVID-19. Viruses are among the main causes of this illness and it is defined as obligate intracellular parasites for their need to have a host cell to live and reproduce, since they won't produce proteins and compete for nutrients and metabolites leading to the alteration of the host metabolome. The diagnosis of these viral infections can be done by detecting viral particles or components, isolating the virus in cell culture, or even by evaluating immune responses. In this context, metabolomics comes as a very useful tool that reflects all "omics" techniques and best represents the phenotype. Since water-soluble metabolites and lipids are the major molecular constituents of human plasma, their abnormalities are commonly observed during disease, which contributes to the understanding of physiology and pathology. Nuclear magnetic resonance (NMR) spectroscopy and mass spectrometry (MS) are the most widely used techniques in metabolomics. NMR spectroscopy has emerged as a valuable application due to its ability to identify compounds with simple sample preparation, in addition, to being a non-destructive, highly reproducible, and quantitative technique (primary ratio method). These features make NMR a valuable tool that is frequently used in metabolomics analysis, and nowadays used in the diagnosis of viral diseases. Therefore, in this chapter, we will address a short integrative description of viral diseases and diagnostics, metabolomics, and NMR concepts. Furthermore, we will explore the advances in NMR-based metabolomics applied in medicine, and finally, the viral diseases discriminated by NMR-based metabolomics.

Keywords NMR · Metabolomics · Viral diseases · Prognosis

B. S. B. Correia · P. M. F. D. Piagge · L. S. Almeida · C. de Souza Peixoto · D. R. Cardoso (✉)
University of Sao Paulo, Chemistry Institute of Sao Carlos, São Carlos, Sao Paulo 13560-970, CP 780, Brazil
e-mail: drcardoso@iqsc.usp.br

G. H. Ribeiro · L. A. Colnago
Embrapa Instrumentation, Brazilian Agricultural Research Corporation, Sao Carlos, Sao Paulo 13570-970, Brazil

F. N. Crespilho (ed.), *COVID-19 Metabolomics and Diagnosis*,
https://doi.org/10.1007/978-3-031-15889-6_7

1 Introduction

Viruses are one of the major causes of human diseases, ranging from mild to several symptoms including death. Influenza viruses have been the most lethal viruses since early 1900. More recently, Acquired Immune Deficiency Syndrome (AIDS) caused by the human immunodeficiency virus (HIV), and COVID-19, caused by the human coronavirus SARS-CoV2 have been the major new virus diseases affecting people around the world. COVID-19 has been declared a pandemic by the World Health Organization (WHO) in March 2020 and until March 2022 (2 years later) caused 6 million people to die [1]. Other viral outbreaks causing severe symptoms and death have emerged in recent decades including Dengue, Zika, and Ebola viruses. Table 1 shows the most common human viral diseases worldwide, their clinical manifestations, and their detection methods [2–21].

Viruses are structures formed by proteins and other compounds that encapsulate DNA or RNA molecules. Therefore, viruses don't have the biological machinery to self-replicate and consequently, they have to infect a specific living cell to use their replicating machinery to form new virus particles and continue the infection process [22]. Consequently, the metabolism of infected cells is strongly affected by virus replication. In multicellular organisms, like animals and plants, virus infections may strongly affect the metabolism of the entire being. Therefore, the metabolomics approach can be a useful technique to monitor the virus's infection and the organism´s response to the infection.

1.1 Metabolomics

Cells are constantly involved in a great variety of chemical reactions, acting on intra- and extracellular communication to provide essential biochemical processes for the survival of the organism as a whole, such as protection and energy. Every single reaction is linked in its way to one another, resulting in a complex network, formed by lots of different pathways. Therefore, metabolism is defined as a set of interconnected biochemical reactions that requires a collective and complementary work of all pathways [23].

Each molecule in the complex network of metabolism has its function, such as signalize other molecules to start a reaction/process. Most biochemical reactions in a metabolic system don't present a pattern and spontaneous behavior since it is considered an open system, which is in constant energy exchange. Hence, released energy from a reaction contributes to the facilitation of another reaction. Enzymes can also act as a facilitator, since they withhold the capacity of catalyzing a reaction, lowering the activation energy barrier required for a given reaction, allowing it to proceed without changing the original arrangement of the facilitator [23].

Metabolic pathways may always provide a synthesis or decomposition of some components of the organism. Anabolism is a set of pathways that requires a load of

Table 1 Most common human viral diseases, their clinical manifestations, and their detection methods [2–21]

Disease	Viral pathogenic	Symptoms	Detection method
Acquired immune deficiency syndrome (AIDS)	Human immunodeficiency virus (HIV)	Fever, malaise, sore throat, muscle pain, and rash	ELISA
Chickenpox	Varicella-zoster virus (VVZ)	Fever, headache, fatigue, pharyngitis, and blisters on the chest, back, and face	PCR
Common cold	Rhinovirus (HRV)	Nasal congestion, runny nose, sneezing, headache, cough, and sore throat	Observation of the symptoms' progression
COVID-19	Coronavirus (SARS-CoV-2)	Fever, fatigue, cough, weakness, nausea, vomiting, diarrhea, shortness of breath, and changes to taste and smell	RT-PCR
Dengue	Dengue virus (DENV)	Severe headache, swollen glands, nausea, vomiting, rash, muscle, joint, and behind the eyes pain	PCR and ELISA
Ebola virus disease (EVD)	Ebolavirus (EBV)	Fever, fatigue, headache, sore throat, vomiting, diarrhea, rash, and muscle pain	RT-PCR and ELISA
Genital warts	Human papilomavirus (HPV)	Sore throat, earache, neck mass, and warts in the genital area	Biopsy
Hepatitis B	Hepatitis B virus (HBV)	Fatigue, nausea, vomiting, abdominal pain, dark urine, and jaundice	ELISA
Hepatitis C	Hepatitis C virus (HRV)	Fatigue, weakness, nausea weight loss, anorexia, joint, and muscle pain	PCR and ELISA
Infectious Mononucleosis	Epstein-Barr virus (EBV)	Fever, headache, splenomegaly, lymphadenopathy, and sore throat	Immunofluorescent test
Influenza A	Influenza A virus (IAV)	Fever, malaise, cough, sore throat, runny nose, muscle, and joint pain	RT-PCR and viral culture

(continued)

Table 1 (continued)

Disease	Viral pathogenic	Symptoms	Detection method
Measles	Measles virus (MV)	Fever, headache, abdominal and pharynx pain, photophobia, swelling of lymph nodes, coryza, cough, and conjunctivitis	ELISA and viral culture
Mumps	Mumps virus (MuV)	Fever, headache, malaise, anorexia, parotid swelling, and muscle pain	RT-PCR and immunofluorescent test
Oral Herpes	Herpes simplex virus (HSV)	Fever, muscle pain, headache, swollen lymph nodes, and blisters or ulcers at the oral mucosa	Viral culture
Poliomyelitis	Poliovirus (PV)	Fever, fatigue, headache, vomiting, limb pain, and stiff neck, followed by paralysis	PCR and viral culture
Rabies	Rabies virus (RABV)	Fever, pain, and paraesthesia around the wound site	RT-PCR
Respiratory viral sepsis	Adenovirus (ADV)	Fever, cough, sore throat, nasal congestion, and runny nose	PCR and viral culture
Smallpox	Variola virus	Fever, headache, backache, abdominal pain, vomiting, rashes on the face, arms's and legs	PCR and viral culture
Yellow fever	Yellow fever virus (YFV)	Fever, fatigue, headache, nausea, vomiting, jaundice, and muscle pain	PCR and ELISA
Zika fever	Zika virus (ZIKV)	Fever, headache, sore throat, conjunctivitis, rash, joint, and muscle pain	PCR

PCR: polymerase chain reaction**, RT-PCR:** reverse transcription-polymerase chain reaction**, ELISA:** enzyme-linked immunosorbent assay

energy to complete the synthesis of complex molecules, using smaller and simpler ones as precursors. On the other hand, catabolism presents a collection of pathways that performs the rupture of chemical bonds, creating some small molecules from one complex structure to create energy-storing molecules, which can be used in anabolic pathways in an endless cycle [23].

Metabolites are the byproduct or the intermediate of such metabolic process. As the final product of a reaction, these compounds may indicate disturbances in some specific pathways, since it reflects each alteration that the organism has suffered because the organism will contribute in a different way to the formation or decomposition of these small molecules. Thus, metabolites analysis may offer a complete vision of one's phenotypical responses that other macromolecules cannot. Proteins may suffer post-transcriptional adaptations, as well as genes, may suffer epigenetic regulations, making it difficult to directly correlate these macromolecules with the organism's phenotypic behavior [23].

Metabolomics is an emerging field within the "omics" sciences, concerning the biochemical processes that take place within a cell, tissue, or organism, involving a specific group of metabolites in a metabolome, as an approach to assimilating biological mechanisms and map functions of metabolic pathways. Metabolites profile and/or levels being monitored can help predict the biological structure, as well as the function, of a phenotype, leading to the understanding of the response of the organism to environmental stressors, such as nourishment, exposure to toxin e infections, that lead to perturbations in cellular homeostasis. Since the phenotype is directly linked to the genotype and its behavior, genetic variations will also generate phenotypic variations [24–26].

To develop an experimental study using this "omics" technique, some basic steps must be performed as illustrate in Fig. 1. Before starting the metabolomics analysis, the determination of the study strategies and the design of the experiments are required. Untargeted metabolomics is a methodology based on the global profiling of all the metabolites in a biological sample, including chemical unknowns, whereas targeted methodology presents a more specific approach, with a characterized metabolite as a valid standard, focusing on particular metabolites signals. The study strategies can be developed from one of these concepts in an arrangement with the most appropriate analytical techniques [25, 26].

Furthermore, a large amount of biochemical information gathered can be correlated through statistical and chemometric analysis. Metabolomics samples carry a complex load of metabolites, which generates cross information that can't be visualized considering individual biomarkers. Data analysis greatly depends on preprocessing, which has the aim of transforming the data to improve the data analysis through a simplification of the dataset to be comparable [25].

After data preprocessing, several statistical tools can be used to find discriminative features within the sample set. Data analysis involves the application of the different univariate and multivariate methods that can be of parametric (e.g. student *t*-test, multivariate linear regression) or non-parametric (e.g. Mann–Whitney test, random forests) nature. The methods can be also divided into unsupervised techniques (i.e. methods where labeling of the samples is not involved in calculations, e.g. principal

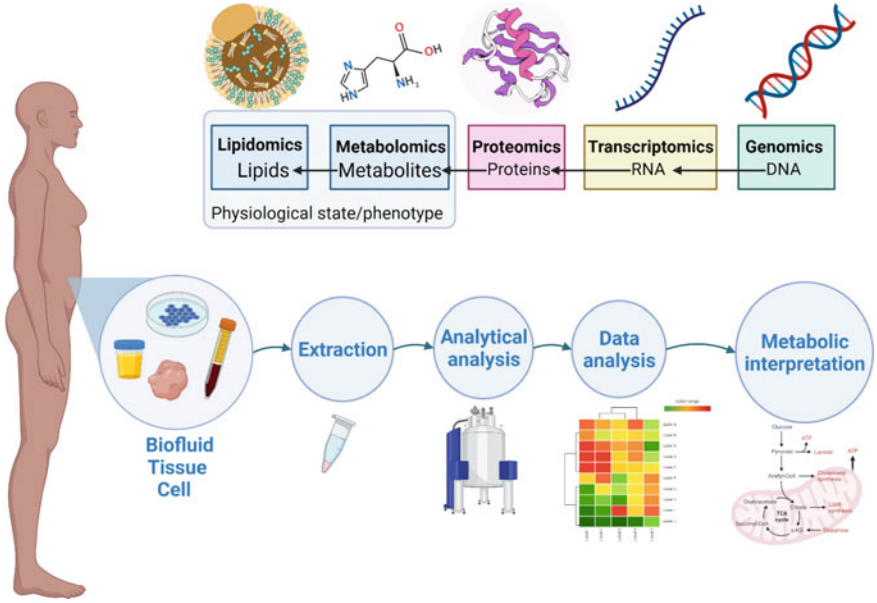

Fig. 1 Metabolomics scheme showing the sequence of macromolecules to small molecules and their respective omics science, the metabolomics steps from the human sample as biofluid, tissue or cell until final results as metabolic interpretation. Created with Biorender.com

component analysis (PCA), hierarchical cluster analysis (HCA), and supervised techniques (i.e. methods where calculations involve the information regarding sample labels, e.g. linear discriminant analysis (LDA), k-nearest neighbor (KNN). A supervised multivariate technique, partial least squares discriminant analysis (PLS-DA), is a particularly useful tool in metabolomics studies [27].

The application of statistical analysis aims to see a general correlation between the metabolites in a simpler interpretation. Principal Components Analysis (PCA) is commonly used in these cases for its ability to reduce the range of a database, minimizing information loss while retaining the main features. In a PCA plot, it is possible to analyze similarities and differences between samples and the control, considering the distance between the points. On the other hand, ANOVA and Student's *t*-test, with a *P*-value of < 0.05, are univariate analyses that can be used to analyze the parameters of an isolated metabolite, since it doesn't depend on other variables [25].

Scores and loadings are the usual visual results from the multi statistical analyses in which the scores describe samples and the loadings show the features. The scores must present a cluster (group) or a tendency for a cluster to claim that the metabolites are distinct in the different samples. Loadings features correlating with score clusters are relevant to establishing what metabolites distinguish the samples. Thus, the feature may be presented as clearly as possible with the aim of emphasising which metabolites are important. One of the possible loading charts is the heatmaps based on VIP (variable importance in projection) [28].

For metabolism investigation, the Pathway Analysis is used which module combines results from powerful pathway enrichment analysis with pathway topology analysis to help researchers identify the most relevant pathways involved in the conditions under study. This analysis uses enrichment techniques as key tools for understanding complex biological systems. These tools reduce the complexity of the data, improve interpretation and understanding of biological systems, and help to generate hypotheses. The presentation of the pathways usually is a map of the metabolome view [29].

1.2 NMR as a Tool in Metabolomics

There are several analytical tools to study metabolomics, among them, the most used are nuclear magnetic resonance (NMR) and mass spectrometry (MS). MS has excellent sensitivity, and a large coverage of metabolites, and can be coupled with separation techniques, being important for the analysis and identification of a wide variety of compounds, but reproducibility and quantitation is a current issue. However, in this chapter we will delve deeper into the use of NMR in metabolomic analysis, addressing the operation and the main advantages of the technique [30–32].

Nuclear magnetic resonance (NMR) spectroscopy is a rapid and non-destructive technique that allows a high analytical reproducibility, identification of chemical compounds without the use of standards, and information about molecular dynamics. NMR can detect a gamma of metabolites in a complex sample with minimal sample preparation when compared to other analytical methods [33, 34].

When it comes to the actual experiment in human beings, the samples can be collected as biofluids (urine, saliva, blood, plasma, serum, cerebrospinal fluid, stool) or also as tissues (biopsy tissue), and cells. To obtain a sample with minimal alterations for reproducible experiments, the preparation is quite simple. It starts with the homogenization of the collected sample by the centrifuge followed by the metabolite's extraction, adding some deuterated solvent. The extraction of metabolites can also be promoted by the biomolecules' precipitation, as a result of the addition of methanol: chloroform mixture, or only the methanol itself, that also provides the inactivation of enzymes. After that, the sample is centrifuged and the floating part is evaporated. Then, the reference standard is added, as well as the deuterated solvent or buffer is added. It is important to maintain the physiological pH during the sample preparation, since its variation may induce unwanted reactions [35].

In the final step samples can be filtered or not to remove macromolecules that may get in the way during the spectral analysis. If the macromolecules are not physically removed, the choice of NMR experiment must be well planned (a Carr-Purcell-Meiboom-Gill—CPMG—pulse sequence must be required). The samples are transferred to the equipment's tubes and the analysis may begin. It is important to avoid a sequence of thawing processes under the same sample. At the end of this process, it is obtained a well-preserved biological sample, making it possible to

use nuclear magnetic resonance (NMR) as the analytical technique, since it is non-destructive and allows other types of analysis later, or the reproduction of the same one. Less processed samples provide a result loaded with information, with larger width and more overlaps, as well as the possibility to correlate all these features in a bigger view analysis. Besides, a rawer sample supports the idea of a replicable experiment, since it hasn't been overly modified, and is best used in NMR analysis [36]. A graphical illustration of the sample handling process is available in Fig. 2.

Several nuclei can be studied by the NMR, but the most commonly available ones are hydrogen-1 and carbon-13 isotopes [37, 38]. One-dimension ^{1}H and ^{13}C are the most common NMR experiments. More sophisticated multidimensional experiments involving for example ^{1}H–^{1}H and ^{1}H–^{13}C, such as COSY (correlated spectroscopy) and HSQC (heteronuclear single quantum coherence) [38] among many others also are common. Solution or liquid-state NMR, and HR-MAS (High-Resolution Magic Angle Spinning) are the two main approaches employed in metabolomics. Solution NMR is used in the analyses of soluble metabolites in biofluids, cell lysates, or polar/apolar tissue extracts, and HR-MAS for the measurement of metabolites in heterogeneous samples containing solid and liquid components, like intact tissues [39].

Liquid-state NMR in high resolution (600 MHz) is the preferred instrument to perform metabolomics analyses in biological samples containing many compounds

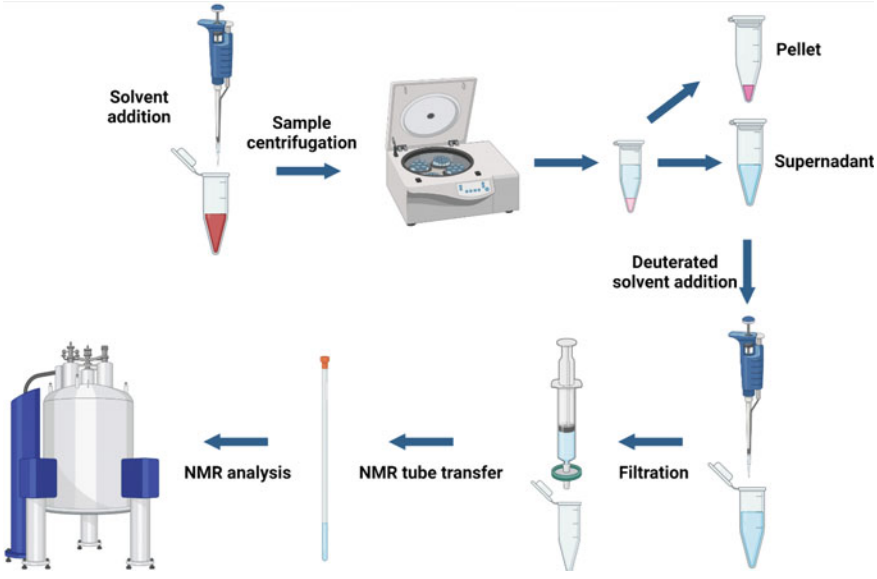

Fig. 2 Representation of sample handling process to NMR-based metabolomics analysis. Initially, the solvent is added for protein precipitation, centrifugation, and separation of the supernatant and pellet fractions. Then, a deuterated solvent is added to the supernatant, followed by filtration, insertion of the sample into the NMR tube and, finally, the sample is inserted and analyzed in the NMR spectrometer. Created with Biorender.com

in different degrees of abundance. Usually, 1H NMR the spectrum is acquired with a pulse sequence including water presaturation to suppress the solvent signal [39–42]. Additionally, in selected samples, some bidimensional experiments, usually COSY, HSQC, and JRES are performed to aid the process of metabolites identification. The metabolites identification relies on the comparison of chemical shifts, and spin–spin couplings to information available in chemical databases such as HMDB, Chenomx NMR Suite (Chenomx, Canada), and literature [27]. After carrying out all the steps described, it is possible to obtain a spectrum as shown in Fig. 3.

Under appropriate quantitative NMR (qNMR) conditions, NMR spectra may provide direct quantitative information since the area of each signal in the spectrum is directly proportional to the number of equivalent nuclei responsible for that signal, or in other words, is directly proportional to the molar amount of the detected isotope nuclei [37, 43]. Thus, absolute concentrations of the metabolites can be determined by NMR using internal, external, or electronic generated signal [33, 43, 44].

The qNMR spectra must be acquired under a set of appropriate conditions to obtain accurate results. For a maximum error of 1% it is necessary to set the relaxation delay (delay before the excitation) equal to at least 5 times the longitudinal relaxation time (T_1) for a 90° pulse, and an acquisition time longer than 3 times the transverse relaxation time (T_2), and at least 50:1 signal to noise ratio. Careful processing of NMR spectra is also required to extract accurate peak areas [33, 37].

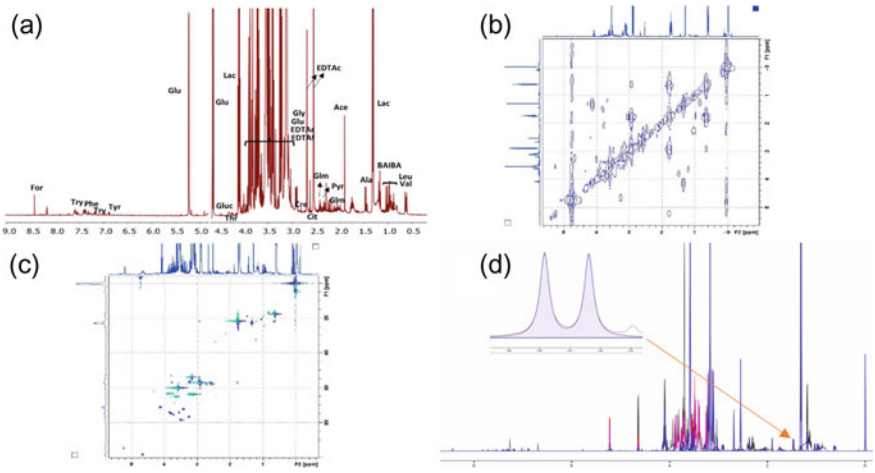

Fig. 3 Spectra 1H NMR and bidimensional experiments were obtained from blood plasma samples of covid-19 patients at the time of hospitalization. **a** 1H NMR spectrum with identification of the most intense metabolites; **b** Correlation Spectroscopy (COSY) showing scalar couplings between hydrogen atoms; **c** Heteronuclear Single Quantum Correlation (HSQC) showing the correlations between carbon and hydrogen nuclei that are directly bonded; **d** Quantification by Chenomx NMR Suite (professional version 8.1). Superposition of the obtained spectrum (black line) with the software library containing the reference compounds (filled in blue) allows spectral deconvolution, identification, and individual quantification of metabolites

NMR spectra preprocessing usually involves baseline correction, alignment, binning, normalization, and scaling [28].

2 Advances in NMR Based Metabolomics to Apply to Diagnostic Diseases

As mentioned so far, metabolomics is an efficient tool to optimize viral disease metabolome profiling overdue the generation of detailed chemical pathology fingerprints enabling the association to diagnostic and therapeutic interventions [45]. This personalized approach in medicine is probably the most important paradigm change in medical diagnosis and appears to be the future of modern medicine [46]. Hence, to improve its performance and promote a gradual transition from standardized clinical protocols to personalized medicine. NMR Metabolomics has been improving its methodologies to obtain better data resolution, avoid peak overlap, improve sensitivity, and also maintain an auto sustainable work regarding the high demands in clinical studies as a semi- or fully-automatization process from preparation steps to data results.

Regarding the NMR acquisition to improve data quality, researchers in the past decade studied and validated advanced NMR experiments through different approaches (1D and multidimensional NMR). Considering that biofluids are a complex matrix that not only comprises small metabolites but is also rich in proteins and lipids, applying a diffusion-edited pulse sequence like Carr-Purcell-Meiboom-Gill (CPMG) for the NMR analysis is typically necessary, suppressing the protein and lipids signals and allowing the analysis of small molecules without matrix interference. The CPMG does not represent the last advance, however worth mentioning once certainly was the historical advance in biofluids analysis.

The CPMG relies on molecules' transversal relaxation time (T_2). A spin-oriented chemical compound under an external magnetic field presents a longitudinal (T_1) and a transversal (T_2) relaxation rate - back to the z and y-axis, respectively. These properties are related to the magnetization axis the spin is oriented. CPMG pulse sequence starts with a 90° pulse to the y axis. The time required for the spin to lose its magnetization on the transversal axis (y) is smaller in macromolecules, compared to small molecules. Hence, to record only small molecules of T_2, there is a sequence of 180° pulses and a T time acting as a spin echo. This enables the NMR equipment to filter T_2 on samples [47, 48].

However, this CPMG approach commonly causes a broadening of the baseline, complicating posterior quantitative data analysis [35]. Alternatives to avoid this problem is physically removing the macromolecules from the samples [36, 45] or balancing the fast data and efficiency within additional experiments, which is the case with the use of the Bruker proprietary In Vitro Diagnostics research (IVDr) method for the entire biofluid sample [35].

Considering saving time while handling hundreds of samples, research using the newest NMR Bruker metabolomics protocol named In Vitro Diagnostic research (IVDr) to characterize the metabolic profile and quantify metabolites in biofluids samples seems to be the latest innovation in viral diseases metabolomics.

As shown in Fig. 4, for IVDr protocol the instrument is calibrated before the analysis, and the automated methods are performed on each sample. For plasma sample, IVDr performs four experiments in automation mode: a standard 1D experiment with solvent presaturation (noesy); a 1D—Carr – Purcell – Meiboom – Gill (CPMG) spin – echo experiment; a 2D—J-resolved experiment, and a 1D diffusion-edited spectrum. The methods rely on using short relaxation times within some corrector factor strategy to expedite quantitative analysis. The quantification data is automatically calculated for a standard metabolite list for each biofluid (blood, urine, and cerebral spinal fluid—CSF) based on the electronic signal ERETIC (Electronic Reference To access In vivo Concentrations) [49].

Novel IVDr protocols focus on fast and efficient quantification profiles of both small metabolites and lipoprotein fractions [50]. Elaine Holmes, John Lindon, and Jeremy Nicholson group have reported a series of studies trying to provide a standard protocol for IVDr methodology to ensure its reproducibility and robustness [45, 50–52]. This strategy showed to be appropriate for the SARS-CoV-2 metabolic profile due to previous reports of the high demand for lipid metabolism on Covid-19 pathology. Their results are promising for the differentiation of SARS-CoV-2 infected patients from healthy patients based on lipid profile (Table 2). They could also relate cytokine levels in both groups and compare them with lipid quantification and the disease evolution [53]. More about Covid-19 studies are discussed in Sect. 3.1.

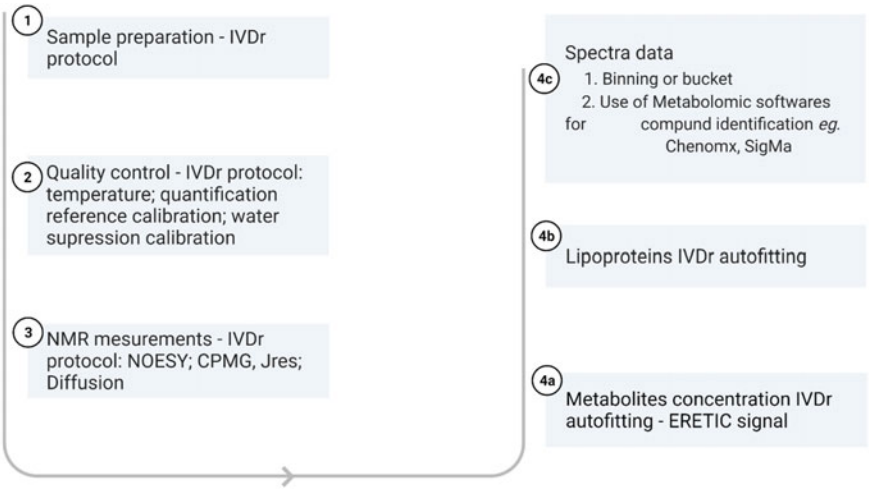

Fig. 4 Scheme showing the Bruker IVDr protocol analysis steps to perform metabolomics analysis

Table 2 Distinct metabolite types for SARS-CoV-2 infected patients from healthy patients

Group	Metabolites in abundance
SARS-CoV-2 infected patients	LDL cholesterol (LDCH), LDL phospholipids (LDPL), LDL-free cholesterol (LDFC), LDL apolipoprotein B, HDL cholesterol (HDCH), and phospholipids (HDPL)
Healthy patients	VLDL cholesterol (V1CH, V2CH, and so forth) and triglycerides (V1TG, V2TG, and so forth)

Metabolites assigned by PCA analysis. Data extract from Lodge's paper [53]

Besides the advantage of fast data acquisition to cohort studies samples, IVDr enables NMR metabolomics researchers to manage multivariate data from different centers and compare their data due to the IVDr protocol required to be the same, making it a universal protocol. One example is the cooperation between the Australian National Phenome Center (ANPC) with Bruker in an attempt to deliver COVID-19 diagnostic and prognostic solutions [54].

Many efforts have been putting on mainly in metabolomics data, more precisely in metabolites identification. Standardized methods were created such as SigMa which focuses on analyzing biofluids Lipoproteins, LipSpin which are lipidic NMR databases, Chenomx, and COLMARm whose software identifies and quantifies small metabolites [55, 56].

2.1 qNMR Strategies to Overcome the Metabolomics Issues

The accurate quantitation of larger numbers of metabolites has some challenges. The overlapping signals and lower sensitivity continue to be a struggle in metabolomics. To overcome these issues some strategies are being developed and explored by researchers (Fig. 5) [44, 57].

Strategy 1 consists of the 1D NMR solutions to spectrum overlapped issues involving deconvolution and heteronuclear experiments [58]. Deconvolution experiments use mathematical deconvolution of 1D NMR line shapes to separate individual 1D spectra of the different analytes present in the sample; while heteronuclear experiments separate the data at the acquisition stage using another nucleus, such as ^{13}C,^{15} N, ^{31}P, or ^{17}O, different of ^{1}H [38, 44]. In the meantime, 1D NMR with isotope labeling is another strategy to not only identify a metabolite set but also track down their metabolic pathway and cell influx/efflux. This is a methodology that alleviates a major challenge in NMR experiments involving low natural abundant nuclei, which could involve the isotopes of ^{13}C, ^{15} N, ^{2}H [59]. The use of labeling ^{13}C quantitative one-dimensional HMQC (Q-1D-HMQC) 1H NMR analysis has been reported for HBV infection. The combination of an isotope labeling and quantification technique provided a quantitative pathway description of this disease and made it possible to point out discussions about HBV infection [60]. Yet, isotope labeling improves

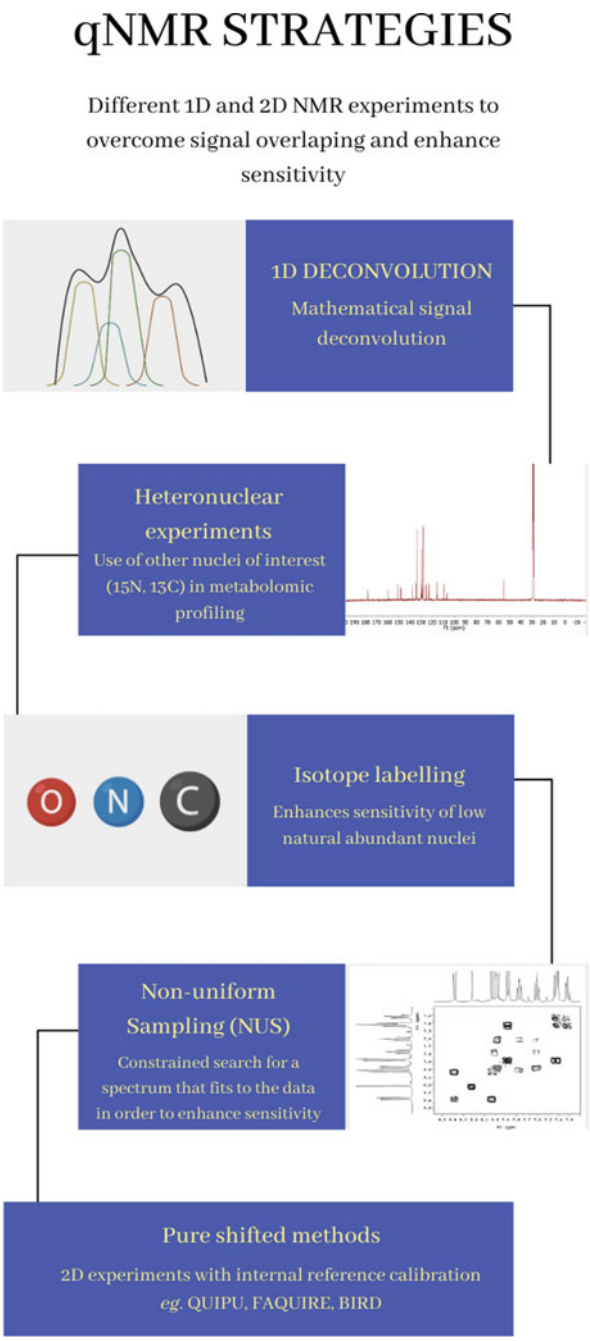

Fig. 5 Scheme illustrating the qNMR strategies to overcome the metabolomics limitations in the quantitative approach

the technique sensitivity, overcoming a major problem in heteronuclear experiments [61].

The deconvolution of peak areas is an efficient alternative to simple data integration when peaks are overlapped, as described in Fig. 6 [27, 37]. The deconvolution method achieves the integration of the signals more accurately in 1D spectra since errors are minimized in quantitative parameters such as noise in the NMR spectrum, phasing errors, baseline approximation, and also, careless adjustment of slope and bias correction on integrals [37, 43]. In deconvolution, a peak (or peaks) is fitted to the observed spectrum using, for instance, a least-squares-based method. Initial values for line-fitting analysis (frequency, width, height, and line shape of a signal) can be either defined manually or obtained from a database that contains the model spectra of the compounds. The spectral parameters can be fitted depending on the software as shown in many scientific articles [37, 62].

Strategie 2 and 3 consist in expanding the 1D spectrum to another dimension, running a two-dimensional (2D) experiment regarding the factors that influenced the peak areas as the peaks are spread along with one (or more) orthogonal dimension(s) [37, 38, 44]. 2D NMR solutions are also available for qNMR, which can involve pulse sequence modifications, theoretical calculations, or calibration approaches with fast 2D acquisition methods, all carefully thought to account for the peak-specific response of the 2D NMR signal. The quantitative application of 2D NMR in the field of metabolomics is recent, and already are being developed more practical approaches. The intrinsically quantitative 2D NMR method is one of them [38].

The intrinsically quantitative 2D NMR method development relies on the use of a simple internal reference without the need to rely on multiple external standards, which would directly yield quantitative results in a way similar to 1D NMR. The "intrinsically" quantitative 2D approaches such as qHSQC and its variants and applications of pure shifted and NUS (nonuniform sampling) methods to 2D NMR experiments are strongly investigated [43, 63, 64].

Despite the benefits of the methods mentioned above, conventional 2D NMR suffers from long acquisition times because of the need to repeat numerous 1D

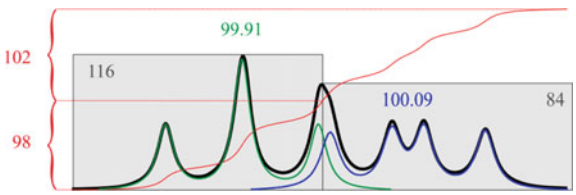

Fig. 6 Different methods to determine peak areas. The black line represents the observed spectrum where a triplet (t) and a doublet of doublets (dd) are overlapping. The red curve is the step curve used in the classical integration, in which their relative step heights determine the areas of 98 and 102 for the t and dd, respectively. Using the two bins from the equidistant binning procedure (grey boxes) areas of 116, and 84 for the t and dd were found, respectively. The most accurate results were obtained with deconvolution: the area of the t (green line) is 99.91 and the area of the dd (blue line) is 100.09. Reprinted with permission from Soininen et al. [37]

experiments with incremented delays to obtain a well-resolved 2D matrix. Therefore, many NMR methods have been developed to reduce the acquisition time of multi-dimensional experiments [44, 65]. Two main strategies seem to be a solution to overcome this situation: reducing the interscan sequence delay, e.g. band-Selective Optimized-Flip-Angle Short-Transient (SOFAST), Acceleration by Sharing Adjacent Polarization (ASAP), and Small Recovery Times (SMART). Another option is to introduce multiplexing instead of sequential sampling in the indirect dimension, by spatial encoding [61], as occurs in the ultrafast (UF) 2D NMR.

An operator must weigh the benefits of those first alternatives to attend to their research demand. SOFAST sequence is applied in HMQC experiments with an excitation pulse within a flip angle leading to a partial restoration of proton magnetization by a subsequent 180° pulse. This leads to an increased signal-to-noise ratio for high repetition rates of the experiment, nevertheless, SOFAST only is efficient for systems in which spin diffusion is an effective relaxation mechanism, such as macromolecules or small molecules in viscous solvents [61, 66]. ASAP sequence for HMCQ relies on proton-proton coupling while a mixing stage retains the residual Z-magnetization. It is an advantage for small molecules, nonetheless, this sequence is restricted to heteronuclear experiments for samples at natural abundance or slightly enriched [61, 67]. SMART sequence eliminates artifacts from previous scans in 2D experiments through a pulse field gradient (on the x, y, and z-axis), dephasing them (Fig. 7). It could be applied for COSY and TOCSY sequences. Despite the use of smaller recovery delay times, it requires rather high concentrations and access to triple axis gradients [61, 68]. Within the approaches mentioned, medical studies were reported studying macromolecules and hormones. The evaluations performed so far were focused on chronicle metabolites syndromes [69, 70]. These studies may enable further metabolic investigation in biofluids.

The ultrafast (UF) 2D NMR is a generic approach that can record any kind of 2D experiment in a fraction of a second as shown in Fig. 8 [38, 71].

The ultrafast (UF) 2D NMR proposes to reduce the sampling of the indirect time domain by recording the complete 2D NMR dataset in a single scan. This can relatively decrease the sensitivity, however, this can be solved by relying on hybrid methods offering a reasonable compromise between the experiment duration

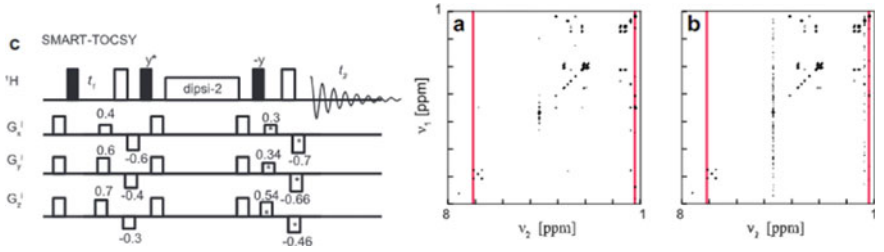

Fig. 7 SMART pulse sequence for a TOCSY **a** experiment. Comparison of a regular TOCSY **b** spectra and a SMART TOCSY **c** spectra containing Alanine, Arginine, Histidine, Threonine, and Tyrosine. Reprinted (adapted) with permission from [68]

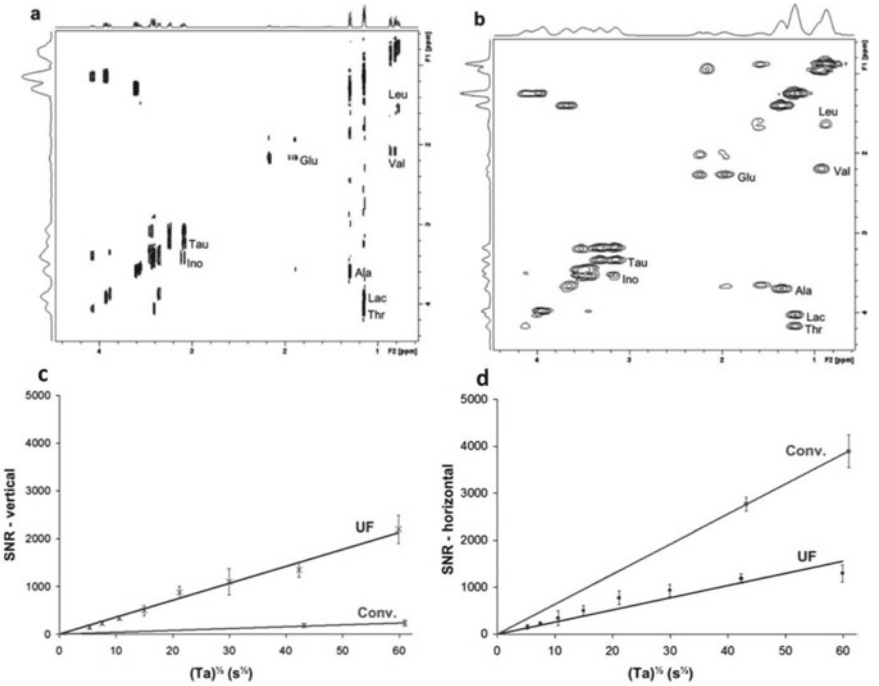

Fig. 8 Conventional **a** and ultrafast **b** COSY spectra of a 5 mM metabolic mixture of Alanine, Glutamic acid, Inositol, Lactic acid, Leucine, Taurine, Threonine, and Valine, acquire in 34 min on a 500 MHz spectrometer with a cryoprobe. Signa-to-noise ratio (SNR) as a function of the acquisition time, in the vertical **c** and horizontal **d** dimension of ultrafast (UF) and conventional (Conv.) constant-time COSY. Reprinted (adapted) with permission from [71]. Copyright 2011 Royal Chemical Society

(a few minutes) and the sensitivity (micromolar concentrations can be detected on homonuclear 2D spectra of biological extracts) [71]. The ultrafast method must be allied to the external calibration approach. Despite the similarity with other analytical methods, here the calibration curve is obtained from a single series of standard samples containing all the targeted analytes in known concentrations for each peak of interest [44]. Thus, hundreds of samples can be analyzed from the same calibration curves if the experiment is repeatable, leading to a fast method as reported in many scientific articles [44, 72–74].

Guennec and coworkers have presented the application of these experiments to cancer cells. The UF NMR could assign metabolites, most of the amino acids, in three different cell lines. Their results could be exploited in biological fluids due to the efficiency of UF NMR to identify metabolites in complex mixtures and point out their concentration [75].

There are quantitative 2D methods using a simple internal reference and without the need to rely on multiple external standards which would directly yield quantitative results in a way similar to 1D NMR. The “intrinsically” quantitative 2D approaches

such as Q HSQC and its variants ($HSQC_0$, or Q QUIPU HSQC) were developed to yield quantitative data from a single 2D spectrum [63, 64]. These approaches all rely on the HSQC pulse sequence. Therefore, they offer a better separation than UF COSY, thanks to the broader ^{13}C chemical shift range, but they are also less sensitive due to the low natural abundance of ^{13}C.

The QUIPU HSQC (QUantItative Perfected and pUre shifted HSQC) method is strongly recommended when strong overlap occurs once 2D ^{1}H, ^{13}C NMR allows an enhancement of the spectral resolution compared to ^{1}H homonuclear 2D NMR (2D COSY), and an enhancement of the sensitivity compared to Q HSQC. However, this method consumes time due to the 2D acquisition mode combined with the long recycling times required by the quantitative requirements (5 times the longest longitudinal relaxation time T1), and due to the higher number of scans needed to access low concentrated metabolites [63]. Additionally, the BIlinear Rotational Decoupling (BIRD) HSQC method stands as a prominent strategy to enhance spectral resolution and avoid sensitivity loss. This experiment uses a pulse sequence with a double spin-echo containing a bilinear rotational decoupling pulse cluster and a non-selective 180° proton pulse. This strategy provides a J-selective spin inversion and enhances the signal-to-noise ratio with isotope labeling and proved to be an effective tool for multidimensional NMR metabolomics analysis [76, 77].

The Nantes group has developed an accelerated version of this experiment named FAQUIRE (FAst, QUantitative, hIghly Resolved and sEnsitivity enhanced NMR) [63], an approach that combines the Q QUIPU (quick QUIPU) with spectral aliasing, NUS (nonuniform sampling), and VRT (variable repetition time) methods. The FAQUIRE approach promises to accelerate the access to quantitative data based on 1H, 13C correlations while preserving the spectral resolution and the sensitivity, without the need for external calibration.

In Fig. 9 we show that the acquisition time of 2D quantitative maps using the FAQUIRE approach is reduced by a factor of 6–9 while conserving a high spectral resolution due to the pure shift approach. The “pure shift” spectrum is generated when homonuclear broadband decoupling is applied resulting in a greatly simplified NMR spectrum with the multiplet pattern removed [43]. Even so, this approach may result in sensitivity loss due to the selective J-refocusing elements [76]. The pure shift concept can be applied in both dimensions in a 2D NMR experiment.

3 Viral Diseases Discriminated by NMR Based Metabolomics

In this section, the scientific findings in the use of NMR-based metabolomics approaches for viral diseases will be discussed. NMR spectroscopy has been one of the most common platforms for metabolomic analysis in human infectious diseases caused by viruses [78–80]. The metabolomics research has been mainly based on comparisons and identification of differences between metabolic profiles

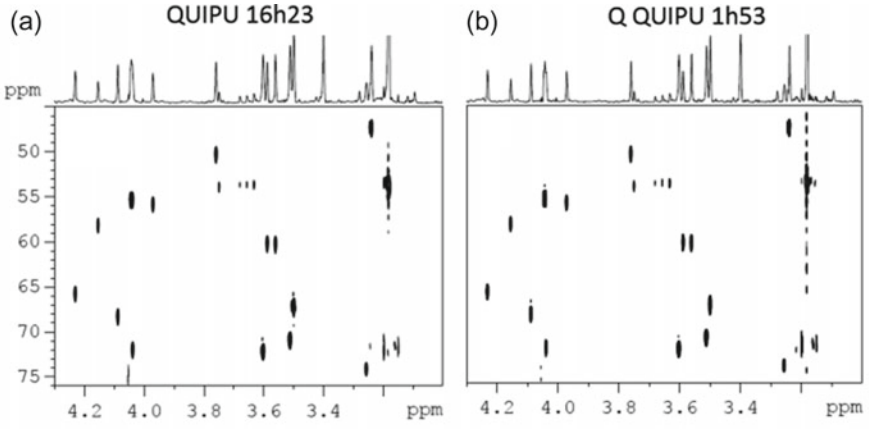

Fig. 9 2D maps of the methylene/methane area for a metabolite model mixture in ~16 h **a** using QUIPU and in less than 2 h **b** using Q QUIPU with 25% NUS and VRT function vd3. Reprinted (adapted) with permission from [63]. Copyright 2018 American Chemical Society

of study and control groups, such as the comparison of healthy and diseased individuals. Therefore, the objective of untargeted metabolomics in viral studies is to observe metabolic alterations associated with specific factors under study, aiming the discovery of diagnostic and prognostic biomarkers, and disease staging of viral infections. Metabolomics has been more employed in the past years for several viral infections as shown in Fig. 10. Here, we will focus primarily on those viruses in which a greater number of NMR-based metabolomics studies in patients with viral infections. Viral hepatitis B (HBV) [81], C (HCV) [82–88] and E (HEV) types [89], and human immunodeficiency virus (HIV) [90–96], are the most studied, as well as the response to many other viruses, such as West Nile virus [97], H1N1 influenza virus [98, 99], dengue virus [100] and other [101–103]. However, the COVID-19 pandemic disrupted this scenario, the metabolic profiles from patients with viral infection due to severe acute respiratory syndrome coronavirus 2 (SARS-CoV-2) have also been researched [51, 104–111]. The main works within the theme are listed in Table 3 which point to relevant remarks.

Most of NMR based metabolomics viral studies demonstrated high-level discrimination between the group of individuals with viral infection analyzed and the group of individuals not carrying viral infection analyzed or with a difference between the groups of individuals analyzed. These studies showed that metabolites present in plasma, urine, and to a lesser extent in saliva are differentially produced in response to HIV infection. In general, dysregulated metabolic pathways of patients caused by viral infection were also identified, such as TCA cycle, glycolysis, glutaminolysis, pentose phosphate pathway (PPP), fatty acid (FA) and lipid biosynthesis, β-oxidation, respiratory cycle (electron transport chain, ETC), and nucleotide and amino acid metabolism (Fig. 11).

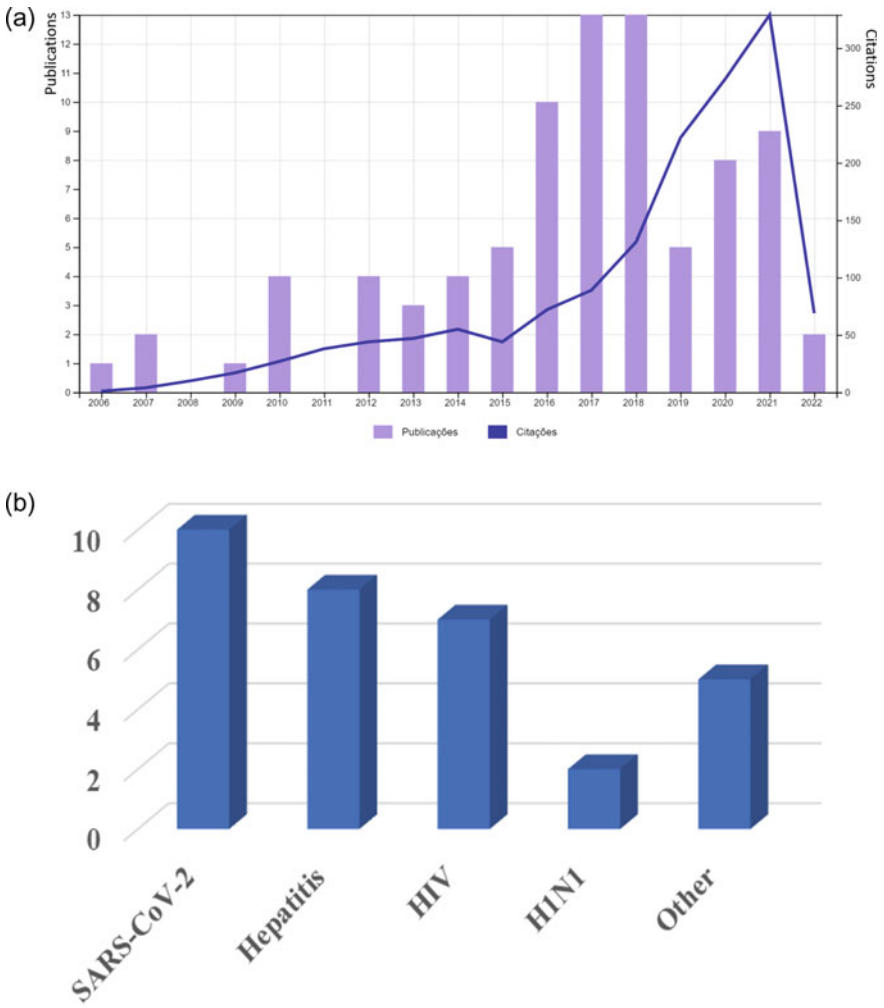

Fig. 10 **a** Trend in the virus NMR metabolomics publications and citations obtained using the keywords NMR metabolomics virus from the web of knowledge (http://apps.webofknowledge.com). **b** Number of scientific articles on NMR-based metabolomics studies of patients with infectious diseases caused by different viruses

The metabolism of viral studies is based on metabolites findings. The common metabolite NMR assignments are as follows in Table 4.

Table 3 Relevant remarks of NMR-based metabolomic studies of patients with infectious diseases caused by a virus

Virus	Sample	patients and/or individuals	Relevant remarks	References
HBV	Serum	HBV-liver cirrhosis (LC) HBV Healthy individuals (HI)*	Serum histidine as a potential biomarker for HBV patients Acetate, formate, pyruvate, and glutamine as potential biomarkers for progressing from HBV to HBV-LC Phenylalanine, unsaturated lipid, *n*-acetylglycoprotein, and acetone in the serum could be considered as a potential common biomarkers panel for these patients	Zheng et al. [81]
HBV and HCV	Urine	HCV HBV	Differentiating between the HCV and HBV patients The metabolites responsible by difference no were revealed	Godoy et al. [82]
HBV and HCV	Serum	HCV-fibrosis HCV-no fibrosis	Biologic pathways altered, mainly energetic metabolism involving glutamine/glutamate, carbohydrates, ketone bodies, and lipids Serum glucose is upregulated in HCV-fibrosis patients Acetoacetate at lower levels in HCV-fibrosis 3-hydroxybutyrate is downregulated in cirrhotic patients Serum creatine and creatinine at significantly lower levels in HCV-fibrosis	Embade et al. [112]

(continued)

3.1 Metabolomics Analysis in Severe Acute Respiratory Syndrome Coronavirus 2 (SARS-CoV-2) Infection

Coronavirus disease (COVID-19) is an infectious disease caused by severe acute respiratory coronavirus type 2 (SARS-CoV-2). Molecularly, severe COVID-9 disease is characterized by uncontrolled inflammatory syndrome caused by immune system

Table 3 (continued)

Virus	Sample	patients and/or individuals	Relevant remarks	References
HBV and HCV	Serum	HBV or HCV with schistosomiasis mansoni HBV or HCV monoinfected	Lactate and HDL are responsible for discrimination between the groups of patients Lactate at higher levels in coinfected patients in comparison to mono-infected HDL at lower levels in coinfected patients in comparison to mono-infected	Gouveia et al. [85]
HBV and HCV	Serum	HCV-before DAAs treatment HCV-after DAAs treatment Naïve HBV Healthy individuals	Distinction between the metabolomic profile of HCV patients before and after effective DAA treatment Tyrosine and formate at higher levels and potential biomarkers for the severity of HCV 3-hydroxybutyrate, formate, and acetate levels were significantly higher before DAAs therapy in HCV patients 2-oxoglutarate and 3-hydroxybutyrate at high levels in HCV patients when compared to HC and HBV individuals	Meoni et al. [86]
HCV	Serum	HCV (patients with different liver disease severity) Healthy individuals	Choline and histidine at high levels in HCV patients with late-stage of fibrosis when compared to early-stage fibrosis HCV individuals Choline/uric acid ration as a potential biomarker for differentiation of liver disease severity Serum 5-oxo-proline at higher levels in HCV in comparison to non-HCV individuals	Shanmuganathan et al. [87]

(continued)

Table 3 (continued)

Virus	Sample	patients and/or individuals	Relevant remarks	References
HEV	Serum and urine	HEV HBC Healthy individuals	L-isoleucine, acetone, and glycerol at reduced levels, while glycine at higher levels in the plasma in HEV patients Imidazole, 3-aminoisobutanoic acid, 1-methyl nicotinamide, biopterin, adenosine, 1-methylhistidine, and salicyluric acid at lower levels on the urinary fluid in HEV patients Both HEV and HBV, l-proline at high levels on the plasma and urinary when compared to HI	Munshi et al. [89]
HIV	Serum	HIV/AIDS-antiretroviral therapy; HIV/AIDS-no antiretroviral therapy HIV—negative (healthy individuals)	Discrimination between three analyzed groups	Hewer et al. [90]
HIV	Plasma	HIV/AIDS-antiretroviral therapy; HIV/AIDS-naïve therapy HIV-negative (healthy individuals)	Multivariate statistical analyzes unraveled distinct metabolic phenotypes and pathways among groups Glycolysis, TCA cycle, amino acid metabolism altered of the HIV/AIDS children	Kaur et al. [91]
HIV	Serum	HIV/AIDS-antiretroviral therapy; HIV/AIDS-naïve therapy; HIV-negative (healthy individuals)	Serum alanine at higher levels in HCV-negative, when compared to individuals with infection caused by HIV Alanine, glutamine, valine, taurine, and glucose levels can be altered due to viral infection and/or during antiretroviral therapy Alanine levels decrease, while glutamine and glucose increase with disease severity	McKnight et al. [92]

(continued)

Table 3 (continued)

Virus	Sample	patients and/or individuals	Relevant remarks	References
HIV	Serum	HIV/AIDS-antiretroviral therapy; HIV/AIDS-naïve therapy HIV-negative (healthy individuals)	Lipids, including low-density lipoprotein (LDL) and very-low-density lipoprotein (VLDL) mainly responsible for discrimination between infected individuals and HIV-negative	Philippeos et al. [93]
HIV	Serum	HIV/AIDS-antiretroviral therapy; HIV/AIDS-naïve therapy HIV-negative (healthy individuals)	Significant differences in glucose, lipids, phenylalanine, glutamic acid, aspartic acid, and branched amino acids compounds Aspartic acid, phenylalanine, and glutamic acid up-regulated in HIV individuals when compared to HIV-negative Tryptophan and tyrosine at lower levels in HIV-naïve therapy as compared to other groups Cystine at higher levels in HIV-naïve therapy as compared to other groups 11 metabolic pathways to be significantly altered by infection and/or treatment	Sitole et al. [95]

(continued)

hyperactivation. According to the World Health Organization (WHO), the standard method for diagnosis of acute SARS-CoV-2 infections is based on the detection of unique viral sequences by nucleic acid amplification tests (NAATs), such as rRT-PCR, however other methods are also used as microscopy, culture, antigen tests and antibody tests [120]. In this sense, intense efforts have been put into research on the application of single and multi-omics-based strategies have been carried out on several fronts to dissect a plethora of aspects involved in the SARS-CoV-2 infection. The understanding of the molecular processes altered by viral infection due to targeting host-response, providing the discovery of diagnostic and prognostic biomarkers for infectious diseases caused by SARS-CoV-2. However, the broad spectrum of severity of the COVID-19, and unpredictability in the outcome of the viral infection outcome make the metabolomic study of patients particularly challenging. Since the host response can be highly variable, the application of metabolomics

Table 3 (continued)

Virus	Sample	patients and/or individuals	Relevant remarks	References
HIV	Plasma, saliva, and urine	HIV/AIDS-antiretroviral therapy; HIV/AIDS-naïve therapy HIV-negative (healthy individuals)	Plasma and urine biofluids proportion better discrimination between HIV-infected individuals and HIV-negative than saliva Neopterin from urinary can be potential biomarkers for HIV-positive individuals Choline and sarcosine from serum can be potential biomarkers for HIV-positive individuals Serum sarcosine, Methylmalonic acid, D-Glucose, Choline, and L-Aspartic acid at high levels in HIV-infected individuals, when compared to HIV-negative individuals Metabolic pathways, such as metabolic cycles, glucose metabolism, hormone biosynthesis and amino acid biosynthesis pathways to be significantly altered by infection and/or treatment	Munshi et. al. [96]
HIV	Plasma		In HIV-infected individuals, atherogenic profile in terms of lipid and lipoprotein compositions and functions Classification of HIV-dyslipidemia from HIV normolipidemic VLDL particles, lactate, and LDL-TG compounds as potential biomarkers of dyslipidemia in patients on stable NNRTI-based ART and HIV-dyslipidemia predisposition	Rodriguez-Gallego et al. [94]

(continued)

Table 3 (continued)

Virus	Sample	patients and/or individuals	Relevant remarks	References
SARS-CoV-2	Plasma	COVID-19-hospitalized patients Healthy controls COVID-19-nonhospitalized patients (3 and 6 months pos-covid)	Tyrosine and formate at higher levels and potential In vitro diagnostics research (IVDr) protocol COVID-19 biomarker signatures in many Pos-COVID-19 patients At the elevated level the taurine, and reduced glutamine/glutamate ratio in Pos-COVID-19 patients in comparison to healthy controls Glutamate at an elevated level, glutamine at a reduced level, and a low glutamine/glutamate ratio in COVID-19 hospitalized patients in comparison to Pos-COVID-19 patients Gly A and Kynurenine/tryptophan ration at elevated levels in Pos-COVID-19 patients, when compared to healthy individuals The HDL parameters H4A1, H4A2 (apolipoproteins A1 and A2 in HDL subfraction 4), and kynurenine were partially normalized in Pos-COVID patients Glyc A and Glyc B at higher levels in COVID-19-hospitalized patients, when compared to among groups	Holmes et al. [107]

(continued)

in COVID-19 becomes a major challenge in potential biomarkers for its diagnosis [121–123].

The metabolomics profile of COVID-9 patients has displayed dyslipidemia at every level of complexity [53]. Remarkably, the works have described rich lipoprotein information from plasma samples obtained by NMR spectroscopy, and several are using in vitro diagnostic research (IVDr) information on quantitative lipoprotein profiles [53, 104, 107–109]. In the studies described by Günther and collaborators [53], the NMR-based metabolomics experiments were conducted by the Bruker

Table 3 (continued)

Virus	Sample	patients and/or individuals	Relevant remarks	References
SARS-CoV-2	Plasma	COVID-19; Healthy controls	In vitro diagnostics research (IVDr) protocol 116 metabolic variables derived from NMR spectroscopy and 41 from mass spectrometry α-1-acid glycoprotein signal A (Glyc A) at elevated levels and an increased kynurenine/tryptophan ratio were discriminant metabolites between groups and inflammation markers Higher level of VLDL class parameters and a high Apolipoprotein B100/A1 ratio in COVID-19 patients Major HDL class particles and components at lower levels in COVID-19 patients Elevated glutamine/glutamate ratio as marked for liver dysfunction	Kimhofer et al. [108]

(continued)

in-vitro Diagnostic Research (IVDr) protocol, aiming to distinguish the metabolic profile between COVID-9 patients and healthy individuals. From the spectra collected using a pulse program noesygppr1d and cpmgpr1d, 39 metabolites and 112 lipoproteins were found by slash Instant 20% using Bruker Quantification in plasma/serum B.I Quant-Ps 2.0.0 and Bruker IVDr Lipoprotein Subclass Analysis B.I-Lisa (Bruker BioSpin). The study of individuals with severe SARS-CoV-2 hospitalized in an intensive care unit (ICU) exhibited a distinct serum metabolic profile when compared to healthy individuals. Metabolic differences were also found between COVID-19 patients and patients also submitted to ICU with respiratory distress as a consequence of cardiogenic shock. The lipoprotein profile investigated has whether showed severely altered in the COVID-19 patients about among analyzed groups, which signature to predict the severity of COVID-19 infection. When compared with healthy individuals, the individuals with COVID-19 prominently displayed dyslipidemia: Very-low-density lipoprotein and intermediate-density lipoprotein and associated apolipoprotein B and intermediate-density lipoprotein cholesterol; as well as the VLDL, IDL, and large-sized low-density lipoprotein (LDL)-1 particles were

Table 3 (continued)

Virus	Sample	patients and/or individuals	Relevant remarks	References
SARS-CoV-2	Plasma	COVID-19 Healthy controls Patients with Influenza-like and SARS-CoV-2 negative	In vitro diagnostics research (IVDr) protocol Glucose and α-1-acid glycoprotein are responsible for discrimination between the COVID-19 and healthy individuals Glyc A and Glyc B at higher levels in COVID-19 in comparison to Influenza-like (SARS-CoV-2) groups Alanine, lactate, and pyruvate at higher concentrations in COVID-19 than healthy controls · LDL cholesterol (LDCH), LDL phospholipids (LDPL), LDL-free cholesterol (LDFC), LDL apolipoprotein B, HDL cholesterol (HDCH), and phospholipids (HDPL) in higher levels in the healthy individuals VLDL cholesterol (e.g., V1CH, V2CH, and so forth) and triglycerides (e.g., V1TG, V2TG, and so forth) subclasses in higher levels in the COVID-19 individuals	Lodge et al. [51]

(continued)

increased, and triglycerides for nearly all lipoprotein subfractions. However, cholesterol and apolipoprotein A2 were decreased. In general, a severely disturbed lipoprotein profile with remarkably increased TG levels potentially contributes to atherosclerosis. Another important aspect addressed in the studies was demonstrating metabolic and lipoprotein profiles from asymptomatic individuals infected with SARS-CoV-2 were similar to healthy individuals absent antibody-negative [53].

The analyses and quantification of routine lipids, lipoprotein subclasses, fatty acids, and their saturation, as well as the low-molecular-weight metabolites, have been shown to play a relevant role in the metabolomic studies of the patients with SAR-CoV-2 [109, 110]. According to Izquierdo-Garcia et al. [111], the disease severity of the COVID-19 patients may be associated with serum 56 metabolites ($p < 0.05$), being mainly lipid and lipoprotein subclasses. Notably, increased triglyceride

Table 3 (continued)

Virus	Sample	patients and/or individuals	Relevant remarks	References
SARS-CoV-2	Plasma	COVID-19- ICU patients Healthy controls Pneumonia (negative SARS-CoV-2) patients	• 162 metabolites analyzed by DI-LC–MS/MS and NMR • Creatinine alone and creatinine/arginine ratio predicted ICU mortality with 100% accuracy • Kynurenine, arginine, and creatinine as potential biomarkers for diagnostic and prognostic for COVID-19 patients, as well as for patients stratification Lysophosphatidylcholines (LysoPCs) also helped discriminate between COVID19 patients and healthy individuals	Fraser et al. [105]
SARS-CoV	Serum	COVID-19	• In vitro diagnostics research (IVDr) protocol • Apolipoproteins, both Apo-A1 and Apo-A2, at lower levels in COVID-19 patients • Triglyceride (TG)-rich lipoprotein profile in the serum COVID-19 patient • TG-VLDL, TG-IDL, TG-LDL, and TG-HDL at higher levels in COVID-19 patients • TC-LDL and TC-HDL at lower levels in COVID-19 patients • Acetoacetic acid, 3-hydroxybutyric acid, and acetone were at markedly elevated levels in COVID-19 patients	Bruzzone et al. [104]

(continued)

Table 3 (continued)

Virus	Sample	patients and/or individuals	Relevant remarks	References
SARS-CoV-2	Serum	COVID-19 patients in ICU Healthy individuals (control group) Patients in ICU caused by Cardiogenic shock Asymptomatic SARS-CoV-2 infection	• 39 metabolites and 112 lipoprotein-related parameters determined In-vitro Diagnostic Research (IVDr) protocol • COVID-19 disease is associated with dyslipidemia • SARS-CoV-2 asymptomatic individuals did not develop dyslipidemia • Very-low-density lipoprotein (VLDL) and intermediate-density lipoprotein particles and associated apolipoprotein B and intermediate-density lipoprotein cholesterol at lower levels in COVID-19 patients • Glucose and formic acid at higher levels in COVID-19 patients, when compared to healthy individuals • Lactic acid and the lactic acid/pyruvic acid ratio were decreased in COVID-19 patients when compared to healthy individuals Creatine, creatinine, and phenylalanine at higher levels in COVID-19 suggesting alterations in hepatic or renal metabolism	Schmelter et al. [109]

(continued)

content and very-low-density lipoprotein (VLDL), a decrease in HDL, percentage of cholesterol/cholesteryl esters in HDL and IDL were associated with increased severity of COVID-19 disease. Furthermore, the acetoacetate, 3-hydroxybutyrate, phenylalanine metabolites, as well as the ratio of apolipoprotein B/apolipoprotein A were also biomarkers for the severity of COVID-19 patients.

An assessment of serum metabolites from SAR-CoV-2 patients has indicated a disturbed energy status [109]. The glucose and formic acid levels were increased, and the lactic acid/pyruvic acid ratio decreased compared to healthy individuals. These

Table 3 (continued)

Virus	Sample	patients and/or individuals	Relevant remarks	References
SARS-CoV-2	Plasma	COVID-19 COVID-19-tocilizumab treatment	Changes in the lipoprotein particles levels and composition associated with severe disease – Triglyceride content and VLDL at higher levels; a decrease in HDL – The percentage of cholesterol/cholesteryl esters in HDL, and IDL Acetoacetate, 3-hydroxybutyrate, phenylalanine, and the ratio of apolipoprotein B to A1 (ApoB/ApoA1) can be potential biomarkers for COVID-19 severity Valine levels, triglyceride content of VLDL, and the ratio of the polyunsaturated fatty acids (PUFA) were associated with tocilizumab treatment	Rendeiro et al. [110]
SARS-CoV-2	Serum	COVID-19 Influenza A	Free fatty acids, acetone, creatinine, and lactate at higher levels in COVID-19 Valine, 2-hydroxybutyrate, proline, methyl-guanidine, glucose, and tyrosine at higher levels in COVID-19 Branched-chain amino acids (isoleucine and valine) at higher levels in COVID-19 in comparison with Influenza A patients Lactate-to-glucose ratio can be a potential biomarker for the up-regulation of the glycolysis pathway in COVID-19 patients	Lorente et al. [111]

(continued)

Table 3 (continued)

Virus	Sample	patients and/or individuals	Relevant remarks	References
SARS-CoV-2	Plasma	COVID-19 (survivors) COVID-19 (patients with a worsening condition during the sampling period)	Metabolites described as the most important in the discrimination, not be specific to COVID-19 disease, since associated with inflammation, immune response, and energy metabolism 3-hydroxybutyrate, a ketone bodies representative at higher levels in COVID-19 patients BCAAs (branched-chain amino acids), including leucine and isoleucine at levels similar in both groups of patients Citrate at a lower level in the blood plasma in COVID-19 patients, suggesting changes in the TCA cycle	Baranovicoa et al. [113]

Healthy individuals (HI)* was a term used to describe individuals no-infected with the virus under study; HBV-liver cirrhosis (HBV-LC); direct-acting antiviral agents (DAAs), which are used in the treatment of hepatitis C; Acquired immune deficiency syndrome (AIDS); intensive care unit (ICU); severe acute respiratory syndrome coronavirus 2 (SARS-CoV-2); triglyceride (TG); cholesterol (TC); tricarboxylic acid (TCA) cycle; Very low-density lipoproteins (VLDL), intermediate-density lipoproteins (IDL); low-density lipoproteins (LDL); high-density lipoproteins (HDL); α-1-acid glycoprotein signal A (Gly A); α-1-acid glycoprotein signal B (Gly B) Lysophosphatidylcholines (LysoPCs)

studies identified a decrease in the alanine, glutamine and histidine may be associated with disrupted hepatic amino acid metabolism and hepatic damage. The hepatic or renal metabolism changes were also suggested by increased levels of creatine, creatinine, and phenylalanine in comparison to healthy individuals. Correia et al. also corroborated with this data showing that metabolomics from samples of COVID-19 patients is a powerful tool for a better understanding of the SARS-CoV-2 mechanism of action and metabolic consequences of the infection in the human body. They showed Glycerol, 3-aminoisobutyrate, formate, and glucuronate levels as alternated in COVID-19 patients, affecting the lactate, phenylalanine, tyrosine, and tryptophan biosynthesis, D-glutamine, D-glutamate, and glycerolipid metabolisms. Thus, SARS-CoV-2 infection presents disturbance in the energetic system, supporting the viral replication and corroborating with the severe clinical condition of the patient [124].

Another NMR-based metabolic approach that has been employed is the differential between COVID-19 patients and individuals that developed severe acute respiratory distress syndrome caused by the H1N1 influenza A virus [111]. In studies

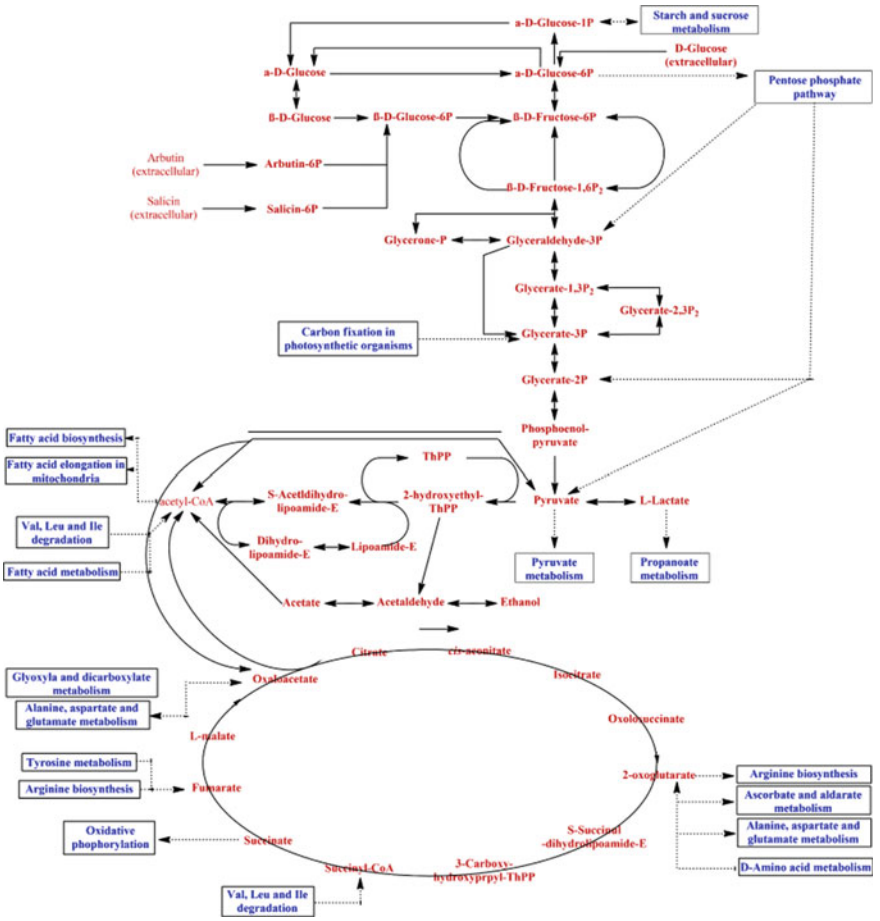

Fig. 11 Dysregulated metabolic pathways of patients caused by viral infections [114]

performed by Izquierdo-Garcia et al., the samples were analyzed by high-resolution magic angle spinning (HR-MAS-NMR), aiming to reduce the linewidth of the NMR due to macromolecules, such as proteins and lipids. HR-MAS reduces the line width of NMR spectra by spinning at a magic angle to a magic angle (54.7°) about the magnetic field. Serum samples of patients with viral infection in the intensive care unit (ICU) were analyzed by HR-MAS NMR at 4 °C to minimize metabolic degradation. From 1H spectra, the metabolites were identified by the Chenomx Profiler tool. Statical modeling of NMR data provided discrimination between the COVID-19 and H1N1 patients. The ICU patients due COVID-19 showed up-regulation of energy-generating pathways, such as glycolysis, fatty acid degradation, CoA biosynthesis, glycerolipids, and glycerophospholipids metabolism. A potential biomarker described for up-regulation in the glycolysis pathway of patients with SAR-CoV-2 infection was increased lactate/glucose ratio, when compared to patients with

Table 4 ^{1}H NMR assignment of common metabolites finding in biofluids [113, 115–119]

Metabolites	Chemical shift (ppm), multiplicity, integrals	Biofluid
Lipids and Lipoproteins		
Lipoprotein	0.82–0.93 (m), 1.20–1.37 (m)	Blood
Alcohols and derivatives		
Ethanol	1.17 (t; 3H) 3.65 (q; 2H)	Blood
Amines and derivatives		
Dimethylamine	2.50 (s; 6H)	Urine
Trimethylamine	2.88 (s; 9H)	Urine
Trimethylamine-N-oxide	3.25 (s; 9H)	Blood, Urine
Urea	5.78 (s; 4H)	Urine
Amino acids and derivatives		
1-Methylhistidine	3.06 (dd; 1H), 3.16 (dd; 1H), 3.69 (s; 3H), 3.96 (t; 1H), 6.99 (s; 1H), 7.89 (s; 1H)	Urine
2-Aminobutyric acid	1.18 (d; 3H), 2.59 (m; 1H), 3.02 (dd; 1H), 3.10 (dd; 1H)	Blood
2-Furoylglycine	3.92 (s; 2H), 6.62 (dd; 1H), 7.20 (dd; 1H), 7.85 (dd; 1H)	Urine
Alanine	1.47 (d; 3H), 3.78 (q; 1H)	Blood, urine
Arginine	1.53 (m; 1H), 1.59 (m; 1H), 1.86 (td; 2H), 3.17 (t; 2H), 3.77 (t; 1H)	Urine
Asparagine	2.84 (dd; 2H) 3.84 (t; 1H)	Blood
Betaine	3.89 (s; 2H), 3.25 (s; 9H)	Urine
Creatine	3.02 (s; 3H) 3.92 (s; 2H)	Blood, urine
Creatinine	3.03 (s; 3H) 4.04 (d; 1H) 4.09 (d; 1H)	Blood, urine
Glutamic acid	2.04 (m; 2H), 2.13 (m; 2H), 3.35 (m; 1H), 3.75 (m)	Blood
Glutamine	2.12 (td; 2H) 2.42 (dt; 1H) 2.46 (dt; 1H) 3.76 (t; 1H)	Blood
Glycine	3.55 (s; 2H)	Blood, urine
Guanidinoacetic acid	3.75 (s;2H)	Urine
Histidine	3.15 (dd; 1H) 3.24 (dd; 1H) 3.98 (t; 1H) 7.07 (s,1H) 7.82 (s; 1H)	Blood, urine
Isoleucine	0.92 (t;3H) 1.00 (d; 2H) 1.00 (d; 1H) 1.25 (m; 2H) 1.97 (m;1H) 3.66 (t; 3H)	Blood
Leucine	0.94 (d; 3H), 0.96 (d; 3H), 1.71 (m; 3H); 3.73 (dd; 1H)	Blood
Lysine	1.43 (m; 2H) 1.72 (tt;2H) 1.90 (dtd; 1H) 2.12 (dtd; 1H) 3.01 (t; 1H) 3.74 (t; 1H)	Blood

(continued)

Table 4 (continued)

Metabolites	Chemical shift (ppm), multiplicity, integrals	Biofluid
Methionine	2.11 (dtd; 1H) 2.12 (s; 3H) 2.19 (dtd; 1H) 2.63 (t;2H) 3.85 (t; 1H)	Blood, urine
Dimethylglycine	2.92 (s; 6H), 3.72 (s; 2H)	Blood, urine
Ornithine	1.78 (tt; 2H) 1.94 (td; 1H) 3.04 (t; 2H) 3.74 (t; 1H)	Blood
Phenylalanine	3.12 (m; 1H), 3.28 (m; 1H), 3.99 (dd; 2H), 7.32 (d; 2H), 7.40 (t; 1H), 7.42 (t; 2H)	Blood
Proline	1.47 (m;1H) 1.75 (m; 2H) 2.20 (m; 1H) 2.99 (ddd; 1H) 3.40 (ddd; 1H) 3.57 (dd; 1H)	Blood
Sarcosine	2.73 (s; 3H) 3.60 (d; 1H) 3.78 (d; 1H)	Blood, urine
Taurine	3.25 (t;2H), 3.41 (t;2H)	Urine
Threonine	1.32 (d; 3H), 3.58 (d; 1H), 4.25 (m; 1H)	Blood
Tryptophan	7.19 (t; 1H), 7.28 (t; 1H), 7.32 (s; 1H), 7.54 (d; 1H), 7.73 (d;1H)	Blood
Tyrosine	6.88 (d; 2H), 7.18 (d; 2H)	Blood
Valine	0.97 (d; 3H), 1.03 (d; 3H), 2.25 (m; 1H), 3.59 (d; 1H)	Blood, urine
Benzene and substituted derivatives		
Benzoic acid	7.47 (dd; 2H), 7.54 (t; 1H), 7.86 (d; 2H),	Urine
Mandelic acid	4.93 (s, 1H), 7.13 (m, 1H), 7.41 (tt, 1H), 7.44 (m, 1H), 7.45 (m, 1H)	Urine
Hippuric acid	3.96 (d, 2H), 7.54 (m, 2H), 7.63 (tt, 1H), 7.83 (dd, 2H)	Urine
Carboxylic acids		
2-Hydroxybutyric acid	0.89 (t; 3H) 1.64 (m; 2H) 3.98 (t; 1H)	Blood
Acetic acid	1.91 (s; 3H)	Blood, urine
Citric acid	2.52 (d; 2H), 2.68 (d; 2H)	Blood, urine
Formic acid	8.45 (s; 1H)	Blood, urine
Fumaric acid	6.38 (s;2H)	Urine
Imidazole	7.26 (s; 3H)	Urine
Lactic acid	1.32 (d; 3H), 4.10 (q; 1H)	Blood, urine
Proline betaine	3.57(s;1H), 3.31 (s; 2H), 3.26 (s; 6H), 2,58 (s; 2H), 2.02 (s; 2H)	Urine
Succinic acid	2.39 (t; 4H)	Blood, urine
Tartaric acid	3.70 (d; 1H), 4.34 (d; 1H)	Urine

(continued)

Table 4 (continued)

Metabolites	Chemical shift (ppm), multiplicity, integrals	Biofluid
Trignolline	4.33 (s; 3H), 8.07 (m; 1H), 8.83 (m; 2H), 9.11 (s; 1H),	Urine
Fatty acids and derivatives		
2-Methylsuccinic acid	1.09 (m; 3H), 2.12 (dd; 1H), 2.51 (dd; 1H), 2.61 (td; 1H),	Urine
Essential nutrient		
Choline	3.19 (s; 6H) 3.50 (m; 2H) 4.10 (s; 2H)	Blood
Keto acids and derivatives		
2-Oxoglutaric acid		Blood, urine
3-Hydroxybutyric acid	1.19 (d; 2H) 2.29 (dd; 1H) 2.39 (dd; 1H) 4.14 (td; 1H)	Blood, urine
Acetoacetic acid	2.27 (s; 3H) 3.43 (s; 2 H)	Blood, urine
Acetone	2.22 (s; 6H)	Blood, urine
Oxaloacetic acid	3.32 (s; 2H)	Urine
Pyruvic acid	2.37 (s; 3H)	Blood, urine
Purine, Pyridine, and Pyrimidine derivatives		
1-Methyladenosine	3.49 (dd; 1H), 3.75 (dd; 2H), 3.97 (s; 3H), 4.12 (td; 1H), 4.68 (dd; 1H), 5.90 (d; 1H), 8.28 (s; 1H), 8.31 (s; 1H)	Urine
1-Methylnicotinamide	4.47 (s; 3H), 8.18 (t; 1H), 8.89 (d; 1H), 8.96 (d; 1H), 9.28 (d; 1H)	Urine
Adenosine	3.49 (td; 1H), 3.49 (dd; 1H), 3.75 (dd; 1H), 3.91 (dd; 1H), 4.62 (d; 1H), 4.73 (dd; 1H), 8.49 (s; 2H)	Urine
Allatoin	4.12 (s; 1H)	Urine
Allopurinol	7.51 (s; 1H), 8.01 (s; 1H)	Urine
Caffeic acid	6.33 (d; 1H), 6.92 (d; 1H), 7.06 (dd; 1H), 7.14 (d; 1H), 7.29 (d; 1H)	Urine
Inosine	3.86 (dd; 1H), 3.93 (dd; 1H), 4.34 (dd; 1H), 4.38 (td; 1H), 4.78 (dd; 1H), 6.09 (d; 1H), 8.49 (s; 2H)	Urine
Sugars and derivatives		
D-Galactose	3.71 (t; 1H) 3.71 (dd; 1H) 3.75 (quint; 2H) 3.81 (dd; 1H) 3.99 (d, 1H) 5.27 (d; 1H)	Blood, urine
D-Glucose	3.25 (m; 1H), 3.41 (m; 2H), 3.48 (m; 2H), 3.54 (dd; 1H), 3.72 (m; 3H), 3.76 (dd), 3.82 (m; 2H), 3.89 (dd; 1H), 4.65 (d; 1H), 5.23 (d; 1H)	Blood, urine

(continued)

Table 4 (continued)

Metabolites	Chemical shift (ppm), multiplicity, integrals	Biofluid
D-lactose	5.18 (s; H), 4.63 (s; H), 4.12 (s; H), 3.84 (s; H), 3.81 (s; H), 3.75 (s; H) 3.63 (s; H) 3. 53 (s; H)	Urine
D-mannitol	3.61 (dd;1H) 3.71 (td;1H) 3.71 (dd;1H) 3.72 (td;1H) 3.83 (dd;1H) 3.84 (dd;1H) 3.88 (dd;1H)	Urine
D-mannose	3.47 (dt; 1H) 3.68 (dd; 1H) 3.75 (dd; 1H) 3.80 (dd; 1H) 3.82 (dd; 1H) 3.95 (dd; 1H) 5.21 (d; 1H)	Urine
Glucuronate	3.27 (m; 1H), 3.49 (m; 2H), 3.57 (dd; 1H), 3.71 (m; 1H), 4.05 (d; 1H), 4.65 (d; 2H), 5.23 (d; 1H)	Blood
Glycerol	3.55 (m; 4H), 3.64 (m; 4H), 3.78 (m; 1H)	Blood
Myo-Inositol	3.87 (t; 1H) 3.87 (dd; 2H) 4.12 (dd;2H) 4.12 (dd; 1H)	Urine
Sulfones		
Dimethylsulfone	3.14 (s; 6H)	Blood

influenza A. The decrease in the amino acid metabolism in COVID-19 patients is mainly due to isoleucine and valine at low levels. The branched-chain amino acids levels may be associated with intense inflammatory of host-response, the authors suggesting that the lower levels of BCAAs in COVID-19 patients may be indicative of less intense inflammatory response in patients infected with SARS-CoV-2 than influenza A patients [111].

The metabolomic data and immune response were used to develop the approach to stratification of COVID-19 patients. Through regularized Canonical Correlation Analysis (rCCA), both NMR and flow cytometry datasets were integrated, and six groups were characterized by distinct clinical parameters and an abundance of immune-metabolic species [110]. The groups characterized by mild COVID-19 patients were differentiated by distinct BMI, liver enzyme levels, and triglyceride content of lipoproteins. While stratifying between "late" and "earlier" severe COVID-19 patients, one of the main factors was creatinine level, being at a higher level in the late group than that the "earlier" severe group [110].

The response of COVID-19 patients to drug therapy is also being monitored by metabolic changes. Salvatore et al. reported a metabolomics study of ten COVID-19 patients hospitalized with hyper inflammation before and after treatment with Tocilizumab. The metabolic profile of the patients treated with Tociluzumab was more similar to patients with milder infection viral. However, the metabolites are associated with the severity of COVID-19 patients [110].

3.2 Metabolomics Analysis in Hepatitis C Viral Infection

Chronic hepatitis C virus infection can lead to progressive liver diseases, such as chronic liver disease, cirrhosis, and hepatocellular carcinoma [125, 126]. Similar to other forms of chronic liver disease, the progression of the viral infections caused by HCV is accompanied by liver fibrosis. The liver biopsy is the gold standard method for detecting liver disease and fibrosis through different semiquantitative and validated histological scores. The METAVIR system scores fibrosis on a scale ranging from 0 to 4, where F0 indicates the absence of fibrosis and F4 is a fully developed cirrhosis. There is currently an immense interest in the diagnosis and prognosis for hepatitis viruses in a non-invasive way. In this context, NMR-based metabolomics studies have been performed to identify potential biomarkers for HCV, as well as HBV and HEV, to effectively distinguish patients in different stages and healthy individuals [125–128].

The liver plays a central role in energy and lipid metabolism. Liver diseases affect lipids levels, including those caused by HCV, hepatitis B virus (HBV), and hepatitis E virus (HEV). Serum lipid profile can be a biomarker of liver insufficiency in fibrosis and cirrhosis patients [112]. According to Millet and collaborators [112], low-density lipids, such as VLDL and VLDL2, were found at higher levels in HCV-cirrhosis patients when compared to healthy individuals. The serum of patients with HBV and HBV-LC also exhibited a high concentration of unsaturated lipid in comparison to healthy individuals. On the other hand, the low-density lipoproteins (LDL) and lipoproteins with higher densities (HDL) were observed at lower levels in cirrhotic-HCV patients compared to HCV non-fibrotic patients [112]. In another study [83], the spectra profile of serum of HCC and HCV patients showed clear differences. From broad signals of the ^{1}H spectra, the fatty acid methyl and methylene moieties were determined, however, lipids with different fatty acid chains were not differentiated due to their overlapping signals [83].

Silva et al. also reported differences between coinfected patients with schistosomiasis and HBV/HCV chronic infection and HBV/HCV chronic monoinfected patients regarding the levels of HDL and triglycerides. By conventional assays, these metabolites did not present any statistically significant in the different analyzed groups [94]. Similarly, Gao et al. [81] reported that HBV-LC and HBV patients had a higher level of saturated/monounsaturated fatty acid and a lower level of polyunsaturated fatty acid than healthy individuals.

Undoubtedly, in the different works reported in the literature, there is a great variation of several metabolites, mainly low molecular weight metabolites, between the groups of patients infected with the hepatitis virus. They are assigned to different metabolites, such as amino acids, organic acids, creatine, creatinine, and choline, among others. Since then, NMR-based metabolomic studies have demonstrated alterations in biological pathways of the patients with viral infection caused by hepatitis, mainly energetic metabolism involving glutamine/glutamate, carbohydrates, ketone bodies, and lipids. The distinction between analyzed groups is reported by comparing the concentrations of only a reduced set of metabolites [86, 87, 112].

A pilot study reported by Simas et al. in 2010 demonstrated the potential of NMR-based metabolomics on urine samples for differentiating patients infected with HCV from healthy individuals with sensitivity and specificity [82].

In the serum metabolite comparison of HBV, HBV-liver cirrhotic and healthy individuals, the histidine, *n*-acetylglicoprotein, phenylalanine, acetone, unsaturated lipid, and citrate were the main metabolites for differentiation of the analyzed groups [81]. Compared to HBV patients, serum phenylalanine and unsaturated lipid concentrations were higher in the serum of patients in the severe stage (HBV-LC), while that *n*-acetylglycoprotein and acetone were found at lower levels. To distinguish HBV patients from healthy individuals, the serum histidine and citrate were described as important metabolites that contributed to the distinction of these groups [81].

The differentiation between the metabolomics profile of individuals with hepatocellular carcinoma (HCC) from the Hepatitis C virus (HCV) population was achieved through OSP-PLS analysis of the NOESY spectra. Therefore, the contributions of lipids were most prominent, however, the lipids responsible for separation were not attributed. About low-molecular-weight metabolites, creatinine, valine, and choline were found at higher levels in HCC patients than in HCV. Choline is an important metabolite in several cancer types in high concentrations, which plays a key role in the synthesis of phospholipids for cancer cell membranes and donors in methylation reactions. The advanced stages of liver fibrosis/cirrhosis in both diseases, HCC and HCV, can lead to a higher concentration of this metabolite [83].

A cross-platform serum metabolomics study compared the performance of MSI-CE-MS and NMR methods standardized protocols [88]. Both platforms offered similar reproducibility with a good mutual agreement to classify HCV individuals in different stages of the disease. The researchers highlighted the NMR metabolomics approach by an automated spectral processing and deconvolution software, as well as the identification and quantification of metabolites by a serum-specific metabolite library. However, there are disadvantages of 1D NMR over MSI-CE_MS. MSI-CE-MS spectrometric was improved resolution and lower detection limits, as result, MSI-CE-MS, 60 serum metabolites were found in the HCV patient samples, while by NMR platform were determined 47 metabolites, being 30 serum metabolites were reliably determined in most non-HCV controls and HCV patients. In both instrumental platforms, serum choline and histidine metabolites were found as the best biomarkers to distinguish between HCV patients in late-stage fibrosis and early-stage fibrosis HCV individuals [88]. In other studies, choline is also one of the most significant biomarkers to assess liver cirrhosis in HCV individuals [112]. It is worth mentioning that several other serum metabolites were determined with increasing liver fibrosis, such as asparagine, arginine, tyrosine, and hydroxyproline [87].

Serum creatine and creatinine levels are also associated as biomarkers to differentiate HCV patients of different fibrosis stages [112]. These metabolites were found at higher levels in HCV patients in the non-fibrotic than HBV-LC patients. Creatine is an important metabolite in the energy transfer process, which is synthesized primarily in the liver and is again involved in the general energy supply [113].

Glucose is a metabolite with significant variations in its concentration in the serum of patients infected with hepatitis virus [85, 112]. As reported by Millet et al.

in NMR-based metabolomics [110], HCV-cirrhosis patients present a high level of serum glucose when compared to HCV-no cirrhosis individuals. Similarly, Embade et al. reported towards patients with mild or severe chronic liver in comparison to healthy individuals. The severity of liver diseases is also associated with glucose metabolism changes. The high level of serum glucose in severe cirrhosis patients may be related to reduced metabolism via the tricarboxylic acid cycle. Also, the upregulation of serum glucose is associated with a lower level of glycerol, which can be metabolized to glucose in the liver and result in energy for cellular metabolism [112].

4 Conclusions and Future Perspectives

Amongst the methodologies reported, communication efforts are required to make end-users aware of recent methodological advances. Otherwise, NMR method improvements may not cross laboratory doors to meet the outside world. Efforts to standardize the metabolomics protocols and solve pattern metabolomics issues allow the integration of international cooperation to determine the metabolism type of a wide range of viral diseases.

Acknowledgements Authors acknowledge the financial support from CAPES (Grant no. 88887.504531/2020-00, from notice no. 09/2020) and FAPESP (grant no. 17/01189-0). DRC acknowledge the continued support from CNPq Research Productivity Program (309212/2019-7).

References

1. World Health Organization, WHO Director-General's opening remarks at the media briefing on COVID-19. https://www.who.int/director-general/speeches/detail/who-director-general-s-opening-remarks-at-the-media-briefing-on-covid-19---11-march-2020
2. S. Crimi, L. Fiorillo, A. Bianchi et al., Herpes virus, oral clinical signs, and qol: systematic review of recent data. Viruses **11**, 1–18 (2019). https://doi.org/10.3390/v11050463
3. M.H. Ebell, Epstein-Barr virus infectious mononucleosis. Am Fam Physician **70** (2004)
4. T. Wilkins, J.K. Malcolm, D. Raina, R.R. Schade, Hepatitis C: diagnosis and treatment. Am Fam Physician **81**, 1351–1357 (2010)
5. World Health Organization, Yellow fever (2019). https://www.who.int/news-room/fact-sheets/detail/yellow-fever#:~:text=Symptoms of yellow fever include, and Central and South America
6. W.J. Wiersinga, A. Rhodes, A.C. Cheng et al., Pathophysiology, transmission, diagnosis, and treatment of coronavirus disease 2019 (COVID-19): a review. JAMA **324**, 782–793 (2020). https://doi.org/10.1001/jama.2020.12839
7. T. Hemachudha, G. Ugolini, S. Wacharapluesadee et al., Human rabies: neuropathogenesis, diagnosis, and management. Lancet Neurol **12**, 498–513 (2013). https://doi.org/10.1016/S1474-4422(13)70038-3
8. P. Davison, J. Morris, Mumps, in *StatPearls* (StatPearls Publishing, Treasure Island, 2022)

9. A. Misin, R.M. Antonello, S. Di Bella et al., Measles: an overview of a re-emerging disease in children and immunocompromised patients. Microorganisms **8**, 1–16 (2020). https://doi.org/10.3390/microorganisms8020276
10. World Health Organization, Influenza (2018). https://www.who.int/news-room/fact-sheets/detail/influenza-(seasonal))
11. World Health Organization, Dengue and severe dengue (2022). https://www.who.int/news-room/fact-sheets/detail/dengue-and-severe-dengue
12. A.R. Xavier, S. Kanaan, R.P. Bozzi, L.V. Amaral, Clinical and laboratory diagnosis of Zika fever: an update. J Bras Patol e Med Lab **53**, 252–257 (2017). https://doi.org/10.5935/1676-2444.20170039
13. World Health Organization, Ebola virus disease (2021). https://www.who.int/news-room/fact-sheets/detail/ebola-virus-disease
14. F. Ayoade, S. Kumar, Varicella zoster, in *StatPearls* (StatPearls Publishing, Treasure Island, 2022)
15. K.A. Simonsen, SJ Smallpox, in *StatPearls* (StatPearls Publishing, Treasure Island)
16. M. Truong Lam, B. O'Sullivan, P. Gullane, S.H. Huang, Challenges in establishing the diagnosis of human papillomavirus-related oropharyngeal carcinoma. Laryngoscope **126**, 2270–2275 (2016). https://doi.org/10.1002/lary.25985
17. S.U. Kalu, M. Loeffelholz, E. Beck, J.A. Patel, K. Revai, J. Fan, K.J. Henrickson, T. Chonmaitree, Persistence of adenovirus nucleic acids in nasopharyngeal secretions: a diagnostic conundrum. Bone **29**, 746 (2010). https://doi.org/10.1097/INF.0b013e3181d743c8
18. World Health Organization, Hepatitis B (2021). https://www.who.int/news-room/fact-sheets/detail/hepatitis-b
19. C. Chu, P.A. Selwyn, Diagnosis and initial management of acute HIV infection. Am Fam Physician **81**, 1239–1244 (2010)
20. Centers of Disease Control and Prevention, Poliovirus diagnostic methods (2021). https://www.cdc.gov/polio/what-is-polio/lab-testing/diagnostic.html
21. G.L. Kirkpatrick, The common cold. Prim Care Clin Off Pract **23**, 657–675 (1996). https://doi.org/10.1016/S0095-4543(05)70355-9
22. B. Alberts, D. Bray, A. Johnson et al., Fundamentos da Biologia Celular. Uma Introdução à Biologia Molecular da Célula. Artes Médicas Sul, Porto Alegre (2006)
23. J.B. Reece et al., *Biologia de Campbell,* 10th edn. (Artmed, Porto Alegre, 2015)
24. C.B. Clish, Metabolomics: an emerging but powerful tool for precision medicine. Mol Case Stud **1**, a000588 (2015). https://doi.org/10.1101/mcs.a000588
25. S.Z. Tan, P. Begley, G. Mullard et al., Introduction to metabolomics and its applications in ophthalmology. Eye **30**, 773–783 (2016). https://doi.org/10.1038/eye.2016.37
26. R.G. Duft, A. Castro, M.P.T. Chacon-Mikahil, C.R. Cavaglieri, Metabolomics and exercise: possibilities and perspectives. Mot Rev Educ Física 23 (2017). https://doi.org/10.1590/s1980-6574201700020010
27. K.S. Smirnov, T.V. Maier, A. Walker et al., Challenges of metabolomics in human gut microbiota research. Int J Med Microbiol **306**, 266–279 (2016). https://doi.org/10.1016/j.ijmm.2016.03.006
28. A. Smolinska, L. Blanchet, L.M.C. Buydens, S.S. Wijmenga, NMR and pattern recognition methods in metabolomics: from data acquisition to biomarker discovery: a review. Anal. Chim. Acta. **750**, 82–97 (2012). https://doi.org/10.1016/j.aca.2012.05.049
29. A. Marco-Ramell, M. Palau-Rodriguez, A. Alay et al., Evaluation and comparison of bioinformatic tools for the enrichment analysis of metabolomics data. BMC Bioinformatics **19**, 1–11 (2018). https://doi.org/10.1186/s12859-017-2006-0
30. C. Lema, M. Andrés, S. Aguadé-Bruix et al., 1H NMR serum metabolomic profiling of patients at risk of cardiovascular diseases performing stress test. Sci. Rep. **10**, 1–10 (2020). https://doi.org/10.1038/s41598-020-74880-6
31. V. Pareek, H. Tian, N. Winograd, S.J. Benkovic, Metabolomics and mass spectrometry imaging reveal channeled de novo purine synthesis in cells. Science **368**, 283–290 (2020). https://doi.org/10.1126/science.aaz6465

32. D.D. Fraser, G. Cepinskas, E.K. Patterson et al., Novel outcome biomarkers identified with targeted proteomic analyses of plasma from critically ill coronavirus disease 2019 patients. Crit. Care Explor. **2**, e0189 (2020). https://doi.org/10.1097/cce.0000000000000189
33. B.L. Marquez, R.T. Williamson, Quantitative applications of NMR spectroscopy. Chem. Eng. Pharm. Ind. 133–149 (2019). https://doi.org/10.1002/9781119600800.ch7
34. J.L. Ward, J.M. Baker, M.H. Beale, Recent applications of NMR spectroscopy in plant metabolomics. FEBS J **274**, 1126–1131 (2007). https://doi.org/10.1111/j.1742-4658.2007.05675.x
35. A.A. Crook, R. Powers, Quantitative NMR-based biomedical metabolomics: current status and applications. Molecules **25** (2020). https://doi.org/10.3390/molecules25215128
36. G.A. Nagana Gowda, D. Raftery, Overview of NMR Spectroscopy-Based Metabolomics: Opportunities and Challenges (2019), pp. 3–14
37. P. Soininen, in *Quantitative 1H NMR Spectroscopy—Chemical and Biological Applications* (2008)
38. C. Deborde, A. Moing, L. Roch et al., Plant metabolism as studied by NMR spectroscopy. Prog. Nucl. Magn. Reson. Spectrosc. **102–103**, 61–97 (2017). https://doi.org/10.1016/j.pnmrs.2017.05.001
39. A. Vignoli, V. Ghini, G. Meoni et al., High-throughput metabolomics by 1D NMR. Angew Chemie. Int. Ed. **58**, 968–994 (2019). https://doi.org/10.1002/anie.201804736
40. M. Schmedes, A.D. Brejnrod, E.K. Aadland et al., The effect of lean-seafood and non-seafood diets on fecal metabolites and gut microbiome: results from a randomized crossover intervention study. Mol. Nutr. Food Res. **63**, 1–8 (2019). https://doi.org/10.1002/mnfr.201700976
41. R. Thøgersen, J.L. Castro-Mejía, U. Kræmer Sundekilde et al., Inulin and milk mineral fortification of a pork sausage exhibits distinct effects on the microbiome and biochemical activity in the gut of healthy rats. Food Chem. **331** (2020). https://doi.org/10.1016/j.foodchem.2020.127291
42. P.S.X. Yap, C.W. Chong, A.A. Kamar et al., Neonatal intensive care unit (NICU) exposures exert a sustained influence on the progression of gut microbiota and metabolome in the first year of life. Sci. Rep. **11**(1353), 1 (2021). https://doi.org/10.1038/s41598-020-80278-1;Sci. Rep. **11**(1–14), 10 (2021). https://doi.org/10.1038/s41598-021-88758-8
43. X. Li, K. Hu, Quantitative NMR studies of multiple compound mixtures. Annu. Reports NMR Spectrosc. **90**, 85–143 (2017). https://doi.org/10.1016/bs.arnmr.2016.08.001
44. P. Giraudeau, Challenges and perspectives in quantitative NMR. Magn. Reson. Chem. **55**, 61–69 (2017). https://doi.org/10.1002/mrc.4475
45. R.L. Loo, S. Lodge, T. Kimhofer et al., Quantitative in-vitro diagnostic NMR spectroscopy for lipoprotein and metabolite measurements in plasma and serum: recommendations for analytical artifact minimization with special reference to COVID-19/SARS-CoV-2 samples. J Proteome. Res. **19**, 4428–4441 (2020). https://doi.org/10.1021/acs.jproteome.0c00537
46. M.P.M. Letertre, P. Giraudeau, P. de Tullio, Nuclear magnetic resonance spectroscopy in clinical metabolomics and personalized medicine: current challenges and perspectives. Front. Mol. Biosci. **8**, 1–25 (2021). https://doi.org/10.3389/fmolb.2021.698337
47. D.L. Pavia et al., Introduction to spectroscopy. Cengage Learn (2009)
48. T.D.W. Claridge, in *High-Resolution NMR Techniques in Organic Chemistry* (Elsevier, 2009)
49. C. Stavarache, A. Nicolescu, C. Duduianu et al., A real-life reproducibility assessment for NMR metabolomics. Diagnostics 12 (2022). https://doi.org/10.3390/diagnostics12030559
50. B. Jiménez, E. Holmes, C. Heude et al., Quantitative lipoprotein subclass and low molecular weight metabolite analysis in human serum and plasma by 1H NMR spectroscopy in a multilaboratory trial. Anal. Chem. **90**, 11962–11971 (2018). https://doi.org/10.1021/acs.analchem.8b02412
51. S. Lodge, P. Nitschke, T. Kimhofer et al., NMR spectroscopic windows on the systemic effects of SARS-CoV-2 infection on plasma lipoproteins and metabolites in relation to circulating cytokines. J Proteome Res **20**, 1382–1396 (2021). https://doi.org/10.1021/acs.jproteome.0c00876

52. R. Masuda, S. Lodge, P. Nitschke et al., Integrative modeling of plasma metabolic and lipoprotein biomarkers of SARS-CoV-2 infection in Spanish and Australian COVID-19 patient cohorts. J. Proteome. Res. **20**, 4139–4152 (2021). https://doi.org/10.1021/acs.jproteome.1c00458
53. S. Lodge, P. Nitschke, R.L. Loo et al., Low volume in vitro diagnostic proton NMR spectroscopy of human blood plasma for lipoprotein and metabolite analysis: application to SARS-CoV-2 biomarkers. J. Proteome. Res. **20**, 1415–1423 (2021). https://doi.org/10.1021/acs.jproteome.0c00815
54. G. Costa Dos Santos Junior, C.M. Pereira, T. Kelly Da Silva Fidalgo, A.P. Valente, Saliva NMR-based metabolomics in the war against COVID-19. Anal. Chem. **92**, 15688–15692 (2020). https://doi.org/10.1021/acs.analchem.0c04679
55. B. Khakimov, H.C.J. Hoefsloot, N. Mobaraki et al., Human blood lipoprotein predictions from 1H NMR spectra: protocol, model performances, and cage of covariance. Anal. Chem. **94**, 628–636 (2022). https://doi.org/10.1021/acs.analchem.1c01654
56. C. Wang, I. Timári, B. Zhang et al., COLMAR lipids web server and ultrahigh-resolution methods for two-dimensional nuclear magnetic resonance- and mass spectrometry-based lipidomics. J. Proteome. Res. **19**, 1674–1683 (2020). https://doi.org/10.1021/acs.jproteome.9b00845
57. B.S. Barbosa et al., Qualitative and quantitative NMR approaches in blood serum lipidomics, in *Investigations of Early Nutrition Effects on Long-Term Health* (Humana Press, New York, 2018), pp. 365–379
58. Y. Navarro, R. Soengas, M.J. Iglesias, F.L. Ortiz, Use of NMR for the analysis and quantification of the sugar composition in fresh and store-bought fruit juices. J. Chem. Educ. **97**, 831–837 (2020). https://doi.org/10.1021/acs.jchemed.9b00651
59. G.A.N. Gowda, D. Raftery, NMR based metabolomics. 19–37 (2022). https://doi.org/10.1007/978-3-030-51652-9
60. Q. Wan, Y. Wang, H. Tang, Quantitative 13C traces of glucose fate in hepatitis B virus-infected hepatocytes. Anal. Chem. **89**, 3293–3299 (2017). https://doi.org/10.1021/acs.analchem.6b03200
61. A.L. Guennec, P. Giraudeau, S. Caldarelli, Evaluation of fast 2D NMR for metabolomics. Anal. Chem. **86**, 5946–5954 (2014). https://doi.org/10.1021/ac500966e
62. Maulidiani, F. Abas, R. Rudiyanto et al., Application of quantitative spectral deconvolution 1H NMR (qsd-NMR) in the simultaneous quantitative determination of creatinine and metformin in human urine. Anal. Methods **11**, 5487–5499 (2019). https://doi.org/10.1039/c9ay00594c
63. J. Farjon, C. Milande, E. Martineau et al., The FAQUIRE approach: fast, quantitative, highly resolved and sensitivity enhanced 1H, 13C Data. Anal. Chem. **90**, 1845–1851 (2018). https://doi.org/10.1021/acs.analchem.7b03874
64. E. Martineau, J.N. Dumez, P. Giraudeau, Fast quantitative 2D NMR for metabolomics and lipidomics: a tutorial. Magn. Reson. Chem. **58**, 390–403 (2020). https://doi.org/10.1002/mrc.4899
65. J. Marchand, E. Martineau, Y. Guitton et al., Multidimensional NMR approaches towards highly resolved, sensitive and high-throughput quantitative metabolomics. Curr. Opin. Biotechnol. **43**, 49–55 (2017). https://doi.org/10.1016/j.copbio.2016.08.004
66. P. Schanda, Fast-pulsing longitudinal relaxation optimized techniques: enriching the toolbox of fast biomolecular NMR spectroscopy. Prog. Nucl. Magn. Reson. Spectrosc. **55**, 238–265 (2009). https://doi.org/10.1016/j.pnmrs.2009.05.002
67. E.R.F. Kupce, Fast multidimensional NMR by polarization sharing. Magn. Reson. Chem. **45**, 2–4 (2007). https://doi.org/10.1002/mrc.1931
68. B. Vitorge, G. Bodenhausen, P. Pelupessy, Speeding up nuclear magnetic resonance spectroscopy by the use of SMAll Recovery Times—SMART NMR. J Magn Reson **207**, 149–152 (2010). https://doi.org/10.1016/j.jmr.2010.07.017
69. M. Quinternet, J.P. Starck, M.A. Delsuc, B. Kieffer, Heteronuclear NMR provides an accurate assessment of therapeutic insulin's quality. J. Pharm. Biomed. Anal. **78–79**, 252–254 (2013). https://doi.org/10.1016/j.jpba.2013.02.016

70. M. D'Onofrio, L. Ragona, D. Fessas et al., NMR unfolding studies on a liver bile acid binding protein reveal a global two-state unfolding and localized singular behaviors. Arch. Biochem. Biophys. **481**, 21–29 (2009). https://doi.org/10.1016/j.abb.2008.10.017
71. M. Pathan, S. Akoka, I. Tea, B. Charrier, P. Giraudeau, "Multi-scan single shot" quantitative 2D NMR: a valuable alternative to fast conventional quantitative 2D NMR. Analyst **136**, 3157–3163 (2011). https://doi.org/10.1039/c1an15278e
72. E. Martineau, P. Giraudeau, I. Tea, S. Akoka, Fast and precise quantitative analysis of metabolic mixtures by 2D 1H INADEQUATE NMR. J. Pharm. Biomed. Anal. **54**, 252–257 (2011). https://doi.org/10.1016/j.jpba.2010.07.046
73. T. Jézéquel, C. Deborde, M. Maucourt et al., Absolute quantification of metabolites in tomato fruit extracts by fast 2D NMR. Metabolomics **11**, 1231–1242 (2015). https://doi.org/10.1007/s11306-015-0780-0
74. S. Akoka, P. Giraudeau, Fast hybrid multi-dimensional NMR methods based on ultrafast 2D NMR. Magn. Reson. Chem. **53**, 986–994 (2015). https://doi.org/10.1002/mrc.4237
75. A.L. Guennec, I. Tea, I. Antheaume et al., Fast determination of absolute metabolite concentrations by spatially encoded 2D NMR: application to breast cancer cell extracts. Anal. Chem. **84**, 10831–10837 (2012). https://doi.org/10.1021/ac3033504
76. I. Timári, C. Wang, A.L. Hansen et al., Real-time pure shift HSQC NMR for untargeted metabolomics. Anal. Chem. **91**, 2304–2311 (2019). https://doi.org/10.1021/acs.analchem.8b04928
77. D. Uhrín, T. Liptaj, K.E. Kövér, Modified BIRD pulses and design of heteronuclear pulse sequences. J. Magn. Reson. Ser. A **101**, 41–46 (1993)
78. N.M. Byers, A.C. Fleshman, R. Perera, C.R. Molins, Metabolomic insights into human arboviral infections: dengue, chikungunya, and zika viruses. Viruses **11**, 1–30 (2019). https://doi.org/10.3390/v11030225
79. E.C. da Nunes, G.A.B. Canuto, Metabolomics applied in the study of emerging arboviruses caused by Aedes aegypti mosquitoes: a review. Electrophoresis **41**, 2102–2113 (2020). https://doi.org/10.1002/elps.202000133
80. V. Tounta, Y. Liu, A. Cheyne, G. Larrouy-Maumus, Metabolomics in infectious diseases and drug discovery. Mol. Omi. **17**, 376–393 (2021). https://doi.org/10.1039/d1mo00017a
81. H. Zheng, M. Chen, S. Lu et al., Metabolic characterization of hepatitis B virus-related liver cirrhosis using NMR-based serum metabolomics. Metabolomics **13**, 1–9 (2017). https://doi.org/10.1007/s11306-017-1260-5
82. M.M.G. Godoy, E.P.A. Lopes, R.O. Silva et al., Hepatitis C virus infection diagnosis using metabonomics. J. Viral. Hepat. **17**, 854–858 (2010). https://doi.org/10.1111/j.1365-2893.2009.01252.x
83. S. Wei, Y. Suryani, G.A.N. Gowda et al., Differentiating hepatocellular carcinoma from hepatitis C using metabolite profiling. Metabolites **2**, 701–716 (2012). https://doi.org/10.3390/metabo2040701
84. N. Embade, O. Millet, Molecular determinants of chronic liver disease as studied by NMR-metabolomics. Curr. Top. Med. Chem. **17**, 2752–2766 (2017). https://doi.org/10.2174/1568026617666170707124539
85. L.R. Gouveia, J.C. Santos, R.D. Silva et al., Diagnosis of coinfection by schistosomiasis and viral hepatitis B or C using 1H NMR-based metabonomics. PLoS ONE **12**, 1–11 (2017). https://doi.org/10.1371/journal.pone.0182196
86. G. Meoni, S. Lorini, M. Monti et al., The metabolic fingerprints of HCV and HBV infections studied by nuclear magnetic resonance spectroscopy. Sci. Rep. **9**, 1–13 (2019). https://doi.org/10.1038/s41598-019-40028-4
87. M. Shanmuganathan, M.O. Sarfaraz, Z. Kroezen et al., A cross-platform metabolomics comparison identifies serum metabolite signatures of liver fibrosis progression in chronic hepatitis C patients. Front. Mol. Biosci. **8**, 1–15 (2021). https://doi.org/10.3389/fmolb.2021.676349
88. C.M. Slupsky, K.N. Rankin, H. Fu et al., Pneumococcal pneumonia: potential for diagnosis through a urinary metabolic profile. J. Proteome. Res. **8**, 5550–5558 (2009). https://doi.org/10.1021/pr9006427

89. S.U. Munshi, S. Taneja, N.S. Bhavesh et al., Metabonomic analysis of hepatitis e patients shows deregulated metabolic cycles and abnormalities in amino acid metabolism. J. Viral. Hepat. **18** (2011). https://doi.org/10.1111/j.1365-2893.2011.01488.x
90. R. Hewer, J. Vorster, F.E. Steffens, D. Meyer, Applying biofluid 1H NMR-based metabonomic techniques to distinguish between HIV-1 positive/AIDS patients on antiretroviral treatment and HIV-1 negative individuals. J. Pharm. Biomed. Anal. **41**, 1442–1446 (2006). https://doi.org/10.1016/j.jpba.2006.03.006
91. S.U. Kaur, B.F. Oyeyemi, A. Shet et al., Plasma metabolomic study in perinatally HIV-infected children using 1H NMR spectroscopy reveals perturbed metabolites that sustain during therapy. PLoS ONE **15**, 1–17 (2020). https://doi.org/10.1371/journal.pone.0238316
92. T.R. McKnight, H.A.I. Yoshihara, L.J. Sitole et al., A combined chemometric and quantitative NMR analysis of HIV/AIDS serum discloses metabolic alterations associated with disease status. Mol. Biosyst. **10**, 2889–2897 (2014). https://doi.org/10.1039/c4mb00347k
93. C. Philippeos, F.E. Steffens, D. Meyer, Comparative 1H NMR-based metabonomic analysis of HIV-1 sera. J. Biomol. NMR **44**, 127–137 (2009). https://doi.org/10.1007/s10858-009-9329-8
94. E. Rodríguez-Gallego, J. Gómez, P. Domingo et al., Circulating metabolomic profile can predict dyslipidemia in HIV patients undergoing antiretroviral therapy. Atherosclerosis **273**, 28–36 (2018). https://doi.org/10.1016/j.atherosclerosis.2018.04.008
95. L.J. Sitole, F. Tugizimana, D. Meyer, Multi-platform metabonomics unravel amino acids as markers of HIV/combination antiretroviral therapy-induced oxidative stress. J. Pharm. Biomed. Anal. **176**, 112796 (2019). https://doi.org/10.1016/j.jpba.2019.112796
96. S.U. Munshi, B.B. Rewari, N.S. Bhavesh, S. Jameel, Nuclear magnetic resonance based profiling of biofluids reveals metabolic dysregulation in HIV-infected persons and those on anti-retroviral therapy. PLoS One 8 (2013). https://doi.org/10.1371/journal.pone.0064298
97. C.D. French, R.E. Willoughby, A. Pan et al., NMR metabolomics of cerebrospinal fluid differentiates inflammatory diseases of the central nervous system. PLoS Negl. Trop. Dis. **12**, 1–17 (2018). https://doi.org/10.1371/journal.pntd.0007045
98. M.M. Banoei, H.J. Vogel, A.M. Weljie et al., Plasma metabolomics for the diagnosis and prognosis of H1N1 influenza pneumonia. Crit. Care. **21**, 1–15 (2017). https://doi.org/10.1186/s13054-017-1672-7
99. J.L. Izquierdo-Garcia, N. Nin, J. Jimenez-Clemente et al., Metabolomic profile of ards by nuclear magnetic resonance spectroscopy in patients with h1n1 influenza virus pneumonia. Shock **50**, 504–510 (2018). https://doi.org/10.1097/SHK.0000000000001099
100. N. Shahfiza, H. Osman, T.T. Hock et al., Metabolomics for characterization of gender differences in patients infected with dengue virus. Asian Pac. J. Trop. Med. **8**, 451–456 (2015). https://doi.org/10.1016/j.apjtm.2015.05.012
101. S.P. Young, M. Nessim, F. Falciani et al., Metabolomic analysis of human vitreous humor differentiates ocular inflammatory disease. Mol. Vis. **15**, 1210–1217 (2009)
102. J. Shrinet, J.S. Shastri, R. Gaind et al., Serum metabolomics analysis of patients with chikungunya and dengue mono/co-infections reveals distinct metabolite signatures in the three disease conditions. Sci. Rep. **6**, 1–12 (2016). https://doi.org/10.1038/srep36833
103. D.J. Adamko, E. Saude, M. Bear et al., Urine metabolomic profiling of children with respiratory tract infections in the emergency department: a pilot study. BMC Infect. Dis. **16** (2016). https://doi.org/10.1186/s12879-016-1709-6
104. C. Bruzzone, S. Lu, T. Diercks et al., in *iScience ll SARS-CoV-2 Infection Dysregulates the Metabolomic and Lipidomic Profiles of Serum the Metabolomic and Lipidomic Profiles of Serum* (2020). https://doi.org/10.1016/j.isci.2020.101645
105. D.D. Fraser, M. Slessarev, C.M. Martin et al., Metabolomics profiling of critically ill coronavirus disease 2019 patients: identification of diagnostic and prognostic biomarkers. Crit. Care Explor. **2**, e0272 (2020). https://doi.org/10.1097/cce.0000000000000272
106. A. Valdés, L.O. Moreno, S.R. Rello et al., Metabolomics study of COVID-19 patients in four different clinical stages. Sci. Rep. **12**, 1–11 (2022). https://doi.org/10.1038/s41598-022-05667-0

107. E. Holmes, J. Wist, R. Masuda et al., in *Incomplete Systemic Recovery and Metabolic Phenoreversion in Post-Acute-Phase Nonhospitalized COVID-19 Patients: Implications for Assessment of Post-Acute COVID-19 Syndrome* (2021). https://doi.org/10.1021/acs.jproteome.1c00224
108. T. Kimhofer, S. Lodge, L. Whiley et al., in *Integrative Modeling of Quantitative Plasma Lipoprotein, Metabolic, and Amino Acid Data Reveals a Multiorgan Pathological Signature of SARS-CoV—2 Infection* (2020). https://doi.org/10.1021/acs.jproteome.0c00519
109. F. Schmelter, B. Föh, A. Mallagaray et al., Metabolic and lipidomic markers differentiate COVID-19 from non-hospitalized and other intensive care patients. Front. Mol. Biosci. **8**, 1–12 (2021). https://doi.org/10.3389/fmolb.2021.737039
110. A.F. Rendeiro, C.K. Vorkas, J. Krumsiek et al., Metabolic and immune markers for precise monitoring of COVID-19 severity and treatment. Front. Immunol. **12**, 1–13 (2022). https://doi.org/10.3389/fimmu.2021.809937
111. J.A. Lorente, N. Nin, P. Villa et al., Metabolomic diferences between COVID-19 and H1N1 influenza induced ARDS. Crit. Care **25**, 1–11 (2021). https://doi.org/10.1186/s13054-021-03810-3
112. N. Embade, Z. Mariño, T. Diercks et al., Metabolic characterization of advanced liver fibrosis in HCV patients as studied by serum 1H-NMR spectroscopy. PLoS ONE **11**, 1–19 (2016). https://doi.org/10.1371/journal.pone.0155094
113. E. Baranovicova, A. Bobcakova, R. Vysehradsky et al., The ability to normalise energy metabolism in advanced covid-19 disease seems to be one of the key factors determining the disease progression—a metabolomic nmr study on blood plasma. Appl. Sci. **11**, 4–6 (2021). https://doi.org/10.3390/app11094231
114. M. Manchester, A. Anand, in *Metabolomics: Strategies to Define the Role of Metabolism in Virus Infection and Pathogenesis*, 1st edn. (Elsevier Inc., 2017)
115. D.S. Wishart, C. Knox, A.C. Guo et al., HMDB: a knowledgebase for the human metabolome. Nucleic Acids Res. **37**, 603–610 (2009). https://doi.org/10.1093/nar/gkn810
116. O. Beckonert, H.C. Keun, T.M.D. Ebbels et al., Metabolic profiling, metabolomic and metabonomic procedures for NMR spectroscopy of urine, plasma, serum and tissue extracts. Nat. Protoc. **2**, 2692–2703 (2007). https://doi.org/10.1038/nprot.2007.376
117. G.F. Giskeødegård, T. Andreassen, H. Bertilsson et al., The effect of sampling procedures and day-to-day variations in metabolomics studies of biofluids. Anal. Chim. Acta. **1081**, 93–102 (2019). https://doi.org/10.1016/j.aca.2019.07.026
118. A.C. Dona, B. Jiménez, H. Schafer et al., Precision high-throughput proton NMR spectroscopy of human urine, serum, and plasma for large-scale metabolic phenotyping. Anal. Chem. **86**, 9887–9894 (2014). https://doi.org/10.1021/ac5025039
119. B. Khakimov, N. Mobaraki, A. Trimigno et al., Signature mapping (SigMa): an efficient approach for processing complex human urine 1H NMR metabolomics data. Anal. Chim. Acta. **1108**, 142–151 (2020). https://doi.org/10.1016/j.aca.2020.02.025
120. R.W. Evans, Diagnostic testing for headache. Med. Clin. North. Am. **85**, 865–885 (2001). https://doi.org/10.1016/S0025-7125(05)70348-5
121. B. Shen, X. Yi, Y. Sun et al., Proteomic and metabolomic characterization of COVID-19 patient sera. Cell **182**, 59-72.e15 (2020). https://doi.org/10.1016/j.cell.2020.05.032
122. M.R. Hasan, M. Suleiman, A. Pérez-López, Metabolomics in the diagnosis and prognosis of COVID-19. Front. Genet. 12 (2021). https://doi.org/10.3389/fgene.2021.721556
123. M. Costanzo, M. Caterino, R. Fedele et al., COVIDomics: the proteomic and metabolomic signatures of COVID-19. Int. J. Mol. Sci. **23**, 2414 (2022). https://doi.org/10.3390/ijms23052414
124. B.S.B. Correia et al., ^{1}H qNMR based metabolomics discrimination of COVID-19 severity. J. Proteome. Res. (in press)
125. V. Khullar, R.J. Firpi, Hepatitis C cirrhosis: new perspectives for diagnosis and treatment. World J. Hepatol. **7**, 1843–1855 (2015). https://doi.org/10.4254/wjh.v7.i14.1843
126. R.H. Westbrook, G. Dusheiko, Natural history of hepatitis C. J. Hepatol. **61**, S58–S68 (2014). https://doi.org/10.1016/j.jhep.2014.07.012

127. R.F. Schwabe, J.J. Maher, Lipids in liver disease: Looking beyond steatosis. Gastroenterology **142**, 8–11 (2012). https://doi.org/10.1053/j.gastro.2011.11.004
128. F.S. Macaluso, M. Maida, M.G. Minissale et al., Metabolic factors and chronic hepatitis C: a complex interplay. Biomed. Res. Int. 2013 (2013). https://doi.org/10.1155/2013/564645

Application of Quality Statistical Tools for the Evaluation of Diagnostic Tests for SARS-CoV-2 Detection

Carolaine de Oliveira Rodrigues and Igor Renato Bertoni Olivares

Abstract This chapter explores the use of quality statistical tools for the development of diagnostic tests for SARS-CoV-2 and the different metrological parameters recommended to laboratories towards guaranteeing the quality assurance of the tests, according to ISO/IEC 17025. Tools such as validation, uncertainty estimation, and proficiency testing are presented and the importance of their application to the current scenario and their perspectives and scarcity in the tests developed and made available are discussed.

Keywords SARS-CoV-2 · Qualitative analysis · Diagnostic tests · Metrological tools

1 Introduction

The current global pandemic caused by Severe Acute Respiratory Syndrome 2 (SARS-CoV-2) is considered constant challenge for global public health. Diagnostic methods, or in vitro tests, developed for the detection and diagnosis of the contagion of viruses act towards a quick and effective response in a crisis, contributing to the screening, diagnosis, follow-up/treatment of patients, and recovery/epidemiological surveillance [1]. Their performance must be qualified and reported so that their compliance with legislation can be assessed. However, the currently available database has revealed a mismatch between existing or reported results of method/test/device information from metrology tools applied and performance criteria, which requires the performance characteristics of the method be defined so that it is scientifically consistent under the conditions for its adoption [1]. A set of qualitative analysis checks should therefore be applied to the method through

C. de Oliveira Rodrigues · I. R. B. Olivares (✉)
Research in Quality Assurance for Laboratories (RQA Labs), Institute of Chemistry of São Carlos (IQSC), University of São Paulo (USP), São Carlos, São Paulo 13560-970, Brazil
e-mail: igorolivares@iqsc.usp.br

C. de Oliveira Rodrigues
e-mail: carolainerodrigues@usp.br

F. N. Crespilho (ed.), *COVID-19 Metabolomics and Diagnosis*,
https://doi.org/10.1007/978-3-031-15889-6_8

different metrological tools (e.g., validation, uncertainty estimation, and proficiency testing) for ensuring the tests are suitable and compliant with their application.

This chapter addresses the importance of a correct application of metrology tools for ensuring both quality and reliability of the results of SARS-CoV-2 detection methods. The analysis is based on a review and an evaluation of such tools and their best practices are highlighted.

2 SARS-CoV-2

Emerging and re-emerging infectious diseases are regarded as ongoing challenges for global public health. Among such diseases, the current Severe Acute Respiratory Syndrome 2 (or SARS-CoV-2), formerly known as novel coronavirus (2019-nCoV), has been considered a global pandemic. It is transmitted by a new zoonotic agent that emerged in Wuhan, China, in December 2019, and has caused respiratory, digestive, and systemic manifestations articulated in the clinical picture of a disease called COVID-19 (Coronavirus Disease 2019). COVID-19 spreads to humans from an animal host and, according to its origin, SARS-CoV-2 virus is known to be 96% identical to a bat coronavirus, which spreads through intermediate hosts and now from human to human (Fig. 1) [2, 3].

SARS-Cov-2 is a β-coronavirus type virus that uses angiotensin-converting enzyme II (ACE II) for cell adhesion and subsequent replication [4]. It is transmitted by various means [e.g., aerosols (coughing/sneezing)], direct contact (e.g., fomites, handshake, kissing, and hugging), and possibly through sexual contact [5]. COVID-19 can develop asymptomatically or with symptoms such as runny nose, fever, cough, diarrhea, and, in more advanced cases, severe pneumonia [6].

The virus is known to have a high transmission rate and cause an acute respiratory syndrome that ranges from mild cases—approximately 80%—to very severe ones—between 5 and 10%—with respiratory failure and a variable fatality rate, mainly according to age group [2, 5], thus requiring specialized treatment in intensive care units (ICU).

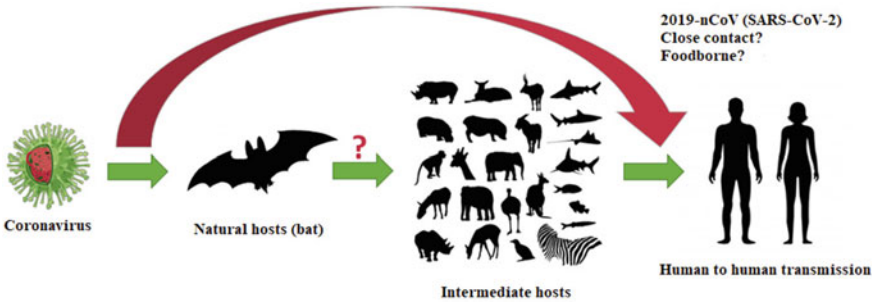

Fig. 1 Potential transmission cycles of SARS-CoV-2 (based on Ahmad et al. [3])

An early diagnosis of COVID-19 is essential for the identification of cases and control of the pandemic [7]. Suspected cases can be confirmed by SARS-CoV-2 ribonucleic acid amplification molecular tests, immunological tests for antibody detection, clinical presentation, and clinical-epidemiological investigation [8].

2.1 Diagnostic Tests for SARS-CoV-2 Detection

Diagnostic methods developed for confirming diagnoses and better estimating contagion of SARS-CoV-2 have emerged in the pandemic as essential tools that monitor cases at a population level, understand the immune response, and assess the exposure of individuals and possible immunity from reinfection [7]. Such tests are simple and usually do not require equipment; moreover, they enable the visualization of the result in a few minutes (10–30 min on average, depending on the type of test applied) [9].

The use of different diagnostic methods for detecting SARS-CoV-2 infection should consider their purpose of detection, since their characteristics vary according to the context of infection (e.g., timing of symptoms, type of sample, among others). Their use can help from clinical decision-making to the development of a health surveillance strategy [10, 11]. Among other aspects, individuals to be tested, clinical stage of their disease, definition of samples to be used, and minimum acceptable requirements for clinical performance (Fig. 2) [12] must also be identified.

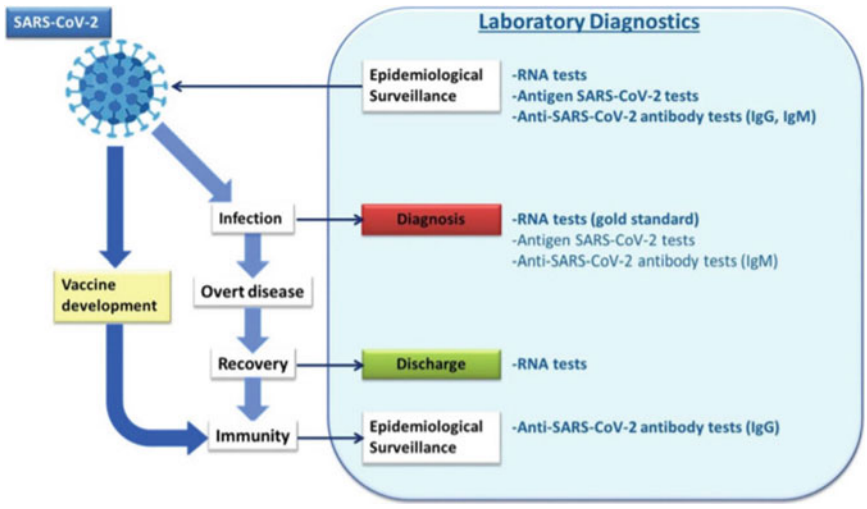

Fig. 2 Testing in the context of SARS-CoV-2 disease. Reprinted from European Commission [13]

The tests can be classified into two groups, i.e., those that can detect the presence of the virus (RNA and antigen tests) for supporting the diagnosis of patients with symptoms similar to those of 2019-nCoV, and tests with detection of the immune system and body response against SARS-CoV-2 virus, which identify previous infections or current infections in the presence of the virus (antibody tests) [12, 13].

Technologies based on polymerase chain reaction (PCR) and high-throughput sequencing are commonly used in the molecular approach for replicating nucleic acids and detecting the virus in respiratory samples [14]. Different targets include genes E, S, and Orflab, and in RDT tests, antigens or antibodies detect the presence of the virus. Antibody-based tests use ELISA or immunity-based technologies to detect antibodies in patients and identify if a patient has been previously infected. Antibodies of IgG, IgM, and IgA types related to SARS-CoV-2 infection are detected by qualitative methodology [7, 15]. Antibody tests use blood, plasma, or serum samples, and antigen-based testing methods can detect the presence of viral antigens in respiratory samples and diagnose an active infection using S and N proteins as the main targets of such antigens [7, 14].

A variety of laboratory parameters assists in monitoring the virus; apart from the aforementioned methods, radio imaging such as computed tomography (CT) monitors the shape of the chest throughout an infection, and inflammatory biomarkers [e.g., interleukin-6 (IL-6)] have also been detected in patients with COVID-19 [8, 12].

In addition to playing an essential and effective role in a crisis, diagnostic tests, contribute to a rapid response to patient triage, diagnosis, monitoring/treatment, and epidemiological recovery/surveillance [13]. Some of the several commercially available diagnostic tests for SARS-CoV-2 have received authorizations for use by national and international regulatory agencies [10].

Manufacturers of diagnostic methods for SARS-CoV-2 should evaluate the performance of the test device and report the performance parameters and the technical documentation of the device in the instructions for use—usually through performance studies—towards assessing the compliance of the test specifications with the legislation. Furthermore, after the commercialization of a diagnostic test, the performance of the methods should be validated for helping public health decision-making, especially in the context of the current crisis [9, 16].

According to a study conducted by the European Union [13], the current performance of test methods and devices for 2019-nCoV (Working document of Commission services) has shown a clear mismatch between the existing or reported quality assurance and the information about the tests/devices and performance criteria, which are based on good analytical practice principles and corresponding international standards such as ISO/IEC 17025 [16] and ISO 15189 [17]. The study has shown a current need for ensuring the performance characteristics of a test method are understood and certifying the method is scientifically consistent under the conditions for its use, which requires a set of checks regarding an analytical method, such as validation.

3 Quality Assurance

Quality assurance was considered quite revolutionary for laboratories a few years ago, since it justified laboratory credibility and proved effective in increasing the reliability of results [18]. It has been adopted in the daily processes of laboratory management, therefore, several organizations have implemented quality management systems in their routine [19].

The concept of quality is mainly associated with the reliability and traceability of analytical results in laboratories. A quality management system provides tools for the management of factors that may affect the quality of laboratory results according to documented procedures so that tools are properly applied and always in the same way [18, 19].

In clinical laboratories, the implementation of a quality control system represents all the systematic actions necessary to provide reliable results for satisfying patients' needs and avoiding errors [20]. A regular testing of quality control samples and samples from diseased individuals, as well as comparisons of quality control results with specific statistical results already known are required for ensuring quality in diagnostic tests [17].

Among the specific standards that regulate the implementation of a quality management system in laboratories is ISO/IEC 17025:2017 [16], more flexible for any type of laboratory and applied by several routine laboratories. However, GLP [21] (Good Laboratory Practice) focuses on each study performed and on the organizational processes and conditions under which non-clinical environmental health and safety studies are planned, performed, monitored, recorded, archived, and reported. As shown in Fig. 3, research laboratories apply quality principles and practices towards guaranteeing their activities.

Among the management requirements in NBR ISO/IEC 17025:2017 [16] for the functioning of the quality management system and the administration of the laboratory, laboratories must assure their customers they provide data with the expected quality through tools related to technical requirements and considered essential for the reliability and traceability of the results associated with each other by AQAC (*Analytical Quality Assurance Cycle*) [23] (see Fig. 4).

I. **Method validation:** refers to the evaluation of a method's suitability for an intended use;
II. **Uncertainty estimation:** the confidence level of a result is evaluated with data obtained in the validation stage;
III. **Quality control:** refers to a continuous evaluation of the validity of results after the validation and uncertainty estimation stages. The method is continuously monitored and data provided are incorporated into the validation ones.

After the evaluation of a method (during validation) and obtaining of the confidence level of the result (knowing the uncertainty), the quality control is applied towards demonstrating the method can provide reliable results in each test batch. The use of "calibrated equipment" and "certified standards" assists in proving the

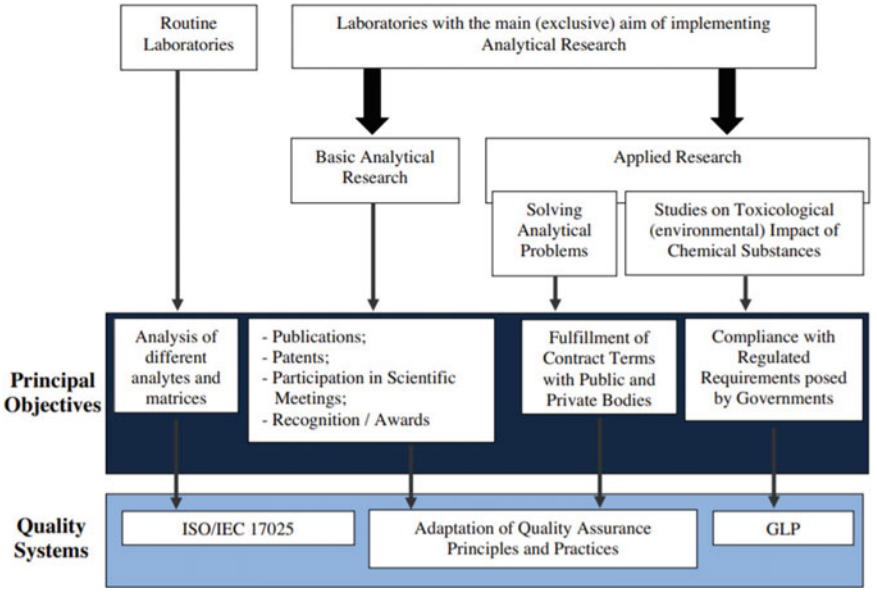

Fig. 3 Major goals and quality systems from different kinds of laboratories, classified according to their activities. Reprinted from Valcárcel and Ríos [22]

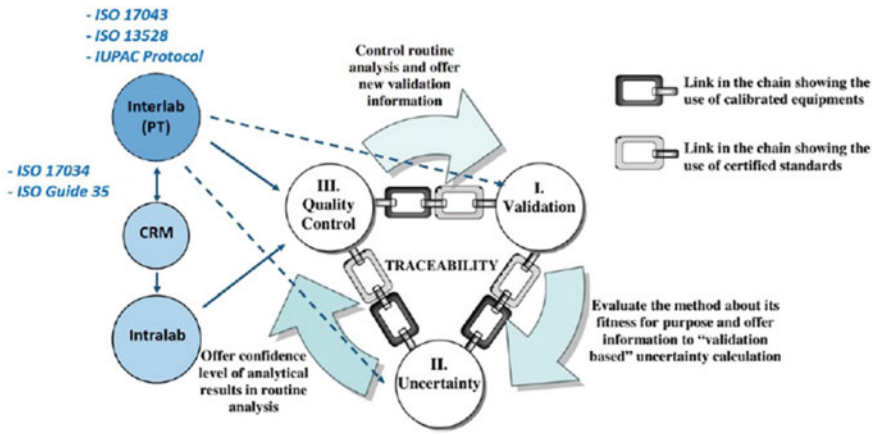

Fig. 4 Analytical quality assurance cycle (AQAC) with CRM and PT concepts. Modified from Olivares et al. [24]

reliability and traceability of the results and provides sustainability to the application of validation, uncertainty, and quality control [19, 25].

Quality Control can be applied either inter-laboratorial, or intra-laboratorial. The inter-laboratory control employs proficiency tests (PT) periodically elaborated by

laboratories and that help the traceability control of a given standard, whereas the intra-laboratory control uses reference material (RM) or certified reference material (CRM) [26].

3.1 Qualitative and Quantitative Methods

Analytical methods can be classified as quantitative or qualitative. A quantitative method establishes the amount of substance analyzed through a numerical value with the appropriate units [23, 24], whereas a qualitative method classifies a sample based on its physical, chemical, or biological properties. A binary response can be provided by a measurement instrument and test kits, which involve sensory changes detected through the presence or absence of a microorganism, directly (mass or volume) or indirectly (color, absorbance, impedance, etc.) in a given sample [23, 24].

Semi-quantitative methods of analysis lie between qualitative and quantitative ones; they provide an approximate answer regarding the quantification of an analyte and usually assign a certain class to a test sample (e.g. concentration can be high, medium, low, or very low) [27].

Prior to the validation process in the analysis of samples, studies on the performance parameters of a qualitative method, i.e., parameters analyzed during the validation of quantitative methods, must be conducted [27, 28]. Qualitative methods provide a response on the presence or absence of a particular analyte in a sample; therefore, the results of a qualitative analysis are binary responses such as present/absent, positive/negative, or yes/no. The parameters evaluated (Table 1) for qualitative methods are generally specificity, sensitivity, precision, false-positive rate, and false-negative rate, whereas repeatability and reproducibility are assessed for quantitative methods.

Quantitative methods can be described by a well-established set of performance characteristics to be used. In a comparison of such characteristics with those of qualitative methods, only the limit of detection (LOD) provides essentially the same

Table 1 Relationship between performance parameters studied in quantitative and qualitative analyses

Quantitative method	Qualitative method
Accuracy: trueness, precision	False positive and negative rates
Range and linearity	Cut-off limit
Uncertainty	Uncertainty region
Detection limit	Detection limit
Selectivity	Selectivity: interferences
Sensitivity and specificity	Sensitivity and specificity
Precision: reproducibility and repeatability	Accordance and concordance
Robustness	Robustness

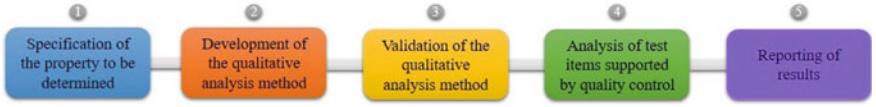

Fig. 5 Qualitative analysis process: (1) problem description, (2) method development and (3) validation, (4) tests on unknown items checked through quality control, and (5) reporting of results (Based on EURACHEM/CITAC Guide (2021) [30])

meaning for the methods, while concepts related to selectivity are important for both. The major features of qualitative methods are measures of "correctness" (ie, indications of false response rates), which have no direct counterpart in quantitative methods [29].

Qualitative analyses have gained importance in laboratories and several sectors, since they provide fast, objective, low cost, simple, and error minimization results due to the shorter interval between sampling and analysis frequently selected for screening [27].

A qualitative analysis (Fig. 5) requires both specification of the property and assessment of the suitability of the analysis for the intended use. The reporting of a qualitative analytical result must be supported by valid procedures and an adequate quality control of the test, and the way the results are reported depends on the purpose of the analysis and the recipient of the report [30].

The aforementioned analyses can be implemented in several analytical areas. For example, rapid testing methods, including qualitative tests, detect microbiological contaminants, heavy metals, pesticides, foreign bodies, mycotoxins, allergens, and other analytes in foods [27].

3.2 Method Validation

The quality of a method must comply with national and international regulations in all areas of analyses. Therefore, a laboratory must take appropriate steps (e.g., use of validated methods of analysis, internal quality control procedures, proficiency testing, and accreditation to an International Standard such as ISO/IEC 17025 [20, 23]) towards providing high quality data.

During the development of a method or a test, its performance characteristics must be evaluated towards their optimization and undergo preliminary validation studies [25] for the establishment of criteria for their performance parameters. Validation refers to confirmation and involves the provision of evidence that the minimum requirements for acceptance of a specific intended application or use have been met, thus proving its applicability for a particular purpose [16].

Method validation is an essential component of the measures implemented by a laboratory for the production of reliable analytical data, as shown in Table 2.

Table 2 Definitions of 'validation'

Definition	Reference
Confirmation through examination and provision of objective evidence that the particular requirements for a specific intended use have been fulfilled	ISO/IEC 17025 [16]
Confirmation through the provision of objective evidence that the requirements for a specific intended use or application have been fufilled	ISO 9000 [19]
Verification through analyses of whether specified requirements are adequate for an intended use	VIM [31]

The validation process consists of evaluation of the performance characteristics of a method and their comparison with analytical requirements [16]. Therefore, prior to the implementation of tests, the laboratory must prove it can properly operate a standardized method and provide objective evidence that the specific requirements for an intended use have been met. It must also define the validation parameters and criteria that best demonstrate the suitability of the method for that use [25].

Figure 6 illustrates the general process of validation of qualitative methods that involves both experimental and qualitative non-experimental steps. If the final result has been satisfied, the method can be considered "validated"; otherwise, it is necessary to return to the previous steps [32].

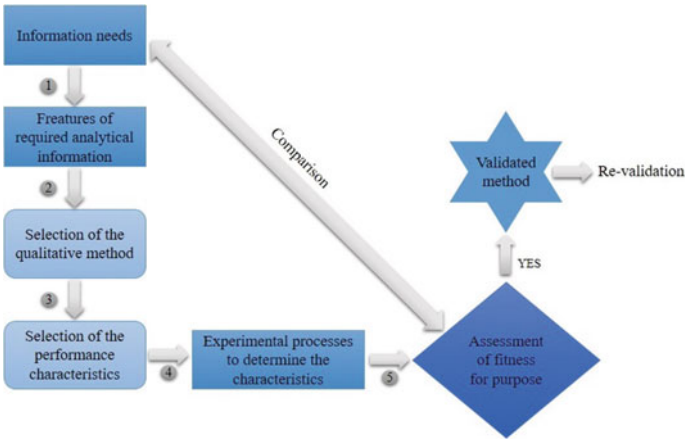

Fig. 6 General validation process of a qualitative method: (1) Conversion of the client's information needs (e.g., threshold limit and % reliability required) into the expected characteristics of the analytical information provided by the qualitative method; (2) A priori selection of the qualitative method (e.g., standard, standard modified or developed by the laboratory) most appropriate to solve the analytical problem; (3) Selection of the key characteristics of the qualitative method; (4) Establishment of the set of experimental processes for the determination of the selected characteristics of the method; and (5) Comparison of the characteristics in step (4) with those established a priori (i.e., confirmation of the fitness for the purpose of the qualitative method). (Based on Cárdenas and Valcárcel [32])

If an existing method has been modified towards meeting specific requirements, or if an entirely new method has been developed, the laboratory must ensure their performance characteristics meet the requirements of the intended analytical operations. Regarding modified methods (standardized or not) or those developed by a laboratory, a series of parameters defined by the laboratory must be evaluated for ensuring the suitability of the method for the intended use [33].

The main characteristics of the methods during the validation process are selectivity, limit of detection (LOD) and limit of quantification (LOQ), working range, analytical sensitivity, trueness (bias, recovery), precision (repeatability, intermediate precision, and reproducibility), measurement uncertainty, and ruggedness (robustness) [25].

Harmonized IUPAC [34], AOAC [35], and EURACHEM [25] protocols, among others, describe the way validation studies must be conducted and the way the results must be analyzed regarding the performance of quantitative methods. The validation of qualitative methods is an important bottleneck for the recognition of the competence of laboratories. Although several publications on validation procedures for qualitative methods are available in the literature, no harmonized document has established the parameters to be evaluated in each process, as in quantitative methods [27, 36]. A specific approach to this topic can be found in Trullols et al.'s "Validation of qualitative analytical methods" [27].

3.3 Uncertainty Estimation

An assessment of the risk of misclassification is recommended in the development of any test procedure; therefore, a laboratory is commonly expected to establish or have access to information on the risks of incorrect results [25]. Regarding standardized test procedures established by groups outside the laboratory and suitable for an intended purpose, access to performance data may be limited or even non-existent [16].

The aforementioned evaluation can provide a detailed test specification; moreover, relevant factors under the control of the laboratory often satisfy the requirements of a test procedure [25]. The evaluation may involve the demonstration that the uncertainty of the control parameters and the performance of the test are adequate to the ultimate objective of the testing [37].

Measurement uncertainty is defined as a parameter that characterizes the dispersion of values assigned to measurement, this is non-negative, based on the information used, according to the International Vocabulary of Measurements—VIM [31].

The establishment of an uncertainty usually requires a range related to a measurement result, which is expected to cover a large fraction of the distribution of values attributed to a quantity subjected to measurement [37]. The method should readily provide an interval with a scope probability or confidence level that realistically corresponds to the required level for the assessment and expression of the measurement uncertainty [38].

Laboratories are currently not expected to assess or report uncertainties associated with qualitative analysis results. However, some specifications, such as ISO/IEC 17025 [16] and ISO 15189 [17], require laboratories ensure they can obtain valid qualitative and quantitative analysis results and are aware of their reliability. When necessary, such laboratories report limitations for interpreting results and accurately answering customers' questions about reliability [28].

The assessment of uncertainties associated with quantitative parameters or analysis results has been the subject of considerable efforts [1]. On the other hand, uncertainties in qualitative analysis have received much less attention due to challenges for the establishment of uncertainty parameters associated with the method of analysis [39].

Despite a wide variety of metrics that express uncertainty in qualitative results, only a limited consensus on those to be used has been reached [5]. The most basic way to quantify the performance of qualitative analysis is to calculate rates of false results, which leads to "positive" or "negative" results, reported as "true positive" and "false positive" or "true negative" and "false negative" rates, respectively. However, such rates can be related to the total number of a specific type of case or result or to the total number of possible causes or results [30].

"Assessment of performance and uncertainty in qualitative chemical analysis" [30], a recently published guide produced by a joint Eurachem/CITAC working group, is based on experiences from several analytical fields through performance and qualitative uncertainty analyses and provides some performance alternatives to express the quality of qualitative analytical results (see Table 3).

3.4 Proficiency Testing

The laboratory must implement a quality assurance (QA) system that includes the monitoring of its performance through comparisons with results from other laboratories, when available and appropriate, for controlling the validity of its measurements [26, 30], which are an important aspect of the requirements for accredited laboratories or those seeking accreditation [16].

Participation in a proficiency test (PT) complements a laboratory's internal quality control (IQC) procedures, since it provides an additional external measure of the laboratory's measurement capability [26, 30].

Proficiency tests are considered interlaboratory studies used as tools for external evaluations and demonstration of the reliability of laboratory analytical results. They help the identification of failures and enable corrective or preventive actions to be taken. Moreover, they are one of the items required for laboratory accreditation by ISO/IEC 17025:2017 [16].

According to ISO/IEC 17043 [40], the proficiency testing provider must follow some steps, such as instruction to participants, handling of PT items, distribution, data analysis, and evaluation, as shown in Fig. 7.

Table 3 Alternative performance characteristics for expressing the quality of qualitative analytical results

Performance characteristics	Expression
True positive rate, *TP* (sensitivity, SS)	$tp/pc = tp/(tp + fn) = 1 - FN$
False positive rate, *FP*	$fp/nc = fp/(tn + fp) = 1 - TN$
True negative rate, *TN* (specificity, SP)	$tn/nc = tn/(tn + fp) = 1 - FP$
False negative rate, *FN*	$fn/pc = fn/(tp + fn) = 1 - TP$
Precision or positive predictive value, *PPV*	$tp/p = tp/(tp + fp)$
Negative predictive value, *NPV*	$tn/n = tn/(p + n)$
Efficiency, *E*	$(tp + tn)/(p + n)$
Youden Index, *Y*	$SS(\%) + SP(\%) - 100$
Likelihood ratio of positive results, *LR*(+)	TP/FP
Likelihood ratio of negative results, *LR*(−)	TN/FN
Posterior probability*	$O(A) = \frac{P(A)}{1-P(A)}$; $P(A) = \frac{O(A)}{O(A)+1}$

tp—number of true positive results; *fp*—number of false positive results; tn—number of true negative results; *fn*—number of false negative results; *p*—number of positive results ($tp + fp$); *n*—number of negative results ($tn + fn$); *pc*—number of positive cases and *nc*—number of negative cases

*A probability *P* is usually expressed as a number between 0 and 1. However, it can also be expressed in the form of "odds", a term perhaps most familiar in sports betting. If the probability of an event *A* is *P*(A) and the alternative possibility is simply "Not *A*", the odds O(A) in favor of *A* can be calculated. Unlike probabilities, odds can take any non-negative value; 10^6 or "a million to one" odds are possible and can be converted back to probabilities through rearrangements

Fig. 7 Steps of a proficiency test according to ISO/IEC 17043:2011 [40]

The interlaboratory ensures a validated method whose uncertainty has been calculated continues working satisfactorily. In principle, method validation and internal quality control are sufficient to ensure a method's accuracy; however, in practice, they are often not perfect [41]. Regarding method validation, unknown influences can interfere with the measurement process and Certified Reference Materials (CRMs)

are not available in several industries [27]. Given these factors, it is difficult to establish traceability of results and unidentified sources of error may be present during the measurement process. Proficiency testing has the advantage of providing a means for participants to obtain an external and independent assessment of the accuracy of their results [42].

In a general context, some of the benefits of PTs are [40]:

- Laboratory performance evaluation and continuous monitoring;
- Evidence of reliable results and identification of problems related to the testing system;
- Possible corrective and/or preventive actions;
- Evaluation of the efficiency of internal controls;
- Determination of performance characteristics and method validation; and
- Standardization of market-facing activities and recognition of test results at national and international levels.

The development and application of PT involve a series of steps that include different approaches chosen according to the matrix and analytes to be evaluated, e.g., assignment of values obtained by consensus or by a reference value calculated by different strategies, performance evaluation (z-score, Zeta-score, etc.), graphical methods (Youden plot, histograms, etc.), and evaluation of stability and homogeneity of PT items, among others [24].

The use of PT or other external control schemes in quality control enables the laboratory to guarantee the effectiveness of the quality control implemented internally, an external reference of the accuracy of the results, and their comparison with those provided by other laboratories. Among the several parameters calculated for assessing the quality of a laboratory's performance is the homogeneity of the results from the participating laboratories [16, 40].

ISO/IEC 17043 [40] describes requirements for the competence of PT providers and ISO 13528 [42] provides an approach to data for qualitative methods. Some practical information on how to select, use, and interpret PT schemes can be found in the Eurachem Guide [25]. However, no fully appropriate scheme has been developed for emerging fields of analysis or rare applications.

4 Application of Quality Statistical Tools in Tests for the Detection of SARS-CoV-2

Quality control, one of the tools strongly related to metrology [19], involves a set of measurement operations that ensure the products manufactured by a company meet the technical specifications to be introduced in the Market [20].

An increasing number of SARS-CoV-2 RNA tests (mostly through RT-PCR) and tests for antibodies against coronavirus (mostly immunoassays) have been reported, whereas a small number of antigen tests is available [13].

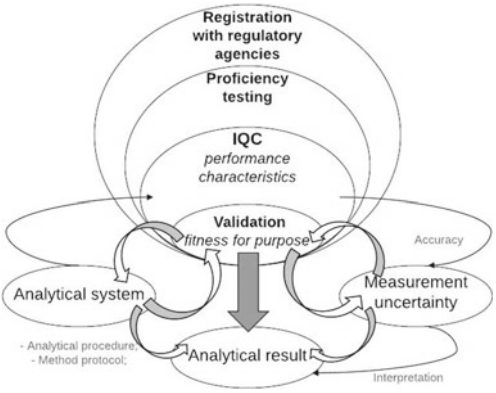

Fig. 8 Different levels of quality validation categories for analyses of diagnostic methods for SARS-CoV-2. Adapted from Olivares and Lopes [23]

The pandemic crisis caused by SARS-CoV-2 and the need for tests that diagnose the virus have required adequate evaluations (i.e. validations) of the performance of the emerging test methods, as well as the development of protocols that standardize their specification of quality, safety, and efficacy, which involves validation of the methods and determination of their uncertainty for ensuring public health safety during their use. Furthermore, the development of proficiency tests in the public domain enables laboratories to prove their competence in test design.

Among the main metrological quality tools are validation, uncertainty estimation, and proficiency testing, as discussed elsewhere. Figure 8 displays a complete set of measurements to be performed by laboratories towards high-quality results. Apart from validation and/or standardized methods, internal quality control (IQC) procedures (use of reference materials (MRs), control charts, etc.), participation in proficiency tests, accreditation to an international standard, usually ISO/IEC 17025 [16], and registration of the test with regulatory agencies such as ANVISA [23] are effective measures.

SARS-CoV-2 diagnostic tests have been performed worldwide in laboratories with extensive experience and technical capacity for nucleic acid amplification testing. Although such tests, which have been commercialized, have been validated and approved by regulatory agencies, few data on their efficacy in wide implementations are currently available.

According to a survey on SARS-CoV-2 diagnostic tests in use, of those registered with Agência Nacional de Vigilância Sanitária (ANVISA) [10], 64 were analyzed, as shown in Fig. 9, and no standardization of the performance parameters has been established for ensuring the quality of their results, thus leading to public health risks.

Most parameters analyzed by the manufacturers (e.g., sensitivity and specificity) have shown discrepancies and followed no standard. The low sensitivity of a diagnostic test may lead to false negatives, thus interfering mainly in cases of asymptomatic individuals.

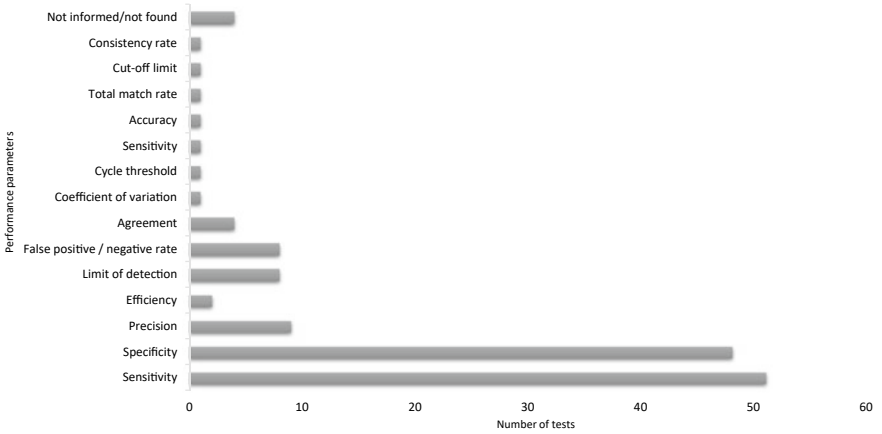

Fig. 9 Main performance parameters used in tests for the diagnosis of SARS-CoV-2 in Brazil, according to ANVISA (2020) [10]

A study developed by the European Commission [13] on the current performance of COVID-19 test methods and devices revealed an urgent need for adequate assessments (i.e. validation) of the performance of both existing and emerging test methods with a view to SARS-CoV-2 viral RNA, such as antigen or antibody tests [1].

We can conclude no standardization has been established for the detection of the quality of tests and no data or parameters for their measurement uncertainty are available.

Regarding the proficiency tests currently available worldwide, only 01 PT has been identified for the diagnosis of COVID-19 in Brazil and only 07 international tests (offered by private companies) have been reported. Therefore, given the importance and urgency of diagnostic methods for COVID-19, the development of a public and widely applicable PT for laboratory comparisons and assurance of results are crucial, since they can be used as a model for other qualitative PTs in emerging disease diagnoses for ensuring interlaboratory testing reliability.

New protocols for validation, calculation of uncertainty, and development of proficiency assays must be implemented not only for the current scenario, but also for future detection tests for SARS-CoV-2 for diagnosing the immunity obtained after infection or vaccination. Once issues of reliability and evaluation of diagnostic tests have been clarified, they will be an essential tool for the development of strategies against SARS-CoV-2 and diseases that may emerge.

5 Conclusions and Future Perspectives

This chapter has discussed statistical quality tools for the quality control of diagnostic tests for SARS-CoV-2.

Among such tools, validation proves an analytical method is suitable for its purpose, thus ensuring routine analyses reproduce consistent values when compared to a reference value. A method is considered validated when evaluated according to a series of established parameters, such as specificity and selectivity, linearity, working range or range, precision, detection limit, quantification limit, accuracy, and robustness (repeatability) and if it has achieved the expected performance.

The uncertainty estimate that provides the confidence level of the result of each test must also be established, and laboratories must be aware of the reliability of qualitative analysis results so that, when necessary, they can report limitations for interpreting results and accurately responding to customers' questions about reliability.

Moreover, well-characterized reference (control) materials that simulate real patient samples and reference test methods should be inventoried, verified, or established towards comparisons of the performance of different tests according to the quality standards required. Other proficiency testing exercises must be organized, so that laboratories can prove their competence in COVID-19 testing.

Despite the importance of application of statistical tools to diagnostic tests for the detection of SARS-CoV-2, no standardization has been established for the registration process with regulatory bodies. Therefore, this chapter has addressed an evaluation and application of statistical tools (validation, uncertainty estimation, and proficiency testing) for the development and monitoring of such tests. The transmission cycles of SARS-CoV-2 must be understood and mechanisms that help the prevention and mitigation of transmission must be developed for use in future risk conditions in the context of emerging zoonotic diseases, including the current one.

Acknowledgements The authors are grateful to CAPES (001 and Pandemias 8887.504861/2020-00) and FAPESP (no. 2020/01238-4) for their financial support and groups MeDiCo and RQA Labs for all support and assistance during the development of this research.

References

1. Eurachem. Trends & challenges in ensuring quality in analytical measurements, *Book of Abstracts*, 01, https://www.eurachem.org/images/stories/workshops/2021_05_QA/pdf/abstracts/Book_of_Abstracts_final.pdf (2021)
2. D. Wang, B. Hu, C. Hu, F. Zhu, X. Liu, J. Zhang, B. Wang, H. Xiang, Z. Cheng, Y. Xiong, Y. Zhao, Y. Li, X. Wang, Z. Peng, Clinical characteristics of 138 hospitalized patients with 2019 novel coronavirus-infected pneumonia in Wuhan, China. JAMA **323**, 1061–1069 (2020). https://doi.org/10.1001/jama.2020.1585
3. T. Ahmad, M. Khan, T.H. Musa, S. Nasir, J. Hui, D.K. Bonilla-Aldana, A.J. Rodriguez-Morales, COVID-19: zoonotic aspects. Travel Med. Infect. Dis. **36**, 101607 (2020). https://doi.org/10.1016/j.tmaid.2020.101607
4. M.A. Shereen, S. Khan, A. Kazmi, N. Bashir, R. Siddique, COVID-19 infection: Origin, transmission, and characteristics of human coronaviruses. J. Adv. Res. **24**, 91–98 (2020). https://doi.org/10.1016/j.jare.2020.03.005

5. A. Patrì, L. Gallo, M. Guarino, G. Fabbrocini, Sexual transmission of severe acute respiratory syndrome coronavirus 2 (SARS-CoV-2): a new possible route of infection? J. Am. Acad. Dermatol. **82**, e227 (2020). https://doi.org/10.1016/j.jaad.2020.03.098
6. B.D. Kevadiya, J. Machhi, J. Herskovitz, M.D. Oleynikov, W.R. Blomberg, N. Bajwa, D. Soni, S. Das, M. Hasan, M. Patel, A.M. Senan, S. Gorantla, J.E. McMillan, B. Edagwa, R. Eisenberg, C.B. Gurumurthy, S.P.M. Reid, C. Punyadeera, L. Chang, H.E. Gendelman, Diagnostics for SARS-CoV-2 infections. Nat. Mater. **20**, 593–605 (2021). https://doi.org/10.1038/s41563-020-00906-z
7. Y. Pan, X. Li, G. Yang, J. Fan, Y. Tang, J. Zhao, X. Long, S. Guo, Z. Zhao, Y. Liu, H. Hu, H. Xue, Y. Li, Serological immunochromatographic approach in diagnosis with SARS-CoV-2 infected COVID-19 patients. J. Infect. **81**, e28–e32 (2020). https://doi.org/10.1016/j.jinf.2020.03.051
8. N.N.T. Nguyen, C. McCarthy, D. Lantigua, G. Camci-Unal, Development of diagnostic tests for detection of SARS-CoV-2. Diagnostics. **10**, 1–28 (2020). https://doi.org/10.3390/diagnostics10110905
9. ANVISA: Information Note - Use of quick tests – Covid-19. 2507, 1–9 (2020)
10. ANVISA: Accuracy of diagnostic tests registered with ANVISA for COVID-19. 1–35 (2020)
11. B. Flower, J.C. Brown, B. Simmons, M. Moshe, R. Frise, R. Penn, R. Kugathasan, C. Petersen, A. Daunt, D. Ashby, S. Riley, C.J. Atchison, G.P. Taylor, S. Satkunarajah, L. Naar, R. Klaber, A. Badhan, C. Rosadas, M. Khan, N. Fernandez, M. Sureda-Vives, H.M. Cheeseman, J. O'Hara, G. Fontana, S.J.C. Pallett, M. Rayment, R. Jones, L.S.P. Moore, M.O. McClure, P. Cherepanov, R. Tedder, H. Ashrafian, R. Shattock, H. Ward, A. Darzi, P. Elliot, W.S. Barclay, G.S. Cooke, Clinical and laboratory evaluation of SARS-CoV-2 lateral flow assays for use in a national COVID-19 seroprevalence survey. Thorax **75**, 1082–1088 (2020). https://doi.org/10.1136/thoraxjnl-2020-215732
12. V. Tiwari, M. Kumar, A. Tiwari, B.M. Sahoo, S. Singh, S. Kumar, R. Saharan, Current trends in diagnosis and treatment strategies of COVID-19 infection. Environ. Sci. Pollut. Res. **28**, 64987–65013 (2021). https://doi.org/10.1007/s11356-021-16715-z
13. European Commission, Current performance of COVID-19 test methods and devices and proposed performance criteria (2020), pp. 1–32. https://ec.europa.eu/docsroom/documents/40805. Accessed 30 June 2020
14. X. Li, M. Geng, Y. Peng, L. Meng, S. Lu, Molecular immune pathogenesis and diagnosis of COVID-19. J. Pharm. Anal. **10**, 102–108 (2020). https://doi.org/10.1016/j.jpha.2020.03.001
15. Z. Li, Y. Yi, X. Luo, N. Xiong, Y. Liu, S. Li, R. Sun, Y. Wang, B. Hu, W. Chen, Y. Zhang, J. Wang, B. Huang, Y. Lin, J. Yang, W. Cai, X. Wang, J. Cheng, Z. Chen, K. Sun, W. Pan, Z. Zhan, L. Chen, F. Ye, Development and clinical application of a rapid IgM-IgG combined antibody test for SARS-CoV-2 infection diagnosis. J. Med. Virol. **92**, 1518–1524 (2020). https://doi.org/10.1002/jmv.25727
16. ISO 17025:2017, A.N.I.: General requirements for the competence of testing and calibration laboratories (2017)
17. ISO 15189: Clinical laboratories - competency quality requirements (2015)
18. I.R.B. Olivares, Quality management in laboratories. Publishing company Átomo, Campinas, SP (2019)
19. ISO 9001: Quality management systems (2021)
20. M.C. de Souza, A.L. Korzenowski, F.A. de Medeiros, C.S. ten Caten, R. Herzer, Standards for quality management in clinical analysis laboratories. Espacios. **37**, 363–368 (2016)
21. E. Directorate, C. Group, M. Committee, OECD series on principles of good laboratory practice and compliance monitoring. Ann. Ist. Super. Sanita. **33**, 1–172 (1997)
22. M. Valcárcel, A. Ríos, Quality assurance in analytical laboratories engaged in research and development activities. Accredit. Qual. Assur. **8**, 78–81 (2003)
23. I.R.B. Olivares, F.A. Lopes, Essential steps to providing reliable results using the analytical quality assurance cycle. TrAC—Trends Anal. Chem. **35**, 109–121 (2012). https://doi.org/10.1016/j.trac.2012.01.004

24. I.R.B. Olivares, G.B. de Souza, A.R. de Araujo Nogueira, V.H.P. Pacces, P.A. Grizotto, P.S. da Silva Gomes Lima, R.M. Bontempi, Trends in the development of proficiency testing for chemical analysis : focus on food and environmental matrices. Accredit. Qual. Assur. (2021). https://doi.org/10.1007/s00769-021-01487-3
25. Eurachem Guide—Second Edition 2014, The fitness for purpose of analytical methods—a laboratory guide to method validation and related topics second edition (1999)
26. E.P.T. Guide, Selection, use and interpretation of proficiency testing (PT) schemes by laboratories (2000)
27. E. Trullols, I. Ruisánchez, F.X. Rius, Validation of qualitative analytical methods. TrAC—Trends Anal. Chem. **23**, 137–145 (2004). https://doi.org/10.1016/S0165-9936(04)00201-8
28. C. de Souza Gondim, O.A.M. Coelho, R.L. Alvarenga, R.G. Junqueira, S.V.C. de Souza, An appropriate and systematized procedure for validating qualitative methods: its application in the detection of sulfonamide residues in raw milk. Anal. Chim. Acta. **830**, 11–22 (2014). https://doi.org/10.1016/j.aca.2014.04.050
29. S.L.R. Ellison, T. Fearn, Characterising the performance of qualitative analytical methods: statistics and terminology. TrAC—Trends Anal. Chem. **24**, 468–476 (2005). https://doi.org/10.1016/j.trac.2005.03.007
30. QAWG: Assessment of performance and uncertainty in qualitative chemical analysis, Draft 03/2021 (2021)
31. National Institute of Metrology, Q. e T., The international vocabulary of metrology (2012)
32. S. Cárdenas, M. Valcárcel, Analytical features in qualitative analysis. TrAC—Trends Anal. Chem. **24**, 477–487 (2005). https://doi.org/10.1016/j.trac.2005.03.006
33. National Institute of Metrology, Quality and Technology (INMETRO): DOQCGCRE-089 (2017)
34. M. Thompson, S.L.R. Ellison, R. Wood, Harmonized guidelines for single-laboratory validation of methods of analysis (IUPAC technical report). Pure Appl. Chem. **74**, 835–855 (2002). https://doi.org/10.1351/pac200274050835
35. B. Pöpping, J. Boison, S. Coates, C. Von Holst, R. MacArthur, R. Shillito, P. Wehling, AOAC international guidelines for validation of qualitative binary chemistry methods. J. AOAC Int. **97**, 1492–1495 (2014). https://doi.org/10.5740/jaoacint.BinaryGuidelines
36. C.S. Gondim, R.G. Junqueira, S.V.C. Souza, Tendências em validação de métodos de ensaios qualitativos Trends in implementing the validation of qualitative methods of analysis. Rev. Inst. Adolfo Lutz. **70**, 433–447 (2011)
37. ISO/IEC GUIDE 98–4, Uncertainty of measurement—part 4: role of measurement uncertainty in conformity assessment. Int. Organ. Stand. GUIDE 98-4 (2012)
38. A. ISO, I.E.C. Guide, ABNT ISO/IEC GUIDE 98-3 (2016)
39. B.L. Mil'man, L.A. Konopel'ko, Uncertainty of qualitative chemical analysis: general methodology and binary test methods. Mendeleev All-Russia Res. Inst. Metrol. **59**, 1129–1130 (2004). https://doi.org/10.1023/B:JANC.0000049712.88066.e7
40. 17043:2011, A.N.I.: Conformity assessment — General requirements for proficiency testing. 46 (2011)
41. A.K. Ávila, L.J.R. Pereira, P.L.S. Ferreira, P.R.G. Couto, R.S. Couto, T.O. Araujo, R.M.H. Borges, Proficiency testing: A powerful tool for national laboratories (2004)
42. ISO 13528:2015: Statistical methods for use in proficiency testing by interlaboratory comparison. 2015, (2015)
43. V. Haselmann, M.K. Özçürümez, F. Klawonn, V. Ast, C. Gerhards, R. Eichner, V. Costina, G. Dobler, W.J. Geilenkeuser, R. Wölfel, M. Neumaier, Results of the first pilot external quality assessment (EQA) scheme for anti-SARS-CoV2-antibody testing. Clin. Chem. Lab. Med. **58**, 2121–2130 (2020). https://doi.org/10.1515/cclm-2020-1183